UNIVERSITY OF Southampton

Faculty of Medicine

Human Development and Health

ENRICHMENT AND CHARACTERISATION OF THE SKELETAL STEM CELL POPULATION

By

Timothy John Noble

Thesis for the degree of Integrated MPhil/PhD

Biomedical Science

September 2018

UNIVERSITY OF Southampton

Abstract

Faculty of Medicine

Human Development and Health

Thesis for the degree of Integrated MPhil/PhD

Biomedical Science

ENRICHMENT AND CHARACTERISATION OF THE SKELETAL STEM CELL POPULATION

By

Timothy John Noble

Throughout the world, the average population age is increasing and, in many areas, nearly a quarter of the population will be over the age of 65 within the next 15 years, 40% of the total NHS budget is spent on people over the age of 65. The UK spends to £13 billion on musculoskeletal treatments, a cost which will increase as the population over 65 also increases. Skeletal stem cells are a rare cell population within the bone marrow, which facilitate bone repair and homeostasis. With no identified markers capable of isolating skeletal stem cells, characterisation, understanding, and subsequent use is limited. Understanding these cells within the skeletal system may help us understand disease states, the causes and, importantly, offer therapeutic solutions.

This thesis approached the study of skeletal stem cells from two alternative angles. The first, a marker discovery direction using aptamers (synthetic binding ligands, normally nucleic acid based) to identify and exploit potential skeletal stem cell-specific markers. The second approach using current enrichment techniques and the application of Drop-Seq to characterise the enriched cell gene expression profiles at a single cell level. Aptamer selection was first applied against a bone-derived cell line, SAOS-2, to ensure a robust methodology was established before the use of precious primary human skeletal tissue. The SAOS-2 selection proved successful, providing ten aptamers which preferentially bound to the SAOS-2 cells over a counter selection target of the Raji cell line. Unfortunately, when carrying out the same aptamer selection method using bone marrow and foetal femur samples unwanted amplification took place within all the attempted selections, resulting in failure of selection. This was narrowed down to amplification products from the cell that was not detected in QC steps.

The use of enrichment markers provided a population (STRO-1^{BRIGHT}+ CD146+) highly enriched for Colony Forming Units - Fibroblastic (CFU-F) capacity. This population was too small for use with Drop-Seq. STRO-1+ CD146+ cells were therefore analysed instead. The analysis highlighted four main cell types within the population, monocytes, lymphocytes, erythrocyte progenitors and CXC chemokine ligand (CXCL) 12-abundant reticular (CAR) cells.

The failure of the aptamer selection against the primary cells presented a setback to the characterisation of the skeletal stem cells. However, with a redesign of the primers and aptamer pool, this methodology should prove fruitful. The identification of the CAR cells is highly intriguing as these cells are studied within the haematopoietic stem cell field, as the CAR cells act as regulatory cells of the haematopoietic stem cells. The CAR cells have been shown to be multipotent, differentiating into adipocytes, chondrocytes and osteocytes, and are a rare population. These characteristics are shared with the characteristics attributed to the skeletal stem cell, and therefore the identification of the CAR cells from a population enriched for the skeletal stem cells suggests a relationship between these cells, whether the SSCs are the CAR cells or are closely related is unclear at this point, with further protein localisation studies this may be elucidated.

Table of Contents

Table of Tables

Table of Figures

Research Thesis: Declaration of Authorship

Print name:	Timothy John Noble

Title of thesis:	Enrichment and Characterisation of the skeletal stem cell population

I declare that this thesis and the work presented in it are my own and has been generated by me as the result of my own original research.

I confirm that:

1. This work was done wholly or mainly while in candidature for a research degree at this University;
2. Where any part of this thesis has previously been submitted for a degree or any other qualification at this University or any other institution, this has been clearly stated;
3. Where I have consulted the published work of others, this is always clearly attributed;
4. Where I have quoted from the work of others, the source is always given. With the exception of such quotations, this thesis is entirely my own work;
5. I have acknowledged all main sources of help;
6. Where the thesis is based on work done by myself jointly with others, I have made clear exactly what was done by others and what I have contributed myself;

None of this work has been published before submission

Signature:		Date:	

Acknowledgements

I would like to thank firstly, my supervisors Professor Richard O. C. Oreffo and Professor Paul A. Townsend for giving me the opportunity to participate in the PhD program and their guidance throughout.

Secondly, I would like to thank the Industrial supervisors Dr Arron Tolley and Dr David Bunka for their input into the project, techniques and materials that the project would not have been possible without.

I would like to thank Louise Hogan and Sarah E. Barton and for proofreading my thesis, picking up on the typing, spelling and grammatical errors to help make my work more capable of communicating my results in a clear and concise manner.

I would also like to thank Patrick Stumpf, for his contribution to my Drop-Seq chapter, working with you was a pleasure, even with the very long hours, the company and the results make it all worthwhile.

Julia Well, you provided some sanity and a sounding board for all things frustrating within the lab, a guru of all techniques, and great company for coffee/tea breaks. Your positive and can-do attitude has helped not only me through our PhDs, and I wish you all the best with your own.

And finally, and most importantly, I would like to thank my partner for being supportive throughout my PhD, giving me confidence when I was lacking, providing adventure and happiness amongst the hard work and long hours of PhD work, and providing motivation when it was needed. You weren’t what I was expecting to come out of my time as a PhD student, but I wouldn’t have it any other way.

To all of you, I say thank you.

Chapter 1 Introduction

1.1 Study rationale

Advances in medical care worldwide, combined with healthier lifestyles, have led to an increase in the global population and lifespan - resulting in a higher proportion of people over 65 (Peterson, 1999, Kinsella and Phillips, 2005). Over 17% of the UK's population currently belongs in this age bracket and is trending towards almost a quarter of the population by 2035 (Figure 1-1). Currently, the elderly population, although a minority, accounts for 40% of the NHS's total expenditure (AgeUK, 2016). This increase in cost with age is most likely due to the capacity of the body to protect and repair itself diminishing with age (Carlson and Conboy, 2007, Oh et al., 2014, Baker et al., 2015), leading to a higher incidence of disease (Wong et al., 2014).

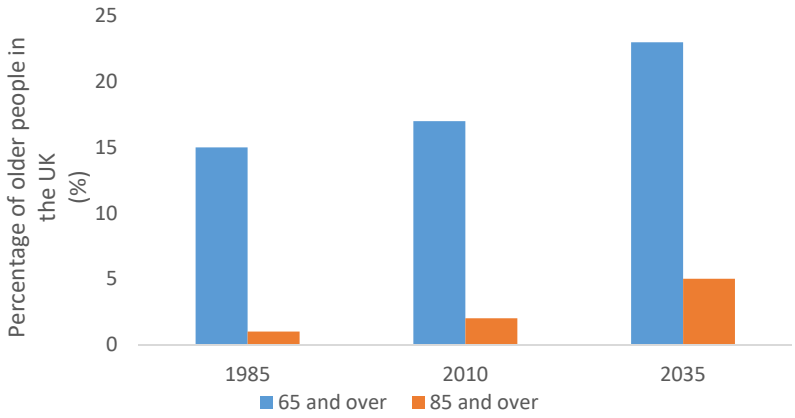

Figure 1-1 - Graph showing the estimated population growth from 1985 to 2035. Approximately a quarter of the population within the UK will be over 65 by 2035. Redrawn using data from the national archives: http://webarchive.nationalarchives.gov.uk/20160108205940/http://www.ons.gov.uk/ons/rel/mortality-ageing/focus-on-older-people/population-ageing-in-the-united-kingdom-and-europe/rpt-age-uk-eu.html?format=print (Accessed 07-07-17)

Musculoskeletal injuries and diseases are mainly associated with the elderly population and result in reduced quality of life before, during, and after treatment - as well as a reduced potential for long-term recovery (Guralnik et al., 1996). Treatments for musculoskeletal injuries and diseases in England cost £12.972 billion between 2013 and 2014, the 4th highest expenditure for medical treatments after mental health disorders, circulation problems and gastrointestinal system problems (NHS_England, 2015). Most treatments for musculoskeletal injury and diseases are reactive, to repair the damage that has taken place. Without preventative treatments and better long-term solutions, these costs will undoubtedly escalate (Etzioni et al., 2003); therefore, a better understanding of the disease initialisation, progression and alternative treatments should be investigated.

The fields of tissue engineering and regenerative medicine offer new insights and potential treatments for a variety of damage and disease states. Tissue engineering and regenerative medicine aim to develop new approaches to improve upon joint replacement surgeries and associated musculoskeletal conditions (Nesic et al., 2006, Correia et al., 2014, Dawson et al., 2014, Gentile et al., 2014, Black et al., 2015, Richardson et al., 2016). Tissue engineering focuses on materials to be implanted and seeded with cells, where regenerative medicine focuses on enhancing bodily functions to repair itself, resulting in multiple approaches to improve public health and quality of life (Nerem and Sambanis, 1995, Lysaght and Reyes, 2001, Roberts et al., 2008, Mason and Manzotti, 2010), (Figure 1-2 A and Figure 1-2 B respectively).

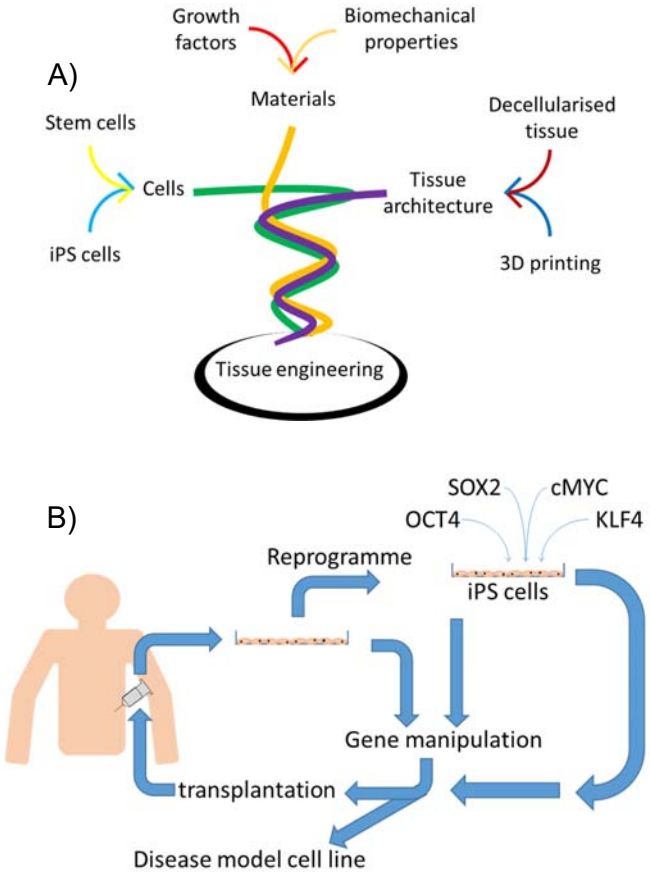

Figure 1-2 - Applications of tissue engineering and regenerative medicine. A) Tissue engineering combines many aspects of biology (left), biological cues (top) and structural components (right) to build solutions to many disease and damage-based issues. B) Regenerative medicine takes cells or tissues from the host and repurposes the cells to treat diseased or damaged tissues or uses them to investigate the disease states through cell lines.

Tissue engineering aims to incorporate engineering and biology to develop materials which function as substitutes for damaged or diseased tissues (Langer and Vacanti, 1993, Howard et al., 2008). To date, a number of materials have been under development to aid in the repair of skin (Monteiro et al., 2015), cartilage (Oka et al., 2000, Nesic et al., 2006, Liao et al., 2013), bone (Gothard et al., 2015b, Tayton et al., 2015, Cox et al., 2015, Xavier et al., 2015) and liver (Che Abdullah et al., 2014).

Material	Target	Publication
Layer by layer Hyaluronic acid scaffold	Skin	Monteiro et al 2015
PVA-H artificial articular cartilage	Articular cartilage	Oka et al 2000
Alginate and Polyacrylamide 3-D woven scaffold	Articular cartilage	Liao et al 2013
Alginate/bone ECM hydrogels	Bone	Gothard et al 2015b
Hydroxyapatite polymer composite scaffold	Bone	Tayton et al 2015
Hydroxyapatite composite	Bone	Cox et al 2015
Nanosilicate enhanced collagen-polymer hydrogel	Bone	Xavier et al 2015
Carbon nanotube scaffold	Liver	Che Abdullah et al 2014

Table 1-1 – Different categories of biomaterials applied in tissue engineering/regenerative medicine. Numerous materials have been developed for tissue repair, here are several tissue engineering and regenerative medicine solutions to tissue damage. They are not limited to bone, and is not an extensive list, but does provide insights into the field and the complex and interesting materials developed.

While these materials are substitutes, they are made in a way that promotes the body to integrate, replace and degrade the materials over time. In contrast, regenerative medicine seeks to stimulate and utilise human cells to repair or grow tissues or organs in order to restore normal function or maintain homeostasis (Mason and Dunnill, 2008). Regenerative medicine requires a greater understanding of the disease and the regenerative properties of the cells being recruited to repair the damaged or diseased tissue (Mahla, 2016, Ge and Fuchs, 2018).

Reactive treatments are essential to developing medical interventions, though wherever possible, preventative solutions are more cost-effective and improve quality of life. To comprehend the bone's repair processes stem cells need to be subject to isolation and characterisation to allow for the stem cells to be utilised and manipulated effectively (Bielby et al., 2007).

1.2 Bone structure

Bone is a hierarchical, heterogeneous, and anisotropic support and a protective structure consisting of collagen, mineral, cells, and non-collagen proteins (Rho, 1998, Reznikov et al., 2014). Bone has varying structural properties and organisations that have evolved for optimal structural strength when loaded from specific directions (Rho, 1997). The macrostructure of bone has two classifications: cortical or cancellous bone. Cortical bone is the dense external layer of the bone making up 80% of the skeletal mass and providing the skeleton with its resistance to physical impact, bending, and torsion, making it critical for the protection of organs, load bearing, and facilitating locomotive abilities. Cancellous bone is the spongy inner mass of bone that provides a high surface area for a variety of physiological functions, including haematopoiesis, calcium ion exchange, and mechanical load distribution (Levrero-Florencio et al., 2016). The macrostructure is the top layer of the bone hierarchy, below are the structural components that make up the bone (Figure 1-3).

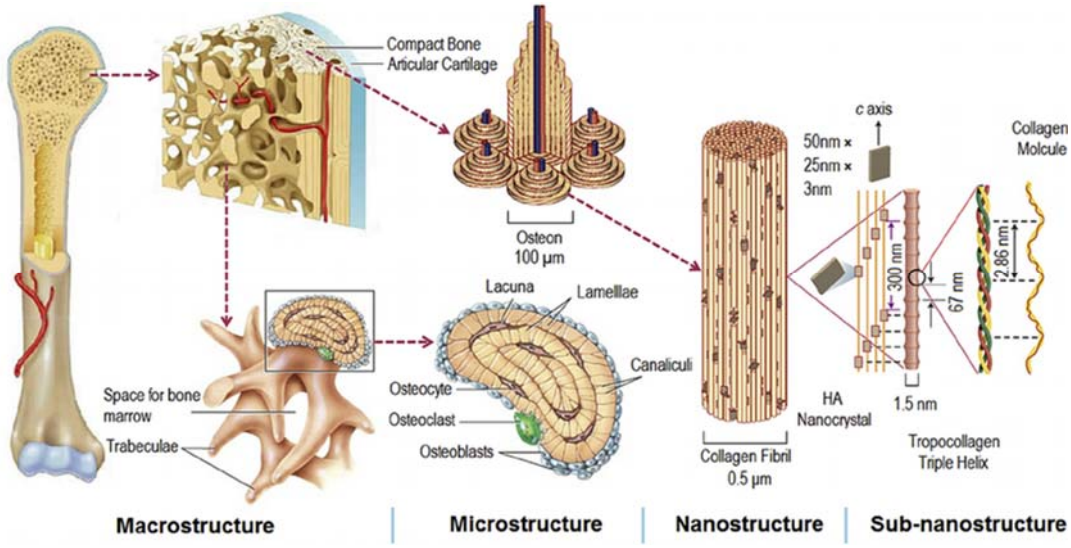

Figure 1-3 - The hierarchical structure of bone. The hierarchical structure of bone is built from the sub-nanostructure up to the macro scale. The sub-nanostructure being the most basic building blocks of bone, the bone crystals and collagen molecules. These build up to make the larger structures and form the macrostructures of cancellous and cortical bone. Image from (Wang et al., 2016).

The cells which support and maintain the bone marrow environment are the haematopoietic cells and the osteogenic cells. The haematopoietic cell populations are responsible for producing the red blood supply and are found within the red bone marrow. In early development red bone marrow is found throughout the cancellous bone, but as humans age, these areas are replaced with yellow bone marrow areas, except for long bone metaphysis, axial skeleton and girdle bones (J B Vogler and Murphy, 1988). The cells which facilitate the change from red to yellow bone marrow are the adipocytes, which increase in number with age (Bianco et al., 1988). The adipose tissue has been shown to be a regulator of haematopoiesis, causing haematopoietic stem cell (HSC) to become quiescent until the adipose tissue is reduced, generally as a reaction to trauma or blood loss to increase haematosis (Naveiras et al., 2009). The osteogenic cell populations maintain and repair the bone structure; these populations include the osteoclasts, osteoblasts and the chondrocytes. Osteoblasts are responsible for active bone deposition and form a dense cross-linked collagen structure called osteoid, which is then mineralised to form bone. Osteoblasts work with the osteoclasts (which resorb bone) to maintain bone structure in the remodelling process (Hadjidakis and Androulakis, 2006). Chondrocytes are responsible for the formation of articular cartilage within the joints (Muir, 1995), as well as being critical in bone fracture repair (Gerstenfeld et al., 2003) in one of four phases of bone fracture repair (Figure 1-4) (Schindeler et al., 2008, Ercin et al., 2017). Phase 1 is inflammation of soft tissues and the recruitment of cells for repair. Phase 2, chondrocytes deposit a cartilaginous template forming a soft callus which is used as a template for the bone repair. Phase 3 the soft callus is ossified and develops into a hard callus of woven bone. Phase 4, remodelling of the callus into cortical and/or trabecular bone takes place via osteoclasts and osteoblasts.

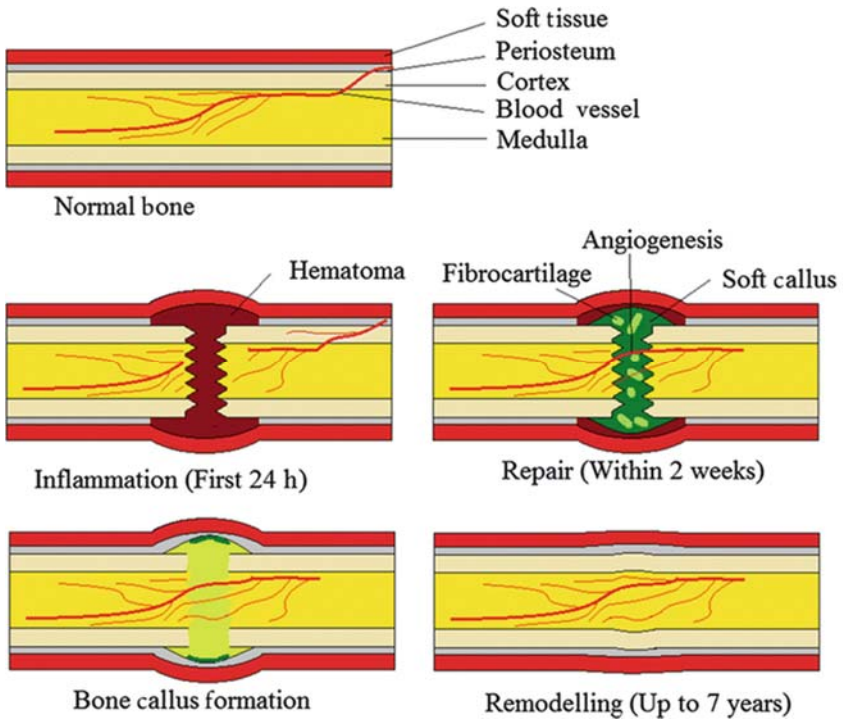

Figure 1-4 - Bone repair has 4 main phases to restore original functionality. Phase 1, inflammation of the damaged site and recruitment of cells for repair. Phase 2, (repair) produces a soft callus and blood vessel invasion ensures adequate nutrient supply for repair processes. Phase 3 (bone callus formation), calcification of the soft callus generating a bony callus. Phase 4 (remodelling), the breakdown of the bone callus woven bone to cancellous or trabecular bone, From (Ercin et al., 2017)

Having an insight into the cells and how they interact allows for a better understanding of the hierarchical structure of bone. Recognising how the bone is formed and maintained allows for treatments to be created for a variety of ailments, from reactive surgeries to set the bones so they heal themselves (Bone, 1986, Wood et al., 2003, Wardlaw, 2009), to chemical and hormonal cues to restore bone to its former structure (Friedlaender et al., 2001, Govender et al., 2002). Occasionally, restoration of the bones to proper structure following a fracture is not completed by the body's repair processes; these are non-union fractures.

Non-union fractures can arise as a consequence of a combination of conditions including fracture site, surgical technique, smoking, and displacement during fracture (Zura et al., 2016). Non-union fractures pose a greater detriment to quality of life compared to a fractured and repairing bone, as the patient continues to have a broken bone and recovery time has been prolonged dramatically. Despite the number of fractures increasing with age, the number of non-union fractures does not follow this trend (Mills et al., 2017), the average percentage of non-union being 1.9% of fractures. The highest incidence of non-union fractures is within the age range 25 to 44 reaching 9% of fractures. The Mills et al. study into over four million adults showed that non-unions are a risk for all age categories, so the detriment to life quality is not just found at ages over 65. However, the number of fractures do increase with age (Mills et al., 2017).

Risk of fracture is an important detail to consider when discussing fractures and potential treatments. Studies have shown that once the risk of a fracture is above 3%, interventions or prophylaxis are more cost-effective and prevent patient injury and associated quality of life deterioration (Schousboe et al., 2007, Zethraeus et al., 2007, Tosteson et al., 2008). Therefore, preventing a disease or breakage is the ideal situation for all, and investigating how bone repairs and maintains itself, and how these processes break down with age, is critical in identifying mechanisms to counter this degradation of function and maintain healthy bone for longer.

1.3 Stem cells

Stem cells are the key to growth, tissue regeneration, maintenance and overall health with the ability for self-renewal and to differentiate into other tissues (Figure 1-5) (Pittenger, 1999, Keller, 2005, Jones and Wagers, 2008, Hogan et al., 2014).

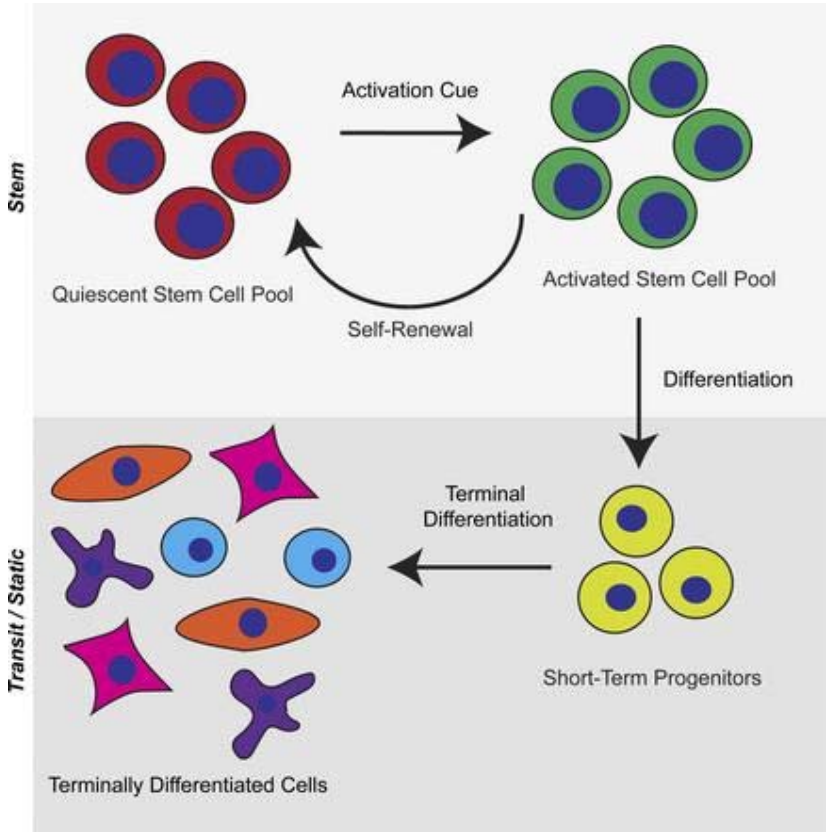

Figure 1-5 - Stem cells are typically a quiescent population, upon activation growth of progenitors as well as self-renewal enable tissue repair. Stem cells are found within niches, and when damage is detected stem cells become activated, produce more cells, which migrate to damage sites to facilitate repair processes differentiation, while maintaining the original stem cell population. from (Keyes and Fuchs, 2018)

There are four primary sources of stem cells: embryonic stem cells, foetal stem cells, induced pluripotent stem cells (iPS), and adult stem cells. Human embryonic stem cells (hESC) are derived from the inner cell mass of a blastocyst, and foetal cells originate from aborted foetuses, while the adult stem cells are derived from adult tissues (Figure 1-6).

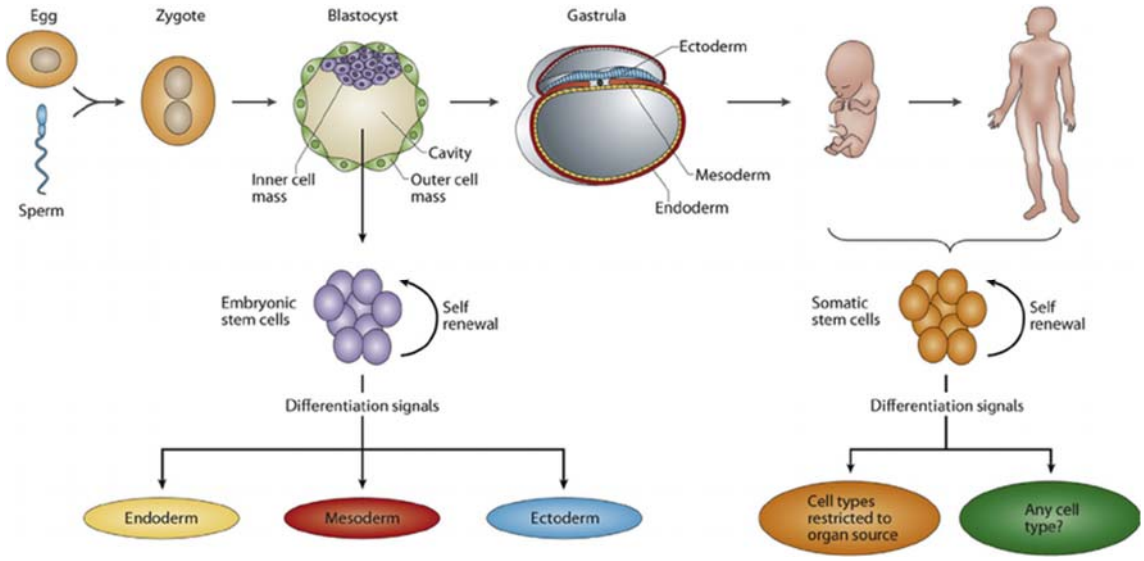

Figure 1-6 - Stem cell sources determine the differential potential of the isolated stem cells. Embryonic stem cells derived from the inner cell mass of a blastocyst have a much broader differentiation capability compared to cells derived from foetal or adult stem sources. The cells from the inner cell mass are capable of differentiation into all three germ layers. Foetal and adult stem cells are generally restricted to differentiation into cell types present from the tissue of origin. However, can be reprogrammed as seen with iPSCs. From (Boppart et al., 2015)

Embryonic stem cells are pluripotent (Evans and Kaufman, 1981, Martin, 1981, Biswas and Hutchins, 2007) and, therefore, have broader differentiation potential than the foetal and adult stem cell counterparts which are multipotent (Pittenger et al., 1999, Beltrami et al., 2003, Gimble and Guilak, 2003). Adult stem cells are from sources that are more readily available, with bone marrow, skin and fat tissues being identified as rich sources (Toma et al., 2001, Zuk et al., 2002, Wexler et al., 2003) as well as being more socially and ethically acceptable.

1.3.1 Clinical need for stem cell understanding and manipulation

Stem cells within the bone marrow become increasingly quiescent and less capable of population expansion as people age (Stenderup et al., 2003), slowing regenerative and reparative processes. The decline in regenerative processes can lead to disease states such as osteoporosis and osteoarthritis (D'Ippolito et al., 1999, Stolzing et al., 2008). With the population ageing resulting in almost a

quarter of the population over the age of 65 by 2035 (Figure 1-1), the number of incidents will only increase, raising the cost from the current £12.9 Billion by at least another 66% by 2035. This results in a significant burden to the NHS, and subsequently society, as well as the individuals who will suffer from potentially debilitating fractures. One potential treatment method that has been shown to have regenerative capabilities is the application of stem cells (Oreffo et al., 2005, Keller, 2005, Le Blanc et al., 2005, Yamanaka, 2009, Dimitriou et al., 2011, Smith et al., 2011, Gowri et al., 2013, Dawson et al., 2014, Vega et al., 2015, Rodriguez-Menocal et al., 2015).

1.3.2 Human embryonic stem cells

Human embryonic stem cells (hESCs) are a pluripotent cell population derived from the inner cell mass of a blastocyst (Thomson, 1998, Pera et al., 2000), capable of differentiation into any of the body germ line cell and tissues types. This differentiation capacity results in significant potential of hESCs for application in regenerative medicine (Figure 1-7). The differentiation potential of the hESCs includes chondrocytes (Odorico et al., 2001) and osteocytes (Kim et al., 2008) which are critical for skeletal repair and maintenance, highlighting the potential of the of hESCs in regenerative medicine for bone repair.

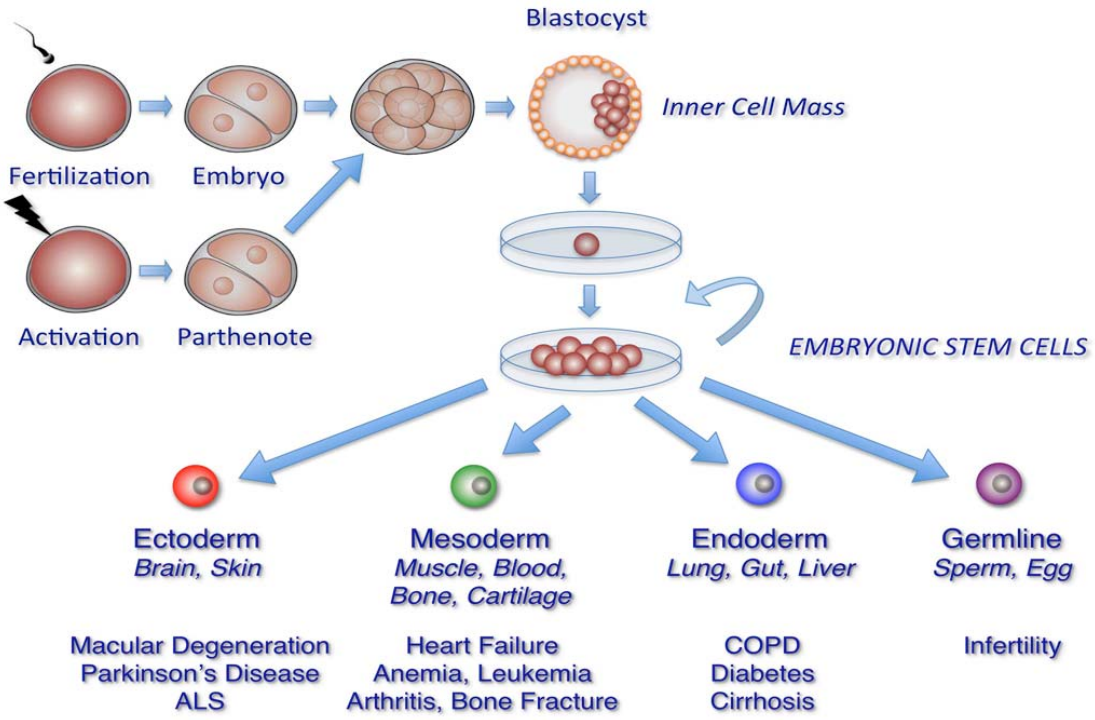

Figure 1-7 - Embryonic stem cells are pluripotent and therefore capable of differentiation into all germ lines within the human body. hESCs are derived from the inner cell mass of a blastocyst; embryonic stem cells have great proliferative capabilities while maintaining a stem cell population which can generate tissues from all germ lines found within the human body. From http://s3.amazonaws.com/libapps/accounts/1768/images/Embryonic_stem_cells_diagram.jpg (accessed 09-09-18)

Despite the potential for regenerative medicine, many questions surround the morality of using hESCs due to their source. The questions stem from the concept of pre-implantation blastocysts as embryos, representative of "life" in their own right: objections centre on the use of, and approval to use, discarded IVF embryos for studies as a dangerous ethical precedent for the broader use of hESCs (de Wert and Mummery, 2003, Baldwin, 2009).

The stemness of the embryonic stem cell population can be maintained by culturing the cells within a hypoxic environment (Forristal et al., 2010), providing a method to culture and expand the hESCs more easily without cell differentiation taking place until cues are added to the culture. Interestingly, hESCs' immune

properties are disputed throughout literature (Fu et al., 2015, Utermohlen et al., 2009, Wu et al., 2008). Some evidence shows that hESCs derived MSCs are immune privileged and perform better than the adult counterpart (Fu et al., 2015), while other evidence states that the hESCs are more readily rejected (Wu et al., 2008, Utermohlen et al., 2009). This indecision within the community makes defining the hESCs populations' immunogenic properties challenging. With the ethical complications in large-scale tissue sourcing and the challenges in directing differentiation, the therapeutic application is currently an unsuitable use of hESCs.

1.3.3 Foetal femur stem cells

Stem cells derived from foetal femurs are multipotent, display tri-lineage potentiality (bone, fat and cartilage) (in 't Anker et al., 2003), with increased proliferative capacity, compared to adult stem cells, as well as a reported broader differentiation potential (neurons, skeletal muscle and blood cells) (O'Donoghue and Fisk, 2004) .

The immunological interactions of transplanted foetal cells have been extensively detailed and characterised compared to hESCs, and the literature shows that foetal MSCs can suppress immune responses while avoiding detection themselves (Götherström, 2011). However, when the immune system is activated foetal cells are destroyed more readily than adult stem cells via the TRAIL pathway (Gotherstrom et al., 2004, Gotherstrom, 2016). This immunosuppressing effect is believed to be a significant advantage to this cell source, and to supplement other treatments to enhance efficacy. Osteogenic lineages have been shown to be generated with foetal stem cells (Le Blanc et al., 2005, Gowri et al., 2013, Gothard et al., 2015a). Given the attributes shared by both hESCs and adult stem cells, this is an exciting population for use in clinical applications.

While more readily available than the hESCs, foetal stem cells still pose ethical concerns regarding their use, and while displaying considerable plasticity and considerable reparative potential compared to adult stem cells, the difficulty in

obtaining foetal tissue remains an issue for therapeutics. However, issues associated with immunogenicity and ethical considerations await resolution before this population can be exploited to its full potential.

1.3.4 Induced pluripotent stem cells (iPS)

Induced pluripotent stem cells (iPS cells) are stem cells generated from adult cells using a series of transcription factors (OCT4, SOX2, cMYC, and KLF4). These transcription factors reprogramme epigenetic regulation and, therefore, expression to a more stem cell-like state (Yamanaka, 2007) (Figure 1-2 B). A small proportion of the adult cells react by modulating epigenetic marks like DNA methylation and histone acetylation; this causes the cells to revert to a more stem-like state (epigenetics is the regulation of gene expression by processes above the underlying genetic code of the genome, it is performed by methylation of DNA, and modification of histones) (Jaenisch and Bird, 2003).

Whether a cell has become pluripotent, and therefore reprogrammed, can be assessed by *in vitro* differentiation to ensure differentiation into the three germ layers (mesoderm, endoderm, ectoderm) (De Los Angeles et al., 2015), or implanting the cells into an immune-compromised mouse and assessing for teratoma formation (Gutierrez-Aranda et al., 2010, Abad et al., 2013). A teratoma is a mass or a tumour that develops from pluripotent stem cells containing tissues from the three germ layers (Przyborski, 2005, Prokhorova et al., 2009). The ability to reprogram adult cells into a pluripotent stem cell is something that has captured the scientific field, like the ability to work with pluripotent stem cells without the need for ethics approval or securing hESC tissue sources, which would allow more in-depth investigations.

While early methodologies of reprogramming iPS cells resulted in low yields (Rodolfa and Eggan, 2006), improvement to the methodologies have been made over many years (Maherali et al., 2007, Okita et al., 2007, Wernig et al., 2007, Yamanaka, 2009, Okita et al., 2011). The main issue with iPS cells generated using these methods is that to produce high yields of the iPS cells; modifications need to be made to the cells such as gene silencing through siRNA, or plasmid

transfection; this renders the iPS cells unsuitable for therapeutic use due to the inclusion of the viral material. However, the improvement in the induction of iPS cells has proved challenging, with the replacement of viral factors by chemical ones, and finally integration of small molecules into the reprogramming phase, the unwanted extra genetic materials can be removed and still produce the desired iPS cells (Zhao et al., 2015, Ma et al., 2017). This advancement in iPS generation holds great promise for the integration of iPS cells into future clinical applications.

1.3.5 Adult stem cells

Adult stem cells are undifferentiated cell types found throughout the body, facilitating growth, repair, and maintenance of tissue and organs during the lifespan of an organism. Asymmetric-renewal attempts to maintain the stem cell population while generating cells required for maintenance and regeneration (Neumuller and Knoblich, 2009) (Figure 1-8).

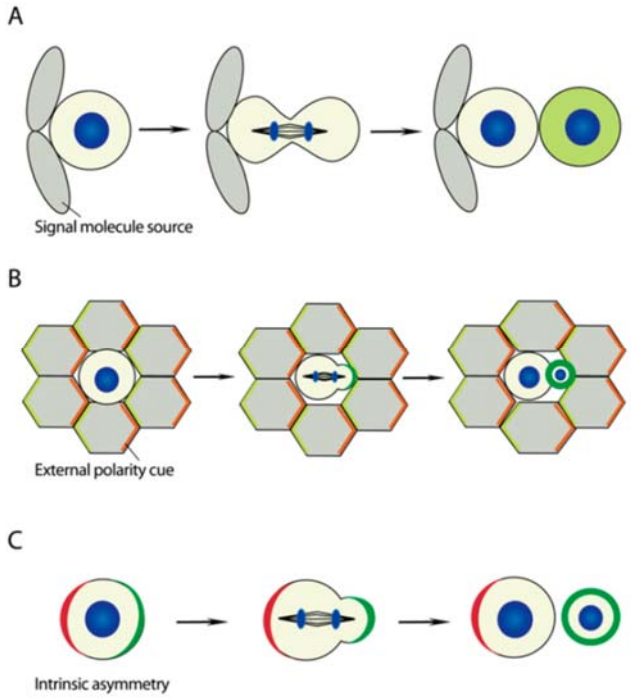

Figure 1-8 - Asymmetric cell division is dependent on cell niche and cues. (A) Niche signal contact retains stem-like activity, where cells without signal contact begin to differentiate. (B) The polarity of the surrounding tissue gives clues to asymmetric cell division and cell fate (green). (C)Cell polarity and protein polarity (red), determines cell fate (green) (DNA, blue). (from (Neumuller and Knoblich, 2009)

Adult stem cells can be found throughout the body in all germ layers (ectoderm, endoderm and mesoderm), forming rare populations within the tissues including: skin (Toma et al., 2001), liver (Herrera et al., 2006), bone marrow (Owen and Friedenstein, 1988), dental pulp (Laino et al., 2005, Laino et al., 2006), muscle (Collins et al., 2005), brain and central nervous system (Johansson et al., 1999), intestine (Barker, 2014), pancreas (Zulewski et al., 2001), and fat (Rodriguez et al., 2005). Despite asymmetric mitosis maintaining the stem cell populations, there is evidence that as a person ages, the number of stem cells decreases (D'Ippolito et al., 1999, Nishida et al., 1999). Reduced numbers of stem cells and reduced stem cell activity hinders maintenance and regeneration within older individuals (Carlson and Conboy, 2007). The cells responsible for the

maintenance and repair of the skeletal system are found within the bone marrow and are often referred to as mesenchymal stem cells (MSCs).

1.3.6 Mesenchymal stem cells

Friedenstein first postulated the existence of a population of adult stem cells responsible for bone formation separate from haematopoietic populations that resided within the bone marrow (Friedenstein et al., 1966). These cells were cultured in diffusion chambers and, when seeded at a critical density, produced bone. Further investigation showed these cells bound to tissue culture plastic and formed fibroblastic colonies. They were initially referred to as fibroblast colony-forming cells (FCFC) (Friedenstein et al., 1974), but are now commonly known by an older term, the colony forming unit – fibroblastic (CFU-F) (Figure 1-9 A) (Friedenstein et al., 1970). CFU-F cells are fibroblastic in morphology, with a nucleus in the centre of the cell with long cell spindles projecting from the centre (Figure 1-9). Upon further investigation, the cells responsible for forming the colonies were referred to as mesenchymal stem cells (MSCs) by Caplan (Caplan, 1991). MSCs were reported to be able to differentiate into mesodermal cells, such as osteoblasts (bone), chondrocytes (cartilage), myocytes (muscle) and adipocytes (fat) (Caplan, 1991). MSCs are not only responsible for the repair of damaged tissue, but also for the regeneration of new tissues as part of routine maintenance. MSC populations have been reported to be present in various organs and tissues such as foetal femur (Mirmalek-Sani et al., 2006), liver (Herrera et al., 2006), bone marrow (Campagnoli et al., 2001), lung (Hogan et al., 2014), spleen (in 't Anker et al., 2003) and synovium (Sakaguchi et al., 2005), giving a variety of sources for cell isolation, which allow for further study and therapeutic uses.

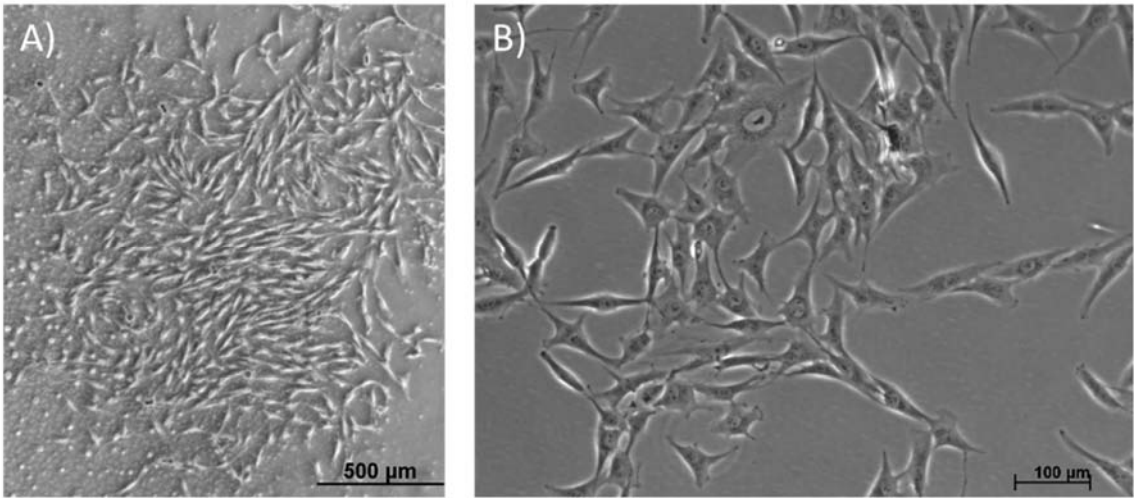

Figure 1-9 - CFU-F colonies and fibroblastic cell lines display the same morphology. Fibroblasts are mononuclear cells with multiple nucleoli, seen as a speckled pattern. The cytoplasm has long extrusions from the centre. Imaged cells are A) STRO-1 isolated BM cells (M72 patient) at 2.5x magnification and B) human osteosarcoma osteoblast cell line SAOS-2 at passage 4 at 10x magnification.

Despite the term MSC being applied to cell populations from many different tissues, each population has been shown to display differences in expression, differentiation, and intercellular signalling (Kern et al., 2006, Mensing et al., 2011, Robey, 2011, Alejandra Lopez-Verrilli et al., 2016). These differences between MSCs from different tissue sources highlight a need for the disaggregation of the term MSC. Therefore, to describe the postnatal cell population found in bone marrow, that is responsible for bone organ maintenance and repair, Paolo Bianco proposed a return to the developmentally restricted and precise term, skeletal stem cell (SSC) (Bianco and Robey, 2004). As opposed to the term MSC or the more specific bone marrow-derived–MSC (BM-MSC) (Caplan, 1991, Bianco and Robey, 2015). Unfortunately, the terms MSCs, BM-MSC and SSCs are used throughout literature to specify MSCs isolated from bone marrow materials, and MSC is a term often used for cells derived from throughout the body, the use varies group to group.

In the case of SSCs, identity, function and utility relate specifically to the various tissues and cell types that compose the bone organ, namely: bone, cartilage, adipocytes, fibroblasts, and stromal tissue (Dawson et al., 2014). Thus, the term SSC is used to refer specifically to the self-renewing stem cell of the bone marrow

stroma responsible for the regenerative capacity inherent to the bone. The heterogeneous population of cultured plastic adherent cells isolated from the bone marrow, which remain the most commonly used (if not acknowledged) population by researchers in the field of bone regeneration, will be referred to as bone marrow stromal cells (BMSCs). Thus, to avoid any confusion, in this thesis the term SSCs will be used to refer to non-haematopoietic cells isolated from the bone marrow that are capable of forming colonies with the capacity to differentiate across the three stromal lineages: bone, fat and cartilage.

1.3.7 Skeletal stem cells

The SSCs population was originally thought to be a self-renewing, multipotent stem cells, capable of tri-lineage differentiation (Pittenger et al., 1999, Kern et al., 2006): bone (osteoblasts) (Jaiswal et al., 1997, Kanczler and Oreffo, 2008, Kollmer et al., 2013, Graneli et al., 2014), cartilage (chondrocytes) (Xu et al., 2008, Serafini et al., 2014, Li et al., 2015) and fat (adipocytes) (Xu et al., 2007, Kollmer et al., 2013, Graneli et al., 2014). Each pathway has a set of specific markers and gene expression profile(s) that can be assessed to identify the differentiation pathways (Pittenger et al., 1999, Xu et al., 2008, Graneli et al., 2014) (Figure 1-10). However, recent work has shown that a heterogeneous stem-like cell population they named as the SSC population, isolated from bone marrow (from mice, foetal femurs and adult bone marrow) is multipotent but only capable of differentiation into osteogenic and chondrogenic cells; and also proliferates in response to skeletal damage (Chan et al., 2018). This presents evidence for a further division of the stem-cell populations within the bone marrow with the SSC (forming the cartilage and bone), HSC (forming the haematopoietic cells), and a population capable of differentiation into lipogenic cells.

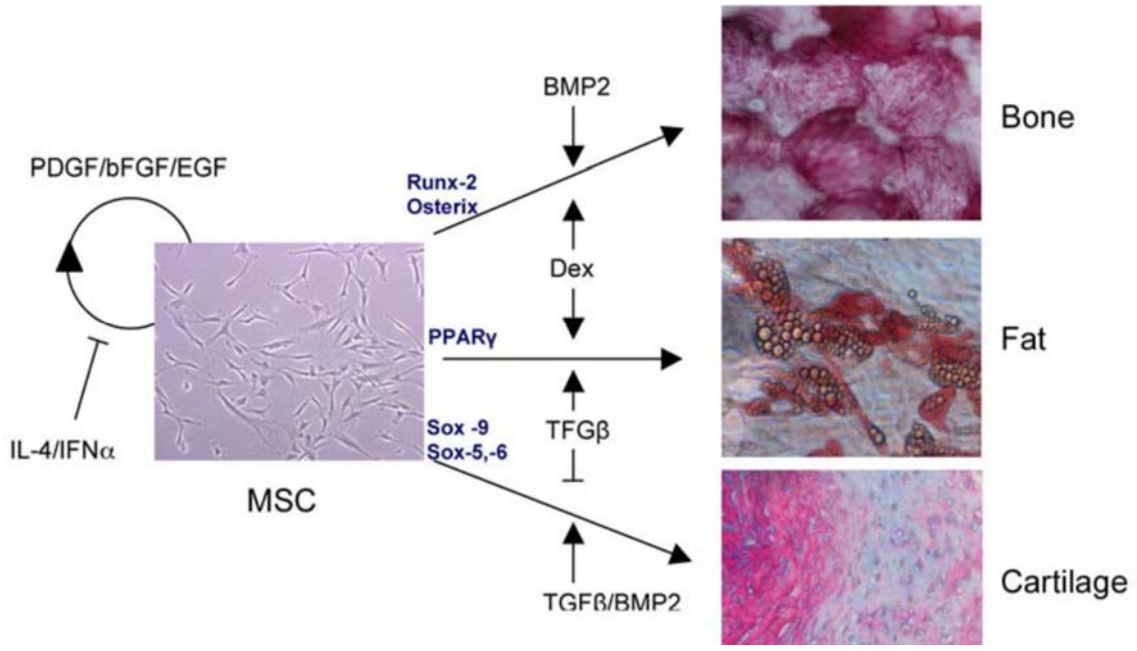

Figure 1-10 - Skeletal stem cell/Mesenchymal Stem Cell differentiation has specific markers for each lineage, and cues the cells take to differentiate down lineage pathways. Skeletal stem cells have tri-lineage differentiation potential and using specific cues in culture the pathway of differentiation can be determined to ensure specific outcomes. Image from (Oreffo et al., 2005)

Together, the three lineages constitute the bone marrow architecture in which haematopoiesis from the host animal can be established (Krampera et al., 2006). When cultured in non-adherent conditions, SSCs form spheroid structures known as ossicles, which are made up of the three bone marrow lineages (Friedenstein et al., 1966, Tavassoli and Crosby, 1968). The cells capable of forming ossicles were initially unidentified but were subsequently described as an adherent, non-haematopoietic cell population within the bone marrow (Owen and Friedenstein, 1988). Though SSCs were found to be non-haematopoietic, they are localised in a specific niche with close associations with haematopoietic stem cells (HSCs) within the venous sinusoids (Mendez-Ferrer et al., 2010, Sacchetti et al., 2007) and capillary beds (Travlos, 2006) within the bone marrow (Figure 1-11 A and B). The close association between the HSC and the SSCs within the capillary beds were found to have a regulatory relationship, which ensures the long-term self-

renewal of the HSCs and exclusivity within bone marrow (Taichman and Emerson, 1994, Taichman et al., 1996, Bianco et al., 2008, Bianco et al., 2013).

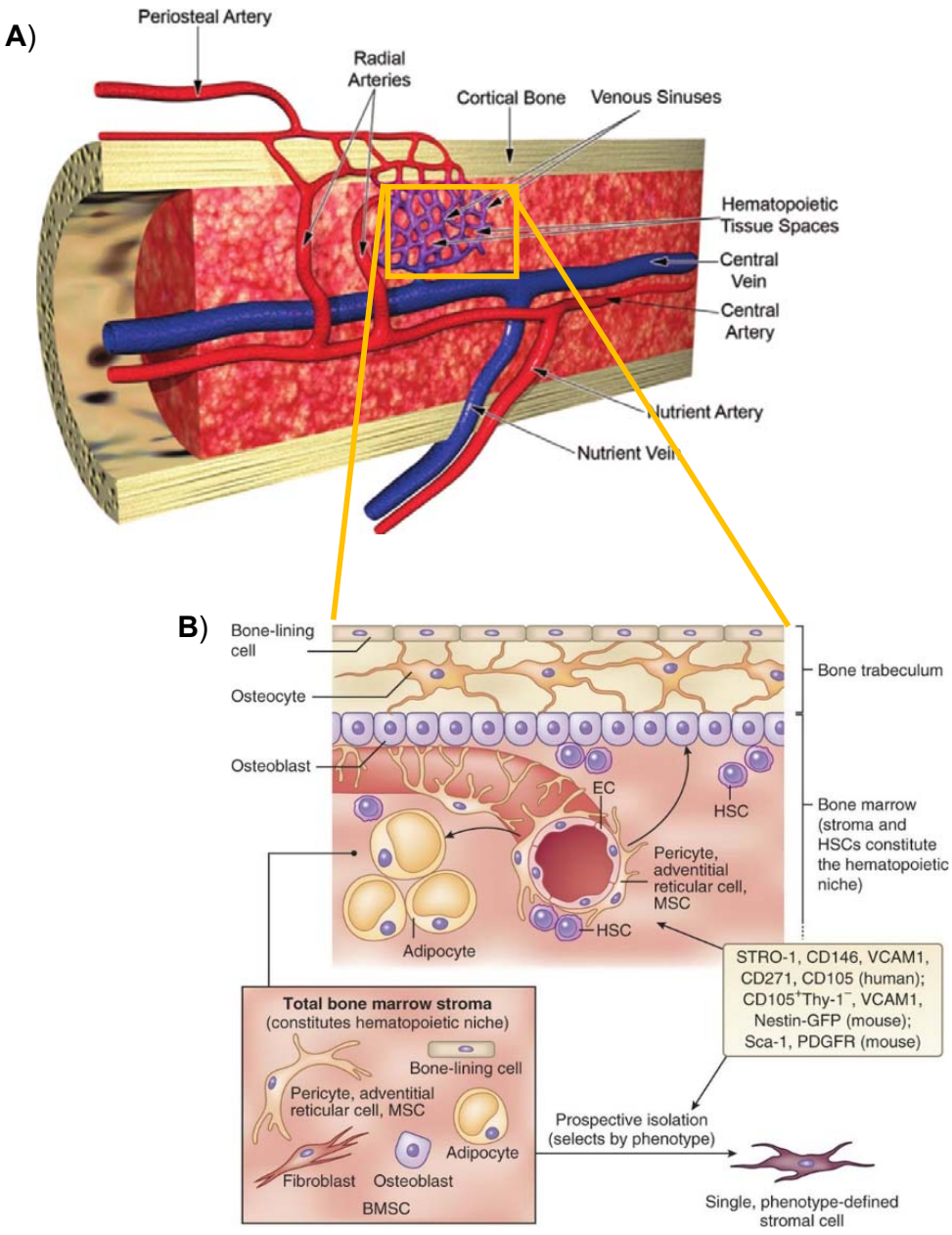

Figure 1-11 - Skeletal Stem Cell (SSC) populations are found within the venous sinuses, proximal to blood supplies. A) Vascular supply diagram of the bone organ highlighting the blood supply structure in bone. Image from (Travlos, 2006). B) A more detailed image of the venous sinuses, highlighting where the MSC/SSC population has been identified, as well as key markers and the cell populations found within the bone marrow. Image adapted from (Bianco et al., 2013).

Recent work has shown that the SSC is multipotent, but only osteo and chondrogenic differentiation, with expansion in response to skeletal damage (Chan et al., 2018). However, until further work is performed to confirm this work, it will be assumed the body of work already present on the SSC population is still relevant.

Despite the close proximity to the HSCs, blood vessel generation does not always take place after fractures. The lack of adequate blood supply to bone tissues is detrimental to repair and is a major contributing factor for non-union fractures (Keramaris et al., 2008). Treatment options for non-union fractures have been investigated, showing that the heterogeneous SSC population seeded onto a ceramic scaffold showed the same degree of repair as that from autograft, the current gold standard for treating non-union fractures. Furthermore, the SSC-seeded ceramic scaffold demonstrated improved integration of bone and vasculature when compared to the scaffold alone or to decellularised bone graft (Giannoni et al., 2008).

Low or inadequate blood supply can also lead to a decrease in pH (acidosis), oxygen (hypoxia), and can cause extracellular ATP to increase, leading to bone resorption, stunted bone repair and remodelling (Utting et al., 2006, Muzylak et al., 2007, Orriss et al., 2007). The fact that bone is resorbed in low pH and oxygen and in high extracellular ATP environments indicates that bone homeostasis requires specific environmental cues. Understanding this environment is critical for effectively directing the use of SSCs for beneficial therapeutics in the future. Understanding of the SSCs is therefore reliant on isolation of a pure SSC population in order to investigate the behaviour and expression profile of the cells.

1.3.8 SSCs applications

Bone marrow-derived non-haematopoietic stem cell-enriched populations have been described as having beneficial effects in the treatment of osteoarthritis

(Buda et al., 2015, Vega et al., 2015), bone and wound repair (Rodriguez-Menocal et al., 2015), immunomodulation (Le Blanc et al., 2008, Kebriaei et al., 2009, Karussis et al., 2010, Kuzmina et al., 2012) and liver cirrhosis (Kharaziha et al., 2009). While showing the beneficial effects of SSCs in therapeutic use, there are considerable variations in the methodologies used for cell isolation between studies, on top of the already heterogeneous enriched SSC populations – thus, isolation of a purer population methodology is urgently needed.

1.3.9 SSC isolation

Isolation of a homogenous population of SSCs is a crucial goal for skeletal regenerative medicine. Attempting to isolate SSCs from a heterogeneous population has proved to be a difficult task due to the rarity of these cells (estimated at 1 in 10,000-100,000) (Gronthos, 2003). Plastic adherence was the first method used to enrich SSCs and remains widely used (Friedenstein et al., 1974, Meirelles Lda and Nardi, 2003, Alhadlaq and Mao, 2003). This technique separated the quickly adherent population from the slower and non-adherent populations. The cells that adhered quickly grew into colonies, the colonies could then be counted to surmise how many stem-like cells were present from the seeded cells. This technique of purification evolved into a cell purity assay known as the CFU-F assay, an assay now performed by seeding and growing cells in tissue culture plate wells to assess stem-like cells.

The cells are then monitored over two weeks, after which the number of colonies formed is counted, which gives an estimate of colony-forming units from a known seeded cell number. Robey described 10-50 CFU-F per 100,000 nucleated bone marrow-derived cells (Robey, 2011). During the incubation time, other cells can also bind to the cell culture plastic, including hematopoietic progenitor cells, which continue to produce non-adherent cells (Gordon et al., 1995). Seeding bone marrow cells in a linear pattern produced a corresponding linear result of colonies, which suggests that a defined proportion of the bone marrow is the stem cell population: 1 CFU-F per 6240 ± 1350 cells (Baksh et al., 2003), giving similar figures of around 1 in 10,000 after depletion of the haematopoietic cells. These figures highlight that plastic adherence alone is not adequate for SSC isolation.

To further enrich the SSC population, various marker-based isolation approaches are being investigated using different cell markers in an attempt to identify the optimal population (Simmons and Torok-Storb, 1991, Pittenger et al., 1999, Bianco et al., 2001, Kuznetsov et al., 2001, Avital et al., 2001, Hung et al., 2002, Quirici et al., 2002, Chan et al., 2018). Several reviews on the matter have been published, showing both positive and negative surface markers for SSCs (Simmons and Torok-Storb, 1991, Quirici et al., 2002, Vogel et al., 2003, Alhadlaq and Mao, 2004, Sacchetti et al., 2007, Kolf et al., 2007, Boxall and Jones, 2012, Lin et al., 2013, Lv et al., 2014, Dawson et al., 2014, Samsonraj et al., 2015, Zhou et al., 2014).

Positive markers	Negative markers
HSC 70 (heat shock cognate 70) targeted by the STRO-1 antibody	CD11b (Integrin alpha M)
CD29 (Integrin beta-1)	CD14 (Myeloid Cell-Specific Leucine-Rich Glycoprotein)
CD44 (HCAM)	CD19 (B-Lymphocyte Surface Antigen B4)
CD73 (ecto-5'-nucleotidase)	CD34
CD90 (Thy-1)	CD45 (Protein tyrosine phosphatase, receptor)
CD105 (Endoglin)	CD79a (B-cell antigen receptor complex-associated protein alpha chain)
CD106 (VCAM-1)	HLA-DR (Human Leukocyte Antigen – DR isotype)
CD146 (MCAM)	
CD166 (ALCAM)	
CD271 (Low-affinity nerve growth factor receptor)	

Table 1-2 - Table of markers used to enrich for the SSC population. Several markers have been used over the many years of research into the bone marrow stem cell. The above table provides a list of a number of markers that have been used in both positive and negative enrichment methods. (Simmons and Torok-Storb, 1991, Quirici et al., 2002, Vogel et al., 2003, Alhadlaq and Mao, 2004, Sacchetti et al., 2007, Kolf et al., 2007, Boxall and Jones, 2012, Lin et al., 2013, Lv et al., 2014, Dawson et al., 2014, Samsonraj et al., 2015, Zhou et al., 2014).

Markers that are known to be associated with the SSC population are STRO-1, CD29, CD44, CD73, CD90, CD105, CD106, CD146, CD166, and CD271. Examples of negative markers include CD11b, CD14, CD19, CD34, CD45, CD79a, and HLA-DR. With a promising selection of markers used in conjunction to isolate a highly stem-like heterogeneous population (PDPN+ CD146- CD73+

CD164+) (Chan et al., 2018). These PDPN+ CD146- CD73+ CD164+ cells differentiate into osteogenic and chondrogenic lineages, forms bone and cartilage tissues *in vivo* when transplanted serially, presenting a highly interesting population to work with when investigating the SSC population.

To utilise these established markers immunolabelling is performed, using specific antibodies raised against molecular targets on the surface of cells. Antibodies are generated by animal immune systems. Lymphocyte progenitors generate many different lymphocytes which have unique receptors on their surface. When these receptors bind to an antigen and are identified as foreign, the lymphocyte differentiates into a lymphoblast and generates clones to ensure a large population of cells with the antigen-specific receptor present to eliminate the foreign antigen. Activated Bursa lymphocytes (B lymphocytes), named for their organ of discovery (Cooper, 2015), proliferate and generate large numbers of plasma cells which then produce antigen-specific antibodies which are released into the body. The antibodies highlight the foreign antigen to phagocytes for subsequent destruction and removal. The antibodies bind to the targets via the variable region which is unique to the lymphocyte through DNA rearrangement and splicing of the heavy and light chain variable region genes, which determine the antibody specificity. The remaining structure of the antibody is the constant region which has little variation and signals to the immune system the fate of the bound antigen (Litman et al., 1993). When generating antibodies for scientific purposes, the desired antigen is injected into a host animal. Once the immune system has had time to respond to the foreign antigen, the antibodies can then be purified from the serum of the hosts for use in various applications, including lab-based tests, assays, cell isolations and purifications.

Magnetic-activated cell sorting (MACS) and fluorescence-activated cell sorting (FACS) are standard techniques that utilise antibodies to facilitate cell separation based on surface marker expressions.

1.3.9.1 MACS sorting

MACS sorting is a technique that uses antibodies attached to magnetic particles to sort cells based on antigen presentation, using magnets to separate cells as they pass through a column allowing for a negative and positive fraction (Miltenyi

et al., 1990). MACS allows for subpopulations to be separated from heterogeneous cell sources with little damage to the cells, allowing for the isolated cells to be cultured, grown and further tested after the isolation. Both positive and negative selections can be performed using MACS, as two fractions of cells are isolated as shown in Figure 1-12.

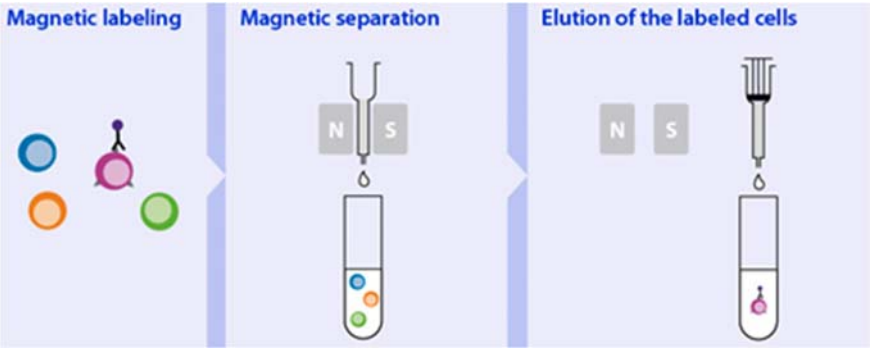

Figure 1-12 - Magnetically-labelled cells can be separated from non-labelled cells using MACS facilitating cell population separation. Application of a magnetic field inhibits magnetically tagged cells, while unlabelled cells pass through the column unimpeded. Marker tagged magnetic particles bound to cells within the column are impeded, preventing extraction of these cells while the magnetic field is present. Once the field is removed, tagged cells can be eluted. (From https://www.elveflow.com/microfluidic-tutorials/microfluidic-reviews-and-tutorials/magnetic-particle-separation-a-short-review) (Accessed 09-09-18)

The primary restriction of MACS is the limited number of markers to be used in conjunction, typically limited by a single negative selection and a single positive selection. Multiple positive or subsequent positive or negative fractionation is practically impossible using MACS, as previous antibodies and magnetic particles would skew subsequent separations. Therefore, to sort the cell populations using more markers, FACS should be used.

1.3.9.2 FACS sorting

FACS is a technique which uses fluorescently tagged antibodies to measure the amount of relevant markers on the surface of the cell via laser excitation and emission, as well as light scattering, to separate the cells into subpopulations (Bonner, 1972) (Figure 1-13).

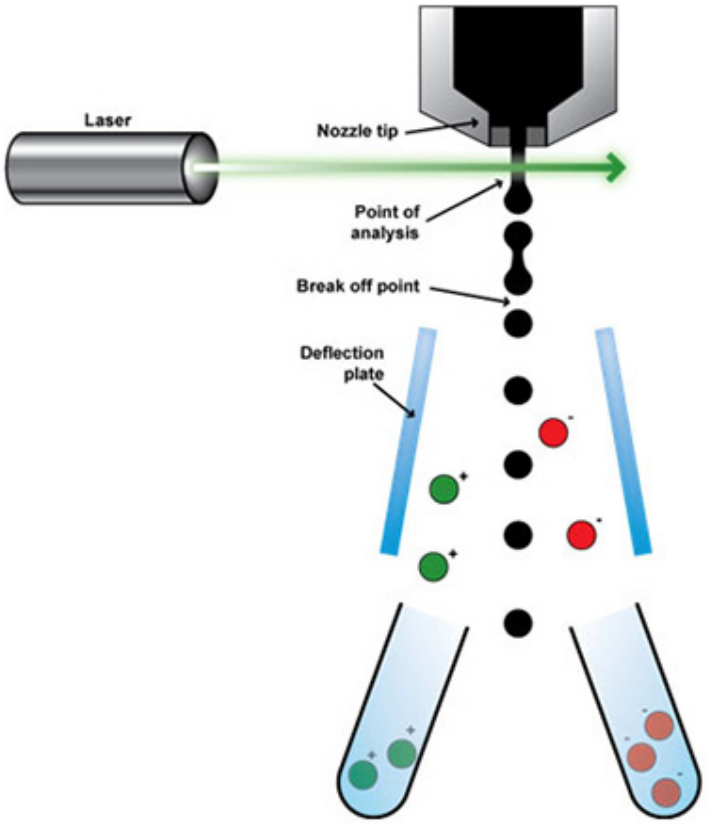

Figure 1-13 - Fluorescently-activated cell sorting. Cells are focused into a single stream and passed in front of a laser, where fluorescence, forward scatter and side scatter are registered by photodetectors. Using the information from the photodetectors, the stream is deflected, or not separating cells, based on optical properties. Image from http://www.abcam.com/protocols/fluorescence-activated-cell-sorting-of-live-cells (Accessed 09-09-18)

Utilising the optical properties of the cell ascertained through the FACS process, specific parameters can be measured. The forward scattering (FSc) measures the size of the cells, where the side scattering (SSc) measures the granularity, or complexity of the internal organelles. The fluorescence is the measure of the amount of marker present on the cell. Using a combination of FSc, SSc and fluorescence, cell populations can be broken down into groups which are then separated using deflection from the charge plates. Advances in FACS technology have enabled faster sorting of more populations of cells; by utilising the optical properties of the cells, and setting gates or thresholds on the measured values, multiple populations can be sorted simultaneously.

Using FACS as a potential solution for SSC isolation, Gronthos investigated a number of markers, as well as a number of different intensities of the fluorescence, detected from the markers, as opposed to the standard positively- versus negatively-expressing status (Gronthos, 2003). In his investigations, he found that the STRO-1 antigen provided enrichment for the SSC population, but an even greater enrichment was seen when sorting for the cells, with the highest 10% of STRO-1 expression referred to as STRO-1^{BRIGHT}.

1.3.9.3 Label-free sorting

While markers specific to cell populations do provide a useful method for isolation, not all cell separation methods require labelling. Both microfluidics and di-electrophoretic separation, for example, have shown promising results in separating cell populations and could potentially be used to isolate SSCs utilising the cell population's structural and chemical properties (Ismail et al., 2015, Xavier et al., 2017b, Xavier et al., 2017a).

Microfluidics is a field with an increasing number of strategies for label-free cell separation (Autebert et al., 2012, Jackson and Lu, 2013, Shields et al., 2015, Xavier et al., 2017b). Microfluidics mainly concentrates on the structural properties, using size filtration mechanisms (Ji et al., 2008), hydrodynamic filtration (Yamada et al., 2007), and hydrophoretic filtration (Choi et al., 2007), or

a combination of size, deformability and stiffness (Inglis et al., 2006, Mohamed et al., 2007, McFaul et al., 2012, Xavier et al., 2017a) (Wang et al., 2000).

Di-electrophoretic separation, or di-electrophoresis (DEP), has been shown to separate a number of cell types, including the removal of human breast cancer cells from normal T-lymphocytes (Wang et al., 2000), CD34+ HSCs from bone marrow (Wang et al., 2000), major leukocyte subpopulations from blood (Wang et al., 2000), the enrichment of leukocytes from blood (Yang et al., 1999a), and the separation of cancer cells from erythrocytes (Yang et al., 1999b). The separations rely on characterising and exploiting the cells' dielectric properties by adjusting a non-uniform electric field within a separation chamber. Cell movements vary by electrical field and population. This property allows conditions to be identified to help separate populations (Hughes, 2002).

1.3.9.4 SSC isolation limitations

Despite the potential of the MACS, FACS, and label-free techniques, they are limited as they rely upon the characterisation of the rare SSC population in order to isolate the cells effectively. With some surface markers identified as capable of enriching for the SSC population (Gronthos, 2003, Lin et al., 2013, Lv et al., 2014), and evidence to demonstrate SSC population size and stiffness differing from the other bone marrow tissues (Lo Surdo and Bauer, 2012, Xavier et al., 2017a) methods have been developed for SSC enrichment. However, no method has currently been identified for pure SSC isolation.

Within MACS and FACS, purity of isolation is heavily dependent on the discriminative power of markers used to identify these subsets of bone marrow cells. A comprehensive meta-analysis of markers and their efficiency at isolating tri-potent cells with colony-forming capabilities (Lv et al., 2014). They looked at various sources of MSCs, including bone marrow (SSCs): the analysis showed variation in expression and differentiation pathways, determined by the tissue origins of MSC isolation. However, of all the markers suggested, CD146 was found to be the most appropriate "stemness" marker due to its presence in all populations of MSC. Several different methods and separations have been used to assess the CFU-F capabilities of cell populations. Jarocha's use of nerve growth factor receptor (NGFR+) cells gave 1584 colonies per 1,000,000 cells

(Jarocha et al., 2008). Gronthos used the STRO-1 antibody as the cell marker, and plastic adherence was shown to be 10 CFU-F per 100,000 cells. MACS separated STRO-1 positive cells provided 50 CFU-F per 100,000 cells; STRO-1^{BRIGHT}, in contrast, gave 8,930 CFU-F per 100,000 cells, a 100-fold increase over STRO-1 alone (Gronthos, 2003). STRO-1^{BRIGHT} is the brightest 5-10% of the STRO-1+ population, as assessed by FACS separation. These values show that while antibody separations do indeed increase the yield of CFU-F capable cells, the populations generated vary depending on the marker used and remain heterogeneous; meanwhile, the standard antibody separations give around the same number of colonies as the plastic adherence method. Thus, until a methodology is developed that yields a high purity of the cell population isolated, antibody separations are only advantageous in terms of the speed of isolation.

As with labelled separation, no pure population has yet been identified using unlabelled separation, despite breakthroughs in the partial characterisation of the SSC population (Lo Surdo and Bauer, 2012, Xavier et al., 2017a). In the absence of a proven technological approach, a range of methodologies continue to be pursued in the field of SSC enrichment, all with the aim of providing the first method for homogenous SSC isolation.

Through a combination of positive and negative markers, a more refined population of SSCs may be isolated from the bone marrow. It should be noted that, to date, the most enriched populations isolated and measured by CFU-F assays are still relatively heterogeneous, with colony-forming cells making up around 1 in 10,000 cells (Alhadlaq and Mao, 2004, Sacchetti et al., 2007, Bianco and Robey, 2015). To date, no standardised process has been established as able to provide a homogenous SSC population. The establishing of new markers for the SSC population is an alternative route that may enable either higher enrichment yields or pure isolation. One potential technology that has been proven for biomarker discovery is aptamers.

1.4 Aptamers

1.4.1 Aptamer history and use

Aptamer selection processes were first described almost simultaneously by three laboratories (Tuerk and Gold, 1990, Ellington and Szostak, 1990, Robertson and Joyce, 1990). Two labs showed that RNA molecules could be used as specific, high-affinity ligands to non-nucleic acid target molecules; the third group showed that RNA could be selected to have DNA-cleaving 'enzymatic' activity. Aptamers are nucleic acid (or peptide) based ligands which bind to a specific target due to their unique three-dimensional structure, which is in turn derived from the base sequence (or amino acid sequence in the case of peptides) and secondary structure components (Laing and Schlick, 2011). Aptamers function similarly to antibodies, in that the diverse conformations derived from their unique sequences allow them to fold into complex shapes and bind to a target. The first targets of aptamers were proteins and small molecules; which allowed a wide range of potential uses (Tuerk and Gold, 1990, Ellington and Szostak, 1990). In 1992, single-stranded DNA (ssDNA) was also shown to have similar utility (Ellington and Szostak, 1992).

Following the initial discovery and publication of aptamer technology, approaches have been developed to use the nucleic acid affinity ligands in place of antibodies in common laboratory applications such as ELISAs (Toh et al., 2015); biosensors (Li et al., 2007, Tang et al., 2007, Cheng et al., 2009, Wang et al., 2011, Bruno et al., 2012, Wu et al., 2012, Su et al., 2012, Smuc et al., 2013); immunoprecipitation (Song et al., 2014, Kim et al., 2014); cell population isolation (Guo et al., 2006, Schafer et al., 2007, Sheng et al., 2012, Wan et al., 2012); delivery vehicles (Zhou et al., 2011, Subramanian et al., 2012, Thiel et al., 2012, Zhu et al., 2014); molecular inhibitors (Nimjee et al., 2005, Lee et al., 2005, Adamis et al., 2006, Iida et al., 2014); and fluorescent imaging (Huang et al., 2005, Fang and Tan, 2010, Jin et al., 2015, Guet et al., 2015, Merkle et al., 2016). In most cases, adapting techniques which already use antibodies typically involves a simple substitution of the antibodies. Aptamers are particularly effective at adapting to these methodologies due to the extensive binding capabilities enabled by their structure.

1.4.2 Aptamer binding

Interactions between aptamers and targets are driven by non-covalent bonds: hydrogen bonds (Espinosa et al., 1998), stacking interactions (Hunter and Sanders, 1990), and Van der Waals forces (Klimes and Michaelides, 2012).

Hydrogen bonds can be the strongest non-covalent bond; a hydrogen atom acts as an intermediary between two molecules, providing a high energy non-covalent bond. As aptamers are single-stranded nucleic acids, and not all bases are used in intramolecular interactions to generate structures, this leaves many potential hydrogen bonding sites (in the non-paired bases) available for intermolecular interaction.

Van der Waals forces are charge-dependent non-covalent bonds, formed from the interaction of molecular dipoles. Dipoles are permanent or induced localised magnetic-pole-like charges on a molecule. These forces are weak, as the charges are only partially positive or partially negative due to sharing of electrons across the atoms. The strength of Van Der Waals bonds is dependent on the molecules involved. Unlike hydrogen bonds, Van Der Waals are not directional, and they have the same bond strength in all directions, whereas hydrogen bonds are rarely observed at angles greater than 90° (Steiner and Desiraju, 1998). These bonding methods further strengthen aptamers' intrinsic binding properties. Combined with the structural complexity of aptamers, these methods make aptamers capable of both high affinity and specificity.

Stacking interactions (π – π interactions) are non-covalent bonds between aromatic rings. In this case, between the nucleic acid bases, and generally providing the second highest bond strengths. The aromatic rings provide charged surfaces (Figure 1-14 A), providing opportunities for other charged molecules to be either repelled by similar or attracted through opposite, charges. Orientation and positioning of the aromatic rings provide opportunities for molecules containing aromatic rings to be non-covalently bonded (Figure 1-14 B and C).

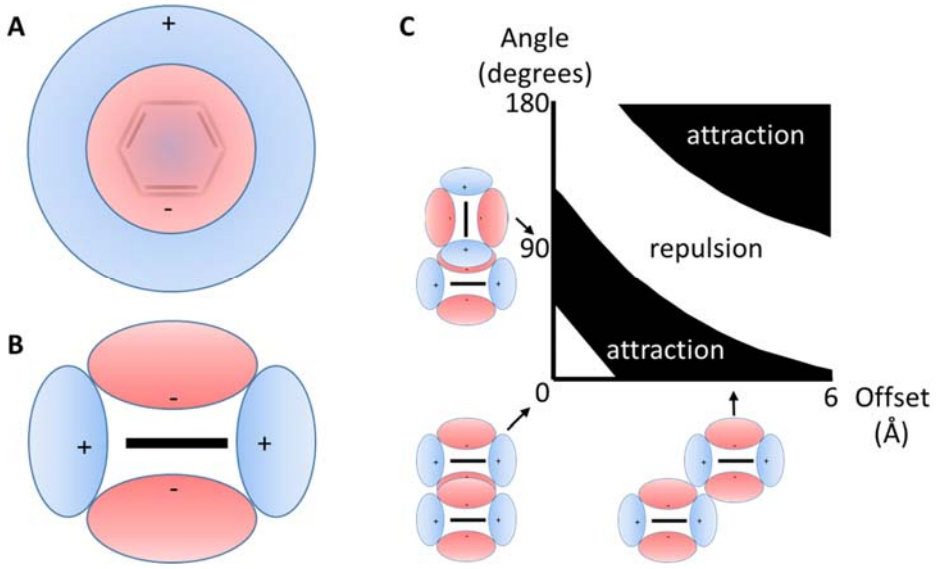

Figure 1-14 - Electrostatic interactions between the aromatic rings generate either attractive or repulsive forces between two molecules. Stacking interactions between aromatic rings are dependent on charge and orientation of the rings. A) Aromatic ring faces possess a negative charge where the edges have a positive charge, better demonstrated from the side view (B). C) Aromatic rings are regions and orientations which facilitate either attraction or repulsion. When placed at 90 ° from one another, or slightly displaced, the aromatic rings become more attracted to each other through the same electrostatic interactions. Adapted and redrawn from (Hunter and Sanders, 1990).

The bond strength depends on the aromatic rings involved, the direction of the bonds, and the orientation of the rings. Identical chemical rings provide the highest bond energy, with a slight displacement between the rings providing optimal attraction, and allowing Van der Waal bonds to contribute additionally (Hunter and Sanders, 1990). Stacking interactions are present in both proteins and nucleic acids. As the nucleic acid bases contain one or two aromatic rings (Figure 1-15), they are capable of forming stacking interactions with one another in their respective strands (forming the helical structure as the highest bond strengths from stacking interactions are formed when the aromatic rings are slightly displaced (Figure 1-14)).

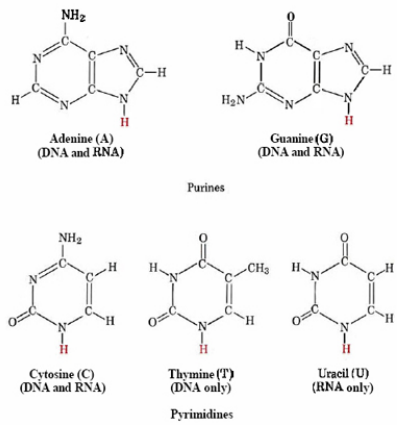

Figure 1-15 - Nucleic acid structures have aromatic rings, which allow for stacking interactions. Purines consist of two aromatic rings, where pyrimidines have a single aromatic ring. These aromatic rings interact to form inter-strand hydrogen bonds but also form stacking interactions with their neighbouring bases in the nucleic acid strand. Similar interactions may be formed with protein-based aromatic rings e.g. those in amino acids such as tryptophan. From https://chem.libretexts.org/Textbook_Maps/General_Chemistry/Book%3A_ChemPRIME_(Moore_et_al.)/20Molecules_in_Living_Systems/20.17%3A_Nucleic_Acid_Structure (accessed 09-09-18)

Stacking interactions, although relatively weak, can comprise up to 40% of interactions between nucleic acids and proteins (Wilson et al., 2014). They therefore contribute to the aptamer-protein non-covalent bonds formed, which provides the affinity and specificity to the target.

Many small molecules also have aromatic rings within their structure; allowing this type of interaction to contribute to small molecule aptamer interactions and selection. Salt concentration, temperature and pH are also critical for aptamer folding and therefore functionality. With the conditions for final use in mind, the appropriate buffer conditions should be maintained throughout selection processes. Once the binding conditions have been decided, the next step is to decide on the library architecture of the aptamer needed to perform a selection.

1.4.3 Aptamer library architecture

The aptamer library architecture can be a very simple; two fixed primer sequences at either end of the aptamer template allow amplification by polymerase chain reaction (PCR). These primers flank a region of random nucleotides (Figure 1-16 A). The random region sequence provides variety in the primary, secondary, and tertiary structures; and is responsible for the unique structures and hence binding properties to each aptamer (Figure 1-16 B and C) (Laing and Schlick, 2011). Figure 1-16 B shows examples of the various structures that nucleic acids can accommodate, including intramolecular base-pairing, nucleotide bulges, hairpin loops, mismatched pairs, internal loops, and stem junctions. These features provide the aptamers with varied secondary and tertiary structures which interact and allow the aptamers to form a complex network of interactions. Many of these individual motifs can be found within a single aptamer, to generate more complex secondary structures (Figure 1-16 C and D). These secondary structures also determine the tertiary or three-dimensional (3D) structure and, along with the natural helical structure of double stranded nucleotides, provide very complex structures (Figure 1-16 E).

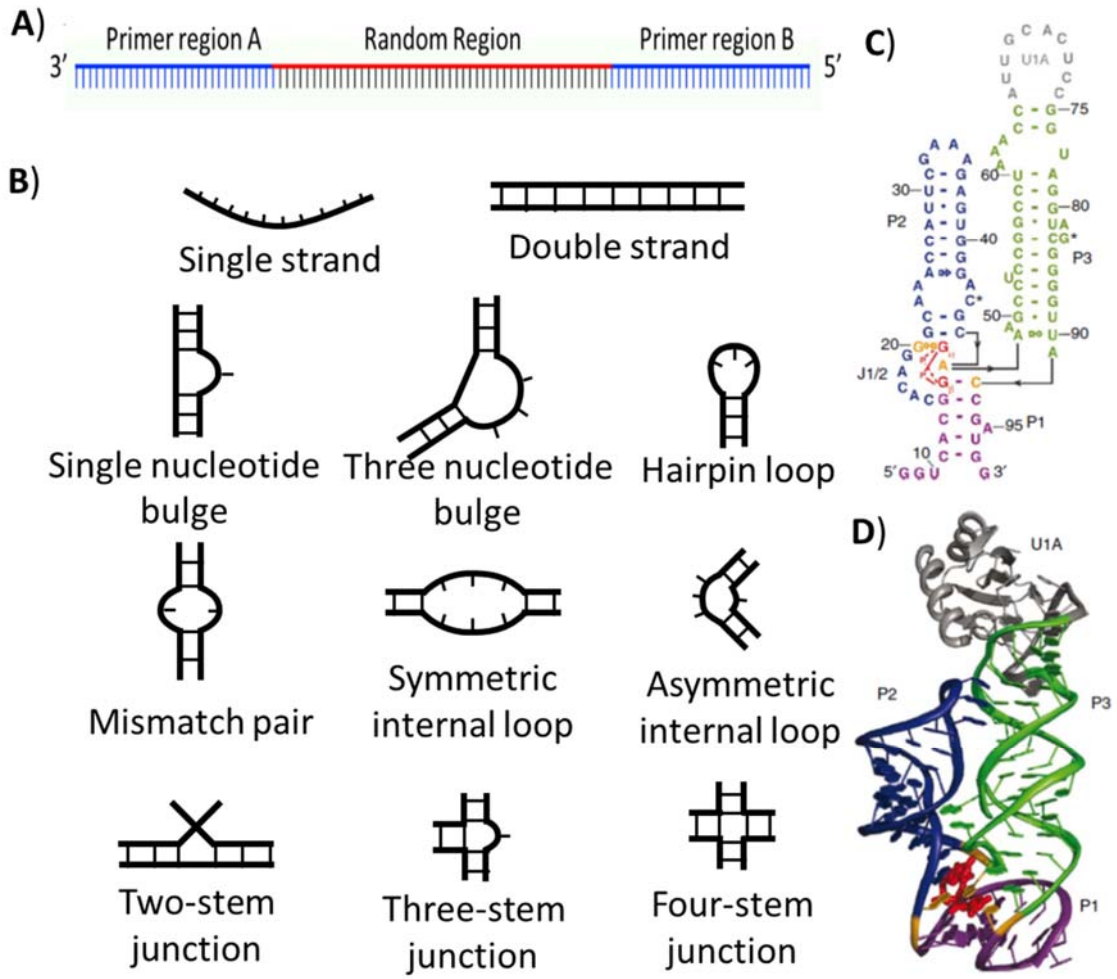

Figure 1-16 - Aptamer functionality is derived from primary, secondary and tertiary structures. – A) Aptamers are single stranded nucleic acids with fixed primer regions (blue) flanking a central randomised region (red). The single stranded nature of aptamers leaves the bases available to form intramolecular interactions to generate secondary and tertiary structures .B) Nucleic acids have several secondary structural motifs that can be formed by single strands, image adapted and redrawn from (Nowakowski and Tinoco, 1997). C) Primary structure of a c-di-GMP binding aptamer, with domains highlighted. D) Tertiary structure of the c-di-GMP binding aptamer primary structure from C, with domains highlighted, demonstrates the high structural complexity of a 98 base long molecule of 32.34 kDa aptamer. Image from (Smith et al., 2009).

Much like proteins, small changes in the primary sequence may not significantly alter the predicted 3D structure but they can alter the binding properties of the

aptamer (Huang, 2003, Katilius et al., 2007). Therefore, a combination of the nucleotides within the structure, as well as the structure itself; provide the necessary elements to allow non-covalent bonding of aptamers to their targets. The structural elements allow for intricate binding motifs and pockets for unique shapes and binding characteristics but known structures can also be included within an aptamer library to facilitate specific tasks desired at the end of an aptamer selection. For example, a library may be designed to have a propensity to form a stem-loop structure if the target protein is known to bind to stem-loops.

1.4.4 Aptamer design

The length of the aptamer random region is one of the first considerations in the design of an aptamer library. The random region provides the structural diversities that are required to generate high affinity and specificity aptamers. Longer aptamers have more material to generate more complex structures (Sabeti et al., 1997). In contrast, shorter aptamers allow for greater coverage of all possible sequences and therefore structural motifs within a practicable setup (Silverman, 2009). The most common random region lengths range from 40 to 70 bases (Sharma et al., 2017). To estimate the maximum possible primary structure variability, a 40 bp random region was used as an example. Calculating the number of available sequences can be performed by taking the 4 common nucleic acid bases (A, C, G, and T) to the power of the number of bases within the random section (40 bases). This gives 4^{40} or 1.20893×10^{24} as the number of potential molecules. To generate a mole equivalent, the number of possible sequences is divided by Avogadro's number (6.022×10^{23}) giving 2.007469376 moles. Once moles have been calculated, it can be converted to grams by multiplying the aptamer molecular weight (81 bases x average molecular weight of a base being 330 Da = 26730 Da) by the number of moles to give a mass of 53659.63 g, or 53.66 kg. Therefore, to use 440 unique sequences 53.66 kg of nucleic acid would be required. This is far more than what is practicable, a mass which increases exponentially with random region length. For this reason, aptamer selections are usually performed with 1×10^{14} – 1×10^{15} molecules for practicality, while still providing a huge potential in structural variance in the

aptamer pool (Guo et al., 2006). This is due to the structural motifs that generate the 3D structure of the aptamers, which are much smaller than the typical 40 base random region (Nowakowski and Tinoco, 1997). Much of the aptamer can be removed at the end of the selection, as only a small proportion of it is required for the purpose for which it was selected (Ellington and Szostak, 1990, Huizenga and Szostak, 1995). However, even with $1x10^{15}$ molecules, further functionality and features can be incorporated to improve the final performance of the aptamer or add specific structures. Known aptamer functions are facilitated by adding specific sequences (discussed below), while others are chemical modifications. Sugar modifications such as 2' fluoro, 2' amino, and 2'-O-methyl modifications can improve serum half-life of aptamers by removing key functional groups required for enzymatic degradation (Ni et al., 2017)

. Locked nucleic acids are nucleic acids with a methylene linkage between the 2' oxygen and 4' carbon, providing resistance to nuclease activity, as well as increased thermal stability if the aptamer is to be used in high temperature environments (Campbell and Wengel, 2011). Modification to the phosphodiester backbone linkages to a methylphosphonate or phosphothioate analog removes the negative charge associated with aptamers (Sacca et al., 2005), allowing for interactions to be made in buffers which do not mask charges (discussed at 1.4.6).

The Spinach aptamer (Kellenberger and Hammond, 2015, Paige et al., 2011) exploits pre-selection sequences to add levels of complexity to the aptamer (Pothoulakis et al., 2014). The Spinach aptamer library is designed to contain a specific dye binding sequence, which binds a dye which exclusively fluoresces only when bound. The binding site for the spinach dye is only stable when the aptamer is bound to a target (Kellenberger and Hammond, 2015), effectively incorporating a reporter system which indicates when the aptamer is bound (Paige et al., 2011, Pothoulakis et al., 2014, Guet et al., 2015). Other modifications include incorporating sequences that bind siRNA, which can be exploited to targeted cell populations (Zhou et al., 2011, Thiel et al., 2012), and binding sequences to allow immobilisation of the aptamers onto beads, and unbind once bound to a target (Stoltenburg et al., 2012, Reinemann et al., 2016), facilitating aptamer selection against targets which cannot be immobilised.

In addition to binding to targets, nucleic acids can also have enzyme-like activities. An example of nucleic acid with enzymatic activity is the ribosome. The ribosome is a necessary organelle for protein synthesis, facilitating the translation from mRNA to protein. The main structure of a ribosome is a nucleic acid (rRNA) which forms a structure with enzymatic activity; building protein structures from mRNA templates. The surrounding proteins provide only structural support for the rRNA complex (Nissen et al., 2000). Other nucleic acid enzymatic activities include cis or trans-cleaving activities seen in 'ribozymes' (Rossi, 2007, Kobori et al., 2015). Here the cleaving activity is used to release fluorophore quenchers from an aptamer structure when the target is present (Kobori et al., 2015). Another activity possible to add to aptamers is a hydrogen peroxidase-like activity. The activity requires the aptamer to be bound to a target to stabilise the region responsible for the enzyme-like activity, providing a colourimetric assay reporter system (Liu et al., 2014). The folding of an aptamer's random region, and intramolecular interactions generating the structures, are only possible when the nucleic acid is single stranded; therefore, steps need to be taken to produce single stranded nucleic acids for aptamer selection.

1.4.5 Single strand generation

RNA aptamers are generally produced through enzymatic approaches which readily yield ssRNA; such as *in vitro* transcription. However, with DNA aptamers (amplified through PCR), additional steps are needed during aptamer selection protocols, to generate ssDNA after amplification. DNA aptamers require removal of the 'template strand' (leaving only the aptamer strand), to allow for intramolecular folding and bonding to restore the structure and function of the 'aptamer strand'. One of the first methods for DNA aptamer selection involved the use of radio labelled primers during the PCR reaction. The amplified dsDNA was then denatured and separated on a denaturing polyacrylamide gel. The radioactively labelled strands were then isolated and eluted (Ellington and Szostak, 1992). Techniques have evolved away from radioactively labelled compounds to safer alternatives. There are three main methods used to generate ssDNA for aptamer selection: the first method is Asymmetric PCR, where the

reverse primer is either not added, or is severely limited. Depletion of the limiting primer leads to an amplification of only one strand; resulting in non-exponential amplification of the 'aptamer strand' (Huizenga and Szostak, 1995), creating a population where the majority of molecules are single stranded (Svobodova et al., 2012). The second method for ssDNA generation involves the use of Lambda Exonuclease. This enzyme has increased activity for phosphorylated strands of dsDNA. Modifying the reverse primer with PO_4 group facilitates the digestion of the 'template strand' (Marimuthu et al., 2012), leaving only the 'aptamer strand'. The third method incorporates a biotinylated reverse primer and uses streptavidin-coated magnetic beads to bind the amplified dsDNA. The two strands are separated and the bead bound template strand is removed (Weber et al., 1989, Espelund et al., 1990, Blank et al., 2001, Rouah-Martin et al., 2012, Zhang et al., 2015). In Chapter 2, the method of aptamer production is a combination of the Asymmetric PCR and Lambda Exonuclease (2.2.11 and 2.2.13 respectively): this allowed generation of many of the forward strands of the DNA through PCR, and the Lambda Exonuclease digestion to remove the few PO_4 modified reverse strands to leave only the forward ssDNA. The uniformity of the material present allows for accurate quantification using the Nanodrop, and therefore accurate quantities of nucleic acids used. As discussed in Section 1.4.2, salt and pH are extremely important in the aptamer functionality and ability to approach target molecules. To this end, the buffer in which the selection is performed also needs to be considered carefully.

1.4.6 Aptamer buffer selection

The medium / matrix in which the aptamers are selected will contribute to the aptamers' overall effectiveness. Slight changes in the ionic strength, ion composition, concentration, and pH within the aptamer environment can alter the aptamer structure and local charge, and hence aptamer performance (Buchanan et al., 2003, Stovall, 2004). Ions within the binding buffers act to shield/mask charged groups on the proteins and the nucleic acids. With the charges shielded from other molecules, similarly charged molecules could interact (Tsumoto et al., 2007). For example, high concentrations of positively charged ions may interact

with a negatively charged region on a protein; masking the region and reducing repulsion of other negatively charged molecules. Changes in ion concentration and composition can change the relationship between the molecules, and even prevent interactions (Stahlberg et al., 1991). The pH of a buffer acts in two ways on proteins; the first is the state of protonation across the protein, and the second is the conformation of the protein. Protonation or deprotonation states of proteins vary with pH: the higher the pH, the more negatively charged the protein. The protonation state affects the charge of the amino acids, carboxyl, and amino-terminal groups on the surface of the protein. These changes in protonation state (and therefore charge), can result in prevention of intermolecular interactions. Areas where charges previously facilitated bond formation may no longer bind or may actively repel the other molecule when the pH is changed (Dumetz et al., 2008). In an aptamer selection, this could either prevent aptamers from binding to the target or enhance binding beyond normal parameters and lead to non-specific binding. Conformational changes can also arise because of pH variance, altering intramolecular interactions to a point where the protein's native structure is compromised, and the protein structure begins to unfold (O'Brien et al., 2012, Di Russo et al., 2012). These conformational changes could, in theory, prevent aptamer binding, due to loss of an essential epitope.

Consideration of these factors and of the final environment for aptamer use is, therefore, essential for optimal function. For target molecules which are typically negatively charged, aptamer selection can be particularly difficult, as the aptamer molecules are also net negatively charged. However, lowering the pH of the selection buffer to the isoelectric point of the target would neutralise the net charge on the target and allow the aptamer to approach and bind. Caution must be taken though, as this may also lead to protein misfolding or even aggregation. Keeping the target and end application in mind can also influence buffer selection. For example, with a live cell selection target; using a buffer that would facilitate aptamer-target binding is pointless if the choice of buffer (or salts) is lethal to cells. With consideration of the elements (buffers, design, salt conditions, structure, and ssDNA generation) the aptamer selection can be performed.

1.4.7 Aptamer selection

In vitro selection and SELEX (Systematic Evolution of Ligands by Exponential enrichment) are the common terms used for the iterative process of narrowing a pool of aptamer sequences from an extremely varied population, to one which binds to a specific molecule (or cell) with high affinity (Figure 1-17) (Philippou et al., 2018, Takahashi, 2018, Yu et al., 2018). The process is used to remove low affinity sequences, which are not specific to the target (Berezovski et al., 2008, Blind and Blank, 2015, Bruno et al., 2012, Takahashi, 2018), while amplifying the recovered, target binding aptamers. The process is then repeated with the refined pool, using more stringent conditions to eliminate further sequences.

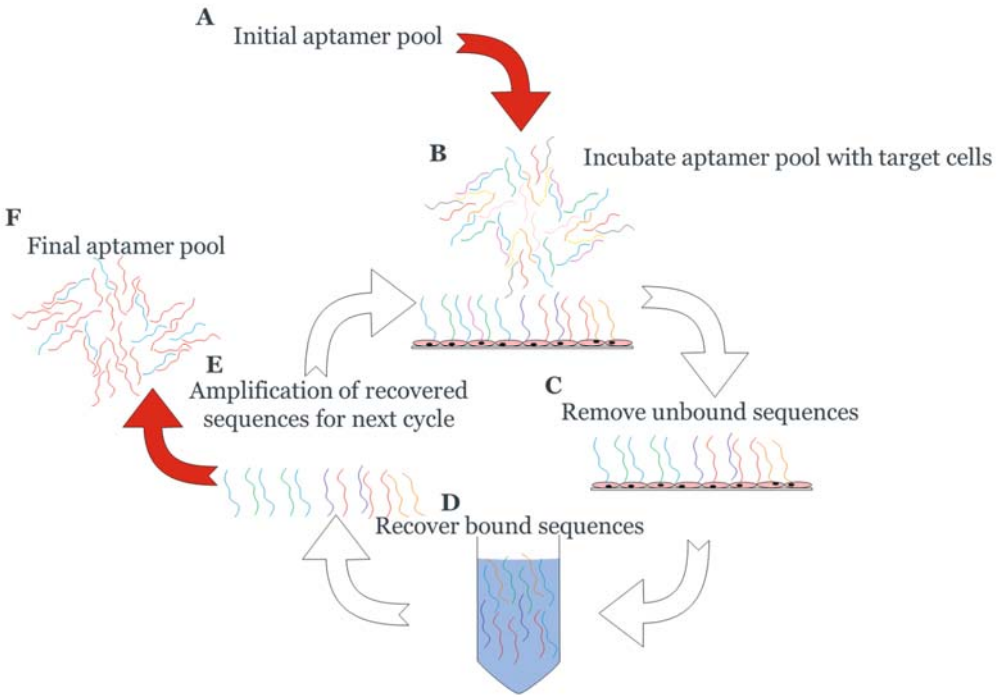

Figure 1-17 - *in vitro* selection (or SELEX) is a cyclical process which narrows a diverse pool of unique sequences, to a pool of highly specific, high affinity sequences. A) Initial pool of 10^{14} nucleic acid molecules of unbiased, random sequences in a single-stranded form. B) The initial aptamer pool is incubated with the target, allowing aptamer binding to the target. C) The targets are then washed; removing sequences that are low affinity, leaving only molecules that have a high affinity for the target. D) The molecules are then recovered from the target. E) The molecules are amplified using PCR. The amplified materials are reduced to single-stranded DNA, and the cycle begins again, increasing the stringency of selection until a small specific population remains. F) The final aptamer population is tested and individual aptamers isolated if the required properties are seen within the pool.

Methods for aptamer selection vary widely throughout the literature. It is therefore important to identify a methodology which works effectively for the chosen target type, from the many methods published (Guo et al., 2006, Schafer et al., 2007, Berezovski et al., 2008, Chang et al., 2013, Shangguan et al., 2015). Several different techniques have been developed to augment the aptamer selection process; most of which are aimed at improving the partitioning efficiency. These include capillary electrophoresis (A. Drabovich et al., 2005, R. K. Mosing et al.,

2005); magnetic sorting (Stoltenburg et al., 2005); and microfluidic sorting (Lou et al., 2009, M. Cho et al., 2010, Oh et al., 2011). AptaBID is another method which utilises the traditional SELEX approach, but incorporates two targets: the positive (or desired target), and a negative target. In this variant of the aptamer selection approach, both of the targets are cell populations (Berezovski et al., 2008). The negative target cell population provides additional selection pressures by presenting epitopes to which the aptamers can bind, which may also be present on the positive target. This negative target facilitates the removal of aptamers which bind to common epitopes: narrowing the aptamer pool to those which bind to cell population specific epitopes.

1.4.8 Aptamer targets

Since 1990, aptamers have been selected against an increasing number of target types. Oligonucleotide synthesis methodologies and nucleic acid chemistry have also improved, providing a range of modifications which may be incorporated into aptamers to impart improved characteristics. This includes resistance to nuclease-rich environments, such as blood. This has expanded the scope for aptamers into clinical applications. A few examples of the different target types are highlighted in Table 1-3.

Year	Target	Target type	Aptamer type	Reference
1990	T4 DNA polymerase	Protein	RNA	(Tuerk and Gold, 1990)
1990	Dyes	Small molecules	RNA	(Ellington and Szostak, 1990)
1992	Dyes	Small molecules	DNA	(Ellington and Szostak, 1992)
1992	Tryptophan	Small molecules	RNA	(Famulok and Szostak, 1992)
1995	Adenosine & ATP	Small molecules	DNA	(Huizenga and Szostak, 1995)
1997	Dopamine	Small molecules	RNA	(Mannironi et al., 1997)
1998	CD4	Protein	RNA	(Davis, 1998)
1998	P-Selectin	Protein	RNA	(Jenison et al., 1998)
1998	Red blood cell membranes	Cell	DNA	(Morris et al., 1998)
1999	Anthrax spores	Small molecules	DNA	(Bruno and Kiel, 1999)
2001	Rat endothelial cell line	Cell	DNA	(Blank et al., 2001)
2002	Cell adhesion receptors of trypanosome cruzi	Whole organism	RNA	(Ulrich et al., 2002)
2003	Angiopoietin-2	Protein	RNA	(White et al., 2003)
2007	Cocaine	Small molecule	DNA	(Li et al., 2007)
2007	Abrin	Small molecule	DNA	(Tang et al., 2007)
2008	LPS O111:B4	Lipopolysaccharide	DNA	(Bruno et al., 2008)
2012	Botulinum	Small molecule	DNA	(Bruno et al., 2012)

Table 1-3 - Literature for various aptamer types and selection targets. The table highlights some of the aptamer types and selections against various targets demonstrating a versatility of the aptamer technology.

1.4.8.1 Small molecule targets

Small molecules were amongst the first targets of aptamers and dominated the early years of aptamer selection literature (Table 1-3). This interest was primarily due to the difficulties in the generation of antibodies to this type of targets. The main issue with small molecules is they are typically either toxic or non-immunogenic. The non-immunogenic nature of small molecules poses a problem for antibody generation. In order to elicit an immune response to generate antibodies, small molecules often need to be conjugated to a larger immunogenic molecule (referred to as a hapten) (Rajesh et al., 2013). The original aptamer selection against small molecules also conjugated the small molecules to a support. In this case, the dye molecules were immobilised on agarose beads (Ellington and Szostak, 1990). An affinity column was prepared using this agarose, and the aptamer library was then passed through the column, allowing the aptamers to bind to the target. Unbound aptamers were removed by washing and discarded; bound aptamers were eluted from the column and amplified for further rounds of selection.

The column-like selection method has continued to be used for aptamer selection (Huizenga and Szostak, 1995, Huang, 2003, Sazani et al., 2004). Agarose beads have been substituted for magnetic beads, removing the need for a column and allowing magnetic separation (Rouah-Martin et al., 2012) and automation of the process. Small molecule selections have been used to isolate aptamers which bind to cocaine (Li et al., 2007), ATP (Wang et al., 2011), theophylline (Cheng et al., 2009), and others (Ruscito and DeRosa, 2016). Other process advances have been made since the conception of the SELEX process. One example incorporates a modification to the process such that it no longer requires the immobilisation of target small molecules. In the Capture-SELEX method, the aptamer library is immobilised on beads through hybridisation to a complementary sequence on the beads (Stoltenburg et al., 2012). The aptamers are released from the beads when they bind to a target. The displaced supernatant is collected, and PCR amplified. Capture-SELEX removes the need for target immobilisation, which is more favourable for small molecules which cannot be readily modified. Also, Capture-SELEX eliminates the problem of the aptamers binding to the support structure rather than the target.

Small molecule toxins pose another problem for antibody generation due to host fatality. The *in vitro* nature of aptamer selection eliminates issues of toxicity to the host animal. Toxins are an area in which aptamers excel compared to antibodies. Aptamers have been raised against several lethal toxins, including anthrax (Bruno and Kiel, 1999), abrin (Tang et al., 2007), and botulinum (Bruno et al., 2012). The ability to specifically bind toxins allows aptamers to be generated for environmental monitoring and to improve security measures, with detection methods having been developed for each of the above toxins.

1.4.8.2 Protein targets

T4 DNA polymerase was one of the first proteins targeted by aptamer selection (Tuerk and Gold, 1990). This eventually led to the isolation of aptamers against proteins associated with diseased states. Disease detecting aptamers include prion diseases in murine (Sekiya et al., 2006) and bovine (Mashima et al., 2009) sources, as well as HIV related proteins (Dey, 2005, D'Atri et al., 2012). Aptamers can also be used in monitoring circulating proteins (Centi et al., 2007), identifying cancerous tissues (Du et al., 2015), and inhibiting signalling molecules (White et al., 2003). Despite the abundance of target proteins for further study, protein composition can often make selection difficult due to charge differences between the two molecules. The aptamer backbone structure is inherently net negatively charged, whereas the protein charge is dependent on the amino acid side chains within the protein (Figure 1-18).

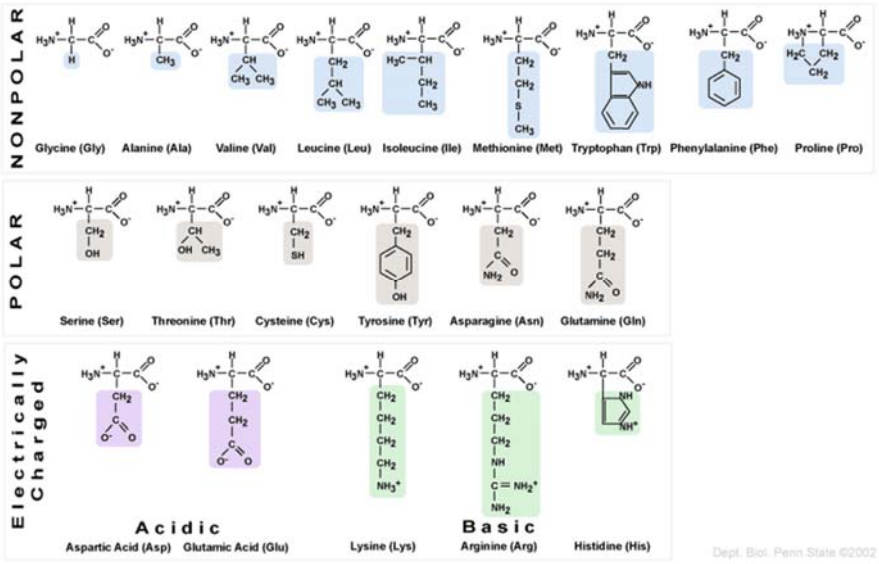

Figure 1-18 - Protein and side chain chemical, structural, and charge properties determine protein characteristics and subsequently aptamer binding. – Non-polar proteins are hydrophobic and will form globular proteins to ensure water cannot interact with these molecules. Polar proteins are highly soluble in water. Charged proteins are either negatively or positively charged dependant on the side chain, this facilitates Van der Waals bonds. Image from http://www.personal.psu.edu/staff/m/b/mbt102/bisci4online/chemistry/chemistry8.htm (accessed 09-09-18)

These charges from the amino acids can pose problems by attracting or repelling aptamers by electrostatic forces through Van der Waals and stacking interactions, causing unspecific binding (if oppositely charged) or no binding (if the same charge). Both unspecific and no binding can result in a failed aptamer selection. As discussed in section 1.4.6; charges can be masked by pH adjustment, ion composition and concentration of the buffer. The masking of the charges allows the proteins to be approached by the aptamers and facilitates other interactions, such as hydrogen bonds to facilitate aptamer-target binding.

1.4.8.3 Lipopolysaccharide targets

Lipopolysaccharides (LPS) are found within gram negative bacteria and are released as endotoxins when the bacteria die. Endotoxins have been shown to cause immune responses in animals, and repeated exposures are thought to be contributory factors to alcoholic hepatitis (Fukui, 2005, Yeluru et al., 2016), obesity (Cani et al., 2007), and auto-immune diseases such as multiple sclerosis (Wang and White, 1999, Walter et al., 2006). Although antibodies allow for specific recognition of endotoxins, the processes of detection are costly in money, time, and labour (Su and Ding, 2015). The original detection method for LPS involved the use of rabbits. The temperature of the rabbits was monitored after injection with the test solution and used as a measure of immune stimulation. This test was later replaced with the Limulus amebocyte lysate (LAL) test, using blood extracted from the horseshoe crab (Limuluspolyphemus); which clots in the presence of LPS (Nachum and Shanbrom, 1981). These methods rely on animals for LPS detection, therefore as an alternative to the assays was developed using aptamers. Aptamers have been raised against endotoxins with success in targeting of bacteria (Bruno et al., 2008, Wu et al., 2012), detection of endotoxins (Su et al., 2012, Su et al., 2013), and protection against endotoxemia (Wen et al., 2009), providing animal-free alternatives to LPS detection, with some methods more rapid than any of the previous assays.

1.4.8.4 Cell targets

Since the first selection against a cellular target (red blood cell ‘ghosts’), cells have been described as ‘complex targets’ (Morris et al., 1998). This is because cells present more than one potential target molecule, to which the aptamer pool may bind. Prior knowledge of the molecular identity of the aptamer target is not required for successful aptamer selection (Guo et al., 2008, Chang et al., 2013, Shangguan et al., 2015). However, identification of the epitopes can be attained through aptamer mediated purification of target molecules from cell lysates, using conventional biochemistry protocols and subsequent molecular characterisation methods (Morris et al., 1998, Fang and Tan, 2010, Hou et al., 2015). For example, the isolated molecules can be identified using an array of tests, including two

dimensional (2D) SDS-PAGE and mass spectrometry (Morris et al., 1998, Fang and Tan, 2010). The data generated from identifying the epitopes can provide important characterisation data on the cells used as the selection target (Berezovski et al., 2008, Chang et al., 2013, Graneli et al., 2014). Using aptamers selected against cell populations, selections have led to interesting uses including sub-population isolation (Wan et al., 2012, Sheng et al., 2012, Zhang et al., 2015); including porcine SSC populations (Guo et al., 2006, Schafer et al., 2007); aid in viral infection (Zhou et al., 2011); delivery mechanisms to specific cell populations (Zhu et al., 2014); and live imaging of specific cell populations (Schafer et al., 2007, Jin et al., 2015, Guet et al., 2015).

1.4.9 Clinical translation

The development of aptamers as a binding ligand enables them to be used in a clinical setting, in similar applications to antibodies and other drugs. While this presents a unique approach to using nucleic acids in a clinical setting, aptamers have issues which potentially limits their clinical application. This includes susceptibility to renal filtration and degradation.

Renal filtration quickly removes aptamers which were not suitably modified for *in vivo* use, due to the small size of an aptamer. To counteract this renal filtration, aptamers may be appended with large molecules, increasing the aptamer/conjugate size above the renal glomerulus cut off (30-50 kDa). Examples of molecules used to reduce renal clearance include cholesterol (Rusconi et al., 2004, Lee et al., 2015); proteins (Dougan et al., 2000, Heo et al., 2016); liposomes (Willis et al., 1998); other aptamers (Kim et al., 2010, Musumeci and Montesarchio, 2012, Soule et al., 2016); or commonly used polyethylene glycol (Burmeister et al., 2005). Using this increased size to prevent renal filtration, other challenges are presented against the aptamers, such as nucleases and immune responses.

Degradation of the aptamers can take place due to numerous nucleases found in bodily fluids.. Aptamers may be modified to increase their nuclease resistance. Typically these are backbone modifications (1.4.4) (Green et al., 1995, Uhlmann

et al., 2000), or amino acids replaced to resistant variants (1.4.4) (Ruckman et al., 1998). Once modified to remain within the human body for extended periods of time; immune reaction becomes the next issue to be presented against aptamers. This immune reaction against the aptamer or conjugated molecules is an issue faced by the REG-1 aptamer treatment discussed below. Once aptamers have been modified to be functional within, and have sufficient time within the body to enact their functionality, using aptamers in clinical setting becomes possible, with Pegaptanib (branded Macugen), is an anti-VEGF165 RNA aptamer that was the first FDA approved aptamer (approved in 2004) developed for the treatment of age related macular degeneration (Ng et al., 2006). The aptamer works by targeting VEGF165 and inhibiting its activity, leading to a significant decrease in symptoms which include overgrowth of blood vessels, vascular leakage, and swelling (Lee et al., 2005, Adamis et al., 2006) (Figure 1-19).

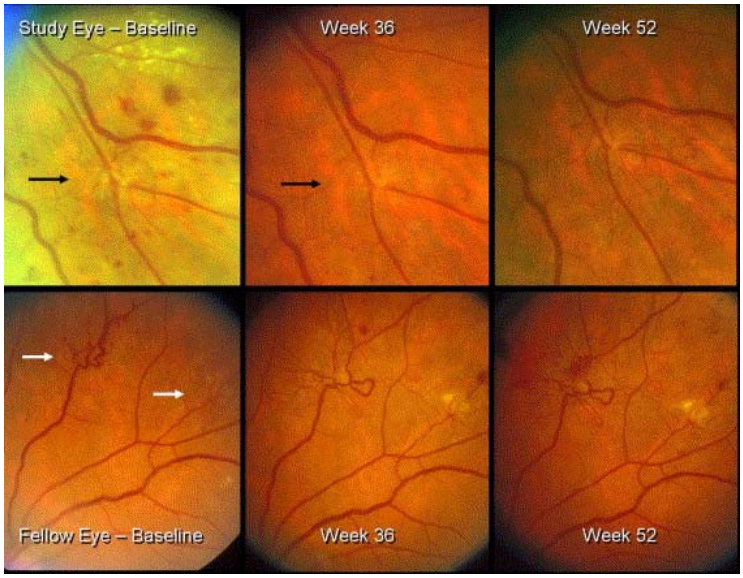

Figure 1-19 - Macugen / Pegaptanib treatments shows regression of neovascularisation. Study Eye was treated 6 times and was 6 weeks from the last treatment at week 36, where neovascularisation was reduced and remained constant at week 52. In contrast, Fellow Eye showed a steady increase in neovascularisation throughout the study without treatment. Image from (Adamis et al., 2006).

Macugen / Pegaptanib was the first aptamer to be approved for use as a therapeutic agent. Once shown to be clinically viable, other aptamers were considered for clinical trials to test efficacy in humans (McNamara et al., 2006,

Shu et al., 2011, Gourronc et al., 2013); though to-date no other aptamer-based treatments have been approved. Despite the success of the Pegaptanib, it has now been superseded by antibody equivalents (Mousa and Mousa, 2010): ranibizumab (Lucentis) (Martin et al., 2012), and aflibercept (Eylea) (Heier et al., 2012).

Another aptamer which was designed to reduce coagulation (REG1) was taken to late stages of clinical trials after showing success in early trials (Vavalle and Cohen, 2012, Povsic et al., 2013). A two-stage aptamer, the first stage Pegnivacogin targeted coagulation factor IXa inhibitor, preventing coagulation during surgical procedures. The second stage, Anivamersen, binds to the first, eliminating its inhibitory effect and restoring coagulation function.

Determination of reversal of the anti-coagulation effect of Pegnivacogin was first carried out before clinical trials, giving a ratio of 1.8 (Anivamersen): 1 (Pegnivacogin), for full reversal (Povsic et al., 2011), but was later increased to 2:1. Using these ratios, and positive control of heparin to prevent bleeding, REG1 treatment demonstrated that 50% reversal of the Pegnivacogin showed similar results to the positive control of heparin (32.8 total bleeding (Pegnivacogin) to 30.6 heparin, and 10.3 major bleeding to 10 % heparin) (Povsic et al., 2013). Moreover, 100% reversal of the Pegnivacogin reduced bleeding significantly below the control heparin (23.4% Pegnivacogin vs 30.6 Heparin total bleeding, and 5.1 Pegnivacogin vs 10.0 % heparin) (Povsic et al., 2013). These results showed promise for the REG-1 treatment as a reversible anti-coagulant, both effectively inhibiting coagulation during treatments, and then striking reversal of the inhibition after treatment had been completed. Phase 2 trials identified three incidents of allergic-like effects in patients; but the treatment was a promising step forward in treatment for acute coronary syndrome (ACS). Unfortunately, during Phase 3 trials, the allergic reactions were much more severe; including 1 death (Mehran et al., 2015, Lincoff et al., 2016). This put a stop the clinical trials of REG1 treatment and cast suspicion across all aptamers within clinical trials. The complications were subsequently attributed to allergic reactions caused by the PEG modification (incorporated to reduce renal clearance and provide prolonged activity within the circulatory system) (Lincoff et al., 2016, Ganson et al., 2016) and patients having pre-existing circulating anti-PEG antibodies.

Despite this setback, aptamers are continually being developed and tested in clinical trials, with 36 hits for aptamers on ClinicalTrials.gov, 6 of the trials being active and 4 currently recruiting (accessed clincaltrials.gov on 03-06-18). The ongoing studies cover a wide variety of conditions including biosensors for bladder cancer, age-related macular degeneration, and inhibition of tyrosine kinase-7. So, despite the setback with REG1, there are still developments within the field to advance aptamers for clinical therapeutics.

1.5 Project rationale and hypothesis

Aptamers are a technology with the potential for application in a number of biomedical applications. Since their first description in 1990, aptamers have been selected against a variety of targets, integrated into numerous assays, and have even been approved for use as a therapeutic agent. With advances in nucleic acid chemistry, synthesis, and sequencing, aptamers are becoming increasingly available for research applications, with a better understanding of many aspects of disease and treatment.

Aptamers have already been proven to perform in cell isolation, as well as stem cell enrichment, providing evidence that isolation of human SSCs is within the remit of this technology. The aptamer technology therefore has potential to aid in furthering the understanding of SSCs and the interactions with the surrounding tissues, as well as providing a methodology for cell isolation that is fast, cheap, and more accurate than current methods.

Hypothesis: Aptamer technology can be used in combination with antibody enrichment methodologies to identify novel individual or combinations of biomarkers to enrich the SSCs population from a heterogeneous bone marrow sample.

Objective I – Development of aptamer selection methodology and optimisation against the immortalised cell line SAOS-2.

Specific aims:

1. To develop a robust protocol for aptamer selection using an osteogenic cell line (SAOS-2 cells) and a non-osteogenic cell line (Raji) as a negative selection population.
2. To identify optimal binding conditions for aptamer selection against the SAOS-2 and Raji cell lines.
3. To raise aptamers against the SAOS-2 cell line, while ensuring limited binding to the Raji cell line.

4. To generate single sequence aptamers using cloning and testing of affinity to identify a selection of the optimum aptamers.

Objective II – Application of aptamer technology to develop an aptamer pool that binds to novel markers on the surface of SSCs.

Specific aims:

1. To raise aptamers against the SSCs population using methodologies developed in Objective I.
2. To incorporate antibody enrichment methodologies from Objective II to raise aptamers more specifically against the SSCs population.
3. To isolate single aptamer sequences through cloning or single molecule PCR, and subsequent testing of affinity to identify the best performing aptamers.
4. To sequence the successful aptamers to identify common sequences and monoclonal equivalent aptamer pool generation.
5. To identify the aptamer binding targets in SSCs.
6. To test single sequence aptamers against SSCs for isolation comparison.

Objective III – Use surface marker mediated enrichment techniques to isolate bone marrow sub populations containing as many SSCs as possible and characterise the SSCs using traditional techniques and Drop-Seq.

Specific aims:

1. To use the STRO-1 and CD146 antibodies to identify a skeletal stem cell population containing the highest CFU-F.
2. To use an enriched SSC population and single cell RNA analysis (Drop-Seq) to enhance the characterisation of the cells' marker expression profile.
3. To identify novel markers using single cell RNA analysis (Drop-Seq which may be used to further characterise and isolate the SSC population.

Chapter 2 Methods

Reagents and materials within this section are listed with product numbers and companies of origin when the material is first mentioned within this chapter.

2.1 Buffers

2.1.1 1x TBE

10.8 g Tris base (93362-500G, SigmaAldrich, UK), 5.5 g Boric acid (185094, Sigma-Aldrich, UK), 4 mL 0.5 M EDTA (BP2482-500, Fisher Scientific, UK) in 1 L deionised water.

2.1.2 10x TBE

108 g Tris base, 55 g Boric acid, 40 mL 0.5 M EDTA in 1 L deionised water.

2.1.3 Culture media

Alpha-MEM (LZBE02-002F, Lonza, UK) supplemented with Foetal Calf Serum (FCS) (1027010, batch 41Q4297P, LifeTechnologies, UK) to make final 10% v/v and 1% v/v Penicillin and Streptomycin (P/S) (A5955-100, Sigma, UK).

2.1.4 RPMI culture media

RPMI-1640 (BE12-702F, Lonza, UK) supplemented with 10% v/v FCS and 1% v/v P/S.

2.1.5 Selection media

Alpha-MEM supplemented with 5 mM $MgCl_2$ (M8266, Sigma-Aldrich, UK), 4.5 mM $CaCl_2$ (223506, Sigma-Aldrich, UK), 80 nM $MnCl_2$ (244589, Sigma-Aldrich, UK), and 77 nM $NiCl_2$ (339350, Sigma-Aldrich, UK).

2.1.6 Folding media

Alpha-MEM supplemented with; 10 mM $MgCl_2$, 9 mM $CaCl_2$, 160 nM $MnCl_2$, and 154 nM $NiCl_2$.

2.1.7 0x optimisation media

Alpha-MEM.

2.1.8 1x optimisation media

Alpha-MEM supplemented with; 5 mM $MgCl_2$, 4.5 mM $CaCl_2$, 80 nM $MnCl_2$, and 77 nM $NiCl_2$.

2.1.9 10x optimisation media

Alpha-MEM supplemented with; 50 mM $MgCl_2$, 45 mM $CaCl_2$, 800 nM $MnCl_2$, and 770 nM $NiCl_2$.

2.1.10 LB agar

In a 500 mL bottle; 5 g Tryptone (95039-50G-F, SigmaAldrich, UK), 2.5 g Yeast Extract (Y1625, SigmaAldrich, UK), 2.5 g NaCl, and 200 mL distilled water were mixed until dissolved. 400 µL 5N NaOH (10306200, FisherScientific, UK) was added to adjust the pH. Water was added until it was a total of 500 mL. To the

mixture 7.5 g agar pellets were added and stirred until dissolved. This mixture was autoclaved.

2.1.11 LB media

In a 500 mL bottle; 5 g Tryptone, 2.5 g Yeast Extract, 2.5 g NaCl, and 200 mL distilled water were mixed until dissolved. 400 µL 5N NaOH was added to adjust the pH. Water was added until it was a total of 500 mL.

2.1.12 Blocking media

17mL a-MEM, 2 mL AB Serum human (H4522-100ML, Sigma-Aldrich, UK), 0.2 g BSA (BP1600-100, FisherScientific, UK), 1 mL FCS.

2.1.13 MACS buffer

1 L 1x PBS, 5 g BSA, 4 ml 0.5M EDTA were mixed for half an hour, and then filter sterilised and de-gassed.

2.2 Aptamer selection and optimisation methods

2.2.1 Agarose gel

A 4% w/v agarose gel was prepared with 4 g agarose (BP1356-500, Fisher Scientific, UK) suspended in 100 mL 1x TBE (2.1.1). This solution was heated in a microwave until the agarose was melted and dissolved into the TBE. 10 µL Gel Red (41003, BIOTIUM, UK) was added and mixed by swirling. The molten agarose was poured into a gel cast (miniPROTEAN plate and 1 mm space, 1653311, BIORAD, UK and miniPROTEAN short plate, 1653308, BIORAD, UK), and a 10-lane comb (1653359, BIORAD, UK) placed into the gel and left to set (approximately 20 minutes). 20 µL each sample was mixed with 4 µL 6x loading buffer (6x orange DNA loading dye, R0631, ThermoScientific, UK). 2 µL

O'RangeRuler 10bp ladder (SM1313, ThermoScientific, UK) was mixed with 4 µL 6x loading buffer and 18 µL water. Once the gel was set, the comb was removed, and the samples and ladder added carefully. The gel was run in 1x TBE, 150 V 20 minutes. The gel was imaged (InGENIUS, Syngene, UK) to ensure aptamer dsDNA, ssDNA, or primers were the only amplification products present within a sample.

2.2.2 Acrylamide gel

A 10% (w/v) acrylamide stock was made with: 125 mL Bis-Acrylamide 40% (v/v) 29:1 (acrylamide: bis-acrylamide) (BP1408-1, Fisher, UK), 100 mL 10x TBE buffer (2.1.2) and deionised water to make the total volume 500 mL. 6 mL the 10% (v/v) acrylamide stock was mixed with 60 µL 10% (w/v) APS in water (A3678, Sigma, UK) and 6 µL TEMED (T/P190/04, Fisher, UK), mixed by gentle swirling and poured into a gel cast (miniPROTEAN plate and 1mm space, 1653311, BIORAD, UK and miniPROTEAN short plate, 1653308, BIORAD, UK) with a 10 lane comb (1653359, BIORAD, UK) and left to set (approximately 20 minutes). 10 µL each sample was mixed with 2 µL 6x loading buffer. 1 µL O'RangeRuler 10 bp ladder was mixed with 2 µL 6x loading buffer and 9 µL water. When set, the gel loaded, and run in 1x TBE at 150 V for 40 minutes (Powerpac Basic, BIORAD, UK). The gel was stained with 1% (v/v) for 1-minute Gel Red in 1xTBE, washed in water for 1 minute and imaged.

2.2.3 SAOS-2 cell culture

SAOS-2 cells are an osteosarcoma cell line with an epithelial morphology. The cells were cultured in culture media (2.1.3). The cells were cultured in T-175 flasks (431080, Corning, UK) with 20 mL media at 37°C, 5% (v/v) CO_2, and passaged when reaching 70-80% confluence (usually 3-4 days).

To passage the cells culture media was removed, and the cells washed with 10 mL PBS. The PBS was removed. 1 mL 10x trypsin solution (BE02-007E, Lonza, UK) was added to 9 mL PBS. 2 mL of the 1x trypsin solution was applied for 5-

10 minutes to ensure all cells were no longer attached to the surface or one another. 8 mL culture media was added. The cell suspension was placed into a 50 mL falcon tube and pelleted by centrifugation (300x g for 4 minutes), the supernatant was removed, and cells were resuspended in 10 mL culture media and seeded at a 1 in 10 dilution in a new flask.

2.2.4 SAOS-2 selection and cell seeding for selection

When cells were required for selection, cells were passaged, and seeded into a T-75 flask (430641U, Corning, UK) at 20,000 cells per cm^2 (1,500,000 cells for a T-75), this allowed 3 days of recovery before the cells approached 80-90% confluence and were suitable for selection purposes.

2.2.5 Raji cell culture

Raji cells are a non-adherent, lymphoblastic cell line isolated from a Burkett's lymphoma; chosen for selection as they lack the STRO-1 antigen present on the SAOS-2 cell line. The Raji cells were cultured in RPMI culture media (2.1.4). The cells were cultured in T-75 flasks with 20 mL media at 37°C, 5% (v/v) CO_2. The cells were passaged every 3-4 days.

For passage, the 20 mL cell suspension was removed from the flask and placed into a 50 mL falcon tube. The tube was centrifuged at 300x g for 4 minutes, the supernatant was removed, and cells were re-suspended in 20 mL RPMI culture media, 1 mL of the cell suspension was added to a new flask containing 19 mL RPMI culture media.

2.2.6 Raji cell seeding for selection

When Raji cells were required for selection, the cells were centrifuged at 300x g for 5 minutes, supernatant removed and cells resuspended in 20 mL RPMI culture media, counted, and 20,000 cells per cm^2 were added to a T-75 (1,500,000 cells), before media was added up to 20 mL. The cells were cultured for 3 days at 37°C,

5% (v/v) CO_2 allowing the cell population to grow and the proportion of dead cells to be minimised. On the day of selection, the cells were counted, and the required number of cells were removed from the growth media and washed in the selection media (2.1.5) for 5 minutes on ice. The cells were centrifuged again (300x g for 5 minutes), supernatant removed, placed in 8 mL new selection media and were ready for selection.

2.2.7 Pre-selection optimisation

250,000 cells were prepared (as 2.2.4 or 2.3.3) and aliquoted into each well of 3, 6 well plates (20,000 cells per cm^2) with 2 mL culture media and cultured for 3 days at 37°C, 5% (v/v) CO_2. Several tests were performed to identify the optimal binding conditions, the variables included; buffer salt content, time and cell number. The tests were performed at approximately 1/20th the cell number, volume and aptamer molecules as a full selection (for easy scaling), therefore, the culture media was removed from all wells. 400 µL of one of the 3 selection media were applied (0x (2.1.6), 1x (2.1.8), and 10x (2.1.9). Cells were incubated on ice for 5 minutes before the media was removed and replaced with identical selection media and volume. 221.9 ng naive re-folded aptamer pool (CCAGTGTAGACTACTCAATGCNx40GGTTGACCTGTGGATAGTAC, IDT, UK) was taken for each condition. This was prepared in either 0x, 2x or 20x media, heated to 95 °C for 10 minutes, cooled to 5 °C to refold the aptamers. The refolded 221.9 ng per well aptamers were applied to the relevant wells (one for T-25 equivalent, or two for T-75 equivalent). The wells were incubated for 15, 30, 45 or 60 minutes, before supernatant was removed, and the cells washed with 400 µl of the relevant media for 5 minutes. The supernatant was again removed and replaced with 120 µL DNase free water added to each condition and the cells scraped (2.2.9.1). The recovered materials were amplified (2.2.10.1) and assessed for recovery percentage (2.2.10.2).

2.2.8 SAOS-2 Selection

Cells cultured and seeded as described in section 2.2.3 and 2.2.4 (20,000 cells per cm^2 in a T-75) were washed twice with 8 mL selection media (2.1.5) and incubated in the final wash for 10 minutes.

During the incubation, aptamers were refolded (4.439 µg ssDNA added folding media (2.1.6) in a 1:1 ratio, heated to 95 °C for 10 minutes and cooled to 4 °C). The refolded aptamers were added to the cells and incubated and washed as Table 3-1, Table 3-2, and Table 3-4.

2.2.9 Aptamer recovery

2.2.9.1 Cell recovery

After selection washing steps (Round of selection dependant, see tables - Table 3-1, Table 3-2, and Table 3-4) and removal of media; 2400 µL DNase free water (BPE561-1, LifeTechnologies, UK) was added to the cells before being carefully scraped with cell scraper (11597692, Fisher Scientific, UK) from the flask, and placed into two 2 mL Eppendorf tubes (623201, Greiner-Bio, UK). This material served as the template for the post recovery PCR (2.2.10.1).

2.2.9.2 Lysis buffer recovery

After washing steps (Round of selection dependant, see tables - Table 3-1, Table 3-2, and Table 3-4) and removal of media; 2400 µL lysis buffer (10 mM Tris pH 7.4 (10376743, FisherScientific, UK), 0.25% v/v Triton X-100 (X100-100ML, SigmaAldrich, UK), and 150 mM NaCl (S7653, SigmaAldrich, UK)) was added to the cells. The cells were incubated for 5 minutes on ice, before being scraped using a cell scraper, transferred to two 2 mL Eppendorf tubes. This material was used as template for the post recovery PCR (2.2.10.1).

2.2.10 Amplification of aptamers by polymerase chain reaction

2.2.10.1 Post recovery PCR

The recovery template (2400 µL) (2.2.9.1 or 2.2.9.2) was added to 2400 µL 2x PCR master mix (M7505, Promega, UK), 96 µL forward primer with a 5' fluorescein amidite modification (FAM) (see Table 2 1), and 96 µL reverse primer with the 5' PO_4 modification (see Table 2 1).

Primer	Sequence
Forward	CCAGTGTAGACTACTCAATGC
Reverse	GGTTGACCTGTGGATAGTAC
FAM Forward	FAM- CCAGTGTAGACTACTCAATGC
PO_4 Reverse	PO_4-GGTTGACCTGTGGATAGTAC
Biotin Reverse	Biotin-GGTTGACCTGTGGATAGTAC

Table 2-1 - Primer sequences, and modifications used for aptamer amplification. Unless otherwise stated, aptamer primers were designed and validated by Aptamer Group (YORK) and synthesised by IDT, UK.

The mix was vortexed briefly, centrifuged, and distributed into a 96 well plate (E1403-8200, Starlab, UK) with 50 µL in each well, sealed (E2796-9793, Starlab, UK) and the 96 well plate centrifuged. PCR was performed for 4 cycles (Verti 96 well thermocycler, Applied Biosystems, UK). Thermal cycling conditions included an initial step at 95 °C for 2 minutes, cycle steps at 95 °C for 45 seconds, 55 °C for 45 seconds and 65 °C for 45 seconds, and a final extension step at 65 °C for 2 minutes.

2.2.10.2 qPCR of recovered material

Once the 4-cycle PCR was complete; three wells were chosen at random from the 96 well plate and 2 µL was taken from each; added to 198 µL DNase free water and mixed. 35 µL the diluted PCR product was added to an equal volume of qPCR master mix (for each 50 µL reaction: 1.2 µL forward primer, 1.2 µL reverse primer, 25 µL GoTaq® qPCR (A6002, Promega, UK). 20 µL of each sample mix was aliquoted into 3 wells, for replicates. The standard curve (1.3317

ng ssDNA (30% of a selection pool) was taken and made up to 25 µL with DNase free water as point 1. Another 1.3317 ng was taken and made up to 25 µL with DNase free water for point 2 and diluted with another 25 µL DNase free water. Point 2 was mixed thoroughly, 25 µL was taken from point 2 and added to 25µL DNase free water to generate point 3 and mixed thoroughly. This process was repeated to generate a 10 point standard curve, these were treated as recovery samples described 2.2.10.1 and 2.2.10.2) was also prepared and distributed following the same method onto the 96 well plate for quantification post qPCR. The plate was sealed, centrifuged and placed in the qPCR machine (7500 Real time PCR machine, Applied Biosystems, UK) for analysis. The qPCR program was run as follows: initial denaturation and activation step at 98 °C for 10 minutes, followed by 30 cycles of; 95 °C for 45 seconds, 55 °C for 45 seconds and 65 °C for 45 seconds. The fluorescence reading was taken at the end of the 65 °C elongation step. During this time the 96-well plate with the 'post recovery PCR' was kept at 4 °C.

2.2.10.3 Secondary PCR optimisation

After the qPCR step, a CT (cycle threshold; the number of amplification cycles required to reach a defined fluorescence threshold) value should be gained for the samples, this CT was used to track recovery of aptamer materials from each round. The CT value also guided the secondary PCR optimisation step. Taking this CT value, a PCR cycle course was run on the remaining material. Post recovery PCR (2.2.10.1) materials were pooled. 192 µL pooled PCR product from 2.2.10.1 was added to 2400 µL 2x PCR master mix, 96 µL forward primer, 96 µL reverse primer, and 2016 µL DNase free water, this was mixed thoroughly. 5x 25 µL aliquots were taken from the mixture and placed into 0.2 mL Eppendorf tubes (I1402-8100, Starlab, UK) and each tube was run at one of the following cycle numbers: CT-1. CT, CT+1, CT+2, CT+3. The amplified cycle course material was analysed by PAGE (2.2.2). The resulting image was used to identify cycle conditions where clean PCR product was obtained (with no aberrant amplification products) the remaining PCR mix was cycled to the same number of cycles as identified in the PAGE.

2.2.11 Asymmetric PCR

For each 50 µL reaction, 2.292 ng of template was added, 25 µL 2x PCR master mix reagents, 1.5 µL forward primer, and water to a final volume of 50 µL. The volumes were amplified in the same conditions as other PCR reactions, for 9 cycles. Amplified material was analysed by PAGE (2.2.2).

2.2.12 Bead purification methodologies

2.2.12.1 Solid Phase Reversible Immobilization

After amplification, the PCR material was recovered and combined, purified using Solid Phase Reversible Immobilization (SPRI) magnetic beads. SPRI bead stock (50mg/ml beads in 28.8% polyol, 1.62 M NaCl) was added at 1.8x volume of PCR product.0.7x volume of isopropanol (2-propanol certified ACS, A416S-4, Fisher Scientific, UK)) was also added to the PCR material and mixed. An example was 100 µL PCR material would be mixed with 180 µL beads (supplied by Aptamer Group) and purification buffer, and 70 µL 100% isopropanol. The mix was incubated at room temperature for 10 minutes before separating the beads using a magnetic tube rack. The buffer was discarded, and the beads washed 3 times in 4 x PCR material volume 80% ethanol (BP2818500, Fisher Scientific, UK) (e.g. 1000 µL PCR material would require three 4 mL washes). After washing, the beads were allowed to air dry (approximately 10 minutes). The purified DNA was eluted in 0.2x original volume DNase free water (e.g. 1000µL PCR is eluted in 200 µL water). The purified material was analysed by PAGE (2.2.2).

2.2.12.2 Streptavidin bead purification

This method only is applicable when using a biotin-modified reverse primer. For each 50 µL PCR reaction, 5 units Exonuclease I was added (M0293S, New England BioLabs, UK). The mix was incubated at 37 °C for 30 minutes. During the incubation, 6 µL streptavidin beads were washed (88817, Pierce Thermo Scientific, UK) in 50 µL PBS three times, magnetically separated each time,

resuspended. After the final wash, the beads were resuspended in 5 µL 5 M NaCl (S6191, Sigma Aldrich, UK) and added to the Exonuclease treated PCR material. Samples were incubated (1 hour, room temperature, 1000 rpm shaking) to capture the biotinylated PCR products. The beads were magnetically separated and washed in 50 µL PBS twice. The beads were magnetically separated from the PBS, the PBS removed, and the beads resuspended in 10 µL 0.5 M NaOH (S318-1, Fisher Scientific, UK), mixed and incubated for 10 minutes, with the sample shaking. The beads were magnetically separated, the supernatant removed, and supernatant added to 10 µL 0.5 M HCl (435570, Sigma Aldrich, UK), to neutralise the NaOH. The eluted ssDNA was quantified using the Nanodrop 1000 (Nanodrop 1000, ThermoScientific, UK).

2.2.13 Lambda Exonuclease

For each 50 µL reaction, 5.1 µL 10x Lambda Exonuclease buffer (B0293S, New England BioLabs, UK) was added and 5 units Lambda Exonuclease (M0262S, New England BioLabs, UK). The tubes were incubated at 37 °C for 30 minutes. The volumes were pooled and analysed by PAGE (2.2.2).

2.2.14 Exonuclease I treatment

For each 50 µL PCR materials, 5.5 µL Exonuclease I 10x buffer and 5 units Exonuclease I was added (M0293S, New England BioLabs, UK). The mix was incubated at 37 °C for 30 minutes.

2.2.15 Workflow

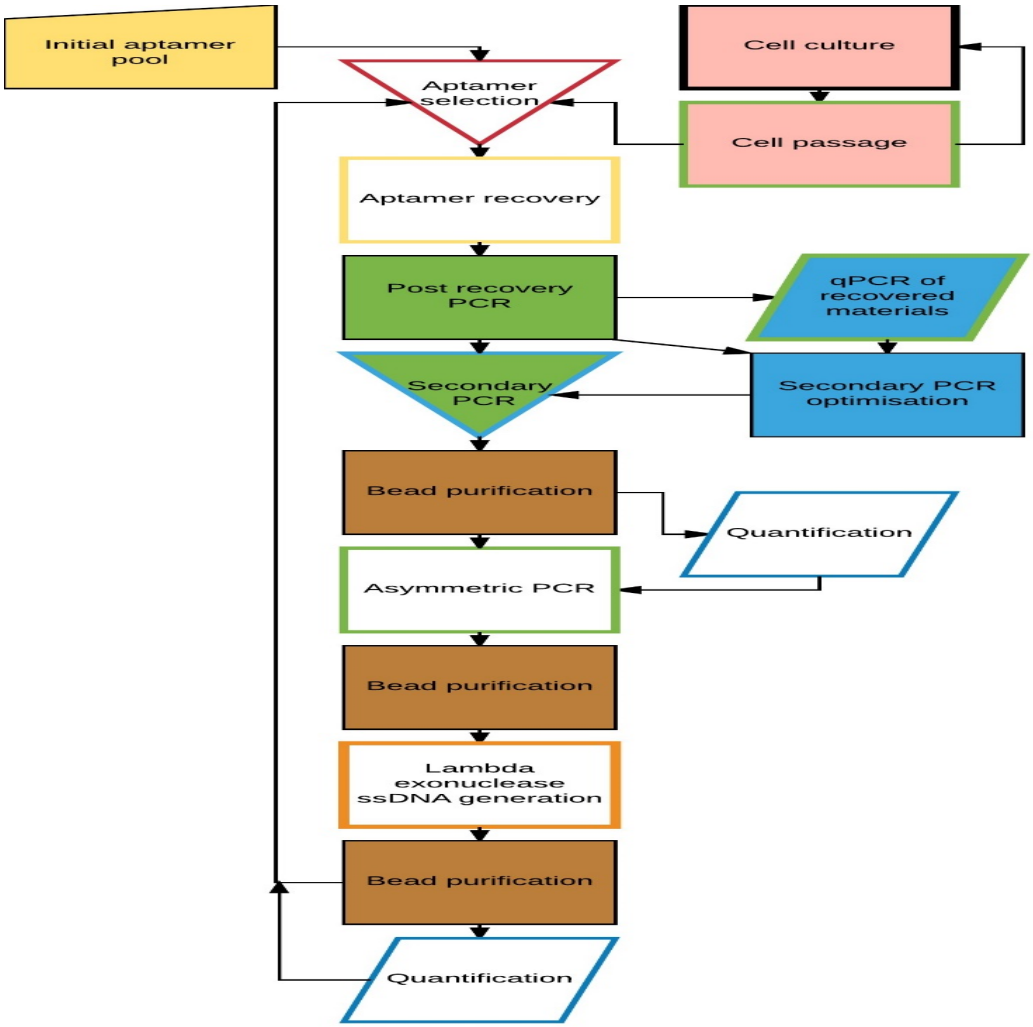

Figure 2-1 - Aptamer Selection workflow highlighting the steps necessary for each round of selection. Cell culture is a cyclical process external to the aptamer selection (seen top right, with the pink boxes) This was performed on a needs basis where cells were grown as needed for the selections for this 20,000 cells / cm^2 were placed in T-75 flasks 3 days before being needed for selection. One other input is required for the selection, the initial aptamer pool (top left) a $1x10^{14}$ unique ssDNA sequences to be tested against the target. The remaining steps are carried out in order, throughout the cycles. Green boxes are PCR stages. Blue boxes are quantification stages, filled in stages are qPCR and a cycle course PCR to determine optimal template levels for the second PCR. Blue outlined boxes are quantification using the Nanodrop 1000. Brown boxes are nucleic acid purification steps using the solid phase reversible immobilisation. Green outlined box is an asymmetric PCR facilitating the generation of ssDNA from dsDNA template. Orange outlined box is the enzymatic digestion stage where any remaining dsDNA is digested into ssDNA.

The workflow (Figure 2-1) shows the final developed methodology used for aptamer selection in this project and the methods to be used when working with primary tissue. With multiple quantifications, gels to check sample purity and qPCR to check the quantity of material recovered from the selection.

2.2.16 Bacterial cloning for single aptamer testing and sequencing

Aptamer materials from the final round of SAOS-2 selection, Round 12 fraction SAOS-2 + Raji was taken, and amplified using the recovery PCR (2.2.10.1), followed by secondary PCR (2.2.10.3). The material was purified (2.2.12.1), Exonuclease I treated (2.2.14) and purified again. The material was quantified using the Nanodrop.

Asymmetric PCR was seeded using this material (2.2.11) followed by purification, Lambda Exonuclease treatment and purification (2.2.13). The ssDNA was quantified using the Nanodrop.

2 picomoles of the ssDNA was used as a template, to which 12 µL 50 µM forward primer, 12 µL 50 µM reverse primer 80 µL Solis HOTFIRE PCR master mix (04-25-02015, Solis Biodyne, Estonia), 40 µL 25mM $MgCl_2$ and water to bring the volume to 400 µL was added. This was split into 50 µL reactions.

This was placed in a thermocycler and treated to 95 °C for 5 minutes. 6 cycles of 95 °C for 45 seconds, 55 °C for 45 seconds and 65 °C for 45 seconds. 65 °C for 2 minutes before a hold at 4 °C.

All materials were pooled, with 5 µL being analysed by PAGE (2.2.2) the successfully amplified material should have 80 bp size. Bead purified twice, the first elution into 50 µL 1x Lambda Exonuclease buffer (10x Lambda Exonuclease buffer mixed with DNase free water in a 1:9 ratio), the second into 50 µL RNase free water. The material was quantified using a Nanodrop.

50 ng the material was taken and made up to a volume of 10 µL.

1 µL the diluted aptamer material, 10 µL 2x reaction buffer (K1232, cloning kit ThermoFisher Scientific, UK), 6 µL nuclease free water and 1 µL DNA blunting

enzyme (K1232, cloning kit ThermoFisher Scientific, UK) were added in turn to a 200 µL Eppendorf tube. This was vortexed briefly and centrifuged on pulse to collect the liquid. This was heated to 70 °C for 5 minutes before a 4 °C hold. The mixture was placed on ice and 1 µL pJET1.2/blunt clone vector (K1232, cloning kit ThermoFisher Scientific, UK) and 1 µL T4 DNA ligase (K1232, cloning kit ThermoFisher Scientific, UK) were added. The mixture was vortexed and centrifuged on pulse to collect the droplets. The mixture was incubated at 22 °C for 5 minutes. This was stored at 4 °C while QC steps were taken.

2µL of the material was taken and placed into a new 200 µL Eppendorf tube. To it 1 µL 10 µM pJET forward primer (K1232, cloning kit ThermoFisher Scientific, UK), 1 µL 10 µM pJET reverse primer (K1232, cloning kit ThermoFisher Scientific, UK), 10 µL 5x solis HOTFIRE PCR master mix, and 13 µL RNase free water were added. The materials were mixed, and PCR was performed. 95 °C for 10 minutes, 16 cycles of 94 °C for 45 seconds, 60 °C for 45 seconds, 60 °C for 45 seconds, and 72 °C for 45 seconds. Followed by 72 °C for 2 minutes and a 4 °C hold.

1 µL of the resultant PCR material was assessed by PAGE. 200 bp material signifies successful ligation.

500ml LB agar was prepared (2.1.10). Once cooled but not set 100 µg/ml ampicillin was added. LB agar plates were poured, until the petri dish was half full, (producing approximately 15 plates).

A vial of competent *Escherichia coli* (*E. coli*) (C2987H, New England BioLabs, UK) was thawed on ice. Once thawed 2 µL of the ligated materials was added and mixed by flicking the tube. The mixture was placed on ice for 2 minutes. The sample was heat shocked by placing the mixture in a 42 °C water bath for 30 seconds. The mix was placed immediately back on ice for 2 minutes. 250 µL LB media (2.1.11) was added to the tube. The tube was gently mixed using a pipette before transferring 50 µL of the broth onto the labelled LB agar plates. The plates were cultured upside down at 37 °C overnight.

A PCR mixture of 39 µL 10 µM pJET forward primer, 39 µL 10 µM pJET reverse primer, 390 µL 5x Solis HOTFIRE PCR master mix, and 1482 µL water was prepared. 20 µL of the mixture was added to each well of a 96 well plate. Using 10 µL pipette tips and a pipette set at a volume of 8 µL single colonies were

picked, and the cells and pipette tip were placed into a well of the 96 well plate before being vigorously mixed until the cells are released from the tip into the PCR mix. The 96 well plate was placed on a thermocycler. The PCR program was 95 °C for 10 minutes, followed by 8 cycles of 94 °C for 45 seconds. 60 °C for 45 seconds, and 72 °C for 45 seconds. Followed by a 72 °C for 2 minutes and a 4 °C hold.

2 µL of each of the PCR materials were taken and added to 8 µL of water and 10 µL 2x DNA loading buffer. Each material was assessed by PAGE with a 50 bp ladder (N3236L, New England BioLabs, UK) and successful ligations noted (at 200 bp).

A new 96 well plate was taken and 296 µL water was placed into each well. 4 µL of the successfully ligated picked colonies PCR material was transferred 6 well to the new 96 well plate to perform a 1 in 75 dilution.

5 µL of each well was added to a PCR mix within another 96 well plate (147 µL 50 µM forward primer, 147 µL 50 µM reverse PO_4 primer, 980 µL solis HOTFIRE PCR master mix, and 3136 µL water. Mixed and 45 µL aliquoted into each well of a 96 well plate.) The 96 well plate was placed on a thermocycler. The PCR program was 95 °C for 10 minutes, followed by 14 cycles of 94 °C for 45 seconds. 60 °C for 45 seconds, and 72 °C for 45 seconds. Followed by a 72 °C for 2 minutes and a 4 °C hold. The materials were bead purified twice. Leaving pure DNA materials from each of the clones, in aptamer form.

2.2.17 Aptamer clone testing

The successfully ligated clone aptamers were quantified using the Nanodrop. 4 50 µL Asymmetric PCR reactions (as in 2.2.11) were prepared and carried out per successful ligation. The Asymmetric PCRs were bead purified (2.2.12.1) Lambda Exonuclease treated (2.2.13) and purified again.

SAOS-2 cells and Raji cells were prepared for aptamer selection (as described in 2.2.4 and 2.2.6 but in 96 well plates and the cell number equivalent, with a CM^2 of 1 CM in a 96 well plate, 20,000 cells were seeded into each well. Each of the

clones materials for a minimised selection (59 µg) were subject to SAOS-2 and Raji cells separately. Washed three times and recovered (as described in 2.2.8 and 2.2.9.1 but scaled down to 100 µL selection media in each well and washes, and 32 µL DNase free water for the scraping which was performed with a 200 µL pipette tip)

A master mix of 153.6 µL 50 µM forward primer, 153.6 µL 50 µM reverse PO_4 primer, and 3840 µL 2 x PCR master mix was prepared. 32 µL of the master mix was placed into 59 wells of 2 96 well plates. The materials were subject to a recovery PCR using the 32 µL of recovered materials as template for the PCR.

qPCR was performed on each of the clones SAOS-2 recovery and Raji recovery. The results were compared and the sequences with significantly higher SAOS-2 recovery compared to Raji recovery were selected for sequencing.

2.3 Bone marrow and foetal selection

2.3.1 Human bone marrow isolation and enrichment

2.3.1.1 Bone marrow isolation

Methodologies established by the Oreffo lab group were used for bone marrow isolation (Tare et al., 2012). Waste bone marrow from hip replacement surgeries were collected from the Southampton University and Spire hospitals with informed patient consent under LREC 194/99. 20 mL alpha-MEM was added to the bone marrow, and shaken for 1-2 minutes, 10 mL cell suspension was taken and placed into another tube. 10 mL alpha-MEM was added to the bone marrow again, and shaken for 1-2 minutes, this was repeated several times until bone fragments were faint red-white. The cells were centrifuged at 272 g and washed 3 times, before being filtered through a cell strainer to remove larger fragments. The cells were centrifuged again and resuspended in 25 mL per preparation, normally two tubes as one often leads to an abundance of blood cells post lymphoprep stage. In a new tube 20 mL lymphoprep (1114547, Serumwerk, Norway) was added to the bottom of the tube, 25 mL cell suspension was layered on top of the lymphoprep carefully to ensure a clear separation of the two

solutions. The tubes were centrifuged at 914 g for 40 minutes, with no brake, as this can disrupt the separation of the solutions. The cells of interest collect at the interface of the two solutions (the buffy coat), and were removed with a 3 mL pipette (13469108, Fisher Scientific, UK) and collected in a new 50 mL falcon tube.

2.3.1.2 MACS enrichment

Methodologies established by the Oreffo lab group were used for SSC enrichment (Tare et al., 2012). The lymphoprep-separated cells (2.3.1.1) were washed 3 times with alpha-MEM and placed in blocking media (2.1.12) for 30 minutes in the cold room, agitating to avoid clumping. After washing three times with MACS buffer (2.1.13) cells were resuspended in 0.5 mL STRO-1 IgM hybridoma antibody (Bone and Joint Group, UK), this was incubated for 30 minutes in the cold room, being agitated to avoid cell clumping. The cells were washed 3 times in MACS buffer, and counted to calculate the amount of magnetic anti-mouse IgM beads were required for the sample (20 µL per $1x10^7$ cells) with a maximum of 200 µL per column. The cells were incubated with the beads and MACS buffer (80 µL MACS buffer per 20 µL beads (130-047-301, Miltenyi Biotec, UK)) for 15 minutes in the cold room, being agitated to avoid cell clumping. The cells were washed three times with MACS buffer before being resuspended in 3 mL MACS buffer, the separation columns were prepared by hydrating with 3 mL MACS buffer. The cells were added to the column and allowed to drip through, the negative fraction was passed through the column again. The column was washed with 9 mL MACS buffer, the column was removed from the magnetic holder and placed over a new tube, and 5 mL MACS buffer was added before the plunger was applied to remove the cells from the column. These cells were the STRO-1 enriched cell populations.

2.3.1.3 Antibody labelling

Samples of the bone marrow were taken at a variety of stages: pure bone marrow, post lymphoprep, and after MACS separation. Whenever the sample was taken the cells were treated as follows on ice or in a cold room.

STRO-1 hybridoma was added to the cell sample if it had not already been exposed. The cells were incubated under agitation for 30 minutes before being washed 3 times with MACS buffer. Alexafluor ® 488 Goat IgG Anti-mouse IgM (A-21042, ThermoFisher, UK) was added to the cell samples at a dilution of 1 in 200 and incubated for 15 minutes, before being washed 3 times with MACS buffer.

CD146 labelling was performed after the STRO-1 labelling as it was a Alexafluor ® 647 mouse anti-human CD146 IgG (563619, BD Biosciences, UK), once the cells were washed for the third time, the anti-CD146 antibody was added to the cells in a 1 in 100 dilution. The cells were incubated agitated for 15 minutes before 3 washes with MACS buffer.

2.3.1.4 FACS

Once all cells were labelled, cells were resuspended in 1 mL MACS buffer per 1 million cells. The unselected cells were loaded into the FACS machine. Size (forward scattering) and granularity (side scattering) thresholds were decided for debris within the sample. Eliminating those as cells, so nucleated cells can be counted for data processing. The mononuclear cells within the population were identified within the cell population using the same thresholding method.

Once the mononuclear cells had been identified, the next step was to threshold for the fluorescent channels, using a histogram that shows FITC/Alexafluor® 488 signal against cells counted with said fluorescence. Using the thresholding tool, a line was drawn at the level where 1% of the unstained population would be counted as positive. This allows for a clear increase in signal to be detected even in rare populations. The same was done for CD146 on the PE/Alexofluor®647 channel. The positive fraction of the MACS assay that has been labelled with the STRO-1 reporting (goat anti-mouse IgM) was loaded so that the thresholds for the $STRO^{BRIGHT}$ may be designated. The $STRO^{BRIGHT}$ threshold was done by

having a threshold encompass the far right portion of the histogram, indicating the brightest fluorescing cells. The threshold was moved along the histogram until it encompassed the top 5% of the STRO population.

A hierarchy of populations was developed that allowed for sorting of the cells, but also for an in depth characterisation of the bone marrow's population markers that have been tested.

2.3.2 Bone marrow cell culture

STRO-1 isolated bone marrow cells (2.3.1.2) were cultured in T-175 flasks with 20 mL culture media at 37°C, 5% (v/v) CO_2, and passaged when reaching 70-80% confluence (usually after 3-4 days).

To passage the cells the culture media was removed and the cells washed with 10 mL PBS. The PBS was removed. 1 mL 10x trypsin solution was added to 9 mL PBS. 2 mL of the 1x trypsin solution was applied for 5-10 minutes to ensure all cells were no longer attached to the surface or to one another. 8 mL culture media was added. The cell suspension was placed into a 50 mL falcon tube and pelleted by centrifugation (300x g for 4 minutes), supernatant was removed, and cells were resuspended in 10 mL culture media and seeded at a 1 in 10 dilution in a new flask.

2.3.3 Bone marrow cell seeding for aptamer selection

When cells were required for selection, cells were passaged, and seeded into a T-75 flask at 20,000 cells per cm^2 (1,500,000 cells), this allowed for 3 days of recovery before the cells approached 80-90% confluence and were suitable for selection purposes. The cells used in each round of selection are summarised in Table 2-2.

Patient (sex and age)	Passage	Selection	Round of selection
F59	P1	1	1
F59	P3	1	2
M69	P0	2 (FACS)	1
F75	P0	2 (FACS)	2

Table 2-2 - Sample information of bone marrow samples used for bone marrow related selections. Several bone marrow samples were used in the course of aptamer selection. These samples are recorded here, with their age, sex, passage used, and which selection they were used for and the round of selection.

2.3.4 Bone Marrow aptamer selection

Cultured BMC were washed twice with 8 mL of selection media (2.1.5) and incubated on ice in the final wash for 10 minutes. During the incubation, 4439 ng ssDNA was added to folding media (2.1.6) in a 1:1 ratio. The mix was heated to 95 °C for 10 minutes and then cooled quickly to 5 °C to fold the aptamers. The selection media (2.1.5) was then removed from the cells and replaced with 8 mL of new selection media (2.1.5). The aptamers were added to the cells and selection media for selection for 45 minutes as determined by the pre-selection optimisation (methodology section 2.2.10.3 and 2.2.7). The cells were placed on ice with selection media (2.1.5) used to wash and pre-condition the cells; throughout the incubation and washes, all were kept on ice. During the incubation, the cells were regularly rocked to redistribute the media across their surface.

2.3.5 Bone marrow FACS aptamer selection

This protocol was carried out with the materials at 4 °C. Bone marrow cells were isolated using the methodology outlined in sections 2.3.1.1 and 2.3.1.2, taking cells after lymphoprep, and after MACS for characterisation. The MACS +ve fraction was treated labelled with anti-mouse IgM Alexafluor 488, and anti-human CD146 IgG antibodies as in Section 2.3.1.3. After washing to remove excess antibodies, the cells were centrifuged at 300x g for 5 minutes and the supernatant carefully removed. The cells were re-suspended in 8 mL selection media (2.1.5) and incubated for 10 minutes. During this incubation, the aptamer materials (4.439 µg) were added to folding media (2.1.6) in a 1:1 ratio. This mix was heated to 95 °C for 10 minutes, before it was rapidly cooled to 4 °C. The cells were again centrifuged at 300x g for 5 minutes, and the supernatant removed. The cells were resuspended in 8 mL selection media (2.1.5) and the aptamer materials added. This was placed on a roller for 45 minutes at 4 °C. During this incubation, the FACS machine was set up and the unlabelled cells were characterised to define positive and negative gates. After the 60 minute total incubation, the cells with aptamer material were washed by being centrifuged at 300x g for 5 minutes, before the supernatant was removed and replaced with 8 mL of selection media (2.1.5), this was incubated for 5 minutes. The cells were centrifuged at 300x g for 5 minutes and the media removed. The cells were resuspended in 8 mL of selection media (2.1.5). The cells were characterised and sorted to isolate the cells and bound aptamers of interest.

The separated cells and aptamer were then made up to 2400µL with DNase free water before amplification as 2.2.10.1 and subsequent processing (2.2.15).

2.3.6 Foetal cell isolation

Foetal femurs are used by the Bone and Joint group under the ethics approval Local REC number 296100. Before dissection of the foetal femur sample, 5 ml of alpha-MEM was added to a 20 mL universal tube. 5 mg/mL of collagenase B was added to the media. The media was mixed on a rotating mixer for 30 minutes. The media was filter sterilised using a 0.22 µm sterilising filter (Z227501, Sigma-Aldrich, UK). The femur was dissected, with careful removal of the soft tissues.

The remaining femur was dissected into small pieces and placed into a 6 well plate well to which the 5 mL of media with collagenase B was added. The dissected femur in collagenase B was incubated overnight at 37°C, 5% (v/v) CO_2. After incubation, the cell suspension was passed through a 70 µm cell strainer (402/031/604, VWR, UK). The cells were centrifuged at 800x g for 5 minutes. The supernatant was removed and the cells resuspended in 20 mL culture media (2.1.3). The cell suspension was placed into a T-175 culture flask and cultured for 3-4 days at 37°C, 5% (v/v) CO_2.

2.3.7 Foetal cell culture

The foetal bone marrow isolated cells were cultured in 20 mL culture media (2.1.3) in a T-175 flask, and passaged when reaching 70-80% confluence, usually after 3-4 days.

To passage the cells the culture media was removed, and the cells washed with 10 mL PBS. The PBS was removed. 1 mL 10x trypsin solution was added to 9 mL PBS. 2 mL of the 1x trypsin solution was applied for 5-10 minutes to ensure all cells were no longer attached to the surface or to one another. 8 mL culture media was added. The cell suspension was placed into a 50 mL falcon tube and pelleted by centrifugation (300x g for 4 minutes), the supernatant was removed, and the cells were resuspended in 10 mL culture media (2.1.3) and seeded at a 1 in 10 dilution in a new flask.

2.3.8 Foetal cell seeding for selection

When foetal cells were required for selection, cells were passaged, and seeded into a T-75 flask with 20 mL culture media (2.1.3) at 20,000 cells per cm^2 for selection in 3 days, 15,000 cells per cm^2 for selection in 4 days, or 10,000 cells per cm^2 for selection in 5 days. After the indicated number of days, the cells were at 80-90% confluence and suitable for selection purposes. The cells used in each round of selection are summarised in Table 2-3

Sample	Passage	Selection round
14017 CS23	P1	1
14017 CS23	P2	2
14017 CS23	P3	3
14046 17 PCW	P1	4
14046 17 PCW	P2	5

Table 2-3 - Sample name and age, passage and the round of selection the sample was used for. Carefully seeding and culturing the foetal cells it was possible to ensure that few samples were needed for the selection to be completed. Using only 2 samples, and a maximum of Passage 3 used 5 rounds of selection was completed.

2.3.9 Foetal cell aptamer selection

The selection method for the foetal cells was identical to the bone marrow selection without FACS. It was performed at 4 °C to prevent aptamer uptake. The confluent cells were taken and culture media (2.1.3) was removed, and 8 mL replaced with selection media 2.1.5). This was incubated for 10 minutes. During this incubation, the aptamer materials (4.439 µg) were added to folding media (2.1.6) in a 1:1 ratio. The aptamer materials were heated to 95 °C for 10 minutes before being rapidly cooled to 4 °C. The selection media was removed from the cells and replaced with 8 mL of new selection media (2.1.5) and the aptamer materials were added additionally. This was incubated with occasional agitation for 60 minutes. The media was removed and replaced with 8 mL of new selection media (2.1.5) and incubated for 5 minutes. The media was removed and replaced with 2400 µL of DNase free water. The cells were scraped and used as a template for amplification and further rounds of selection.

2.4 Human skeletal stem cell enrichment

2.4.1 STRO-1 MACS

MACS was performed as described in 2.3.1.1 and 2.3.1.2

2.4.2 Bone marrow cell FACS

FACS was performed as described in 2.3.1.3 and 2.3.1.4.

2.4.3 CFU-F assay of sorted bone marrow cells

Selected cells from the FACS analysis were isolated and placed individually into a well of a 96 well plate with 300 µL culture media with 20% FCS rather than the usual 10%, this was done with 10 cells per well. The cells were cultured for a week in alpha-MEM supplemented with 20% FCS before the media was changed, and cultured for another 7 days. The samples used for this analysis are summarised in The media was removed from the wells, washed with PBS and fixed in cold 95% ethanol for 10 minutes in a cold room. The ethanol was removed. The well plates were assessed for colony growth using a light microscope; counting each visibly unique colony present allows for the purity of the cell population isolated using the FACS to be assessed, with higher purities of SSCs having much higher colony counts.

Sample (sex and age)	Osteoporotic/Osteoarthritic
M67	Osteoarthritic
F56	Osteoarthritic
F72	Osteoarthritic

Table 2-4 - Samples used for CFU-F assessment of combinations of STRO-1 and CD146 FACS isolation. Using combinations of two markers and FACS five conditions were assessed for the highest CFU-F across several samples.

2.4.4 Single-cell RNA-sequencing (Drop-Seq)

The bone marrow cells from sample ‘F47’ were sorted by MACS based on the STRO-1 antibody, and subsequently sorted by FACS gating for only the CD146+and STRO-1+ cells.

The STRO-1+ CD146+ cells were then taken by Patrick Stumpf and separated into droplets with ‘Macosko’ beads for RNA binding (CSO-2011, Chemgenes, USA). While the cells were being prepared for Drop-Seq, the cell sorting for CFU-F assessment was continued.

To generate single-cell RNA-sequencing data, the original Drop-Seq methodology developed by Macosko et al. 2015 and their detailed written protocol available from the MacCaroll lab (www.dropseq.org) were followed closely.

Once the cells were isolated by FACS, droplets were then disrupted by removing an oil layer, 30 mL of 6x concentration saline-sodium citrate (6x SSC) (0.9 M NaCl2 and 0.09 M sodium citrate (BP327-500, FisherScientific, UK)) was then added and 1 mL Perfluorooctanol (PFO) (370533-25G, Merck, UK) before the tube was shaken 4 times forcefully. The tube was then centrifuged at 1000 g for 1 minute. The top layer was carefully removed and discarded, this was followed by the addition of 30 mL of 6x SSC. The oil was allowed to settle before the supernatant was removed to another tube avoiding oil transfer.

The new tube was centrifuged at 1000 g for 1 minute and all but 1 mL of the supernatant removed. The remaining 1 mL was agitated to suspend the beads. The suspension was transferred to an Eppendorf tube before being 1000 g for 1 min and the supernatant removed and discarded.

The beads were washed twice with 1 mL 6x SSC centrifuging between each wash to retain the beads, once with 300 µL 5x RT buffer. The buffer was removed carefully. To the remaining beads 200 µL of RT mix was added (75 µl H2O, 40 µL Maxima 5x RT buffer (EP0741, ThermoFisher, UK), 40 µL 20% Ficol PM-400 (F4375-25G, Merck, UK), 20 µL 10 mM dNTPs (4030, Clonetech), 5 µL RNase inhibitor (30281-1, Lucigen), 10 µL 50 µM Template switch oligo (AAGCAGTGGTATCAACGCAGAGTGAATrGrGrG), 10 µL Maxima H- RTase (EP0741, ThermoFisher, UK)). The mix was incubated at room temperature for

30 minutes and agitated gently, followed by incubation at 42 °C for a further 90 minutes with gentle agitation.

After 90 minutes the reaction was stopped by washing the beads with 1 mL TE-SDS (10 mM Tris pH 8.0, 1 mM EDTA, and 0.5% SDS). The beads were washed with 1 mL TE-TW (10 mM Tris pH 8.0, 1 mM EDTA, and 0.01% Tween-20). Exonuclease I digestion was performed to remove the unused primer from the reaction, by washing with 1 mL 1 mL 10 mM Tris pH 8.0, before removing the supernatant carefully without removing the beads. To the beads 20 uL 10x Exo I buffer, 170 uL H2O, and 10 uL Exo I was added and mixed. The mixture was incubated at 37 °C for 30 minutes. The beads were washed with 1 mL TE-SDS, twice with 1 mL TE-TW and finally with 1mL water.

After the water wash, the supernatant was removed, 1 mL of water was added and the beads resuspended. 20 µL of the bead suspension was taken and counted by placing 20 µL of the suspension into a haemocytometer. 2000 beads were aliquoted into each PCR tube, the supernatant removed and 24.6 µL H2O, 0.4 µL 100 µM SMART PCR PRIMER (AAGCAGTGGTATCAACGCAGAGT), and 25 µL 2x Kapa HiFi Hotstart Readymix (KK2601, Roche, UK) was added. The suspension was mixed before PCR was performed with the following programme:

95 °C for 3 minutes, 4 cycles of 98 °C for 20 seconds, 65 °C for 45 seconds, 72 °C for 3 minutes, 13 cycles of 98 °C for 20 seconds, 67 for 20 seconds, 72 for 3 minutes, then final extension at 72 °C for 5 minutes followed by 4 °C hold.

Purification was performed by adding 30 µL of room temperature AMPure XP beads (A63881, Beckman Coulter, UK) to each PCR tube. The samples were agitated for 5 minutes before magnetically separated and washed 2 times with 200 µL 70% ethanol and eluted in 10 µL of H2O.

The sample was run on a BioAnalyzer (Agilent) to assess purity and size of the cDNA libraries; followed by the incorporation of the sequencing adapters using the Nextera XT kit (Illumina). The thermocycler was heated to 55 °C. For each sample, 600 pg of purified cDNA was made up to 5 µL in H2O. To each sample 10 µL of Nextera TD buffer (FC-121-1031, Illumina), 5 µL Amplicon Tagment enzyme (FC-121-1031, Illumina) was added before the samples were mixed and

incubated at 55 °C for 5 minutes. Subsequently, 5 µL of neutralisation buffer was added and mixed, incubated at room temperature for 5 minutes. To each sample 15 µL Nextera PCR mix (FC-121-1031, Illumina), 8 µL H2O, 1 µL 10 µM New-P5-SMART PCR hybrid oligo (AATGATACGGCGACCACCGAGATCTACACGCCTGTCCGCGGAAGCAGTG GTATCAACGCAGAGT* A*C), and 1 µL 10µM Nextera N70X oligo (FC-121-1031, Illumina) was added.

To tag the fragmented library with the custom read 1 annealing site and the read 1 indices Nextera N70X, PCR was performed with the following programme:

95 °C for 30 seconds, 12 cycles of 95 °C for 10 seconds, 55 °C for 30 seconds, and 72 °C for 30 seconds. Then 72 °C for 5 minutes and finally 4°C hold.

Purification was performed by adding 30 µL of room temperature AMPure XP beads to each PCR tube. The samples were agitated for 5 minutes before magnetically separated and washed 2 times with 200 µL 70% ethanol and eluted in 10 µL of H2O.

The sample was run on the BioAnalyzer (Agilent) to assess quality followed by being assessed and run on a MiSeq next-generation sequencer. The RAW data was tagged with individual cell tags and individual protein tags. Excess tags from the tagmentation and poly A tails were removed. The remaining sequences were aligned to the human genome to identify genes which were associated with each of the sequences.

2.4.5 Analysis of the Drop-Seq data

Analysis of the Drop-Seq data was performed with a slightly altered pipeline, which is described in detail by Satija Labs (https://satijalab.org/seurat/pbmc3k_tutorial.html).

The data were first filtered to remove cells with unique gene counts over 2500 or less than 200, before being log normalised with a scale factor of 10,000. The data was regressed, based on the nUMI but not mitochondrial genes (percent.mito) as this reduces the impact of some cell types which may be within the analysis.

Principal Components (PC) were generated using Principal Component Analysis (PCA) (runPCA) within R. The PCs were assessed as to which should be used in further analysis. Jackstraw plots suggested that the first 11 PCs should be used with significance, the elbow plot suggested the first 2 PCs should be used being much higher significance than other PCs, and assessment of the heat maps from each PC suggested the first 3 should be used. For cluster identification, a resolution of 1.7 using the PC 1 to 3 was used to find the clusters and visualise them on the t-Distributed Stochastic Neighbour (tSNE) plot.

2 markers from each cluster were identified using the 'bimod' statistical test. The 'bimod' statistical filtering was also applied when determining the genes of significance within a cluster, rather than the default Wilcoxon rank sum test. With the resultant genes and STRO-1 and CD146, each was overlaid on the TSNE plot to identify the gene expression location within the clustering of the genes. Using the genes as population signifiers, the groups of clusters were identified and labelled.

2.5 Statistics

qPCR experiments were run in triplicate, data shown as mean CT values, with bars representing standard deviation. For the Drop-Seq analysis the statistical filtering methods 'bimod' found within the Seurat analysis application for R (McDavid et al., 2013), a test specifically designed to aid in single cell expression analysis, allowed for single cell expressions to be assessed for quality of data, and testing of differential expression.

Chapter 3 Aptamer selection against the skeletal cell line SAOS-2: Protocol and selection technique development

3.1 Introduction

Aptamer selections can be used for a host of different applications as discussed in Chapter 1, including applications within the area of biomarker discovery. Utilising the potential of aptamers to bind to unknown targets on the surface of cell populations allows for a set of molecules to be isolated that are specific to the target population (Berezovski et al., 2008). Aptamer approaches for the identification of novel markers are particularly attractive in the area of skeletal stem cell enrichment and isolation, as previously outlined (1.4.8.4), given the current limitations in available markers for skeletal stem cell identification. A key strength of aptamer selection is the ability for aptamers to be selected against targets in a hypothesis-free manner, allowing novel markers to be discovered. Thus aptamers and aptamer-based biomarker discovery methodologies present an exciting opportunity to enhance current isolation procedures to improve skeletal stem cell enrichment.

Aptamer selection is a complicated, multi-staged process (with a number of protocols enrolled within), and optimisation of the selection procedure is necessary to ensure that the entire process can run to completion. Identifying the experimental design, the necessary quality control steps, and optimising these into a single comprehensive work plan requires rigorous standardisation of protocols and sample handling techniques.

Developing a complex protocol using skeletal stem cells, which vary from patient to patient (and are a limited resource), would be a suboptimal approach. Using primary cells as the materials to optimise against would be a poor choice as many variables are added each time a new patient sample is used, and several different

cell types are present. In order to provide consistency, a stable cell line similar enough to cells found in bone marrow should be used to optimise methods in the early rounds of selection, to be applied to later selection rounds against primary sources of skeletal stem cells.

The SAOS-2 cell line, a human osteosarcoma cell line, has comparable morphology, and similar expression phenotype, to a mature human osteoblast cells (Rifas et al., 1994, Togari et al., 1997). The cell line's attributes include some of the common stem cell markers (Guillot et al., 2007) and di-electrophoretic properties of known enriched (STRO-1) bone marrow cells (Ismail et al., 2015).

Another viable option for this project is the MG-63 cell line, another human osteosarcoma cell line. The MG-63 present a less differentiated cell population in comparison to the SAOS-2 cell line, more similar to that of an osteoprogenitor. These differences in the differentiation stage do not affect the di-electrophoretic properties greatly and have a similar profile to the STRO-1 enriched cells (Ismail et al., 2015). However, the more stem-like characteristic also provides an issue with aptamer selection. Because the MG-63 are less differentiated, once cultured above 70% flask confluence the cells begin to differentiate. As culture flasks are treated (usually by charging the surface slightly) to allow cells to be cultured on the surface, areas of flasks exposed during a selection may bind the aptamers. This unspecific binding can cause aptamers to be retained during selections which are not cell specific. The differentiation is not guaranteed to be an issue with the selection but may have caused inconsistencies between rounds of selection.

A previous study carried out in another collaboration between the University of Southampton and Aptamer Solutions Ltd. used the MG-63 cells as a positive target and the Raji cell line as a negative cell line. This project ended with selection failure due to primer dimers being formed, creating a laddering effect when visualised using PAGE. Since that project new primers were designed and provided for this project. Therefore, for this study, the SAOS-2 cell line was chosen as a bone marrow substitute to enable optimisation of the aptamer selection methodology, due to its ease of culturing and stability at higher confluences.

In addition to the positive selection against the SAOS-2, utilising a negative selection population removes aptamers which bind to markers that are common between cell populations (as well as those which are non-specific), thereby enriching for more cell-specific aptamers. To this end, the Raji cell line was chosen as a negative selection target as it is non-adherent, lacks expression of the STRO-1 antigen (used in enriching for the SSC population (Gothard et al., 2014)), and lacks typical skeletal progenitor markers. On top of these features, previous experience from another aptamer selection with the cells enabled faster integration of the cells into another aptamer selection, therefore with advice from Aptamer Solutions Ltd. to limit the changes between previous selection the Raji cell line was chosen as the negative selection target.

The cell selection process is an iterative method, which consists of: i) selection phase, ii) amplification phase, and iii) purification phase. With the use of two cell lines, there are two selection phases sequentially, which adds to the complexity of the identification of the aptamers (Figure 3-1).

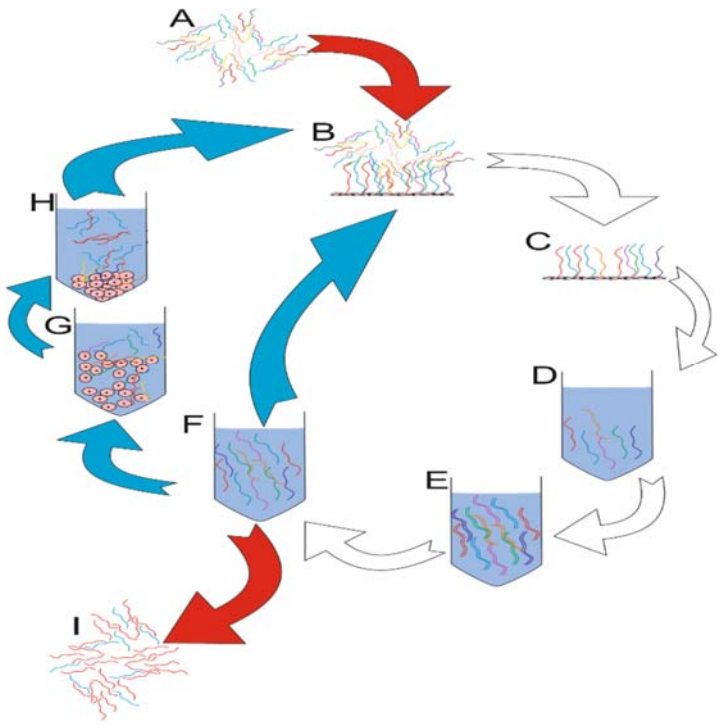

Figure 3-1 - SELEX diagram for selection including negative cell target. Red arrows are beginning (top – initial library introduction to selection conditions) and end (bottom – final aptamer pool) points. Blue arrows show two alternative routes, with negative selection (left), and positive selection only (middle). White arrows are necessary for each round of selection. A) The initial aptamer pool of 1 x 10^{14} molecules. B) Initial and positive selection conditions against the SAOS-2 cell line. C) Washing and removal of the unbound aptamers. D) Recovery of the bound aptamers. E) Amplification of recovered aptamers. F) Removal of the antisense/reverse DNA strands to leave ssDNA. G) Negative selection against the Raji cell line. H) Pelleting of the Raji cells and removal of the unbound aptamers to the positive selection against the SAOS-2 cells. I) The final aptamer pool after multiple rounds of selection.

By incubating the aptamer pool with the Raji cells first, then moving the unbound aptamers onto the positive cells to be further incubated, aptamers which bind to proteins which are not shared between the cell types are selected for, hence narrowing the aptamer pool. This serves to generate aptamer populations that are more specific for the SAOS-2 cell line.

3.2 Hypothesis and aims

3.2.1 Hypothesis

Aptamer technology can be used to generate molecules, which bind specifically to the bone-derived osteosarcoma cell line SAOS-2, and these molecules subsequently can be used for the identification of cell-specific markers.

3.2.2 Aims

1. To develop a robust protocol for aptamer selection using an osteogenic cell line (SAOS-2 cells) and a non-osteogenic cell line (Raji) as a negative selection population.
2. To identify optimal binding conditions for aptamer selection against the SAOS-2 and Raji cell lines.
3. To raise aptamers against the SAOS-2 cell line, while ensuring limited binding to the Raji cell line.
4. To generate single sequence aptamers using cloning and testing of affinity to identify a selection of the optimum aptamers.

3.3 Methodology

The methods used in this chapter are detailed in section 2.2.

The methods follow a workflow for the selection (Figure 3-1), and where methods are referred to links to the methodology are provided.

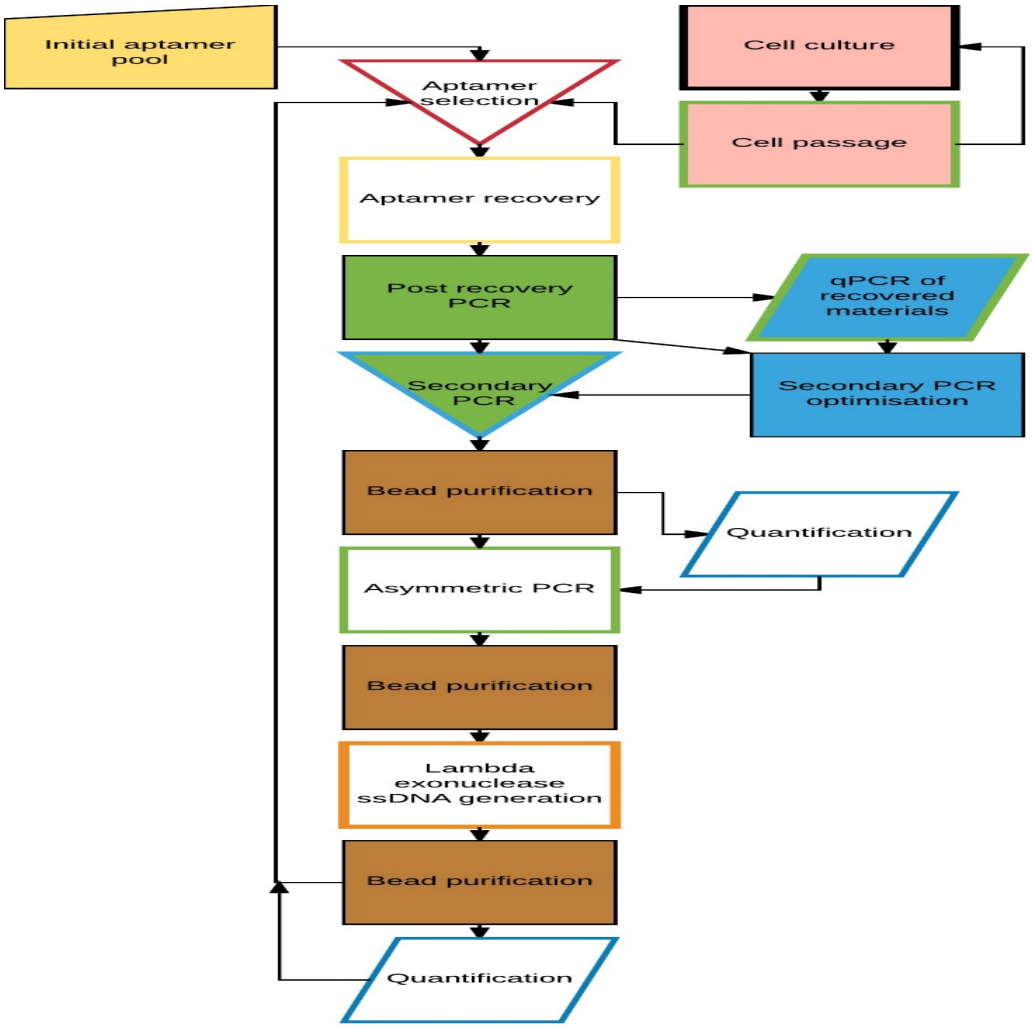

Figure 3-2 - Aptamer Selection workflow highlighting the steps necessary for each round of selection. Cell culture is a cyclical process external to the aptamer selection (seen top right, with the pink boxes) This was performed on a needs basis where cells were grown as needed for the selections For this 20,000 cells / cm^2 were placed in T-75 flasks 3 days before being needed for selection. One other input is required for the selection, the initial aptamer pool (top left) a $1x10^{14}$ unique ssDNA sequences to be tested against the target. The remaining steps are carried out in order, throughout the cycles. Green boxes are PCR stages. Blue boxes are quantification stages, filled in stages are qPCR and a cycle course PCR to determine optimal template levels for the second PCR. Blue outlined boxes are quantification using the Nanodrop 1000. Brown boxes are nucleic acid purification steps using the solid phase reversible immobilisation. Green outlined box is an asymmetric PCR facilitating the generation of ssDNA from dsDNA template. Orange outlined box is the enzymatic digestion stage where any remaining dsDNA is digested into ssDNA.

3.4 Results

3.4.1 Pre-selection optimisation

The first round of selection is essential within any aptamer selection process, as optimising the initial selection conditions generates the highest recovery of aptamer sequences and therefore greatest structural diversity. Therefore, a careful balance of stringency to narrow the pool and use of protocols to ensure recovery of all sequences that bind to the target is necessary.

3.4.1.1 The electrophoretic properties of aptamers

Initial work centred on an understanding of the gel-electrophoretic properties of the aptamer pool in the various states throughout selection and amplification processes. The first step was to determine the most appropriate qualitative method to assess aptamer state and purity. Two commonly used gel types were compared: polyacrylamide (10%), and agarose (4%), determining which method was more appropriate for the analysis of the DNA (80 bp in length). The gels varied in both setup and running conditions: the agarose was run at 150 V for 50 minutes, while acrylamide was run at 200 V for 30 minutes (Figure 3-3).

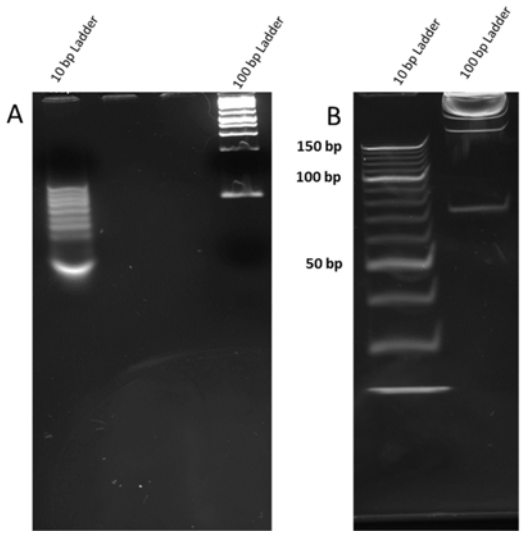

Figure 3-3 - Comparison of 10% polyacrylamide gel and 4% agarose for gel electrophoresis analysis of nucleic acids. (A) 4% agarose gel did not resolve either ladder, making the determining size of any samples extremely impractical. (B) 10% acrylamide gel resolved the 10 bp ladder to a point where each band is separated and would allow for accurate determination of sample size. The 100 bp ladder was not resolved within the 30-minute run time but would have been a less practical ladder for determining the size of aptamer products.

The 10% polyacrylamide gel provided suitable resolution of the 10 bp ladder (Figure 3-3). The 4% agarose gel failed to resolve either of the ladders over the 50-minute runtime (Figure 3-3 A); thus, to provide better resolution of the ladders, the gel would need to be run for a more extended period, making the qualitative tests on agarose gel very time-consuming. In contrast, the 10% acrylamide gel resolved the 10bp ladder in 30 minutes (Figure 3-3 B). The 10 bp ladder provided suitable range and clarity for QC checks of aptamer size throughout the selection, with the ladder ranging from much longer DNA strands to the length of primers. After this test, polyacrylamide gel electrophoresis (PAGE), with 10% polyacrylamide gel and run at 200 v for 30 minutes, was used for all aptamer quality checks, with the benefit of a quick resolution of materials between 10 and 150 bp.

Throughout the selection process, aptamers were present in one of two states, ssDNA or dsDNA; with an intermediary partially dsDNA (incomplete digestions).

Once the running conditions for the ladder had been established, assessment of the aptamer states throughout a selection process was assessed. ssDNA was added to the PCR buffer and then split into three reactions. The first contained the only ssDNA and was not treated; the second primers were added; the mixture was then heated to 95 °C then cooled to 4 °C and the third had primers added; one cycle of PCR was performed to generate the second strand (forming dsDNA). All three conditions were assessed using a 10% polyacrylamide gel (Figure 3-4).

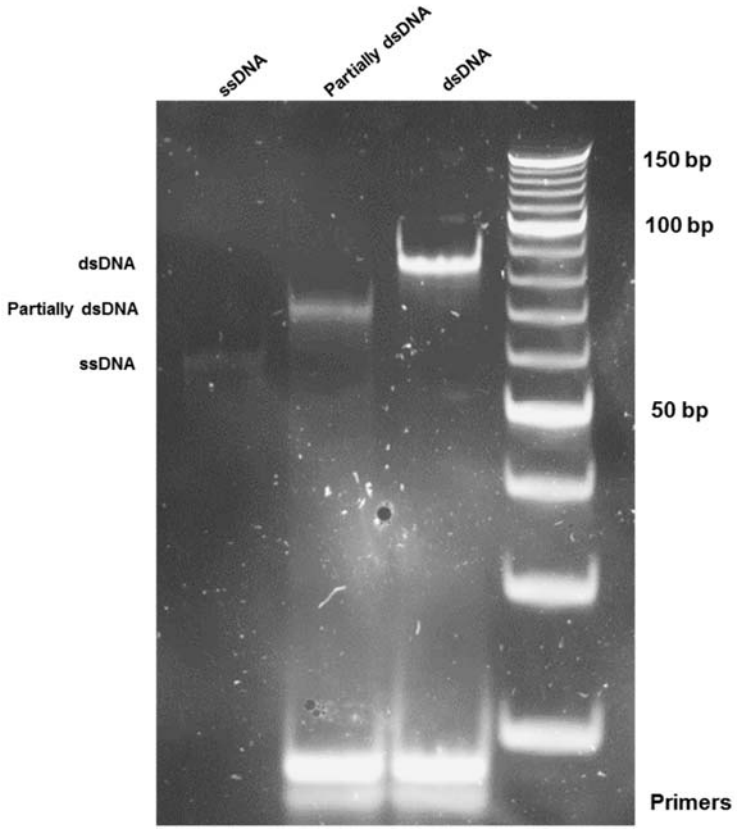

Figure 3-4 - The amplification states of the aptamer determined the apparent size on a polyacrylamide gel. From left to right lanes: lane 1 single-stranded DNA, lane 2 partially double-stranded DNA (ssDNA with primers annealed), lane 3 dsDNA generated with PCR. Each band of the ladder is 10 bp with the brightest bands being the 50, 100 and 150 bp.

Unmodified ssDNA was shown to run at ~60 bp in length (relative to the dsDNA ladder) given the single-stranded nature. Once primers were annealed to the ssDNA (and thus partially double-stranded for 21 bases), the aptamer showed an apparent increase in size to ~70 bp, and a higher fluorescent signal was observed. The dsDNA was shown to run at just above 80 bp, and an additional increase in fluorescent signal was observed. All reactions contained approximately the same number of moles of aptamer. The observed difference in fluorescent signal is due to available sites for Gel Red to intercalate with the molecules. Gel Red does not intercalate into ssDNA as well as dsDNA; hence the difference in band intensity between ssDNA, primer hybridised ssDNA and dsDNA.

Testing of the aptamer states provided insight into the expected band pattern and how the different states appear when analysed on a 10% acrylamide gel, as well demonstrating clear differentiation between the apparent size of the aptamers when it is ss, partially ds, and dsDNA.

3.4.1.2 Testing of nucleic acid purification methods

Streptavidin bead purification utilises the biotin/streptavidin interaction to remove the nucleic acids from buffers, PCR reagents etc., by modifying the second strand of DNA with a reverse biotin primer. The biotin on the modified aptamers binds to the streptavidin on the magnetic beads. Adding 0.5 M NaOH solution to the beads, denatures the dsDNA, leaving the biotin modified second strand on the beads and releasing the first strand into solution. The supernatant and ssDNA was then removed and neutralised using 0.5 M HCl.

The solid phase reversible immobilisation (SPRI) method uses high salts and crowding agents to ‘drive’ nucleic acids onto the beads. These can then be washed and eluted in low salt aqueous solution. The beads were washed in 80% ethanol to remove smaller nucleic acids, enzymes, and salts. The beads were then placed in DNase free water, which eluted the nucleic acids from the beads as the hydrophilic environment allows the nucleic acids to be released from the beads. Lambda Exonuclease was used to digest PO_4 labelled DNA strands.

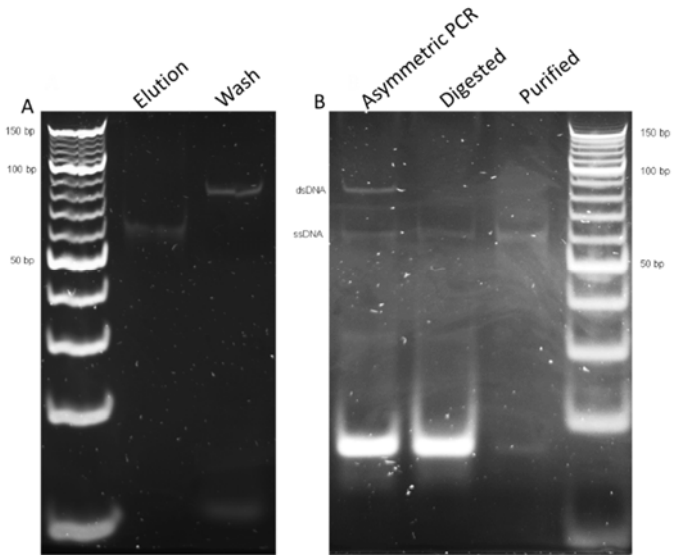

Figure 3-5 - Comparison of nucleic acid bead purification methods. A) Streptavidin bead purification. Wash showed incomplete binding of nucleic acids as materials remained in the wash; despite incomplete binding elution showed nucleic acids at 60 bp, which as previously shown is ssDNA. B) Showed the SPRI purification process, from left to right: Asymmetric PCR showed the generation of ssDNA from dsDNA template, Lambda Exonuclease then digested the PO_4 modified strand leaving the only ssDNA, and finally purification of the ssDNA using the SPRI purification process. The ladder used was a 10 bp ladder, brighter bands are seen at 50, 100, and 150 bp.

Comparison of the two methods showed the biotin and streptavidin bead method facilitated more specific purification (no primer remained), although a lower percentage recovery was noted as not all the material was bound (Figure 3-5 A). The SPRI method was a faster purification but recovered materials in addition to the aptamers, including the primers (Figure 3-5 B), where the biotin/streptavidin method did not. Ultimately, the SPRI methodology was more cost-effective in both time and materials, despite having to incorporate a purification, digestion, purification methodology to ensure only aptamers remain.

3.4.1.3 Selection buffer testing and optimisation

With PCR and purification methods established; selection conditions were determined to maximise aptamer binding, and therefore recovery in Round 1 of selection. Salt concentrations in the buffer change aptamer functionality and thus, identifying an optimal salt concentration (similar to physiological conditions) would allow for aptamer selection against the cells, in a non-damaging environment. To facilitate cell survival during the selection process, physiological levels of salt were tested for selection conditions. 0x (no supplemented salts), 1x (physiological levels of some salts), and 10x (excess in physiological levels of supplemented salts) approximations of physiological levels of salts supplemented into the alpha-MEM culture media were examined (salts detailed in Methods 2.1.7 and 2.1.9). The aptamers were then incubated with the SAOS-2 cells for 20, 40, or 60 minutes with either 0x, 1x, or 10x supplemented buffer, in either T25 or T75 cell number equivalents. These were all washed once before the cells and aptamers were recovered. The recovered materials were then amplified and assessed by qPCR for the CT values indicating the highest levels of recovery (Figure 3-6).

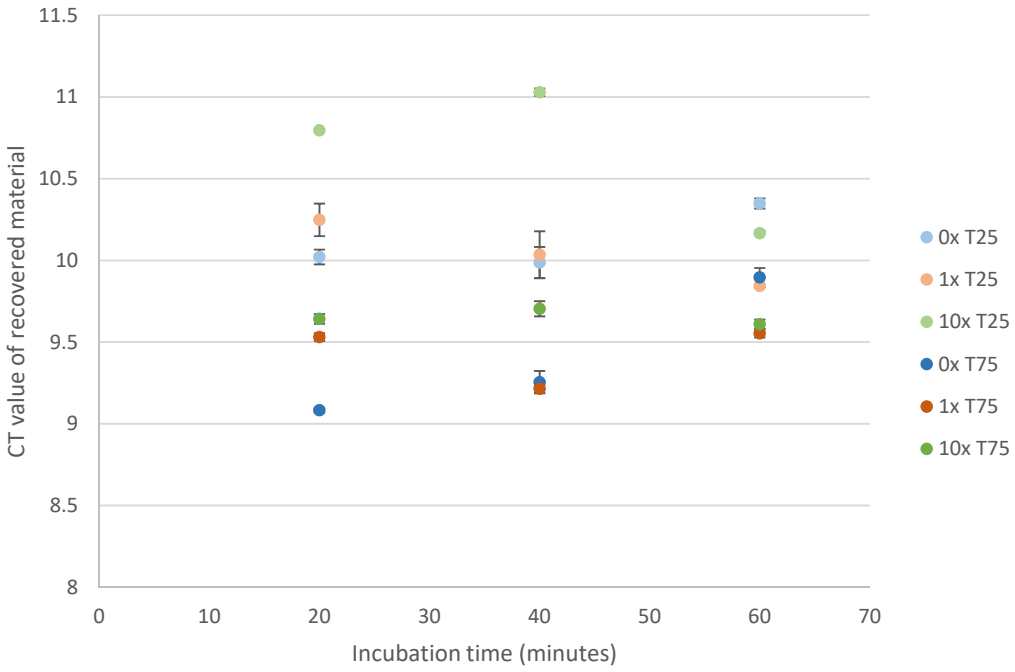

Figure 3-6 - qPCR analysis of recovered aptamers to identify optimum binding conditions for selection. The lowest CT values and therefore highest material recovery was from 0x T-75 for 20 minutes with a CT value of 9.08, closely followed by 1x T-75 for 40 minutes with a CT value of 9.21. Bars show standard deviation calculated by the qPCR software, replicates n = 3.

The highest recovery (lowest CT) was observed using 0x salt, T-75 flask for 20 minutes (Figure 3-6). Despite the highest recovery, the 0x salt conditions were not ideal for aptamer structure formation (1.4.2) or charge masking due to the lack of salts. Without this charge masking, unspecific charge-based attraction and binding may have occurred, increasing recovery. Therefore, the condition which provided the second highest recovery (second lowest CT) was selected: 1x salt, T-75 for 40 minutes of incubation. Although recovery was not as high, the selection media with additional salts provided an improved environment for folding and structure formation within the aptamers. The folding media was based on the selection media at 2x salt.

3.4.2 SAOS-2 First round of aptamer selection

The first round of selection is arguably the most critical of all the selection steps. At this stage, each aptamer sequence should only be represented once in the pool. If they are lost at this stage (due to poor selection conditions); there is no chance for them to be recovered later. Therefore, great care was taken to optimise the selection conditions to permit the greatest level of binding, with the highest levels of aptamer folding potential, and a recovery method which allowed for downstream processes to take place (3.4.1) (1x salts, T-75 of cells and incubated for 40 minutes). The recovered materials were amplified, and a proportion of that amplified material was tested using qPCR to quantify the total recovered aptamer against known standards. This was used as a method of tracking aptamer pool progression (Figure 3-7).

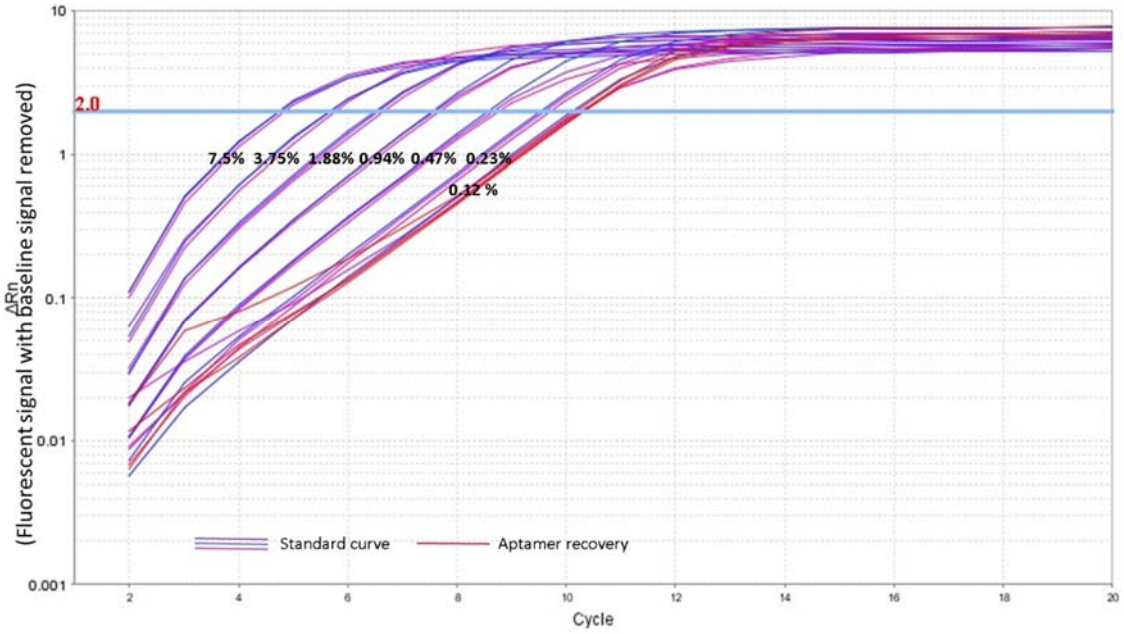

Figure 3-7 - qPCR analysis of recovered aptamers from the first round of selection and standards. The standard curve generated from multiple known DNA concentrations allowed for quantification of the recovered material. Blue lines show the standard curve (from left to right starting at 7.5% of the total aptamer material input into each selection; each subsequent collection of blue lines right of the first is reduced by half (3.75, 1.88, 0.94%, etc.). Red lines show recovered aptamer pool. n = 3 for each sample.

Delta Rn is the fluorescent signal generated from the DNA amplified normalised to the baseline Rn. The number of cycles represents how much amplification was needed to reach the threshold: the higher the number of cycles needed, the lower the amount of template present within the sample. The dark blue lines represent a standard curve (providing CT values for known quantities of nucleic acid), and the aptamers recovered from the first round of selection are shown in red. Figure 3-7 showed that the recovered material from the first round of selection was at the low end of the standard curve, and calculated to be ~0.1% of the material input. While the recovery of 0.1% of the input materials is low, with 1 in 1000 sequences being lost, there are still $1x10^{11}$ molecules recovered. No signal was generated from the no-template control (NTC), nor the cell-only control, therefore, all materials quantified were from aptamer origin and continuation of the aptamer selection was possible.

3.4.3 SAOS-2 aptamer selection Rounds 1-10

Once the first round of selection had been completed, the recovered materials required amplification, followed by purification to give a pool of ssDNA for the subsequent round. This included multiple steps and quality control throughout, as described in Chapter 2 (Figure 2-1).

While the CT values from the qPCR do not provide quantitative data without the corresponding standard curve, the CT values did provide a basis for amplification using a PCR cycle course. CT is the number of cycles of amplification undertaken to generate a fluorescent signal, which crosses a defined threshold: these cycles of amplification are carried out in similar conditions to conventional PCR. The similarity between the two reactions allowed for smaller cycle courses, as the CT of the sample gives an approximate number of cycles at which amplification maximum was reached. The smaller cycle courses were quicker to perform and required fewer materials than an expansive cycle course covering 1-20 cycles. The cycle course provided an optimal number of amplification cycles that generated the maximum amount of DNA possible before aberrant products were produced. Figure 3-7 shows the CT value was between 10 and 11. Thus, 11 was the base of this cycle course, and the cycles tested using gel electrophoresis were 10, 11, 12, 13, and 14, as the CT-2, CT-1, CT, CT+1, CT+2, and CT+3 are tested. The same amplified recovered materials were used as the template for the cycle course PCR (Figure 3-8).

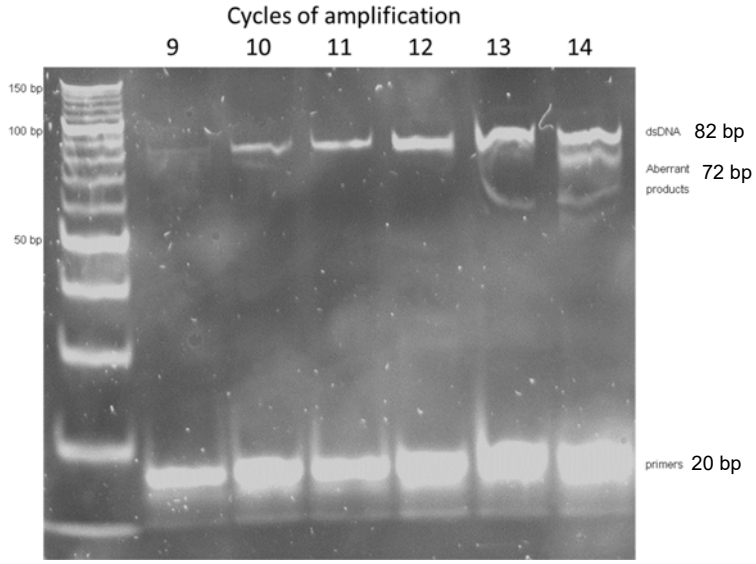

Figure 3-8 - PAGE analysis of an amplification cycle course using recovered aptamers from selection Round 1. As the number of amplification cycles increases, the amount of dsDNA increased. Additional bands are seen after 13 and 14 cycles of amplification. Strong primer bands are seen as the forward primer is fluorescently labelled. The ladder used was the 10 bp the brighter bands are 50, 100 and 150 bp.

Figure 3-8 showed that more dsDNA was generated with increasing cycle number. Aberrant products were observed at cycle 13 and 14 of the PCR cycle course. Aberrant products were likely due to mispriming events caused by primer mispriming. To prevent the desired materials being contaminated with these artefacts, a cycle number was selected before these aberrant materials were generated. Therefore, 12 cycles of amplification were chosen for the Round 1 recovered materials. Each round of aptamer selection required 4439 ng (1 x 1014 molecules at 82 bp) of single-stranded material. 4439 ng of ssDNA can only be produced by a large number of PCR reactions; therefore, sufficient dsDNA template was needed to seed these asymmetric reactions (2.292 ng of purified dsDNA per 50 µL reaction). The double-stranded DNA was purified using the SPRI purification method and quantified using the Nanodrop (Figure 3-9).

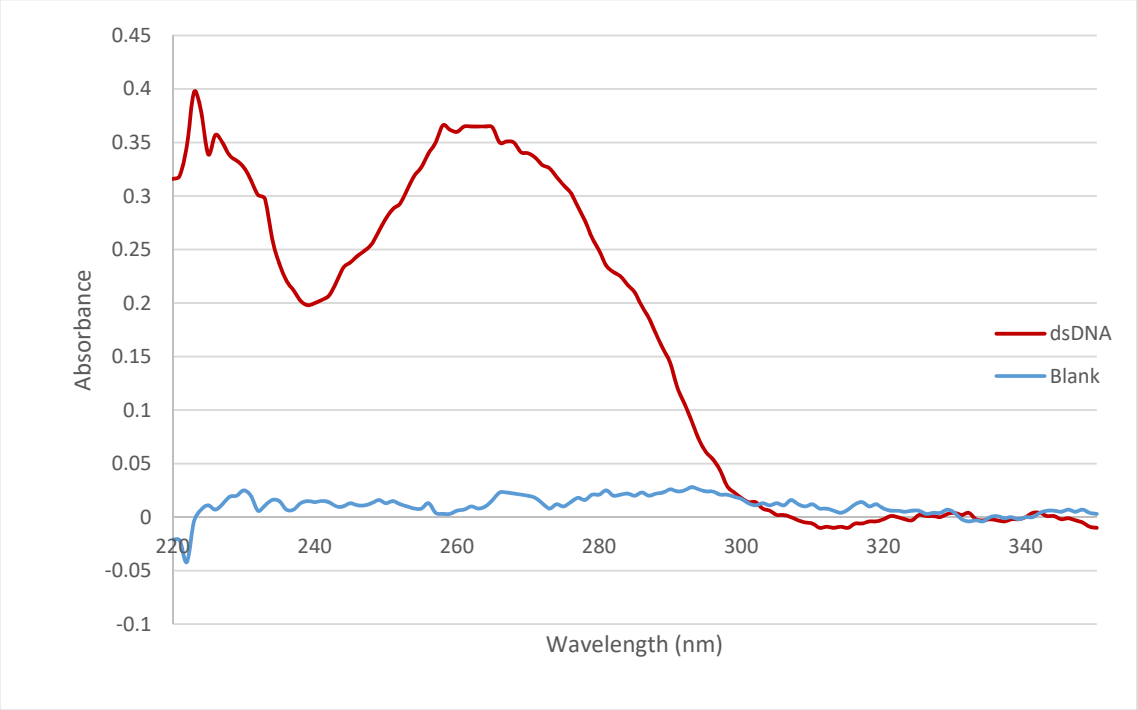

Figure 3-9 - Purified dsDNA generated from selection Round 1 was quantified using a Nanodrop. Nanodrop quantification of dsDNA purified from the secondary PCR. The blue data set is the measurement of absorbance using the blank (RNase free water). The red data set is that of the purified dsDNA.

The Nanodrop was blanked using RNase free water with analysis of absorbance over 220 nm to 350 nm. Values measured at 340 nm are set to zero by the software, and other points are moved to reflect this. Nucleic acids have an absorbance maximum at around 260 nm; while proteins absorb at 280 nm. Therefore, peaks and / or shoulders at 260 nm and 280 nm would suggest protein contamination of nucleic acids, and a single peak at 260 nm is pure nucleic acid. Figure 3-9 showed a flat baseline for the blank (red), and a peak at 260 nm from the recovered dsDNA. The dsDNA sample showed no peak at 280 nm, which would be caused by contaminating proteins. The dsDNA was quantified at 11.87 ng/µl.

Once quantified, the purified dsDNA was then used to seed Asymmetric PCR. Asymmetric PCR is a variant of PCR, which uses only one primer, or a highly limited second primer: in this case, as the forward strand is desired, only the

forward primer is added. The materials generated were then digested with Lambda Exonuclease to remove phosphorylated strands in a dsDNA complex. The digestion leaves only the fluorophore modified forward strand of the aptamer, and the primer. The ssDNA was then purified from the bases and enzymes used in previous steps and resuspended in RNase free water. The products of the Asymmetric PCR, digestion and final purification were then analysed by PAGE to ensure the process was completed successfully (Figure 3-10).

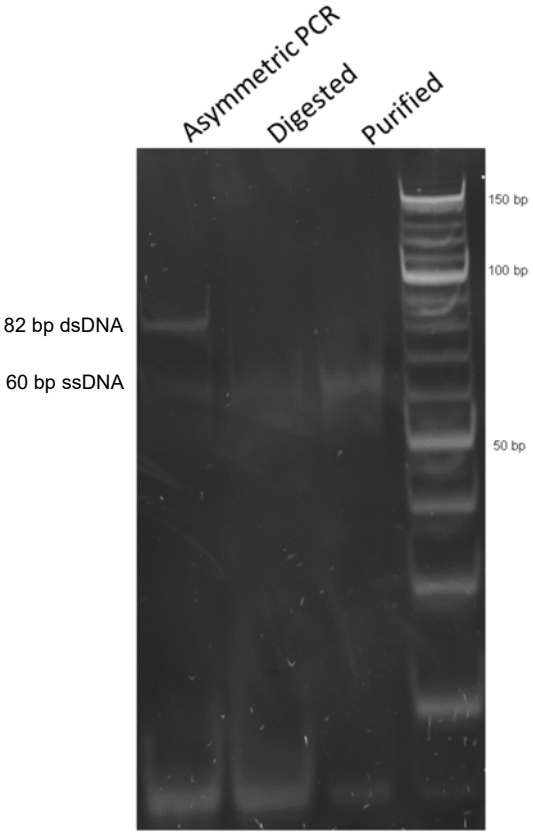

Figure 3-10 - Asymmetric PCR, Lambda Exonuclease digestion and purification of Round 1 aptamer materials. Asymmetric PCR showed the double-stranded template DNA remained at the expected 82 bp, while generating a second band of ssDNA at 60 bp (labelled Asymmetric PCR). The Asymmetric PCR product was then treated with Lambda Exonuclease (labelled digested), leaving only ssDNA and primers, evident by only one band at 60 bp and below 20 bp. The ssDNA was then purified (labelled purified) to remove primers and slightly concentrate the ssDNA, seen in the third lane. The ladder used was the 10 bp the brighter bands are 50, 100 and 150 bp.

The PAGE analysis of the various stages of ssDNA production verify that materials were generated and digested as expected, and that ssDNA was purified from the primers (Figure 3-10). The purified ssDNA was quantified using the Nanodrop (Figure 3-11).

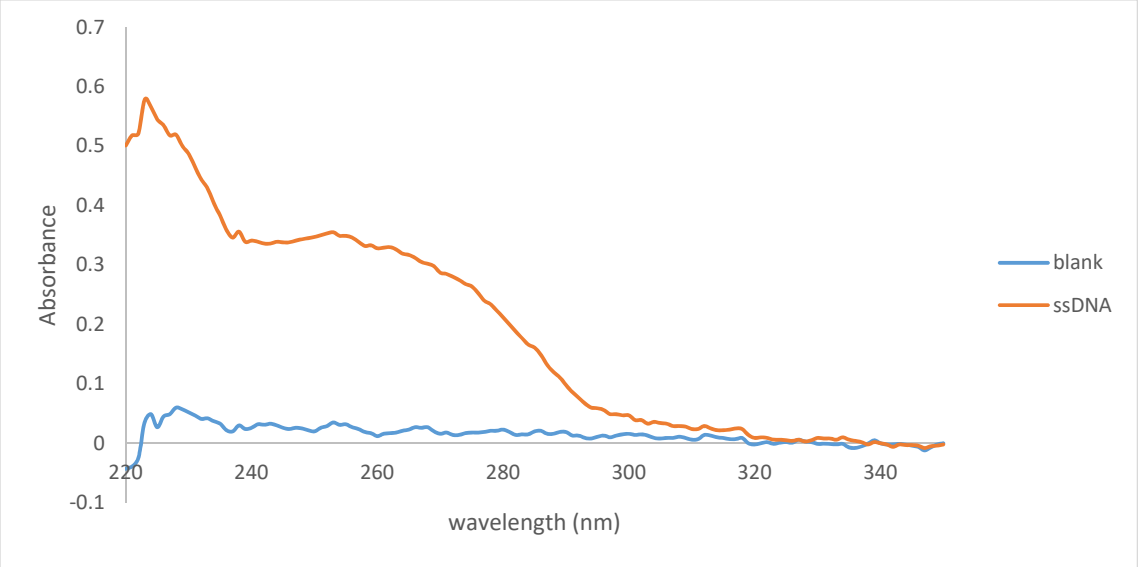

Figure 3-11 - Purified ssDNA prepared after selection Round 1 was quantified using a Nanodrop. Nanodrop quantification of blank (blue) shows no nucleic acid peak. ssDNA (orange).

The combination of Figure 3-10 and Figure 3-11 showed the digestion of dsDNA leaving only ssDNA and primer, followed by the removal of primers by purification (Figure 3-10). Subsequent quantification of the ssDNA using the Nanodrop (Figure 3-11) gives a concentration of 10.81 ng/µl. The concentration and volume of aptamer (480 µL) gives a total of 5188.8 ng of ssDNA. The required amount of ssDNA at each round is 4439 ng. Therefore, this round of the selection and amplification enabled the material to be taken to the second round of selection.

The amplification and single stranded DNA preparation steps outlined above, were repeated in every round of the selection, to ensure that all materials were amplified, purified, and quantified effectively. The gel images and spectra presented in this section are representative of data collected for every round of selection. In situations where errors occurred, materials were re-assessed and protocols repeated until the material passed the quality control steps.

Aptamer recovery was tracked in each round using qPCR (Figure 3-12), and the selection criteria adapted accordingly with recovery quantities. In this case, stringency for selection was increased when two consecutive rounds of selection showed increased recovery (indicated by a red line in Figure 3-12).

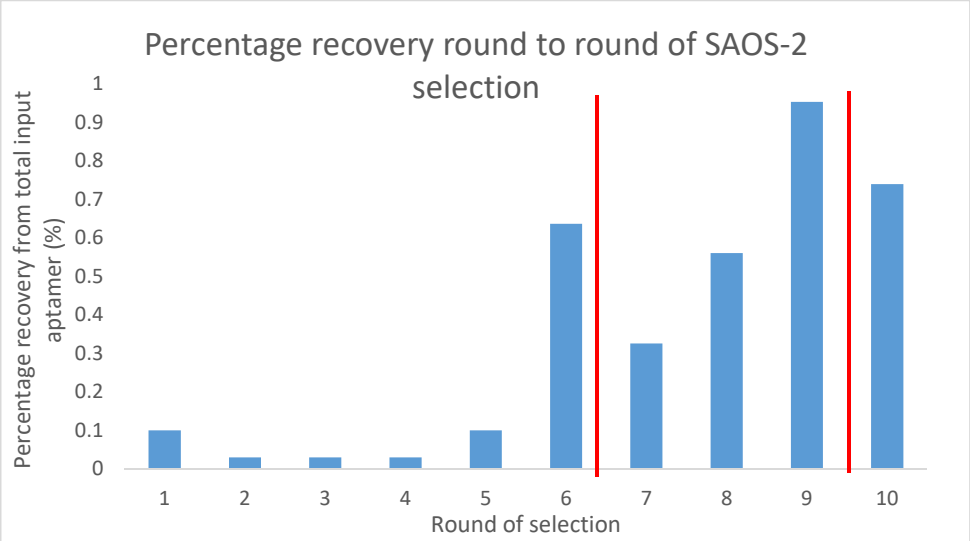

Figure 3-12 - Percentage of the aptamer pool recovered after each round of selection for Rounds 1 to 10. Increased recovery percentage round on round indicated that the aptamer pool was becoming enriched for binders to the SAOS-2 cell line. Red lines indicate where selection stringencies were increased. The percentage recovery was calculated based on known inputs and qPCR data (relative to known standards).

Quantification of the round-to-round enrichment progress allowed a gradual increase of selection stringency to take place to narrow the aptamer pool carefully, and thus increasing stringency only as needed. When two consecutive rounds of selection had shown an increased recovery, the stringency of the selection was increased (as shown in Table 3-1). Figure 3-12 shows tracking of the aptamer recovery from round to round, and highlights when stringency was increased (red lines). The first 5 rounds of selection demonstrated recovery of less than 0.1%, however, from Round 5 onwards recovery increased in all rounds where the stringency was not changed. After the stringency was increased, the recovered amount of aptamer showed an expected drop; but this increased again in the subsequent round of selection. Due to the first 5 rounds of selection provided low recovery, and limited increase observed, only 2 stringency changes were applied

to the selection within the first 10 rounds. The recovery peaked at 0.95% at Round 9, before stringency was increased for Round 10.

Round	Aptamer	Positive cells	Positive incubation time	Positive washes	Negative cells	Negative incubation time	Negative washes
1	4.439 µg	T-75 (approximately 5 x 106 cells)	45 minutes	1 x 8 mL, 5 minutes	none	N/A	N/A
2	4.439 µg	T-75	45 minutes	1 x 8 mL, 5 minutes	none	N/A	N/A
3	4.439 µg	T-75	45 minutes	1 x 8 mL, 5 minutes	None	N/A	N/A
4	4.439 µg	T-75	45 minutes	1 x 8 mL, 5 minutes	None	N/A	N/A
5	4.439 µg	T-75	45 minutes	1 x 8 mL, 5 minutes	None	N/A	N/A
6	4.439 µg	T-75	45 minutes	1 x 8 mL, 5 minutes	None	N/A	N/A
7	4.439 µg	T-75	45 minutes	2 x 8 mL, 5 minutes	None	N/A	N/A
8	4.439 µg	T-75	45 minutes	2 x 8 mL, 5 minutes	None	N/A	N/A
9	4.439 µg	T-75	45 minutes	2 x 8 mL, 5 minutes	None	N/A	N/A
10	4.439 µg	T-75	45 minutes	4 x 8 mL, 5 minutes	None	N/A	N/A

Table 3-1 - Selection conditions used for the first 10 rounds to identify SAOS-2-specific aptamers. Aptamer amount, cells and incubation time were maintained throughout the first 10 rounds of selection, with the washes being doubled at each stringency increase point (Rounds 7 and 10).

3.4.4 The divergence of the aptamer pool to test negative cell selection and the effect on the aptamer pool

Following the first 10 rounds of selection, the aptamer pool was amplified to generate more than 2 x10^{14} molecules and split into two identical aptamer pools. One of the pools was exposed to only the SAOS-2 cells with the same selection conditions as Round 11. The other pool was exposed to the counter selection Raji cell line for 30 minutes: the unbound aptamers in the selection media were recovered and then exposed to the SAOS-2 cells for 45 minutes. These parallel selections allowed for the aptamer pool from Round 10 to be assessed to determine whether counter selection against the Raji cells can be introduced at this late stage. Pre-incubation of the aptamer library with the Raji cell line (prior to incubation with the SAOS-2), will start to remove aptamers that bind to markers common between the two cell lines. If successful, this should improve the specificity of the aptamer population to the SAOS-2 cell line. The recovered materials from both selections were amplified and quantified using qPCR and compared to previous rounds of selection (Figure 3-14).

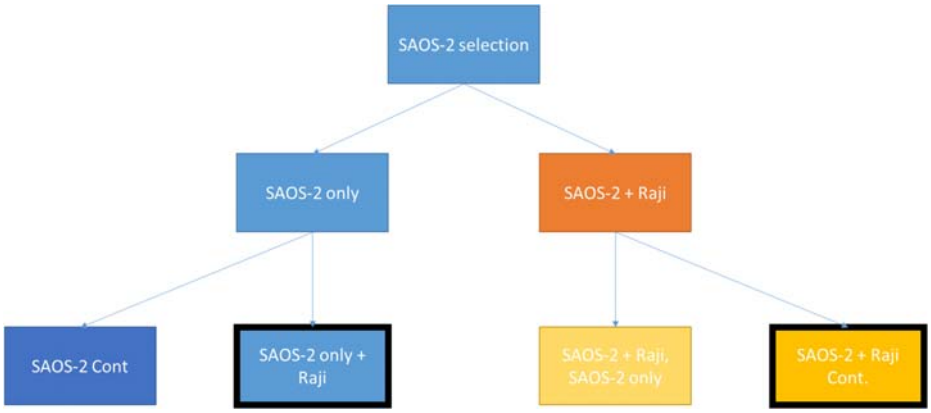

Figure 3-13 - Aptamer selection divergent points. The aptamer selection progresses with divergent points at round 11, and round 13. With the colours followed through to the selection recovery figures to facilitate following of the data and how the different conditions effected the aptamer pool.

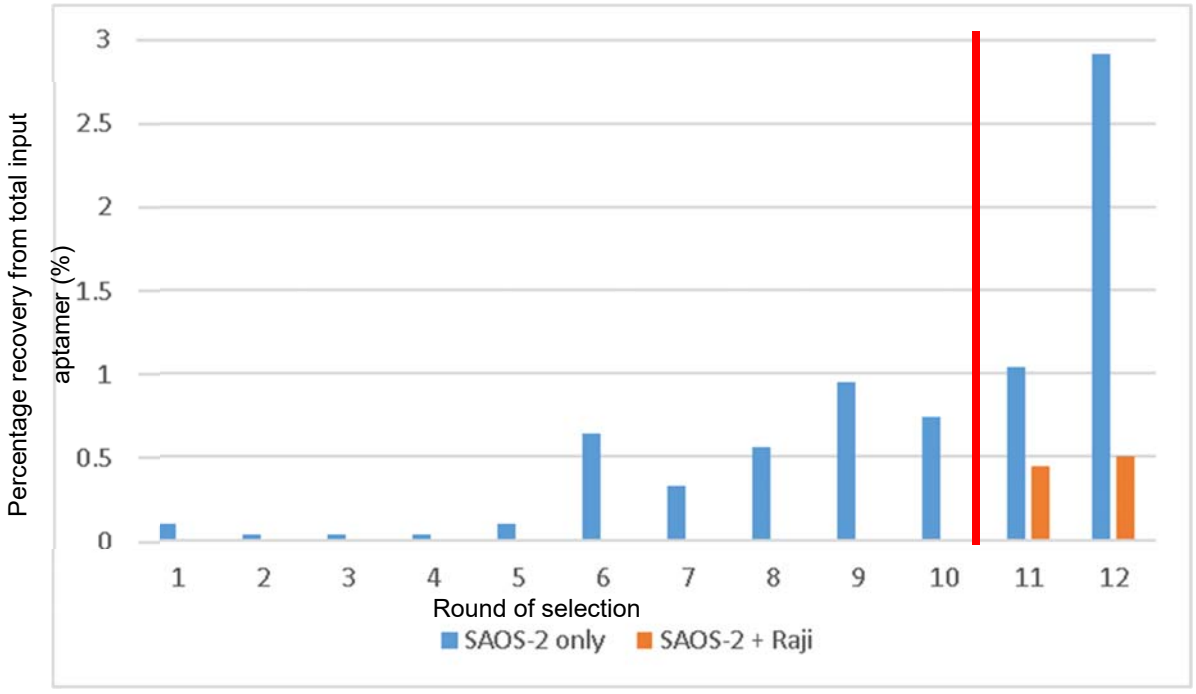

Figure 3-14 - Percentage recovery of parallel aptamer pool after 10 rounds of selection. The aptamer pool was split after Round 10, indicated by the red line. The rounds which lack counter selection are show in blue. The population including counter selection against the Raji cell line are shown in orange.

The parallel selections with and without Raji counter selection demonstrate the effect of introducing counter selection. The selection conditions were fixed for each of the pools for Round 11 and Round 12 (Table 3-2), to compare the effect of counter selection alone. As expected, the population generated following the introduction of the Raji counter selection (orange bars) shows a reduction in recovery, suggesting that a significant proportion of the population has been removed. The population with no counter selection (blue bars) continues to increase. This trend is also seen in Round 12, where the blue population increases further. A slight increase in recovery from the Raji counter selected population is also seen in Round 12 (Figure 3-14). The introduction of the negative cell line reduced the amount of materials recovered, suggesting a narrowing of the aptamer pool to one which is more specific to the SAOS-2 population, by removing aptamers that bind to epitopes common to both cell lines..

Round	Aptamer	Positive cells	Positive incubation time	Positive washes	Negative cells	Negative incubation time	Negative washes
11 SAOS-2	4.439 µg	T-75	45 minutes	4 x 8 mL, 5 minutes	None	N/A	N/A
11 Raji + SAOS -2	4.439 µg	T-75	45 minutes	4 x 8 mL, 5 minutes	Raji 3 million cells	30 minutes	1 x
12 SAOS-2	4.439 µg	T-75	45 minutes	4 x 8 mL, 5 minutes	None	N/A	N/A
12 Raji + SAOS -2	4.439 µg	T-75	45 minutes	4 x 8 mL, 5 minutes	Raji 3 million cells	30 minutes	1 x

Table 3-2 - Aptamer selection conditions for the parallel aptamer pools in Round 11 and 12 of selection. Amount of aptamer, cell number for positive and negative (where applicable) targets, and time of incubations of positive and negative (where applicable) were maintained, as only the divergence of the aptamer pools were tested in Round 11 and 12.

3.4.5 Testing of divergent aptamer pools against both selection conditions

The selection process was ‘branched’ again in Round 13. Aptamer material was generated from both pools of aptamers from Round 12 (SAOS-2 only, and Raji + SAOS-2). Selections were then carried out with and without Raji counter selection. The first condition was the equivalent to the Round 12 SAOS-2 only selection; the second condition was the equivalent to the Round 12 Raji + SAOS-2 selection (Table 3-3).The selections were performed in a reduced format to allow for easier material handling and generation of materials (Table 3-4).

Round				
10	SAOS-2 only			
11 and 12	SAOS-2 only		SAOS-2 + Raji	
13	SAOS-2 Cont.	SAOS-2 only + Raji	SAOS-2 + Raji, SAOS-2 only	SAOS-2 + Raji Cont.

Table 3-3 - Table to show aptamer pool splitting through final rounds of selection. Thick boarders represent where the pools were pools diverged and were kept separate for subsequent rounds.

The 4 recovered aptamer materials were amplified and quantified and compared with previous rounds of selection recovery (Figure 3-15).

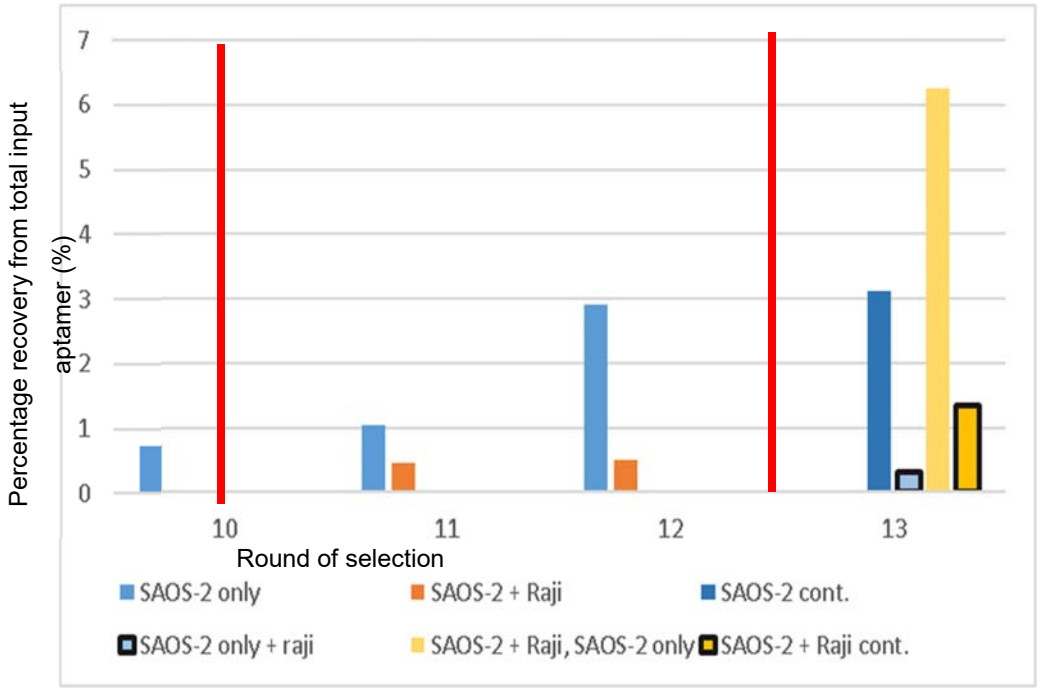

Figure 3-15 - Percentage of aptamer pools after the final rounds of selection comparing the parallel aptamer pools. The aptamer pools were split after Round 10 and Round 12 indicated by the red lines. The black-bordered bars represent the aptamer pools, which were exposed to the Raji cell line in Round 13; the non-bordered bars from Round 12 to 13 represent the pools that were only exposed to SAOS-2 cells.

Figure 3-15 shows the recovery of aptamers from multiple parallel selection conditions; Round 10 to 12 were included in this graph to highlight the previous pools of aptamers recovery. Round 13 highlights the performance differences from aptamers that were from the same selection until Round 10. The SAOS-2 only aptamer pool (blue) steadily increased in recovery from Round 10 to 12. However, this increasing recovery suggests the aptamer pool was not subject to efficient reduction, and therefore high affinity and specificity aptamers were not yet dominant within the pool. As can be seen at Round 13, the SAOS-2 only aptamer pool (blue lines) performed poorly in comparison to the Raji + SAOS-2 pool (red lines), with reduced recovery in both conditions. The discrepancy in recovery between the two pools suggests that despite the 'SAOS-2 cont.' aptamer pool being only selected against the SAOS-2 cells, the incorporation of a negative selection target refined the aptamer pool to aptamers specific for SAOS-2 unique markers.

The same trend was seen when both pools were exposed to the Raji cell lines ('SAOS-2 only + Raji' and 'Raji + SAOS-2 cont.'). The 'SAOS-2 only' pool displayed the largest decrease in recovery from 2.9% in Round 12 to 0.3% in Round 13, indicating that the majority of the aptamers within that pool bound to markers which were common between the two cell lines. The 'Raji + SAOS-2 cont.' pool displayed a trend for rising recovery transitioning from 0.44% in Round 12 to 1.33% in Round 13. The increase from 0.4% to 1.33% was the second increase of recovery in succession, and so if the selection were continued, greater selection pressures would have been applied to this condition to ensure further reduction of the aptamer pool to high specificity aptamers.

Round	Aptamer	Positive cells	Positive incubation time	Positive washes	Negative cells	Negative incubation time	Negative washes
13 SAOS-2 Cont.	2.2195 µg	T-25 (2.5 million cells)	45 minutes	4 x 4 mL, 5 minutes	None	N/A	N/A
13 SAOS-2 only +Raji	2.2195 µg	T-25	45 minutes	4 x 4 mL, 5 minutes	Raji 1.5 million cells	30 minutes	1 x
13 Raji + SAOS-2, SAOS-2 only	2.2195 µg	T-25	45 minutes	4 x 4 mL, 5 minutes	None	N/A	N/A
13 Raji + SAOS-2 cont.	2.2195 µg	T-25	45 minutes	4 x 4 mL, 5 minutes	Raji 1.5 million cells	30 minutes	1 x

Table 3-4 - Aptamer selection conditions for the divergent aptamer pools in Round 13 of selection. The aptamer pools generated in Round 12 were prepared for a 13th round of selection, where half of the aptamer pool was exposed to the SAOS-2 only selection condition, the other half exposed to the Raji + SAOS-2 selection condition.

3.4.6 Cloning and testing of Raji + SAOS-2 Round 13 recovered aptamers

Aptamers recovered from Round 13 from the Raji + SAOS-2 aptamer pool, with the SAOS-2 only conditions, were taken and prepared for cloning, to generate single sequence pools of aptamers which could then be tested against the SAOS-2 and Raji cell lines to identify the most specific aptamers and subsequent sequencing. The aptamer pool was amplified and purified to dsDNA and ligated into a CloneJET plasmid. The resultant plasmids were then analysed by PAGE (Figure 3-16).

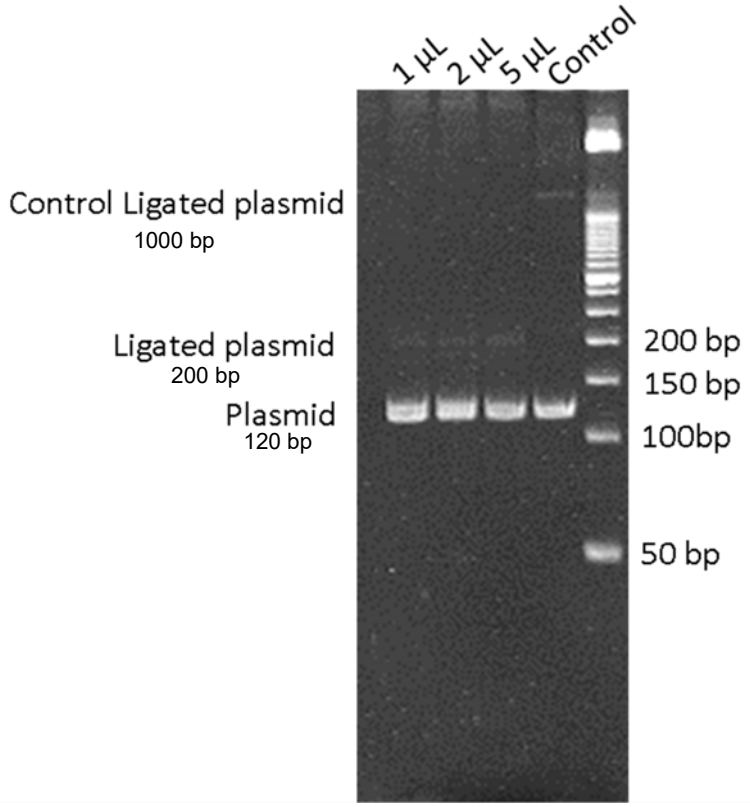

Figure 3-16 - PAGE analysis of plasmid ligation of aptamers and control sequences. Using the CloneJET PCR cloning kit, the aptamer pool was ligated into the kit plasmid. The plasmid running at 80 bp plus the aptamer (80 bp), when ligated, ran at the expected 200 bp size, with the control (976 bp) incorporating a larger insert and resulting in 1000 bp ligation. The ladder is 50 bp increase per band.

Successful ligation was expected to show bands at 200 bp (total plasmid (120 bp) and the aptamer (80 bp)). The control was a much larger, 976 bp, resulting in a total size of 1000 bp within the positive control. 1, 2 and 5 µL of the aptamer pool added to the reaction resulted in successful in low yields of ligation (Figure 3-16). The ligated plasmids were then transformed into competent *E. coli* (C2987H), and plated onto ampicillin spiked agar plates and cultured overnight. The colonies were then assessed for successful transformation, with positive and negative controls to compare to the aptamer ligations (Figure 3-17).

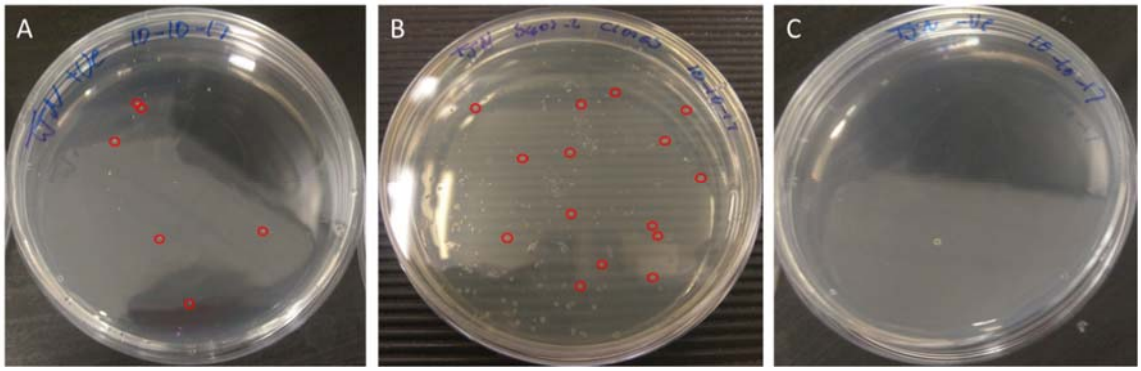

Figure 3-17 - Aptamer/plasmid ligation and transformation necessary for colony formation. A) Colonies were observed growing on the ampicillin spiked plates when the positive control ligation had taken place in the plasmid in two plates. B) Aptamer ligated plasmids transformed into the *E. coli* generated many colonies on each of the six plates. C) Unligated plasmids transformed into *E. coli* did not have colony growth in two plates. Red circles highlight some of the colonies. 10 plates were seeded in total, 2 with the positive control, 2 with negative control and 6 with aptamer ligated sample. No colonies were observed on the negative control plates.

After 24 hours, plates were assessed for colonies. As shown in Figure 3-17, colonies were observed in both the positive control (A), and the aptamer sample (B), and no colonies were present on the negative control plate (C). From the aptamer plates, 96 colonies were picked and placed into a 96 well plate with PCR reagents. PCR was then performed on the 96 samples. Each of the samples was then assessed by PAGE for the product of the correct size (200 bp) (Figure 3-18).

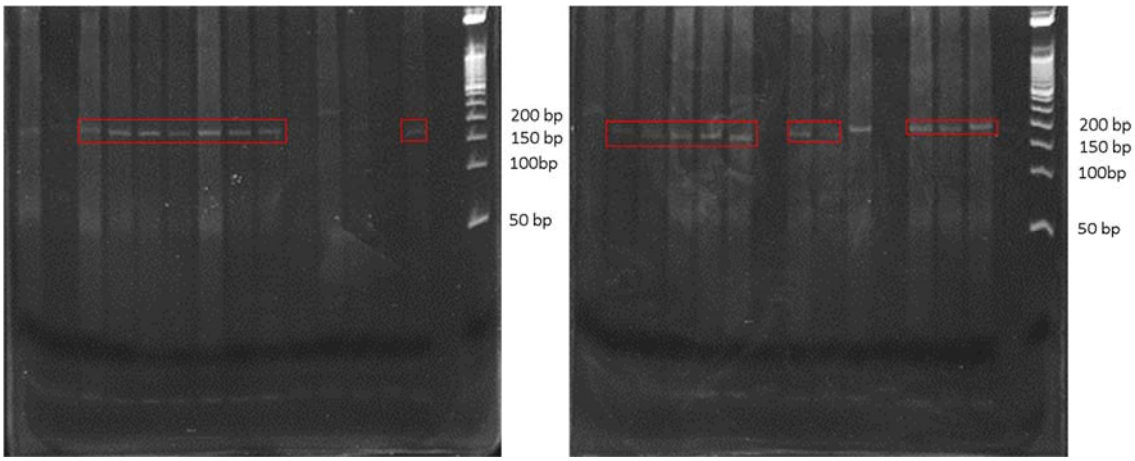

Figure 3-18 - PAGE analysis of picked bacterial colonies with successful ligation to identify correctly ligated plasmids. 15 colonies were run on each gel, All 96 colonies therefore run across 7 gels: this is a representative image of all gels. Successful ligation was determined by the size of the plasmid, as with the previous quality control point 200 bp was the size expected for correct ligation. Red boxes highlight colonies that were successful. The ladder used increased in size by 50 bp per band.

A total of 96 colonies were picked and the remaining colonies left on the growth plates, these plates were stored at 4 °C to maintain colonies that had formed and prevented overgrowth. Following the amplification of the plasmids from picked colonies, each sample was then qualitatively tested using an acrylamide gel. Figure 3-18 shows 2 (30 samples) of the 7 gels (96 samples) generated to test whether correct ligation of the plasmid had taken place. The colonies, which produced a plasmid size at 200 bp, were noted and taken forward for further testing. Those which were larger or smaller than the 200 bp ideal were discarded. From the 59 plasmid samples, ssDNA aptamer pools were then generated using the same methodology as used previously.

These pools were then used in a selection, but with much reduced aptamer, target and volumes. Here, 59 selections were performed simultaneously in 96 well plates for ease of handling. Each cloned aptamer pool was exposed to the Raji cell line for 30 minutes before the supernatant was removed and placed on the SAOS-2 cell line. During the 45 minute incubation with the SAOS-2 cells, the

Raji cells were washed 3 times for 5 minutes each time, before the aptamers were recovered for qPCR. After the 45 minute incubation with the SAOS-2 cells, the cells were washed 3 times for 5 minutes each time before the aptamers were recovered for qPCR. The 59 samples from the Raji cells, and 59 samples from the SAOS-2 cells (118 wells of samples) were then prepared for qPCR and assessed (Figure 3-19).

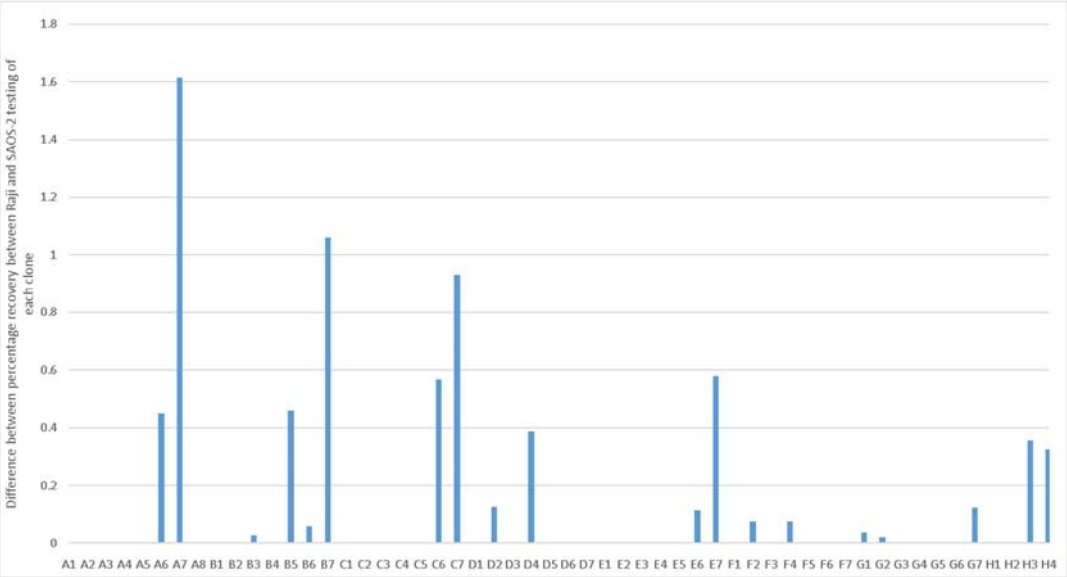

Figure 3-19 - Difference in the percentage of recovery between SAOS-2 and Raji cells for each clone. qPCR quantification from both the percentages of SAOS-2 and Raji testing were compared by subtracting Raji recovery percentage from SAOS-2 recovery percentage for each clone. These values were not a percentage difference between the recoveries but represented a percentage number of molecules, which preferentially bound to the SAOS-2 population.

Assessing the difference in percentage recoveries between the cell lines for each clone removed the background binding for each of the clones. Analysing the data from the qPCR revealed 10 clones that had preferential binding to the SAOS-2 cell line (Figure 3-19). Clone A7 had the highest difference in percentage binding in favour of the SAOS-2 cells, with a difference of 1.61; this equates to 1.61 x 1012 molecules with preferential binding. The other clones that were recognised for having preferential binding were A6, B5, B7, C6, C7, D4, E7, H3, and H4.

3.5 Discussion

This chapter aimed to investigate the technology of aptamers in biomarker discovery, by generating aptamers which were specific to the SAOS-2 cell line, testing individual aptamer sequences to determine the best performing, and identifying the epitope that the best performing aptamers bind to, resulting in the identification of new biomarkers.

3.5.1 Pre-selection optimisation

Determining the correct gel for qualitative quality control steps was the first step in this chapter, setting the groundwork on which the other tests would be based. Agarose and acrylamide gels are both used for protein and nucleic acid electrophoresis, and with the size of 80 bp and below, 4% agarose, and 10% acrylamide gels are the standard choice (Chory and Pollard, 2001). However, as Figure 3-3 demonstrates, the acrylamide gel performs better for the size of the material used, as well as being a generally faster protocol. Agarose gels are often run with the ethidium bromide or Gel Red within the gel already, which is known to cause slight differences in mobility through the gel. These differences are most likely the cause of the slower running times and less clear bands. With the groundwork set up for many of the quality control tests used throughout this chapter, testing the purification from dsDNA to ssDNA for the subsequent round of selection was the next logical step.

There are several purification methods developed for nucleic acids that can be applied to DNA aptamers. The original use of DNA as an aptamer came in 1992 and purification of the dsDNA to ssDNA was performed by tagging the DNA with radioactive labels, then running the DNA down denaturing polyacrylamide gels, before cutting out the band and eluting (Ellington and Szostak, 1992). The use of radioactive labels is now not standard, and other methods have been developed. The most commonly used purification method is the use of a biotin-modified reverse/antisense primer in amplification: the biotin then binds to a streptavidin-coated structure, and the forward/sense strand is released through alkaline

denaturation (Blank et al., 2001, Guo et al., 2006, Shangguan et al., 2015, Bruno et al., 2008, Bruno and Kiel, 1999, Du et al., 2015, Rouah-Martin et al., 2012, Song et al., 2008). As can be seen in Figure 3-5, the streptavidin beads work well with the biotin labelled aptamers as a purification process, confirming why many papers use this method. However, it can also be noted that not all aptamers were bound to the streptavidin beads during this process, so sequence loss is highly likely in the first few rounds of selection. Therefore, another method was investigated, using magnetic beads as a vehicle, and polymer and salt solution to drive dissolved DNA onto the magnetic beads, which can then be washed to remove dNTPs, salts and proteins (Grüttner et al., 2001, Hawkins et al., 1994, Prodělalová et al., 2004, Müller-Schulte et al., 2005). Similar methods are sold commercially for many applications, and Figure 3-5 gives a good indication why, with the proper purification of DNA, with the removal of DNTP and smaller nucleic acids such as primers, the method allows for quick clean-up of reactions, leaving only the desired materials. For the sake of cost, a method used by the York collaboration was employed with magnetic particles paired with salt and polyol solution which provided a cheap alternative to expensive commercially available kits.

The final application of the aptamer must be considered before selection can take place, as the content of selection buffers facilitate aptamer folding and functionality, and deviations from the selection buffer can lead to the dysfunction of the aptamer (Neves et al., 2017, Smestad and Maher, 2013, Catherine et al., 2014). In this chapter, the cell culture medium alpha-MEM was selected as the base of the selection buffer, given that this media is known to not affect cells negatively with extended exposure and provides some salts generally added to aptamer selection buffers, such as $NaCl_2$. The culture media was then supplemented with small amounts of various salts necessary for aptamer structuring (Smestad and Maher, 2013, Lane et al., 2008) and charge masking (Hianik et al., 2007, Yan and Huang, 2009) ($MgCl_2$, $CaCl_2$, $MnCl_2$, $NiCl_2$), while keeping the salt levels comparable to the physiological environment (Elliott and Jasper, 1949). Keeping buffers similar to physiological environments prevents damage to the cells during the selection process but can cause adherent cells to detach from the culture plastic, and therefore one can lose any cells and

aptamers bound to those cells during wash steps. Conversely, cell rupturing may allow aptamers to permeate the cells, and prevent removal of non-specific aptamers during washing. Using this information, buffers had to be selected to correspond with the aptamer selection and tested. Figure 3-6 shows varying aptamer recovery with various salt and cell conditions, with the highest recovery present in the 0x salt conditions. The 0x buffer only contains the salts present within the culture media (KCl, pyruvic acid sodium salt, pyridoxine monohydrochloride, choline chloride, $CaCl_2$, $MgSO_4$, NaH_2PO_4), therefore, supplementing the media with additional salts to allow more complex aptamer structures to be formed would allow for a more varied aptamer pool structurally, and potentially allow higher affinity and specificity.

3.5.2 Aptamer selection

Tracking of recovered aptamers throughout the selection informed not only how well the process was advancing but also roughly how many cycles of amplification were needed for optimal dsDNA production (Figure 3-7 shows qPCR informing cycle course conditions for amplification Figure 3-8). Despite the initial 5 rounds of selection with low recovery, the aptamer pool was narrowed to a point where recovery began to increase round by round, resulting in an aptamer selection that appeared to work well. Duplicating the aptamer pool at Round 10 and diverging the pools, to incorporate a negative selection to narrow the aptamer pool, demonstrated that the selected aptamer pool at Round 10, while having some affinity to the SAOS-2 cell line, could be narrowed further to become more specific. The aptamer pool exposed to the negative selection specificity was highlighted in Round 13 with testing of each of the two divergent pools in both of the selection conditions (Figure 3-15). The inclusion of the Raji cell line facilitated a further selection pressure towards specific aptamers which bind to the SAOS-2 cell line by removing aptamers which bound to markers common to both cell lines. The resultant narrowed pool of aptamers (Raji + SAOS-2) outperformed the aptamer pool which had not previously been exposed to the Raji cell line negative selection (SAOS-2 only). Negative selection played an important role in

narrowing the aptamers to become more specific to the SAOS-2 population, however within this chapter and selection no move to increase affinity, beyond increasing the number of washes, was made. Decreasing the total number of epitopes causes competition between the aptamers which bind to the same or close in proximity epitopes, selecting more heavily for the highest affinity aptamers at the end of the selection (Morris et al., 1998). Decreasing the number of epitopes in this selection could have been accomplished by decreasing the number of cells while maintaining the nanograms of aptamer input. Increasing the number of Raji cells and/or incubation time would have also increased the pressure from the negative selection, ensuring all non-specific binding aptamers, and aptamers which bind to common markers, were removed. Despite not including some of these techniques for further narrowing the aptamer pool, the two aptamer pools generated seemed to show good specificity to the SAOS-2 cell line. The next step was to take the successful selection pool and clone out single sequences to generate single sequence aptamer pools to test more thoroughly against the SAOS-2 and Raji cell lines.

3.5.3 Cloning and testing of clones

Generating the clones for the aptamer pool was relatively easy using the CloneJET cloning kit and support from Aptamer Solutions in York. Ligating the aptamer pool into plasmids and then transforming them into competent *E. coli* allowed for colony growth on ampicillin-spiked agar plates. Colonies were then picked, and each colony of *E. coli* contained a single sequence ligated into a plasmid. Despite the promising results from Figure 3-15, individual aptamers from the final selection round may be non-specific to the target (Shangguan et al., 2015), meaning careful testing of each aptamer sequence needs to be performed before sequencing and epitope identification. In addition to potentially non-specific aptamers, Figure 3-18 highlights that not all ligations were successful and within the standard parameters. Therefore, 59 of the 96 clones (61.46% successfully ligated) picked from the colonies were taken forwards to be tested against the SAOS-2 and Raji cell lines.

qPCR analysis of the generated clones revealed 10 clones that had preferential binding to the SAOS-2 cell line (Figure 3-19). The use of the Raji cell line in the same test allowed for the subtraction of Raji-specific and background binding from the specific SAOS-2 binding. This testing of the clones verified the selection of aptamers specific to the SAOS-2 cell line. However, not all clones generated from the selection were specific to the SAOS-2 cell line and had preferential binding to the Raji cell line. The aptamers which remained bound preferentially to the Raji cell line may be due to aptamers which bound to common markers between the Raji and SAOS-2 populations that were not removed during the negative selections, and therefore bound during the SAOS-2 incubation and subsequently recovered and amplified. These SAOS-2 specific aptamers demonstrate that the aptamer selection process developed in this chapter was capable of isolating cell-specific aptamers. Further work on the SAOS-2 specific aptamers was attempted, in that after cloning and testing, the specific aptamers were then isolated for sequencing. However, the sequencing of these aptamers proved to be problematic returning sequences which were fragments and did not match with the plasmid or primer sequences well enough for identification of the random region of the aptamers. This issue may have been resolved with further expansion of the aptamer sequences using nested PCR to ensure the random region of the aptamer was sequenced successfully. Due to time restrictions and the priority was to move on to primary bone marrow selection, therefore further characterisation of the SAOS-2 specific aptamers was delayed until other aptamers required characterisation. Unfortunately, further aptamer characterisation was never needed.

Characterising the binding target of these aptamers would have been the next step after sequencing. Offering an insight into markers on the surface of the SAOS-2 cell line which are not found on the Raji cell line. To do this aptamers would have been immobilised on streptavidin-coated beads using a biotin-modified primer. The beads placed into a cylinder forming a column, much like immunoprecipitation, but using aptamers where antibodies would have been used. Cell lysate would then be passed through the column, the aptamers binding to their target while the remaining components were washed through. The

proteins could then be identified using protein sequencing. The advantage of identifying the protein targets of the aptamers would be that if these targets are osteosarcoma specific, this may provide a diagnostic tool for detecting osteosarcoma, and if functionalised properly, a targeted therapeutic.

In conclusion, the aptamer selection method developed and used here has been shown to increase recovery of aptamer material round by round, until increased stringency causes the recovery to drop. Continuing the selection with increased stringencies then allowed the recovery of aptamers to increase again, suggesting an aptamer pool that is better-adapted to the target. Final testing of individual aptamer clones revealed several clones which were more specific to the SAOS-2 cell line, and therefore verified the success of the aptamer selection, and the methodologies used to perform it. This selection technique can now be utilised against the primary cells derived from bone marrow or foetal femur sources without the need to validate many of the techniques used, thereby streamlining the selection process against the valuable primary tissues. And despite the lack of information on the targets of the SAOS-2 specific aptamers, a continuation of the selection using the primary cells was carried out next to progress the project using the methods refined in this chapter.

Chapter 4 Aptamer selection against skeletal stem cell populations

4.1 Introduction

As discussed in Chapter 3, aptamer technology is particularly attractive in the area of skeletal stem cell enrichment and isolation. The utility of aptamers for SSC enrichment and isolation is due to the fact that aptamers can be selected against cell surface markers (which may be currently unidentified), and may, therefore, be used as a biomarker discovery platform (Takahashi, 2018, Berezovski et al., 2008). Utilising the methods developed and validated in Chapter 3, cell-based selection of aptamers was undertaken to isolate sequences which bind to primary stem cells isolated from human bone marrow, or human foetal femur sources.

Cell populations directly derived from bone marrow would not be an ideal target for aptamer selection, given that the SSC is a rare sub-population (Bianco and Robey, 2015, Gothard et al., 2011). Any epitopes which are present only on the SSC population would, therefore, be exceptionally rare in a large heterogeneous cell population. The extreme rarity would make isolating aptamers specific to the SSC markers highly unlikely. Therefore, enrichment of SSC cells within the bone marrow population would increase the relative concentration of these epitopes, and provide a more suitable selection target (increasing the proportion of SSCs compared to other cell types). Also, such an approach would decrease the relative number of other epitopes that the aptamers would encounter; thereby increasing the likelihood of successful selection. SSC populations are not restricted to the adult bone marrow; they also reside within foetal femur populations (Gotherstrom, 2016). Thus, foetal femur tissue could be used as an alternative source of significant SSC population for aptamer selection. The foetal femur is, as the adult bone marrow, a source of heterogeneous cells. However, the number of SSCs present in the foetal femur samples far exceeds(one MSC for every 400 cells)(Campagnoli et al., 2001, int ‘t Anker, 2003) those found in

the adult bone marrow sample (sample dependent but around one in one to two million cells). The STRO-1 marker can be used to isolate a subpopulation of the foetal femur-derived cells, however, the STRO-1 immuno-selected sub-population displays a committed osteochondral differentiation pathway (Gothard et al., 2015a). For this reason, so as to not select aptamers against an already semi-differentiated cell population, the unselected foetal femur-derived cells were chosen to be used in this chapter.

To date, no unique markers have been identified for SSC which can be used to fully isolate this sub-population from the heterogeneous bone marrow population. There has been previous work to enrich the SSC population using a number of markers (Gothard et al., 2014, Williams et al., 2013, Sorrentino et al., 2008, Tondreau et al., 2004, Lv et al., 2014): however, a single unique marker would be preferable, as it would lead to a more straightforward SSC isolation process. Combining the work from Chapter 3 with aptamer selection should provide a target population that allows for aptamers to bind to new unique markers. These markers can be used for further enrichment of the SSC population or, ideally, isolation of the cells from the bulk population.

In order to enrich for the SSC population, antibody markers can be utilised to remove or retain cell populations with known protein expressions. For example, the STRO-1 antibody has recently been reported to bind to the heat shock conjugate-70 proteins (Fitter et al., 2017). The SSC population is known to be found within this STRO-1 enriched population (Simmons and Torok-Storb, 1991), though is not the only cell population to be isolated in this step. Red blood cells can still be present after a lymphoprep procedure, but these can be removed through a simple lysis step. This additional step removes more of the red blood cells, and thereby increases the proportion of SSC within the cell population.

Once several rounds of selection have been performed successfully, further enrichment of the SSC population using FACS would further narrow the aptamer pool to create an aptamer pool potentially more specific to the SSC population. This further enrichment will be performed using the STRO-1^{BRIGHT}, and the CD146 (MCAM) markers, both shown to enrich for the SSC population in Chapter

1. As already shown in Chapter 1, around 1:100 cells display stem-like properties once enriched: this is 0.01% of the bone marrow population. Isolation of a large number of cells needed for aptamer selection (5 million) would not be possible. Therefore, using a slightly enriched population, STRO-1 can supply the needed number of cells, and once an aptamer population is established against the BM cells, narrowing the population further using FACS will enable isolation of a more enriched stem cell population, and therefore a more specific aptamer pool.

There is increasing interest in the identification and use of the SSC population within the regenerative medicine and tissue engineering fields. Other work has been performed to develop aptamers against an SSC population (Guo et al., 2006, Schafer et al., 2007), with porcine bone marrow as a target; this subsequently allowed the isolation and imaging of the cells. Although the use of porcine cells demonstrated a useful proof of concept, identifying the aptamer targeted biomarker(s) was not possible as the porcine proteome is, at present, poorly characterised. Despite the lack of target protein identification, these studies offer promise to use similar techniques on human SSCs.

4.2 Aims and objectives

4.2.1 Hypothesis

Aptamer selection methodology developed in Chapter 3 can be combined with antibody enrichment methodologies developed in objective II to select aptamers against SSCs.

Specific aims:

1. To raise aptamers against the SSCs population using methodologies developed in Chapter 3.
2. To incorporate antibody enrichment methodologies from objective II in order to raise aptamers more specifically against the SSCs population.
3. To isolate single aptamer sequences through cloning or single molecule PCR, and subsequently test affinity to identify the best performing aptamers.
4. To sequence the successful aptamers to identify common sequences and monoclonal equivalent aptamer pool generation.
5. To identify the aptamer binding targets in SSCs.
6. To test single sequence aptamers against SSCs for isolation comparison.

4.3 Methods

Methodologies employed in this chapter are detailed in Chapter 2 (2.3).

Selection in this chapter was performed with similar techniques to Chapter 3, as shown in the workflow diagram (Figure 3-1), FACS selection was performed by applying the antibodies after the aptamers have been incubated with the cells, then washes were performed to remove unbound aptamers and antibodies.

Methods used are also referenced in the results chapter, as techniques are used to provide easy understanding of the processes performed.

4.4 Results

Identification of a suitable binding/selection buffer was critical for aptamer functionality, as buffer ions and salts determine aptamer folding and binding capabilities, and therefore maximum performance. The buffer used for aptamer selection should facilitate aptamer folding by containing optimal salts and metal ions. The buffer should also maintain cell viability and not lead to differentiation. The selection described here was based upon alpha-MEM (culture media) used to expand the SSC populations following enrichment and thus keep the culture and selection conditions consistent throughout.

4.4.1 Preselection optimisation

Alpha-MEM was chosen as the basis for the selection buffer. This required salt supplementation to provide the aptamers with the necessary conditions for optimal folding. Non-modified media (0x), physiological levels of salt (1x), and 10 times physiological levels of salt (10x) were applied to STRO-1 enriched SSCs with naive aptamer library (N40B) to test optimal binding conditions (2.2.7). The materials were then recovered (2.2.9.1) and amplified (2.2.10.1) before qPCR analysis was done to assess the best binding conditions to be used for the aptamer selection (2.2.10.2) (Figure 4-1).

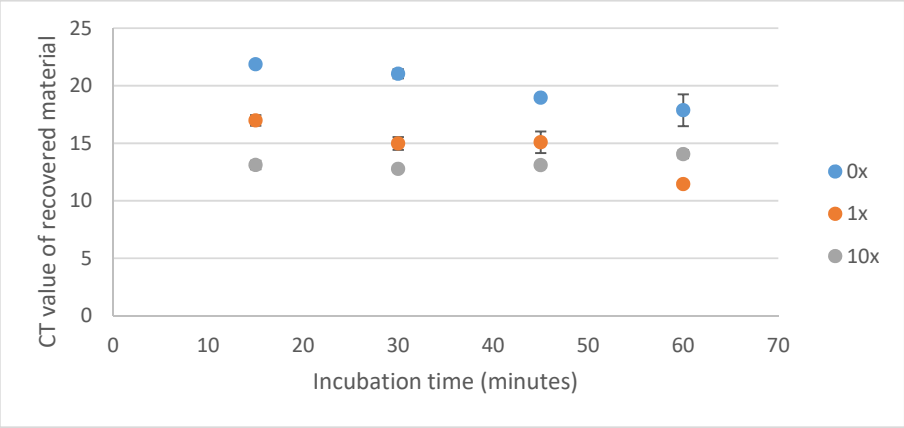

Figure 4-1 - qPCR of recovered aptamers from various buffers and times of incubation with STRO-1 MACS sorted and cultured cells to identify optimal binding conditions. Using qPCR, the effects of incubation time and salt concentrations on aptamer binding to bone marrow-derived cells were tested. 0x, 1x, and 10x refers to the salt supplements added to the media. The lower CT values indicate higher recovery. n = 3, bars show standard deviation.

Results from the buffer optimisation (Figure 4-1) indicated that the lowest CT, and therefore the most aptamer library was recovered from 1x physiological salts with a 60-minute incubation (CT value of 11.44). The no-template control showed no amplification (data not shown) and therefore suggests all recovered materials were from cells/aptamers, rather than from contamination.

4.4.2 Bone marrow selection

Using the conditions established in 4.4.1 aptamer selection was performed on 5 million STRO-1+ MACS sorted and cultured cells. 1X selection buffer was used, and the aptamers were incubated with the cells for 60 minutes. The aptamer materials were then recovered through cell scraping (2.2.9.1), amplified for 4 cycles of PCR (2.2.10.1), before a cycle course was performed to determine optimal amplification cycles. The cycle course of the recovered aptamers was assessed by PAGE (2.2.2) (Figure 4-2).

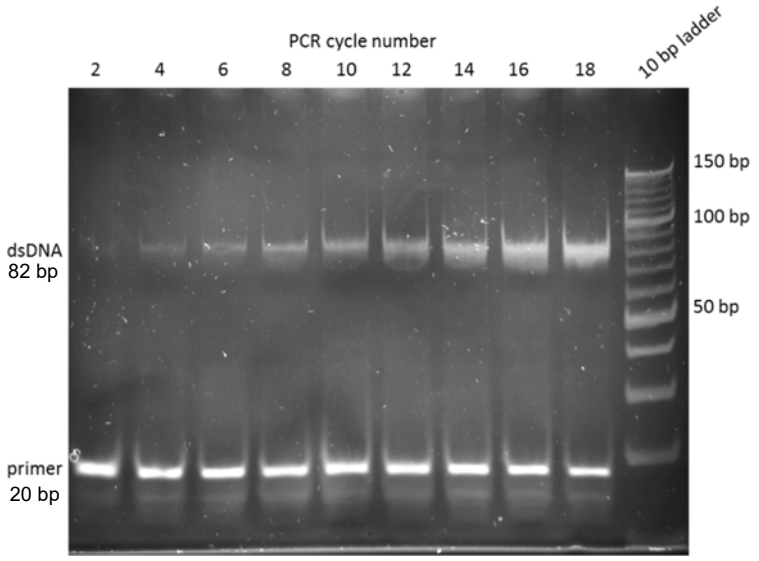

Figure 4-2 - PAGE analysis of the cycle course of bone marrow selection Round 1 recovered materials. High cycle numbers resulted in increased material - note the blurred band below the expected 80 bp dsDNA, thought to be either caused by a large amount of material or aberrant products. The ladder used is a 10 bp ladder, with brighter bands at 150, 100 and 50 bp.

Figure 4-2 showed clean amplification (no amplification artefacts) below 10 cycles. A smear below the 80 bp band was observed with increasing amplification cycles. The smear was most likely a consequence of large amounts of product present in the gel. However, the risk at this early stage of the selection was not taken for the sake of more materials, and 9 cycles of amplification were used for the remaining material.

The amplified materials were then purified (2.2.12.1), primers removed (2.2.14), and purified again. The resultant purified dsDNA was analysed by PAGE (Figure 4-3 A). No primer or aberrant amplification products were seen, so this dsDNA was used to seed an Asymmetric PCR (2.2.11) (Figure 4-3 B).

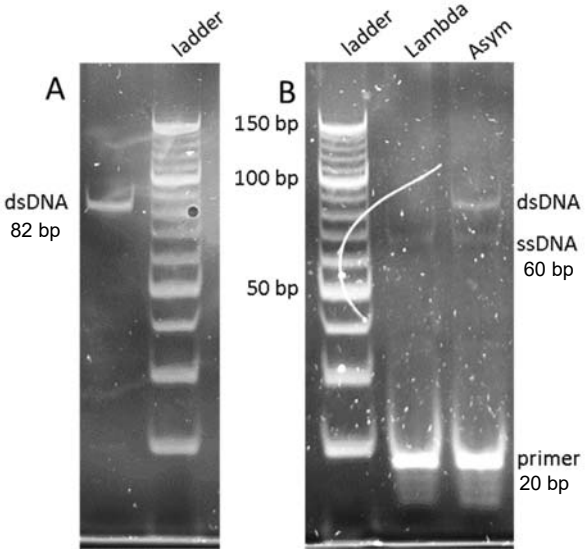

Figure 4-3 - PAGE analysis of purified dsDNA and subsequent Asymmetric PCR and digestions of bone marrow selection Round 1 aptamer materials. A) Purified dsDNA was used to seed an Asymmetric PCR. B) Asymmetric PCR products (Asym) show both ds and ssDNA. PCR products digested with Lambda Exonuclease show only the ssDNA (Lambda). The ladder used is a 10 bp ladder, with brighter bands at 150, 100, and 50 bp.

Figure 4-3 B showed the presence of both dsDNA and ssDNA bands (85 and 70 bp respectively) within the Asymmetric PCR sample (Asym). Subsequent digestion with Lambda Exonuclease leads to the removal of the dsDNA (80 bp) (Lambda). The ssDNA was then purified and subsequently used in Round 2 of selection against the STRO-1+ bone marrow cells.

With the purified ssDNA from Round 1 recovered aptamers, the second Round of selection was performed using the same selection conditions. Aptamers recovered from selection Round 2 were amplified by PCR, then a PCR cycle course to identify optimal amplification, and subsequently purified. The PCR products from the cycle course and the purification were analysed by PAGE to identify the optimum number of PCR cycles (Figure 4-4).

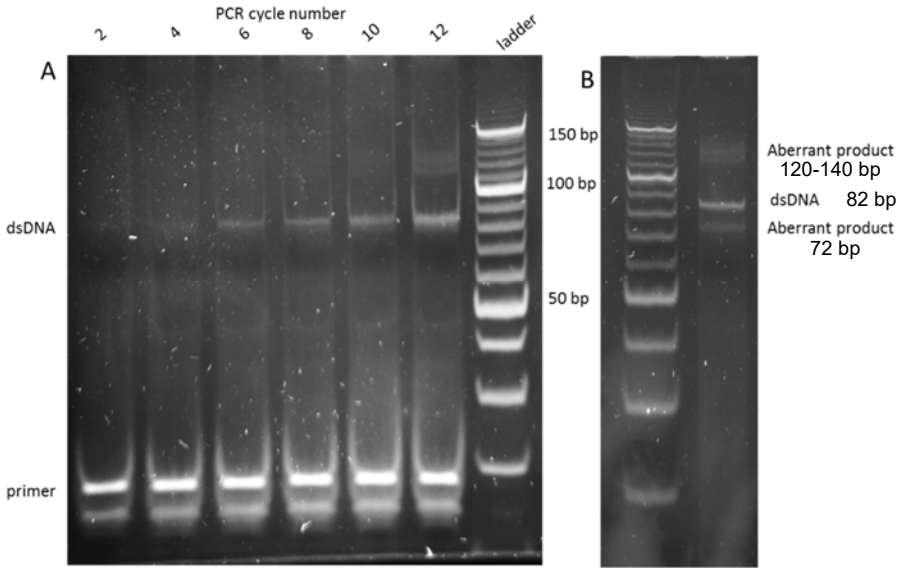

Figure 4-4 - PAGE analysis of cycle course of bone marrow selection Round 2 recovered materials, and subsequent purification of amplified materials. A) Cycle course of recovered materials showed amplification of aptamers with increasing cycle number: at cycle 10 large (120 bp) materials were generated. Cycle 8 was chosen to be used to amplify the remaining materials as no aberrant product was seen. B) Purification of the 8 cycle material showed no primers. However, the large (120 bp) and smaller (70 bp) PCR artefacts were seen. The ladder used is a 10 bp ladder, with brighter bands at 150, 100, and 50 bp.

The PAGE analysis of the PCR cycle course revealed larger aberrant PCR products (120 - 140 bp) generated from 10 cycles onwards (Figure 4-4 A). To prevent these materials being carried forwards in the selection, it was decided that 8 cycles of amplification would be applied to the remaining material. After 8 cycles of PCR the recovered materials were purified, primers digested, and purified again; the resultant product was then analysed by PAGE (Figure 4-4 B). The PAGE of the purified materials revealed the same large amplification product as seen in later PCR cycles in the cycle course (120 - 140 bp), as well as a product which was smaller than the dsDNA aptamer (80 bp), at 75 bp. As these aberrant products were identified in a low selection round, only Round 1 material was available, and thus a new selection was undertaken to avoid any potential

amplification of the same materials which may have been present within Round 1 materials, as well as an opportunity to incorporate FACS into the selection process.

4.4.3 Bone marrow FACS selection

Incorporating FACS into the cell selection protocol provided the added benefit of enabling reduced fraction collection as rounds progressed, by redefining the 'gates' and markers used to sort the cells. The initial round of selection used the fluorescently labelled aptamer library (FAM labelled) and a bone marrow sample. The use of the FACS allowed for not only separation of cells which the aptamer bound to, but also bone marrow characterisation to show differences between samples. The M69 sample was prepared as 2.3.1.1 and 2.3.1.2, and the MACS +ve fraction was treated with the re-folded aptamer, and FACS analysis was performed (Figure 4-5).

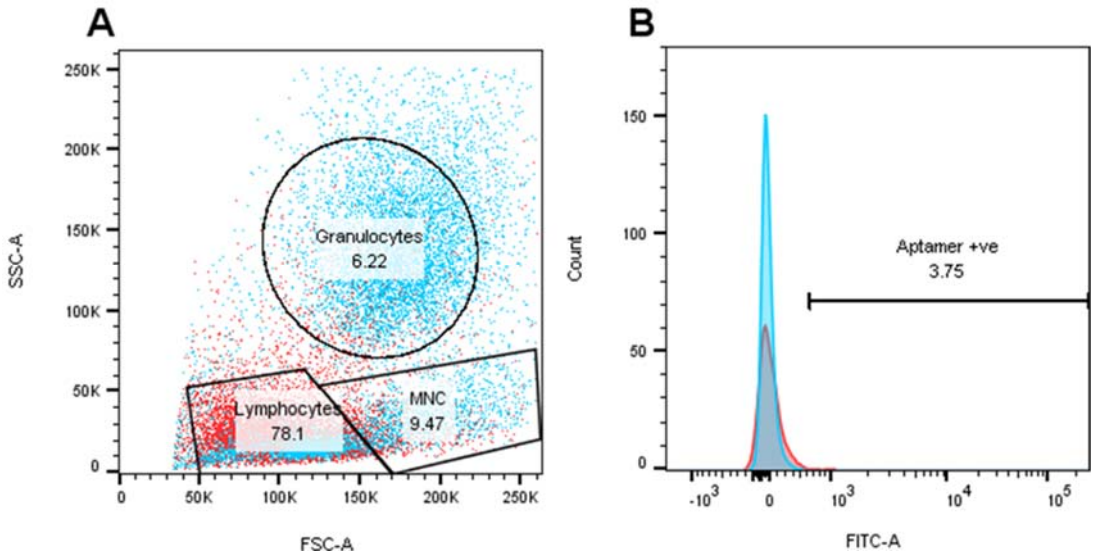

Figure 4-5 - FACS analysis of cell populations and aptamer (FITC) fluorescence of aptamer selection Round 1. Comparison of the Pre-MACS (Blue) and MACS +ve (Red) fraction population, with the numbers on each graph representing the MACS +ve population percentages. A) FSc and SSc diagram of cell populations with the three discernible populations highlighted (Granulocytes, Lymphocytes, and Mononuclear cells (MNC)). B) FITC channel fluorescence of the two populations highlighting the differences in fluorescence population from the pre-MACS at with the gate set at 1% and with aptamer stained section registering at 3.75% stained.

MACS separation shows clear differences before and after, with high enrichment for the lymphocytes and MNCs, with a dramatic reduction in granulocytes between the pre-MACS (blue), and post MACS +ve fraction (red) (Figure 4-5 A). Gating the FITC fluorescence signal to 1% aptamer +ve before the addition of aptamers (blue) allows for precise detection of aptamer after addition and binding (red). The aptamer binding provides an increase in FITC signal from 1% to 3.75% within the MNC population (Figure 4-5 B). The aptamer +ve MNC cells were then sorted to a 15 mL falcon tube.

Sorted cells were made up to 2400 µL with DNase free water, and amplified as 2.2.10.1. The recovered and amplified materials were then analysed through a cycle course and PAGE (Figure 4-6) (2.2.10.3).

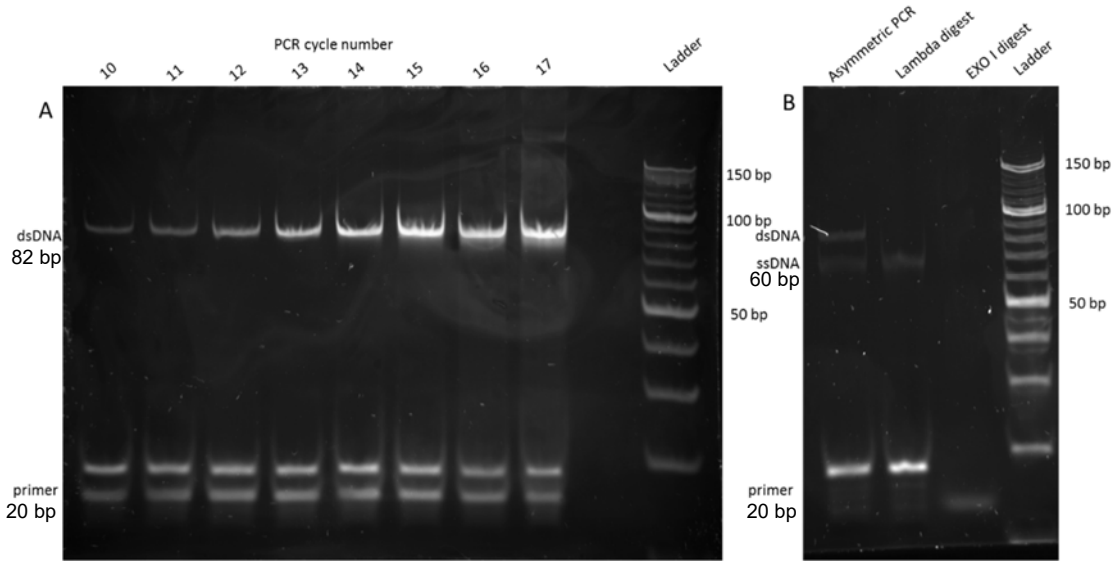

Figure 4-6 - PAGE analysis of Round 1 FACS selection amplification and ssDNA generation. A) Clear amplification of the dsDNA as the cycles of amplification increased, with 16 and 17 cycles showing signs of aberrant products. Therefore, 13 cycles of amplification was chosen to generate dsDNA. B) Asymmetric PCR seeded from the dsDNA generated in A), showed dsDNA as well as ssDNA, subsequent digestion with Lambda Exonuclease showed degradation of the dsDNA, and subsequent treatment with Exonuclease I showed degradation of all DNA material proving the material generated was ssDNA. The ladder used is a 10 bp ladder, with brighter bands at 150, 100, and 50 bp.

The cycle course showed clean amplification of a single 80 bp nucleic acid, which was readily amplified as the PCR cycle number increased (Figure 4-6 A). The nucleic acid recovery was low, as very low amounts of dsDNA were seen at 10 cycles of amplification, and aberrant products and smearing were observed at 15 cycles and higher (Figure 4-6 A). 13 cycles of amplification were chosen for the remaining material. The resulting dsDNA was subsequently purified and used to seed an Asymmetric PCR (Figure 4-6 B). The Asymmetric PCR showed both ds and ssDNA, which when treated with Lambda Exonuclease, removed the dsDNA (80 bp). Subsequent treatment with Exonuclease I also removed the ssDNA (70

bp) and degraded the primers (<20 bp), proving the expected band at 70 bp is ssDNA.

After purification of the ssDNA, the second round of selection was performed on a bone marrow sample, using conditions identical to those in Round 1. For this selection, an F75 sample was used as the aptamer target, treated the same as the M69 sample in Round 1, with MACS separation, and then FACS (Figure 4-7).

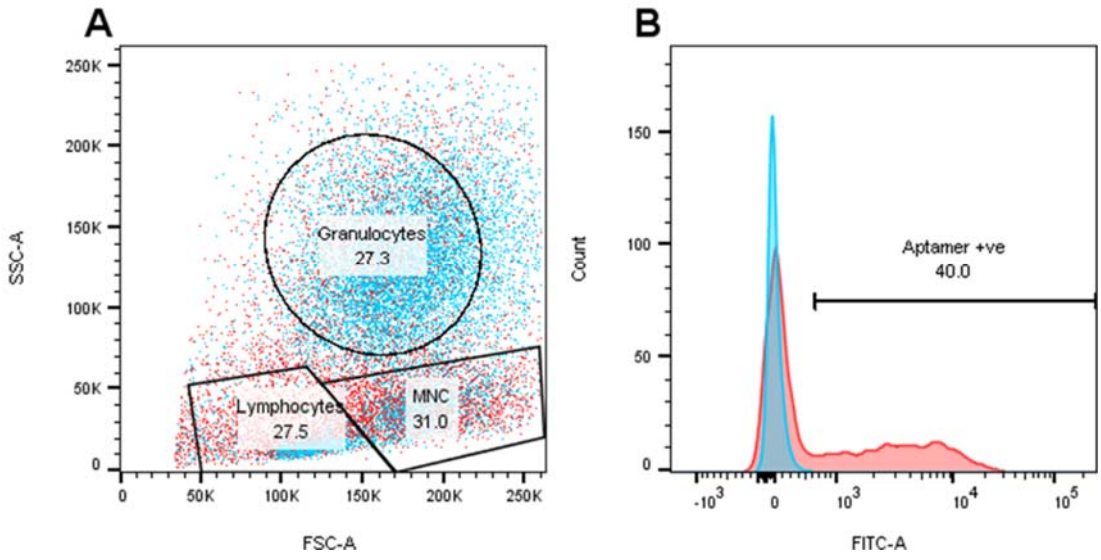

Figure 4-7 - FACS analysis of cell populations and aptamer (FITC) fluorescence of aptamer selection Round 2. Comparison of the Pre-MACS (blue) and MACS +ve (red) fraction population, with the numbers on each graph representing the MACS +ve population percentages. A) FSc and SSc diagram of cell populations with the three discernible populations highlighted (Granulocytes, Lymphocytes, and Mononuclear cells (MNC)). B) FITC channel fluorescence of the two populations highlighting the differences in fluorescence population from the pre-MACS at with the gate set at 1% and with aptamer stained section registering at 40% stained.

MACS separation shows differences before (blue) and after (red), with enrichment for the lymphocytes and MNCs (Figure 4-7 A), though a different population percentage was observed when compared to the sample from Round 1 (Figure 4-5 A), which showed a dramatic decrease in granulocytes between the pre-MACS (blue), and post MACS +ve fraction (red) (Figure 4-5 A). Gating the FITC fluorescence signal to 1% aptamer +ve before the addition of aptamers

allows for precise detection of aptamer after addition and binding. The aptamer binding provides an increase in FITC signal from 1% to 40% within the MNC population (Figure 4-7 B). The aptamer +ve MNC cells were then sorted to a 15 mL falcon tube.

After FACS sorting aptamer recovery and PCR, an amplification cycle course was performed and the PCR products analysed by PAGE (Figure 4-8).

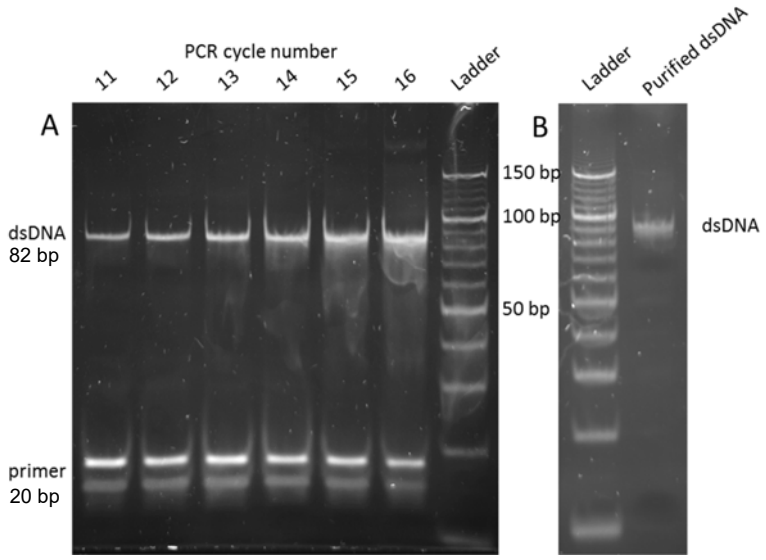

Figure 4-8 - PAGE analysis of Round 2 FACS selection amplification and dsDNA purification. A) Amplification of recovered Round 2 materials showed proper amplification of correct materials until later rounds of amplification (14 onwards), as smears under the 80 bp band began to be more pronounced. Therefore, 11 cycles of amplification was chosen. B) The amplified material was then purified and showed a single band at the expected 80 bp, though it must be noted the band is less well defined compared to other gels. The ladder used is a 10 bp ladder, with brighter bands at 150, 100, and 50 bp.

The results show similar recovery to Round 1: after 11 cycles of amplification, low levels of dsDNA were seen (Figure 4-8 A). However, smearing was also seen from cycle 12, suggesting the materials were over cycled, and a lower cycle number should be used for the rest of the library. Therefore, 11 cycles were

chosen for the PCR amplification. The amplified aptamer library was then purified and analysed by PAGE (Figure 4-8 B). After purification, the dsDNA appeared less well defined on acrylamide gel compared to the amplification cycles, though all primers were removed (Figure 4-8 B). The pure DNA was then quantified using the Nanodrop and used to seed an Asymmetric PCR. The Asymmetric PCR product was then purified, Lambda Exonuclease treated, and a sample Exonuclease treated (Figure 4-9).

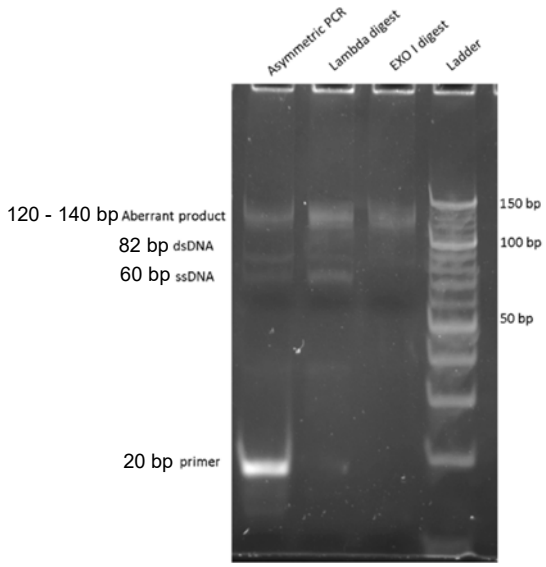

Figure 4-9 - PAGE analysis of Asymmetric PCR of FACS selection Round 2 materials. dsDNA materials were used to seed Asymmetric PCR and generated materials which are much larger (120 – 140 bp) and slightly smaller (70 bp) than the dsDNA (80 bp), while no ssDNA was generated. The Asymmetric PCR products were then subjected to enzymatic digestions to test the generated materials states. Lambda Exonuclease treatment partially degraded the dsDNA and to a lesser extent the larger product. Exonuclease I digestion degraded the primers and materials which were displaying at 70 bp, usually where ssDNA is expected. The ladder used is a 10 bp ladder, with brighter bands at 150, 100, and 50 bp.

Seeding Asymmetric PCR with the purified dsDNA materials generated several products. PAGE analysis of Asymmetric PCR products showed only the presence of the dsDNA band (~80bp) but no ssDNA (~60bp). However, there was also a larger (120 – 140 bp) and slightly smaller (70 bp) bands generated (Figure 4-9).

Subsequent digestion of the PCR product with exonuclease I, removed the primer (<20 bp), but not any of the other material; confirming that these artefacts are dsDNA. Digestion of the purified PCR products with lambda exonuclease partially degraded all material. The 120 - 140 bp bands remained mostly unaffected, suggesting all of the bands displayed were dsDNA. This result was unexpected as the asymmetric reaction PCR contained only one primer.

Generation of these aberrant products was not expected and led to an investigation of the materials and equipment used in the generation of the ds and ssDNA. Two thermocyclers were being used for amplification and incubation purposes. Therefore, differences between the two thermocyclers were assessed. In addition to the two thermocyclers, the 3 forward primers (un-modified, FAM-modified, and cy5.5 modified) which were used were all assessed for differences in amplification. Finally, the aberrant products were more prevalent in the Asymmetric PCR: therefore, symmetric (2.2.10.1) and asymmetric (2.2.11) PCR methods were assessed as well. With all of these conditions identified each was set up, performed, and analysed by PAGE (Figure 4-10).

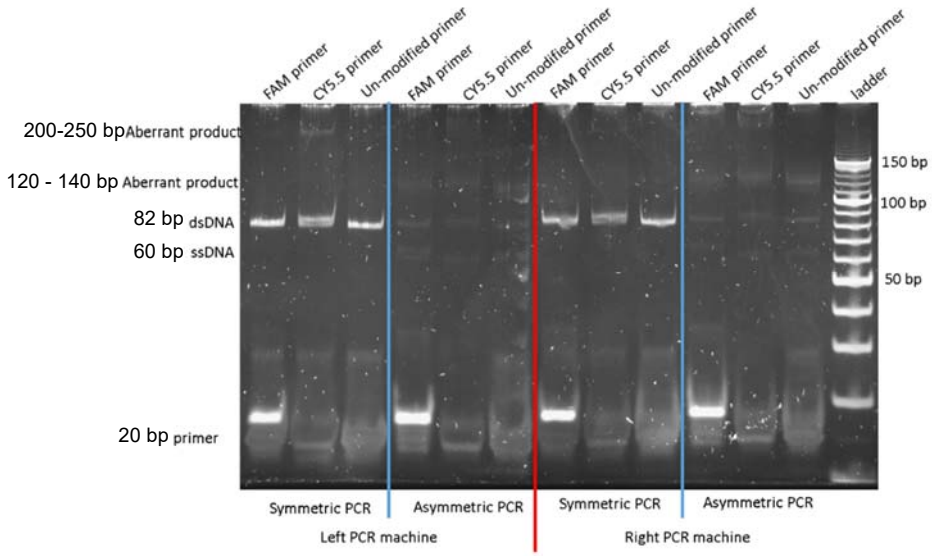

Figure 4-10 - Primer, amplification type, and thermocyclers were tested for the cause of the 120 - 140 bp aberrant products. Reactions were set up in batches and divided before being placed into the two thermocyclers, with each of the used forward primers tested in symmetric and Asymmetric PCR conditions. The red line divides the results between the two thermocyclers (PCR machine), where the blue line divides the symmetric and Asymmetric PCR results. The ladder used is a 10 bp ladder, with brighter bands displaying 150, 100, and 50 bp with each band between representing 10 bp size differences.

The template DNA used for these tests was the recovered materials from Round 1 of the FACS selection: this was the chosen template as, after one round of selection, the aptamer had been subjected to the cells but none of the amplification or purification processes. Therefore, if any amplification products were generated, they were not generated due to over cycling, eliminating that as a possibility compared to the Round 2 materials. Naive aptamer materials would have allowed for assessment of the equipment and the processes, but as soon as cells were introduced the same issue may have arisen again. Comparison of amplification patterns generated using the two available thermocyclers indicated no difference between the materials generated, suggesting that the artefacts are not due to incorrect thermal cycling. Comparison of PCR products generated

through symmetric PCR using the un-modified, FAM, and Cy5.5 labelled forward primers generated slightly differently sized materials, but as each was approximately 80 bp and the labelled dsDNA appears slightly larger; it was assumed that this difference was due to the labelled primer. Asymmetric PCR resulted in the formation of larger products (120 – 140 bp), as seen previously from Round 2 materials, suggesting that the 'contamination' was already within the FACS selection materials after Round 1, and therefore a new selection study would be necessary.

4.4.4 Foetal femur selection

Due to the slow isolation and selection processes involved when using bone marrow-derived cells, human foetal femur-derived cells were used in their place, given their ease of manipulation, proliferation rates and tissue relevance. Cells were seeded onto tissue culture flasks for the selection process, and the selection restarted using the unmodified aptamer library. Recovered cell bound aptamers were amplified in the post-recovery PCR before a cycle course was performed to determine an optimal number of PCR cycles. The recovered, amplified materials were analysed by PAGE (Figure 4-11 A). Moreover, the remaining materials were amplified by the determined optimal amounts, before purification, and seeding of Asymmetric PCR and processing to ssDNA which was also analysed by PAGE (Figure 4-11 B)

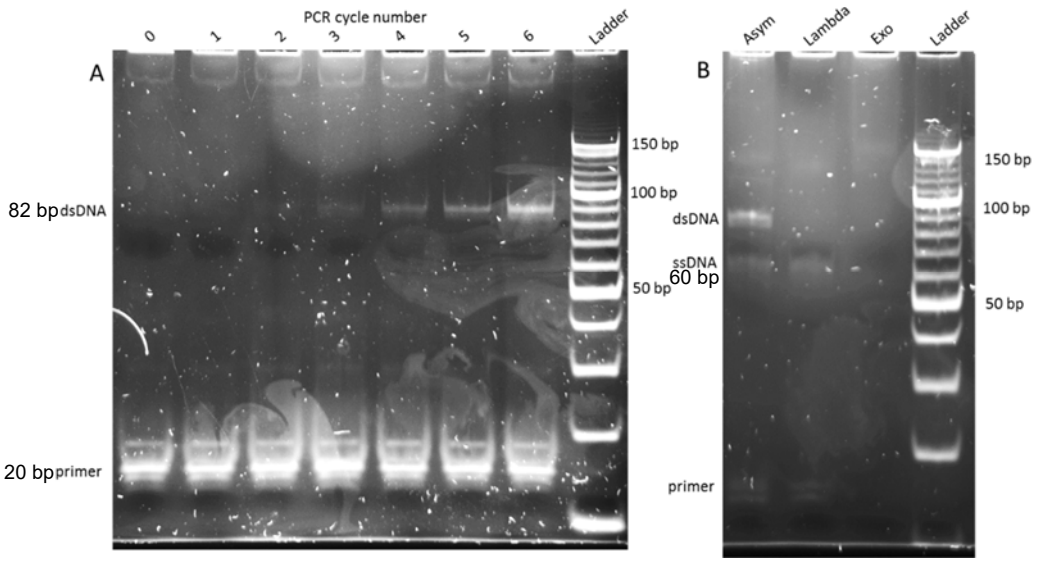

Figure 4-11 - PAGE analysis of cycle course and ssDNA generation of foetal selection Round 1 material. A) Recovered Round 1 material become visible at 3 cycles, and has a good level of materials generated by cycle 6. 5 cycles were chosen for the rest of the materials, B) materials were then purified and used to seed Asymmetric PCR, which showed dsDNA and generated ssDNA: treatment with Lambda Exonuclease removed the dsDNA, and subsequent Exonuclease I treatment removed all ssDNA. The ladder used is a 10 bp ladder, with brighter bands displaying 150, 100, and 50 bp, with each band between representing 10 bp size differences.

PCR products are visible from cycle 3 of amplification and are shown to steadily increase with each cycle (Figure 4-11 A). 5 cycles of amplification were chosen for the remaining materials before purification and seeding for Asymmetric PCR. Asymmetric PCR generated ssDNA (60 bp) as expected. Digestion with Lambda Exonuclease removed the dsDNA, and subsequent treatment with the Exonuclease I removed the ssDNA and primers (Figure 4-11 B). The ssDNA was purified and used for Round 2 of selection.

The selection was continued in this manner, with the cycle course and enzymatic tests until Round 5, where the selection process was interrupted.

Materials recovered from Round 5 were tested for optimal cycles of amplification and testing of the generated ds via PAGE (Figure 4-12).

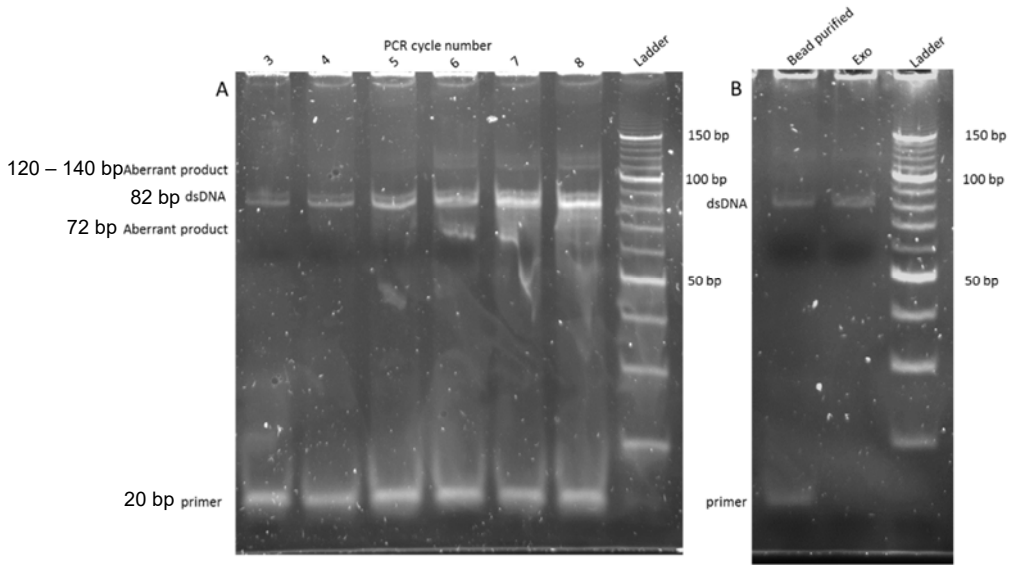

Figure 4-12 - PAGE analysis of cycle course and dsDNA purification of foetal selection Round 5 recovered material. A) amplification of the recovered materials showed aberrant products from Round 5 onwards, and the dsDNA band displayed 2 bands. Despite this second band, 4 cycles of amplification were chosen for the remaining materials, B) purification of the material showed a single band at 80 bp, where the dsDNA is expected to present, and removal of the primers by Exonuclease I treatment did not affect the 80 bp band. The ladder used is a 10 bp ladder, with brighter bands displaying 150, 100, and 50 bp, with each band between represented 10 bp size differences.

All recovered materials generated bands of material slightly larger than the expected 80 bp dsDNA (approximately 85 bp): in addition, a larger second band from 5 cycles onwards was generated (120 - 140 bp) (Figure 4-12A). 4 cycles of amplification were chosen for the remaining materials, which were then purified and treated with Exonuclease I (Figure 4-12 B). The purified materials displayed as a single band, and treatment with Exonuclease I removed the primers. The dsDNA was then purified again, quantified, and used to seed Asymmetric PCR.

As the larger 120 - 140 bp products were seen in the dsDNA cycle course more in-depth assessment of the Asymmetric PCR was carried out, using different ng

of the template to seed the reactions to assess for the aberrant products and identify the method which avoided generating it (Figure 4-13).

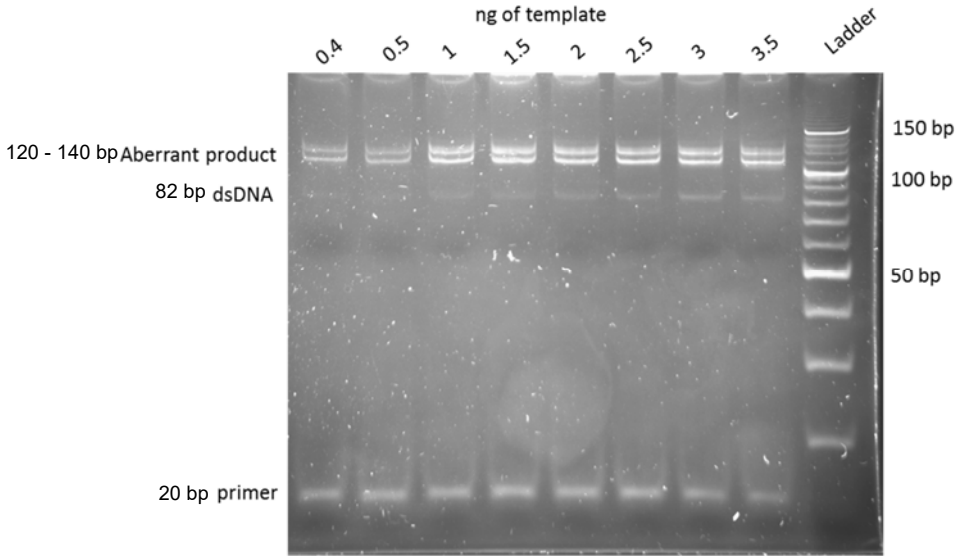

Figure 4-13 - PAGE analysis of Asymmetric PCR of the purified foetal selection Round 5 material. Asymmetric PCR seeded with varying amounts of the purified dsDNA from Round 5 materials showed no generation of ssDNA, and a large aberrant products (120 – 140 bp) which increased in abundance as template was increased. Values across the top denote ng of template in the Asymmetric PCR reaction. The ladder used is a 10 bp ladder, with brighter bands displaying 150, 100, and 50 bp, with each band between represented 10 bp size differences.

Asymmetric PCR from the purified dsDNA was performed with a range of seeding template. PAGE analysis of the Asymmetric PCR products shows different results to the expected 80 bp with 60 bp bands (Figure 4-13). The 80 bp band, corresponding to the dsDNA template, was present, but no ssDNA at 60bp is seen. A pair of larger products at ~120 – 140 bp were seen, similar size to the artefacts seen in the previous primary cell selections (sections 4.4.2and 4.4.3).

A sample of the aberrant Asymmetric PCR products were purified and digested to determine whether the bands were dsDNA (digested by Lambda Exonuclease),

or ssDNA (digested by Exonuclease I) or both. Digested samples were analysed by PAGE (Figure 4-14).

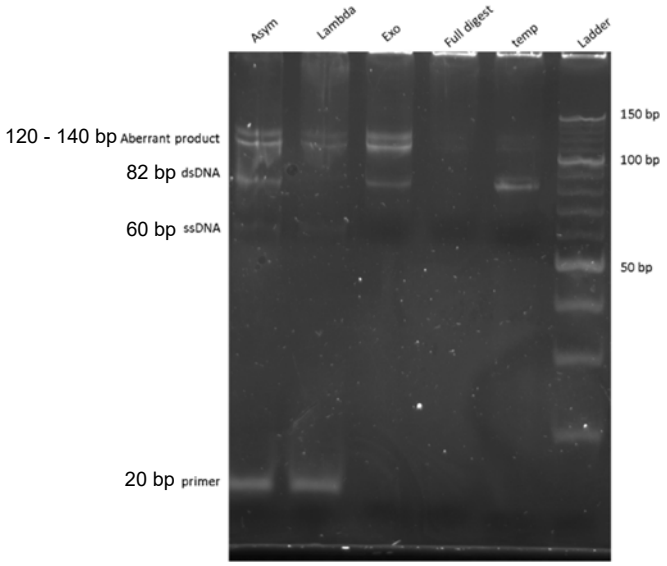

Figure 4-14 - PAGE analysis of foetal selection Round 5 materials which were tested with digestions to identify the 120 – 140 bp material characteristics. Testing of the materials generated at Round 5 another Asymmetric PCR was seeded (Asym) and the aberrant products can be seen, in addition to a low amount of ssDNA. Digestion of the Asymmetric PCR with Lambda Exonuclease (Lambda) showed degradation of the 80 bp and the 120 – 140 bp bands. Treatment of the Asymmetric PCR with Exonuclease I (Exo) showed degradation of the primers. Treating the asymmetric product with both enzymes removed all bands (full digest). The materials used as a template for the Asymmetric PCR were also shown (temp). The ladder used is a 10 bp ladder, with brighter bands displaying 150, 100, and 50 bp, with each band between represented 10 bp size differences.

The 2 larger bands were degraded (Figure 4-14) (but not completely removed) when treated with Lambda Exonuclease, suggesting that they are dsDNA, with a PO_4 modified strand. Treatment with Exonuclease I did not affect any of the upper bands, in agreement with the suggestion that these bands are dsDNA. The

digestion of the primers confirms that the Exonuclease I is active. Digestion with both enzymes degraded all materials.

As both of the upper bands were digested by Lambda Exonuclease, this suggested that material was both dsDNA and carried a PO_4 modification. As only the forward primer was present in the Asymmetric PCR, the 120 – 140 bp amplification products may have been ssDNA which was folded on itself. Testing whether the product was ssDNA was carried out by adding the reverse primer to the 120 - 140 bp materials, and a further cycle of amplification was performed. This reaction would produce the sense strand for any ssDNA present within the reaction and become dsDNA; the results of these tests were then analysed by PAGE (Figure 4-15).

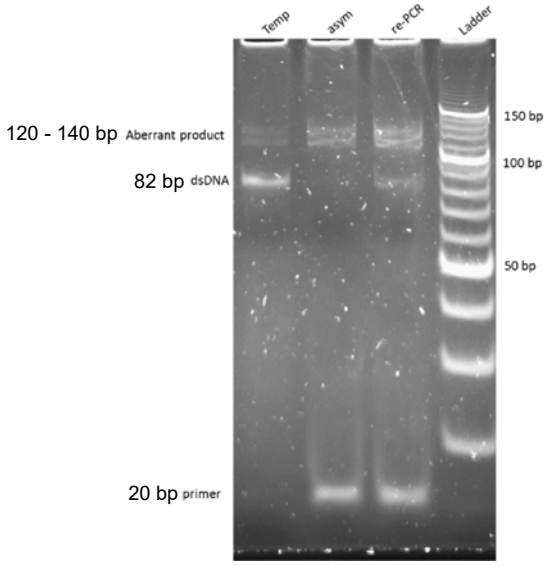

Figure 4-15 - PAGE analysis of tests to prove whether aberrant products were ss or dsDNA. Template (temp) was the same purified materials as used in Figure 4-14, however, when stained for a prolonged period, the larger products (120 - 140 bp) were visible. The template was then used to seed an Asymmetric PCR (Asym). The Asymmetric PCR materials were then taken and reverse primer added to perform a single cycle of symmetric PCR; this resulted in more products of all sizes (re-PCR). The ladder used is a 10 bp ladder, with brighter bands displaying 150, 100, and 50 bp, with each band between represented 10 bp size differences.

As the 120 - 140 bp materials were still present on the gel after the cycle of symmetric amplification, this suggested that the 120 - 140 bp products were not ssDNA which was folded on itself (Figure 4-15). However, it should be noted that the 120 – 140 bp materials were amplified from the amount seeded, which suggests the material was actively amplified in Asymmetric PCR but did not appear to amplify when both primers were present.

As the 120 - 140 bp aberrant PCR artefacts have now appeared across 3 different selections, it was thought that the reagent stocks used within the selections, amplifications and purifications could be the source of this contamination, as the primers and buffers had been remade/reordered in-between each selection iteration. The purification beads were identified as a potential source of contamination as they have been reused. The recycling of the purification beads is standard practice in other labs (personal communication), but it is possible that the washing was insufficient to remove the contaminants. New beads were used to purify the dsDNA from the FACS selection Round 1. If the beads were the source of this contamination, Round 1 materials had not yet been purified using the beads. The purified PCR products were used to seed an Asymmetric PCR, which was then digested and analysed by PAGE (Figure 4-16).

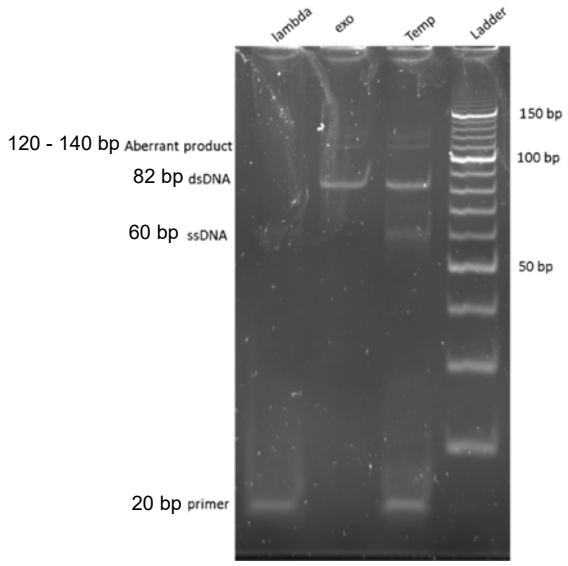

Figure 4-16 - PAGE analysis of amplification of newly purified materials from new purification beads in an attempt to prevent the 120 - 140 bp aberrant products. Round 1 materials were processed with a new batch of beads which then seeded Asymmetric PCR. Temp was the result of the Asymmetric PCR, which was subsequently treated with either Lambda Exonuclease (Lambda) or Exonuclease I (Exo). The template, despite being generated from materials purified with only new beads, still generated the larger products (120 – 140 bp) but also generated ssDNA (60 bp). The enzyme digestions both behaved the same as in Figure 4-15. The ladder used is a 10 bp ladder, with brighter bands displaying 150, 100, and 50 bp, with each band between representing 10 bp size differences.

The 120 – 140 bp bands were still present when using the new beads, suggesting the 120 – 140 bp materials were not contamination from the purification beads. After eliminating the purification beads as a potential source of the contamination further sources were tested, including the cells and water alone. These tests were performed to check if the origination of the contamination is the cells, or the process itself. Each of these was used as ‘templates’ in a mock ssDNA preparation; including the 4 cycles of PCR amplification, 10 cycles of PCR amplification, bead purification, Exonuclease I digestion, bead purification, and

Asymmetric PCR. The resulting amplification products were analysed by PAGE (Figure 4-17).

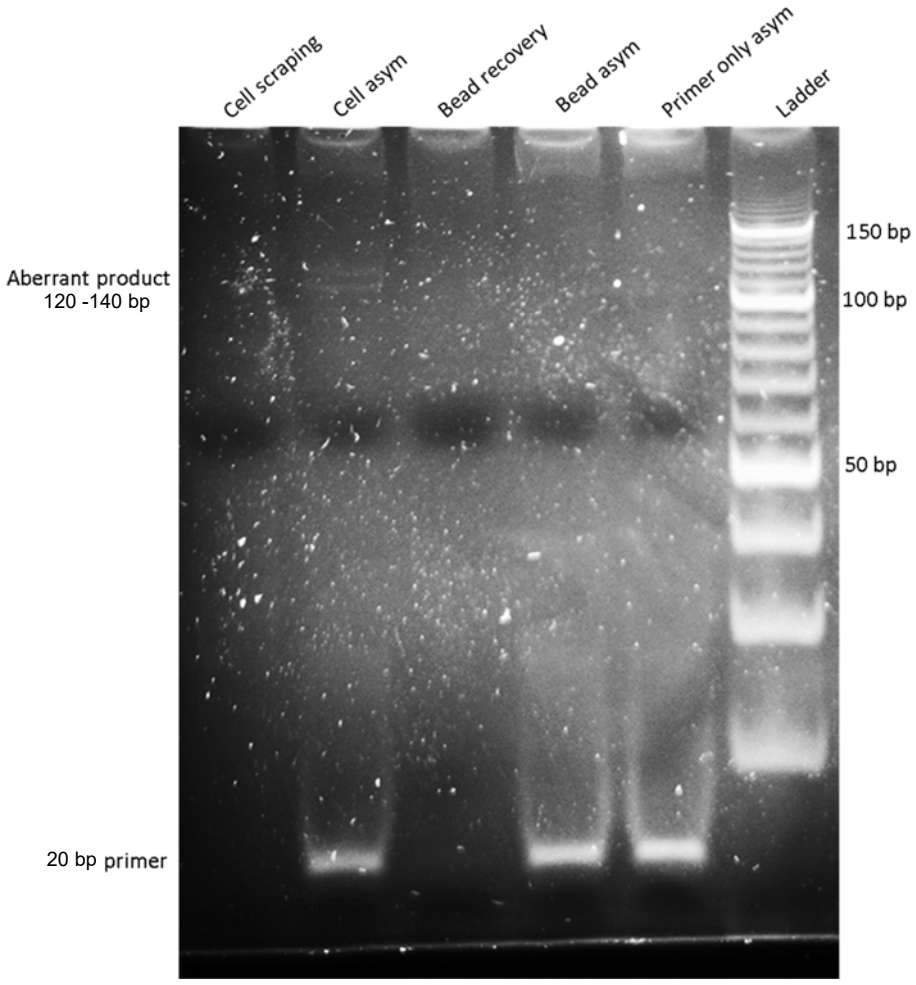

Figure 4-17 - Testing of beads, cells and Asymmetric PCR alone through PAGE to identify the source of the 120 - 140 bp aberrant products. Materials were tested to identify aberrant products source. Cell scraping shows no materials with symmetric PCR (cell scrapping), however, once the subsequent reaction was used to seed as Asymmetric PCR after purification generated large products (120 - 140 bp). Testing of the beads alone showed no materials in symmetric or Asymmetric PCR. Primer alone generated no product in Asymmetric PCR. The ladder used is a 10 bp ladder, with brighter bands displaying 150, 100, and 50 bp, with each band between represented 10 bp size differences.

No PCR products were visible from the symmetric PCR using the cell or bead templates (cell scraping and bead recovery). However, when those same PCR products were used to seed an Asymmetric PCR, the 120 - 140 bp bands were present in the ‘cell scraping only’ sample. No artefacts were seen in the bead recovery or primer alone reactions. This result suggested the material is generated from primary cell material.

4.5 Discussion

This chapter aimed to utilise the same methods used to isolate aptamers specific to the SAOS-2 cell line (Chapter 3), to generate aptamers which were specific to the SSC population. Despite the success observed in Chapter 3, the same methodology was not reproducible in the primary bone cells.

4.5.1 Preselection optimisation

Utilising the same method of pre-selection optimisation as in Chapter 3, the optimal salt conditions and incubation time for selection were assessed. The results indicated an optimal protocol incorporating 60 minutes incubation with a 1x physiological salt equivalent. This selection condition enabled aptamers to fold, approach, and bind to various targets through masking of charges as discussed in Chapter 3. The pre-selection optimisation results did not show similar trends to the pre-selection optimisation in Chapter 3. Time and salt concentrations of 0x and 1x showed decreasing recovery with time, while with 10x salt, recovery was unaffected by time. As discussed in Chapter 3, different salts facilitate the formation of aptamer structure (Smestad and Maher, 2013, Lane et al., 2008), mask repulsive charges (Hianik et al., 2007, Yan and Huang, 2009), and facilitate protein-nucleic acid interactions.

4.5.2 Bone marrow selection

The bone marrow selection was performed on samples which were isolated and grown in tissue culture flasks (T-75) until confluent. This method allowed several flasks to be seeded from a single patient. Different seeding densities of 20,000, 10,000, or 5,000 cells were used for confluence in 3, 4, or 5 days respectively (0), to allow aptamer amplification and purification to be performed before flask confluence. There is an argument that culturing the primary cells on tissue culture plastic can cause changes to the cells' expression profile (Januszyk et al., 2015), which could alter the surface markers on the cells, thereby potentially eliminating

the potential SSC markers being detected through aptamer selection. Therefore, selecting aptamers against cells which have not been cultured offers a cell population which is more representative of the source material and 'normal' expression of biomarker targets for the aptamers to bind.

Despite several controls and quality control steps within the aptamer amplification protocols, an aberrant 120 - 140 bp PCR product was seen in the recovered and amplified aptamer material. The contamination appeared to be readily amplifiable and persisted between purifications, which suggested that it was initially present in lower concentrations but not visualised on the acrylamide gel.

As the 120 - 140 bp products were present in the Round 2 selection material, there were no previous materials to return to within the selection. Therefore, only a new selection could be performed using the naive N40B library as the template. However, the experience of using the primary cells as a target allowed for the development of the methodology, and allowed for other methods to be incorporated into the next selection.

4.5.3 Bone marrow FACS selection

To ensure contamination of the previous selection would not be carried over, new primers and media were used, in an attempt to eliminate the proliferation of template contamination which may have been present.

The incorporation of FACS into the aptamer selection offered an opportunity to monitor the aptamer selection process round on round, as well as after the selection with qPCR. The signal generated from the fluorescently tagged aptamers allowed for sorting of only cells which had bound aptamers, through careful gating and recovery, and cells bound with aptamers from Round 1 to Round 2 significantly increased (Figure 4-5 and Figure 4-7). This process would have allowed for greater population narrowing later in the rounds of selection (and therefore more stringent selection) through the use of the STRO-1 and CD146 antibodies.

The utility of the MACS/FACS isolation, in combination with the aptamer selection, provided a promising platform for SSC biomarker discovery. However, the entirety of the protocol had many stages and took an extended period to perform, with each round of isolation and selection taking approximately 12-13 hours. Despite the protocol length, performing the isolation and selection in one extended methodology without culturing the cells limited any potential changes in expression (and potentially epitopes). The use of this method, therefore, provides the closest natural expression and presentation available outside of a human body, and therefore the most accurate cell source for aptamer selection.

Despite generating and ordering new materials between selections with new forward and reverse primers, selection media, and folding media, and naive aptamer library; the same aberrant 120 -140 bp PCR products were generated in the two separate attempts at the BM selections (Figure 4-4 and Figure 4-9). The fact that the material has been identified after Round 2 but not Round 1 of selection suggests that the materials are in low concentration after Round 1 of selection and are retained, and therefore build up until are visible on the acrylamide gel.

Comparing the materials generated from identical programs on thermocyclers allowed for the testing of whether alternating between available equipment during aptamer preparation affected the outcomes. From the results gathered from the tests, the two thermocyclers produce identical materials in both symmetric and Asymmetric PCR (Figure 4-9), which narrowed the possible sources of aberrant products generation to be within the reaction and not the reaction conditions themselves.

Because of the appearance of the 120 - 140 bp products in two aptamer selections involving the primary BM cells, and the time required for each isolation and selection, an alternative target population was needed. The alternative target of foetal femur-derived MSCs allowed for a more readily available cell source which can be cultured with rapid cell expansion for desired cell numbers, as well as maintaining expression and potential epitopes which may be used to identify and isolate SSCs.

4.5.4 Foetal femur selection

As mentioned above, the foetal femur cells proliferate readily in tissue culture flasks and therefore allow for rapid expansion of the cells to specific densities, which are suitable for aptamer selection. Like the bone marrow selection, seeding cells into flasks at various densities (20, 10, and 5 thousand per cm^2) allowed for several flasks with the same passage from the same patient to be ready for selection several days apart (3, 4, and 5 days respectively) (2.3.8), thereby maintaining the passage at which the selection was performed. Maintaining the passage at a low number, as well as the same number for selections, would reduce any potential expression and epitope changes induced by extended culture.

The foetal femur cells offered a robust, proliferative population to work with, as well as being similar to cells derived from adult bone marrow (Mirmalek-Sani et al., 2006), which provided an excellent population to work with for aptamer selection.

Despite the use of new materials similar to those used before in the SAOS-2 selection (Chapter 3) (unmodified forward primers); new reverse primers; new selection and folding media; new DNase free water; and PCR reagents, the aberrant 120 - 140 bp PCR products were again present within the amplified materials. The presence of this larger material was not seen until much later in the foetal femur selection compared to the BM isolated cells (Round 5 compared to Round 2). Although there was a delay in the identification of the artefact, the fact that the material is present again within selection materials which posed an issue and needed further investigation in order to identify the source of the contamination.

Testing of the material using enzyme digestions showed that the material was dsDNA, despite appearing to be generated during Asymmetric PCR, where only one primer was present (Figure 4-15). Despite this finding, when subjected to the Lambda Exonuclease, the materials were degraded, suggesting that the materials present do have a PO_4 modification on one of the DNA strands.

Having eliminated the thermocyclers as a potential source of the PCR artefact (Figure 4-10), primers and selection materials were eliminated as well as new primer and selection materials for each of the selections. Therefore, the next materials to test for contamination were the purification beads. As the beads are washed and re-used, they have the potential to carry over materials from previous purifications. However, the beads were proven not to be the source for the 120 – 140 bp materials, as performing the purifications using new beads did not affect the emergence of the PCR artefact (Figure 4-16). Regarding troubleshooting the issue, these results left only the primers and the cells as a source; but as the product had not been seen in the SAOS-2 selection (Chapter 3), the primers were an unlikely source. By performing the usual methodology for ssDNA production, with cells only, primer only, and later a primer only Asymmetric PCR, it was seen that the primer process and the primer only Asymmetric PCR did not produce any product. However, the 'cell alone' control did produce the 120 – 140 bp products during Asymmetric PCR (Figure 4-17). This result suggests that there is a sequence within the cells which is amplifiable with the current aptamer primers. Interestingly, the 120 – 140 bp products were not seen within the SAOS-2 selection, which is also of human bone origin. The lack of 120 – 140 bp products in the SAOS-2 cells, but the presence in the primary cells, may suggest that the sequence which is being amplified may be more readily available for amplification within the primary cells.

The identity of the 120-140 bp aberrant product may be discovered through gel purification and next-generation sequencing. As the products have different lengths, Sanger sequencing may not be the correct technique to use as the length differences and potential sequence differences will affect the results. However, this process would have been a rather time-consuming and potentially expensive endeavour, on an already time constrained project. When the 120 - 140 bp product first became an issue in the bone marrow selections the industrial partners discouraged identification of the 120 -140 bp product as it was a failure of the aptamer selection and would not contribute towards a functional aptamer. However, as several selections failed due to this 120 - 140 bp product identification may have been the better course of action as it may have aided in

designing a new aptamer library and primers which are not susceptible to amplification of this sequence in the presence of primary cells.

In conclusion, the aptamer technology, while extremely exciting in the field of biomarker discovery, does have some issues to be resolved for this selection to be completed. The fact that the 120 - 140 bp PCR artefacts were generated only in the presence of the primary tissue suggests that the primer(s), and therefore the aptamer library design, may not be compatible with this kind of cell. Redesigning of an aptamer library to include longer primer regions (to limit unspecific sequence amplification) is one possibility. Another option would be to use more in-depth primer analysis tools to ensure there is no match between the genome and primers. This chapter also highlights that even with the many QC steps within the protocol, these are only as good as the detection levels possible with the acrylamide gel, and materials in low concentrations can go un-noticed until purified or amplified. Analysis of the nucleic acids on a BioAnalyzer would enable a more accurate and specific read into the materials generated and in what quantity in every sample, however, this form of analysis is costly, and a single sample would not fill the chip's 12 sample slots. This method would be more viable if multiple selections were taking place at once, so that the expensive chip and reagents are not used only for a single sample.

To this end, aptamer-based marker enrichment was not performed on the SSC population, and alternative methods of characterisation were carried out. This is the Drop-Seq methodology, which provides single-cell gene expression profiling, thereby identifying populations of cells of interest within the target population: in this case, the bone marrow.

Chapter 5 Skeletal stem cell enrichment and characterisation utilising FACS and Droplet Sequencing

5.1 Introduction

Bone is a complex multicellular structure, comprising some closely associated and structured cells, with discrete functions. However, the relative complexity of the skeletal system and its encompassed cells hampers our ability to characterise its cellular populations, predominantly due to heterogeneity within the bone marrow environment (Mendez-Ferrer et al., 2010, Vogel et al., 2003). Isolation of cell populations using surface markers and either MACS or FACS (Bonner, 1972, Miltenyi et al., 1990) has enabled a more detailed interrogation of cell populations throughout the body (Rifai et al., 2006). Cell marker based isolation can also be used on bone marrow populations (Jarocha et al., 2008, Sorrentino et al., 2008, Worthley et al., 2015); adipo- and osteogenic differentiated populations (Kollmer et al., 2013); and cancerous and non-cancerous populations (Ray et al., 2012, Diamandis, 2004). MACS and FACS can be used for more general population isolation and enrichment. Rare populations, with yet uncharacterised cellular markers, cannot be isolated and investigated as easily. For example, SSCs do not currently have an identified single unique, or set of, marker(/s), which may facilitate isolation for characterisation, or downstream applications such as their use in therapy (Gothard et al., 2011, Bianco and Robey, 2015, Lv et al., 2014).

The rarity of suitable specific stem cell markers has limited the use of FACS and MACS in SSC isolation. However, current markers and cell characteristics can be used for enrichment rather than isolation of the SSC population (Quirici et al., 2002, Gronthos, 2003, Jarocha et al., 2008, Worthley et al., 2015, Xavier et al., 2017a, Xavier et al., 2017b). Assessing the purity of the SSCs can be subsequently evaluated using

approaches like the CFU-F assay (Kern et al., 2006, Gothard et al., 2013), and differentiation assays (Carey et al., 2006, Ramirez-Zacarias et al., 1992). The main advantage of utilising the CFU-F assay is that it provides evidence of colony forming potential, a stem (progenitor) cell-associated trait (Owen and Friedenstein, 1988). The use of the aptamer technology was to provide an alternative approach to the already in-use antibodies used for SSC enrichment, however, as the selections failed, the use of the antibodies provided an alternative approach for investigating the SSC characteristics.

Within this chapter, human bone marrow cells will be sorted based on the CD146 and STRO-1 antibodies, selected due to their association with stem-like properties to enrich for the SSC population (Sorrentino et al., 2008, Gothard et al., 2014). The epitope recognised by the STRO-1 antibody marks a cell population that has been shown to encompass all CFU-F within the bone marrow (Simmons and Torok-Storb, 1991) and has recently been described as binding to heat shock cognate 70 (HSC70) (Fitter et al., 2017). While a member of the heat shock protein family HSP70 and HSC70 do not have similar functionality and perform actions within a normally functioning cell (Goldfarb et al., 2006, Soss et al., 2015). A further subset of the STRO-1 + cells is the STRO-1^{BRIGHT} population, which is a STRO-1 expressing population identified by FACS, identifying the cells with the highest abundance of STRO-1 antigen (the top 10% brightest cells). The STRO-1^{BRIGHT} cells have been shown to have a higher CFU-F capable population (Gronthos, 2003). Another marker, CD146 (M-CAM) (Shih, 1999), has been shown to enrich for the SSC population (Sorrentino et al., 2008, Sacchetti et al., 2007). The clonal progeny of individual CD146+ cells can form heterotrophic ossicles and even reform ossicles following a second transplantation (Sacchetti et al., 2007). The self-renewal and multipotent properties of CD146+ cells suggest that the SSC population is within this CD146+ subpopulation. Also, CD146- cells did not form colonies (Sacchetti et al., 2007): thus, the SSC population should be found within the two populations, which can be identified using STRO-1 and CD146. Here, these antibodies will be combined with MACS and FACS to enrich the SSC population, with FACS providing additional information about the cells isolated from the bone marrow and enriched using MACS (Figure 5-1). Using the FACS characteristics of forward scatter (FSc) and side scatter (SSc) alone, bone marrow

populations can be determined by size and granularity, respectively, with lymphocytes and mononuclear cells having low granularity when compared to granulocytes, but separated by size.

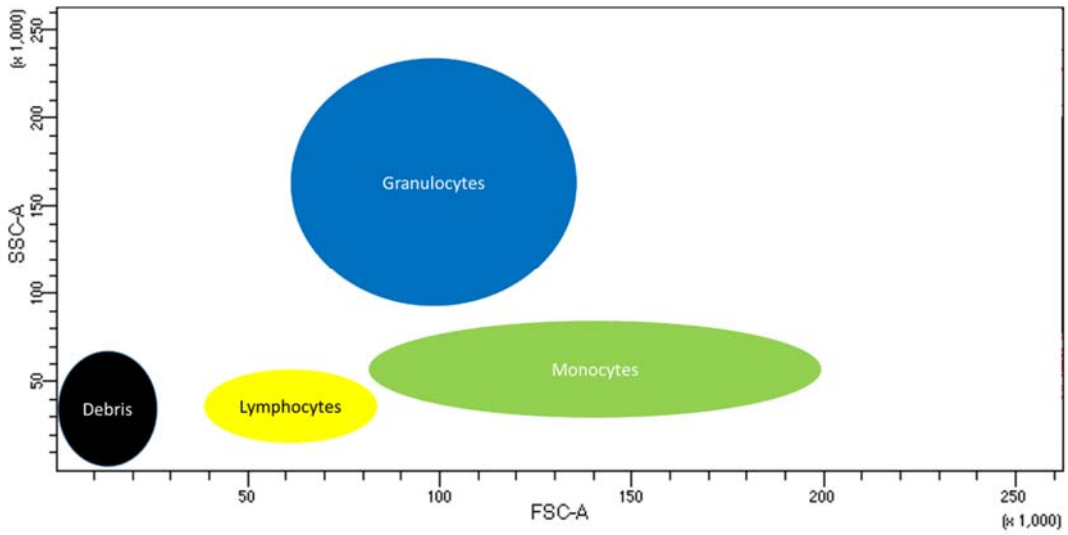

Figure 5-1 - Schematic representation of the FACS plot of forward and side scatter of a bone marrow sample. FACS analysis of the bone marrow show several distinct populations characterised by the side (granularity, or complexity of the structures within the cytoplasm) and forward (size of the cell) scatter.

Once the cells have been enriched from a bone marrow sample, further characterisation via CFU-F assays will be performed, in addition to expression profiles determined using Drop-Seq. Drop-Seq is an innovative, low-cost, single-cell RNA sequencing platform that allows full transcriptome sequencing of many thousands of individual cells (Macosko et al., 2015) within a single experiment. The resultant sequence data would be analysed using Principal Component Analysis (PCA), assessing populations for unique expression profiles that potentially may be used for isolation purposes to further enrich SSCs.

5.2 Aims and objectives

5.2.1 Hypothesis

Bone marrow cells can be sorted using a combination of currently-used antibodies to enable further characterisation of the heterogeneous bone marrow population in combination with single cell RNA analysis to identify the SSC.

5.2.2 Aims

1. To use the STRO-1 and CD146 antibodies to identify a skeletal stem cell population containing the highest CFU-F.
2. To use an enriched SSC population and single cell RNA analysis (Drop-Seq) to enhance the characterisation of the cells' marker expression profile.
3. To identify novel markers using single cell RNA analysis (Drop-Seq which may be used to further characterise and isolate the SSC population.

5.3 Methods

Methods and materials used in this chapter are detailed in Chapter 2 (2.4)

The statistical tests used in this chapter are also references within Chapter 2 (2.5)

The code for analysis is detailed with all figures generated in Appendix 1.

Due to the complexity of the processes performed in this chapter, a workflow diagram has been included to aid in the replication of this technique Figure 5-2.

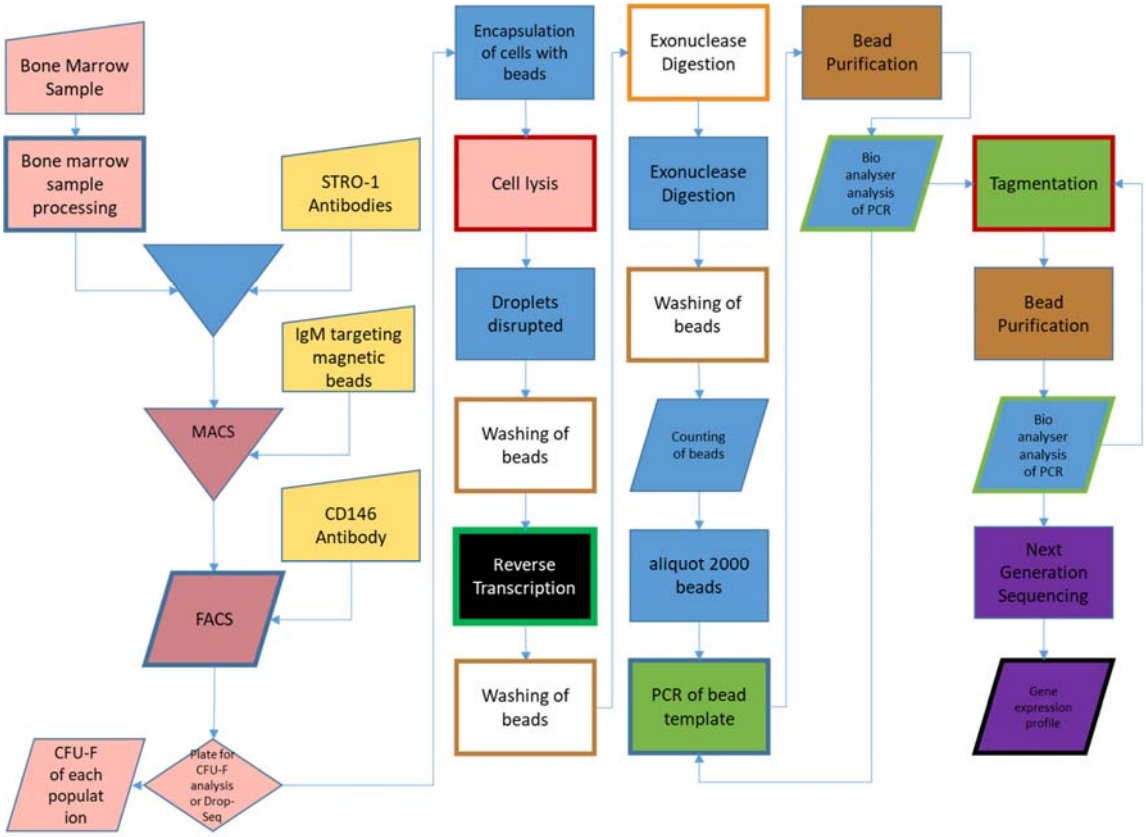

Figure 5-2 - Workflow diagram of Bone marrow Drop-Seq.

Preparation of samples for Drop-Seq analysis is not easy, however, the data that can be gained from this complicated makes this process a worthwhile endeavour. Pink boxes are related to the cells, beginning with the sample preparation. Then the inclusion of the antibodies (yellow) for the MACS and FACS processes (dark pink). Output from the FACS can then either be used for CFU-F analysis of the samples, or Drop-Seq analysis. The preparation of a Drop-Seq library is linear from this point, with two decision steps with the quantification using the BioAnalyzer to ensure the Library preparation has been performed correctly until that point, as well as informing on next steps. The final output of the process is the next generation sequencing data which is the gene expression profile of many individual cells, (maximum of 2000 due to number of beads used).

5.4 Results

5.4.1 MACS and FACS sorting of primary cells

Several human bone marrow samples were magnetically and fluorescently cell-sorted to be enriched based on STRO-1 and CD146 markers. Each of the samples was assessed at multiple points: specifically, after erythrocyte lysis, after MACS isolation (with the two fractions negative and positive assessed), and after immunolabelling with FITC labelled anti-mouse IgM antibody and Alexa Fluor 647™ anti-human CD146. The samples were analysed via FACS (Figure 5-3).

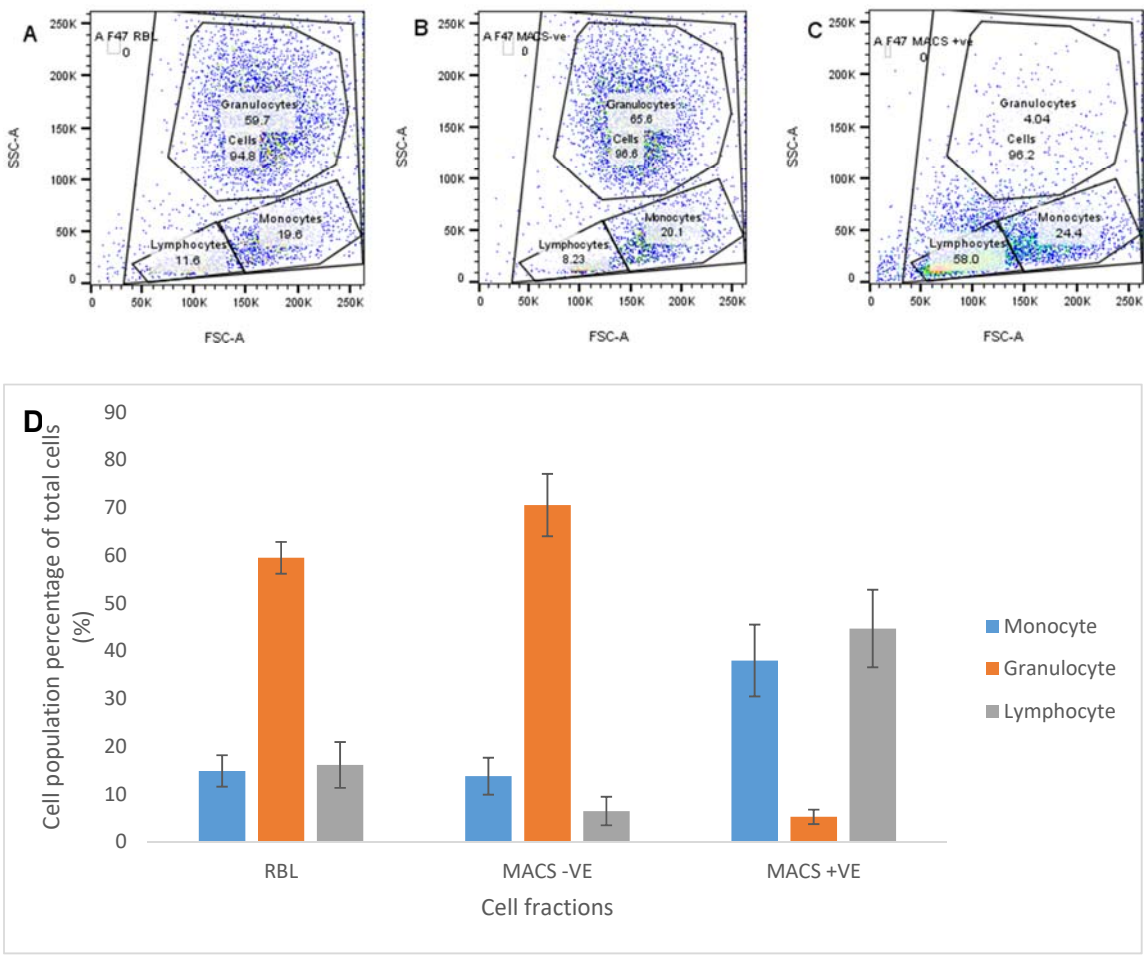

Figure 5-3 - FACS assessment of cell populations before and after MACS separation using the STRO-1 antigen. RBL (red blood lysis) represented the fraction of cells after lymphoprep and red blood cell lysis, before MACS separation, MACS –ve and +ve represented the two fractions generated by MACS separation using the STRO-1 antigen. A-C illustrate cell populations and their FSc and SSc characteristics following MACS separation. (A) FACS characterisation of cells after lymphoprep and red blood lysis. (B) MACS –ve fraction or STRO-1 –ve cells. (C) MACS +ve fraction or STRO-1 +ve cells. (D) The composition of cell populations post MACS based STRO-1 antigen sorting. Granulocytes reduced in the MACS +ve fraction and enriched in the MACS –ve population. Monocyte and lymphocyte fractions increased in proportion following MACS enrichment. n=5, bars represent standard deviation.

The proportions of the cell types are altered through a stepwise separation with clear enrichment of the mononuclear and lymphocyte fractions following MACS separation,

predominantly through the removal of the granulocytes (Figure 5-3 A, B, and C). FACS based STRO-1 antigen application demonstrated a clear population enrichment for the monocyte and lymphocyte fractions with depletion of the granulocytes before labelling with antibodies (Figure 5-3 C and D). Following MACS separation of the cells based on the STRO-1 antigen, immunolabelling of the MACS +ve fraction was performed, and the subsequent shifts in fluorescence were assessed using FACS. The STRO-1 antibody (mouse anti-human STRO-1 IgM), the secondary (goat anti-mouse IgM Alexafluor 488), and the CD146 antibody (mouse anti-human CD146 Alexafluor 647) provide the binding to antigens and the fluorescent signal shifts away from the baseline level, seen in the unlabelled population (Figure 5-4).

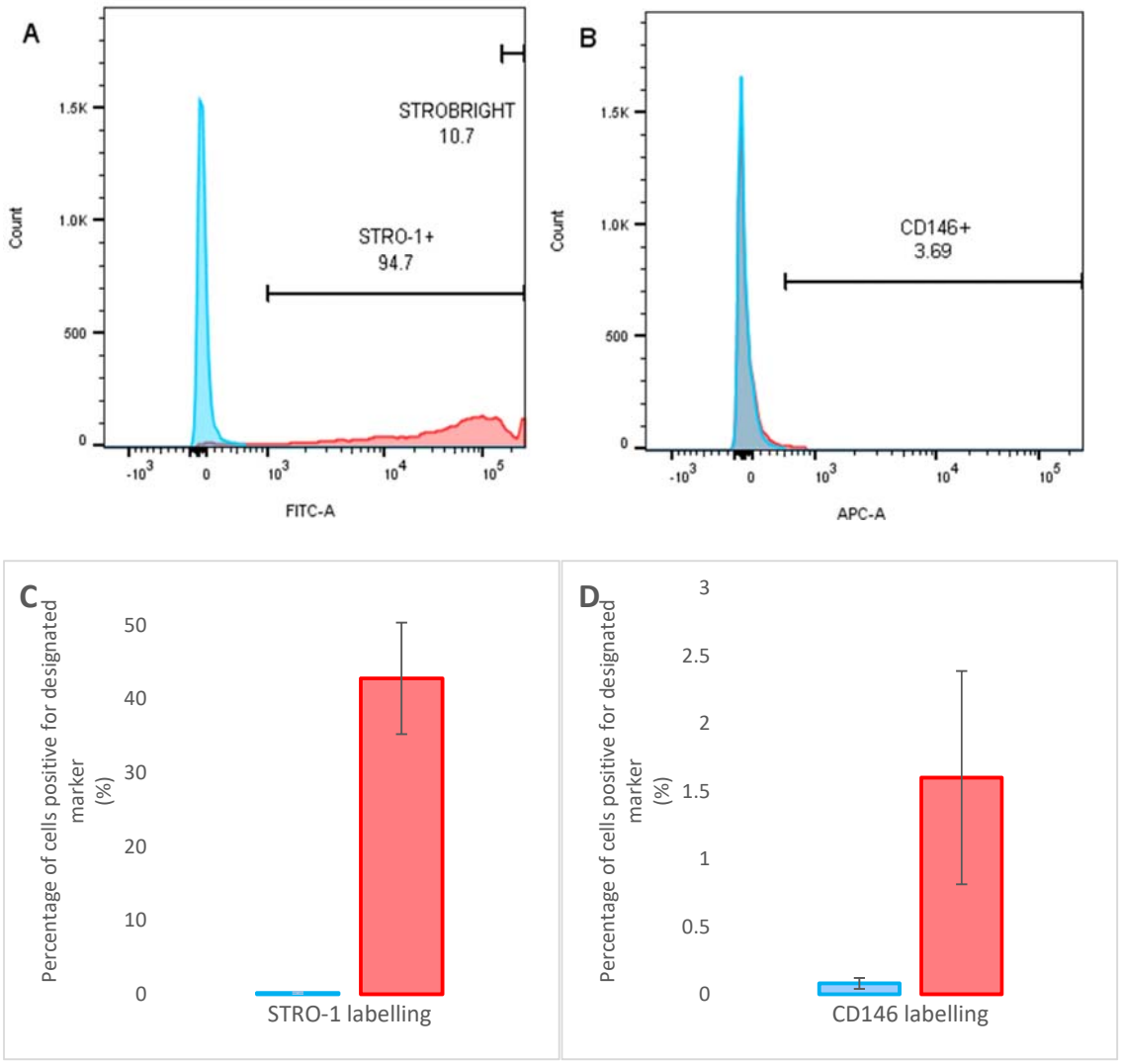

Figure 5-4 - Immunolabelling of the MACS +ve fraction allowed for cell population differentiation based on the fluorescence levels. A) Shift in STRO-1+ MACS fractions highlighting MACS enrichment with a STRO-1+ population (94.7%) in the STRO-1+ gate. Of this STRO-1+ population the cells with the highest expression, and therefore more bound antibodies, produce a brighter fluorescent signal, the brightest 5-10% of the STRO-1+ population known as STRO-1^{BRIGHT}. B) CD146 detection before and after immunolabelling of the MACS STRO-1+ fraction demonstrated a shift to 3.69% of cells expressing. C) Total events which were detected with isotype labelling and STRO-1 labelling. D) Total events which were detected with isotype labelling and CD146 labelling. (A and B) Fluorescence data from the F47 sample before and after STRO-1 and CD146 labelling respectively highlighting the percentage of MNCs within the positive gate. (C and D) Data from n = 5, showing total population percentage changes. Error bars were determined from standard deviation.

The FACS analysis showed the STRO-1 enrichment of the BM population with a corresponding enhanced percentage of STRO-1+ cells (94.7%) (Figure 5-4 A). In contrast, CD146+ cells represented a smaller proportion of the STRO-1+ cell population (3.69%) (Figure 5-4 B) following assessment by FACS. Analysis of populations isolated using MACS and FACS demonstrated a significant shift in the STRO-1+ cells (from 1% to 94.7%) as expected following enrichment. The CD146+ expression demonstrated a modest shift from 1.36% to 3.69% of cells, and thus CD146+ cells represent a smaller population within the STRO-1 enriched population. The successful immunolabelling allowed for the isolation of specific populations to be assessed for colony forming capacity.

Figure 5-4 C and D showed a comparison of total events registering positive with isotype and marker immunolabelling, which highlighted similar population proportions across 5 samples. Total events were used instead of cells or MSCs, as the samples varied with proportions of populations, and assessing what the proportions were after MACS would be important if the population were used after MACS alone.

5.4.2 CFU-F assays of sorted cells

Sorting of the cells provided many different sub-populations using MACS and FACS. However, the MACS and FACS alone do not indicate the level of enrichment for the stem-like cells. Therefore, the cells isolated using FACS based on the STRO-1 and CD146 expression were plated at 10 cells per well of a 96 well plate. The cells were cultured for two weeks, changing the media after week one, and assessed for colony formation. Distinctively individual colonies containing at least 50 cells were counted and the data collected and assessed to display the population which had the highest number of CFU-Fs, and therefore the greatest enrichment for the stem-like cells (Figure 5-5).

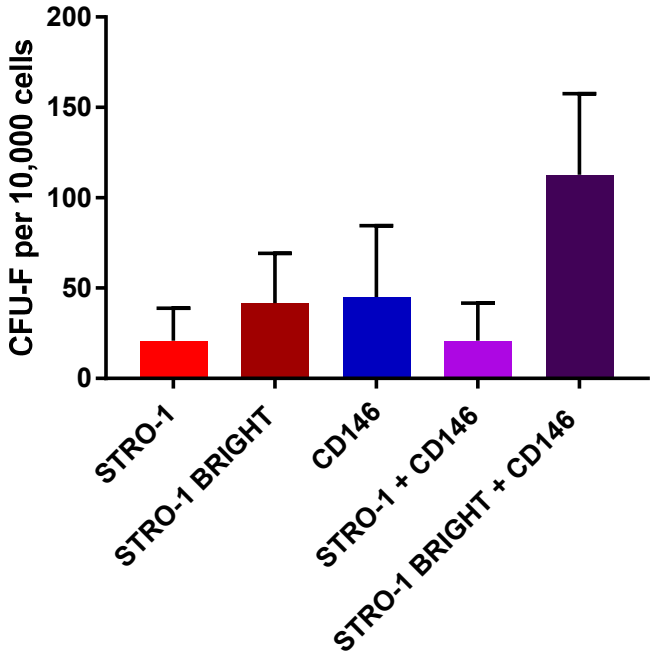

Figure 5-5 - The number of CFU-F following MACS and FACS separation was compared across different marker separation variations. Colonies were isolated using specified markers, 10 cells plated into each of a 96 well plate, which were subsequently cultured for 2 weeks before being fixed and counted. The colony numbers were calculated to the CFU-F potentially present within 10,000 cells. n=3. Statistical analysis was performed with Mann Whitney tests, no statistical significance was detected. Error bars were calculated and shown as standard deviation.

The sorting of several samples provided data from a multitude of patients, which highlighted patient-to-patient variability in the number of CFU-F that were present in each of the samples. For example, some samples produced a high number of colonies across all conditions, where some had very few colonies form. However, there was a clear trend that the combination of the STRO-1^{BRIGHT}+ (the highest STRO-1+ expressing cells identified by fluorescence intensity, gated at the top 10% brightest STRO-1 + cells) and CD146+ had a higher number of colony forming units (Figure 5-5).

Despite a trend for enhanced colony formation from STRO-1^{BRIGHT} + CD146+ skeletal populations, compared to the other cell populations, no significant difference in CFU-F was observed using the Friedman statistical test, comparing each of the populations with a P-value set at 0.05. Another issue with sample-to-sample variation was that some samples had minimal CD146+ expression.

Different isolation strategies yield different subsets of cells, which may display different morphologies. Therefore, imaging and comparison of the isolated sub-populations should be carried out to ensure morphology was not affected by the markers used for isolation. After the colonies were counted, the colonies were imaged and assessed for morphological differences caused by the difference in the markers used for isolation (Figure 5-6).

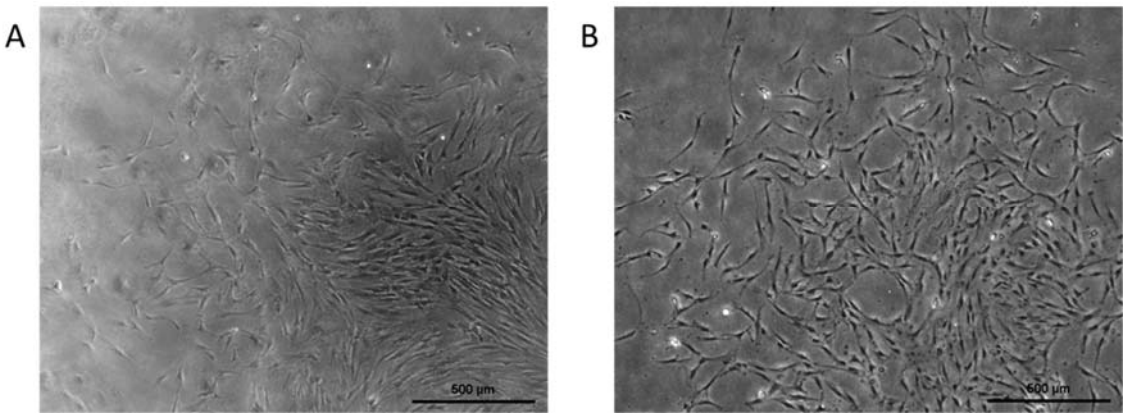

Figure 5-6 - BM cells were isolated and grown on tissue culture plastic and morphologies compared to assess morphology differences based on marker separation methods. A) Showed STRO-1+ isolated 10 cells per well, which were cultured for 2 weeks before being fixed and assessed for colonies. B) Showed STRO-1^{BRIGHT}+ CD146+ isolated 10 cells per well, which were cultured for 2 weeks before being fixed and assessed for colonies. A and B 2.5x magnification.

Colonies generated from either the STRO-1+ marker or the STRO-1^{BRIGHT} + CD146+ did not display any differences in morphology within the colonies from each fraction. 4x magnification Figure 5-6 A and B showed similar morphological features between STRO-1+ isolated and STRO-1^{BRIGHT}+ CD146+ isolated cells.

Despite the increased trend for higher colony forming units within the STRO-1^{BRIGHT} CD146+ cells, this population represented a tiny proportion of the samples (with only 48 cells identified within a 10,000 cell snapshot of the sample during cell characterisation before cell sorting). This limited cell number proved insufficient to perform Drop-Seq, as 100,000 cells are necessary for encapsulation and subsequent sequencing of the cells because of the probability of beads and cells being co-encapsulated allowing for analysis, and losses within the microfluidic chamber. Therefore, a population of cells from which a more substantial number of cells could be isolated was required. To this end, a combination of the STRO-1+ MACS and CD146+ based FACS was chosen to generate sufficient cells to enable single cell RNA (Drop-Seq) characterisation. Therefore the STRO-1 and STRO-1 + CD146 cells

needed to be compared to ensure there are no significant differences morphologically (Figure 5-7).

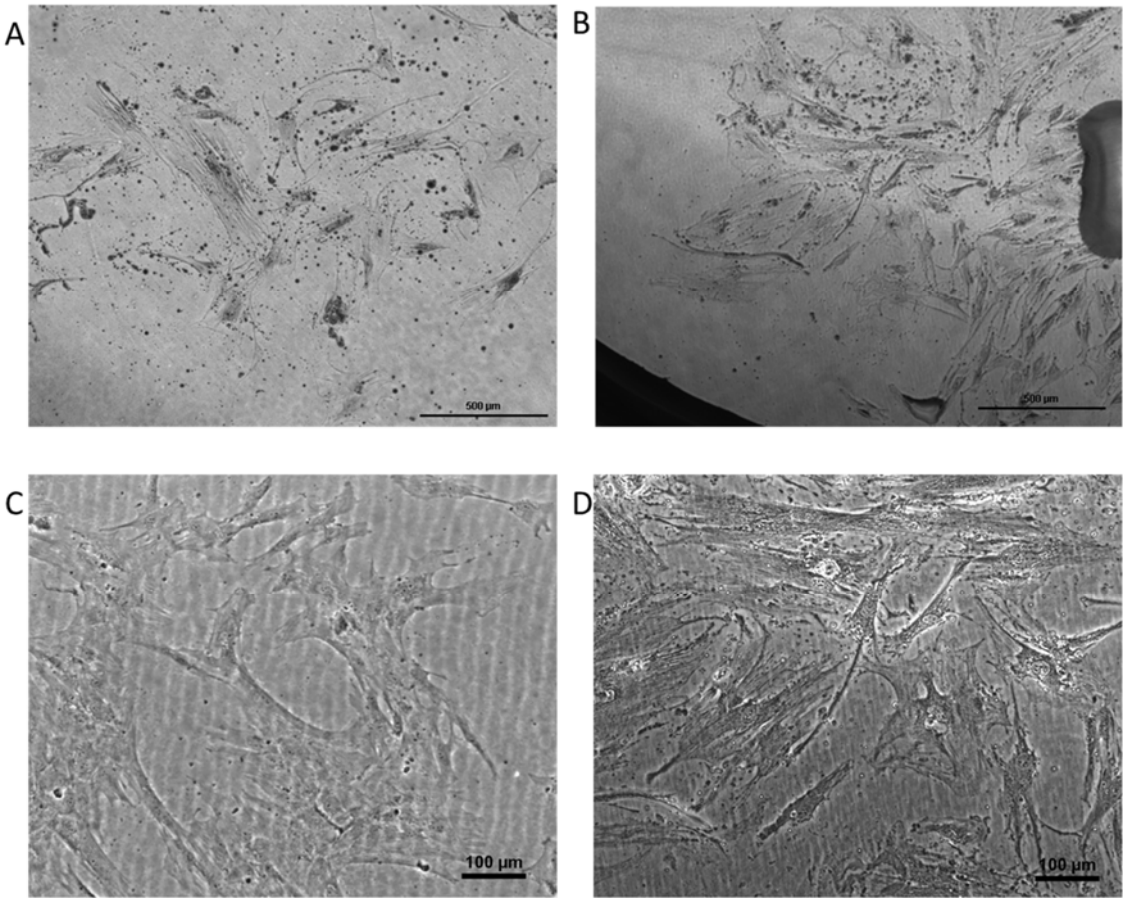

Figure 5-7 - STRO-1 and STRO-1 + CD146 isolated cells compared in morphology. Cells were isolated using either STRO-1 only or STRO-1 then CD146 antibodies using FACS, these two cell populations were then cultured and imaged to assess cell differences between these populations before their use in Drop-Seq. A and C are STRO-1 isolated cells at 5x and 10x. B and D are STRO-1 + CD146 isolated cells at 5x and 10x. Cells were isolated based on STRO-1 + or STRO-1 + CD146 + and 10 cells placed into each 96 well plates, before being cultured for 2 weeks. When the cells were fixed and assessed for colonies. The wavy patterns on C and D are an effect at higher magnifications on tissue culture plastic.

As can be seen in Figure 5-7 colonies formed from STRO-1 isolated, and STRO-1 CD146 isolated cell populations did not vary in morphology. However, it can be noted that this sample grow more slowly than the sample used for STRO-1 + and STRO-

1^{BRIGHT}+ CD146+ comparison (Figure 5-6). However as the cells showed no difference in morphology, the STRO-1+ CD146+ cells were then used for Drop-Seq analysis.

5.4.3 Drop-Seq of enriched SSC

Using STRO-1+ MACS followed by STRO-1+ CD146+ FACS based separation, human bone marrow cells were sorted to enrich for the SSC population, which were subsequently processed for Drop-Seq. After ensuring library purity and integrity following PCR and ‘tagmentation’ using the BioAnalyzer, the resultant materials were sequenced. The raw reads from the next generation sequencing were aligned to the human genome (hg19) and analysed by Digital Gene Expression (DGE) matrix (Rodriguez-Esteban et al., 2015). The genes were then assessed for PCA, and the PCs assessed using the heatmaps generated for each to assess for gene importance to cell population differences (Figure 5-8).

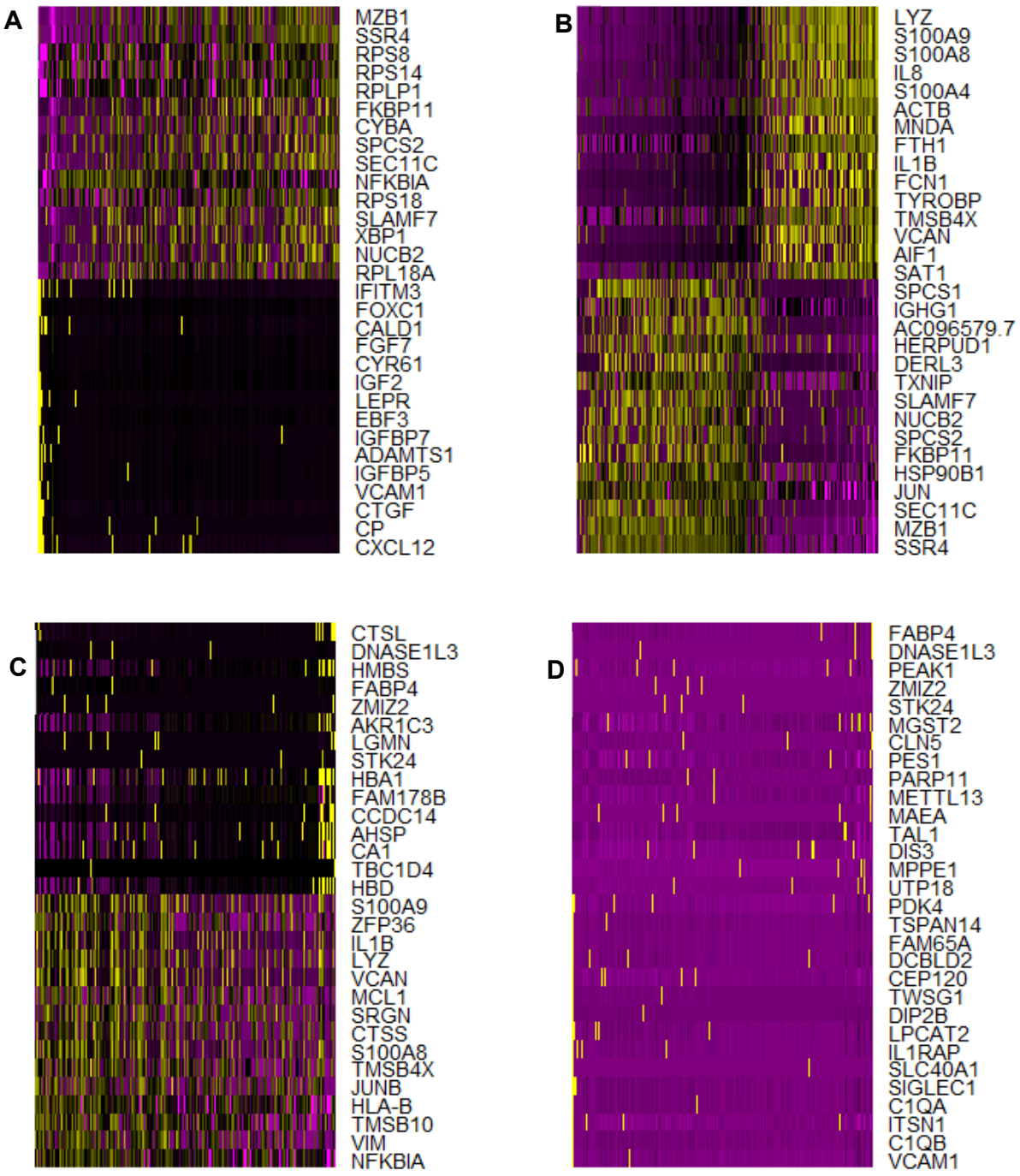

Figure 5-8 - The principal components were assessed for substantial variance for those which should be included in the cell clustering analysis. A) Principal Component 1 (PC1) showing 2 distinct expression profiles. B) Principal Component 2 (PC2) showing 2 distinct expression profiles. C) Principal Component 3 (PC3) showing 2 distinct expression profiles. D) Principal Component 4 (PC4) showing no distinct expression profiles. Yellow represents up-regulation, purple represents down-regulation, and black represents no expression.

Figure 5-8 showed that the Components 1, 2, and 3 (Figure 5-8 A, B, and C, respectively) displayed distinct gene groupings within them that can be used for clustering of cell populations in the tSNE analysis. Figure 5-8 D showed no real variation in the expression of genes within the principal component, and therefore, would most likely only add noise to the analysis, reducing the ability for cluster identification. Therefore, only the first 3 PCs were used in further analysis.

The first 3 PCs were used to identify cells with common and different expressions. Common expressions of genes located cells within proximity were different expressions of genes located cells further apart within the TSNE plot (Figure 5-9). The TNSE plot allows for ease of visualisation of multiple dimensions (PCs) with similarly expressing clusters being grouped. The apparent groupings relate directly to expression similarity. However, the distance between the clusters should not be used as a measure of cluster differences or similarity, and should not be used for making statements about the data without further analysis.

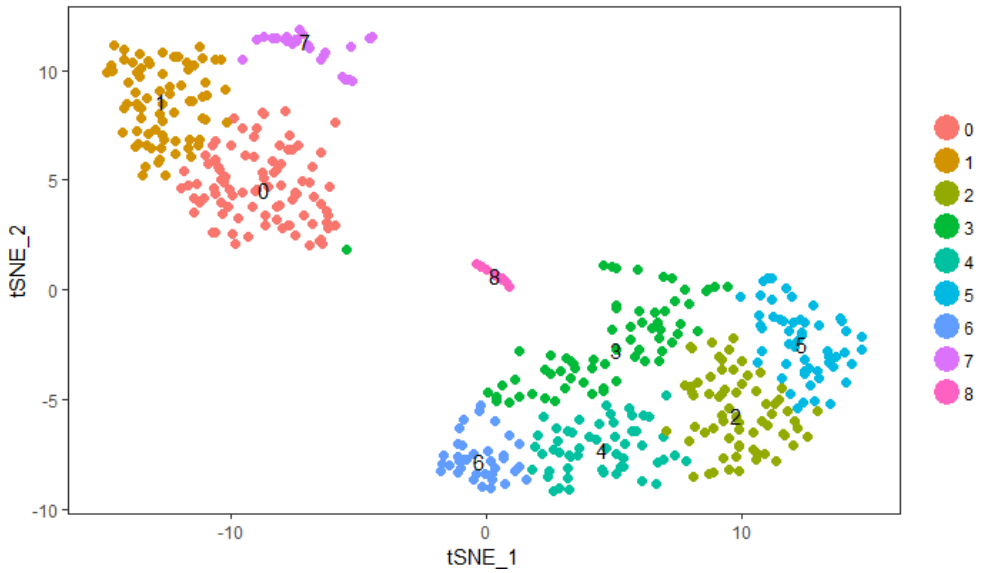

Figure 5-9 - A TSNE plot was generated using the first 3 PCs to identify cell clusters based on gene expression profiles. The clusters were identified using a resolution of 1.2 by the Seurat FindClusters command. Clusters 0, 1 and 7 are grouped into one cell population, Clusters 2 to 6 were grouped into a further cell population, and Cluster 8 was observed to be independent of the other two larger groups.

A resolution of 1.7 during the FindClusters command identified 9 clusters due to their expression profiles. The 9 clusters were localised into 3 distinct locations within the TSNE plot (Figure 5-9). Clusters 0, 1, and 7 were localised into one grouping; Cluster 2, 3, 4, 5, and 6 into another grouping; and Cluster 8 represents a unique population, different from the other 2 groupings.

As the clustering identified 9 unique clusters, each of the clusters was interrogated for the 2 genes with the highest significance from other clusters (determined using the 'bimod' statistical test). These genes were superimposed on the TSNE plot to demonstrate where the genes were expressed (Figure 5-10).

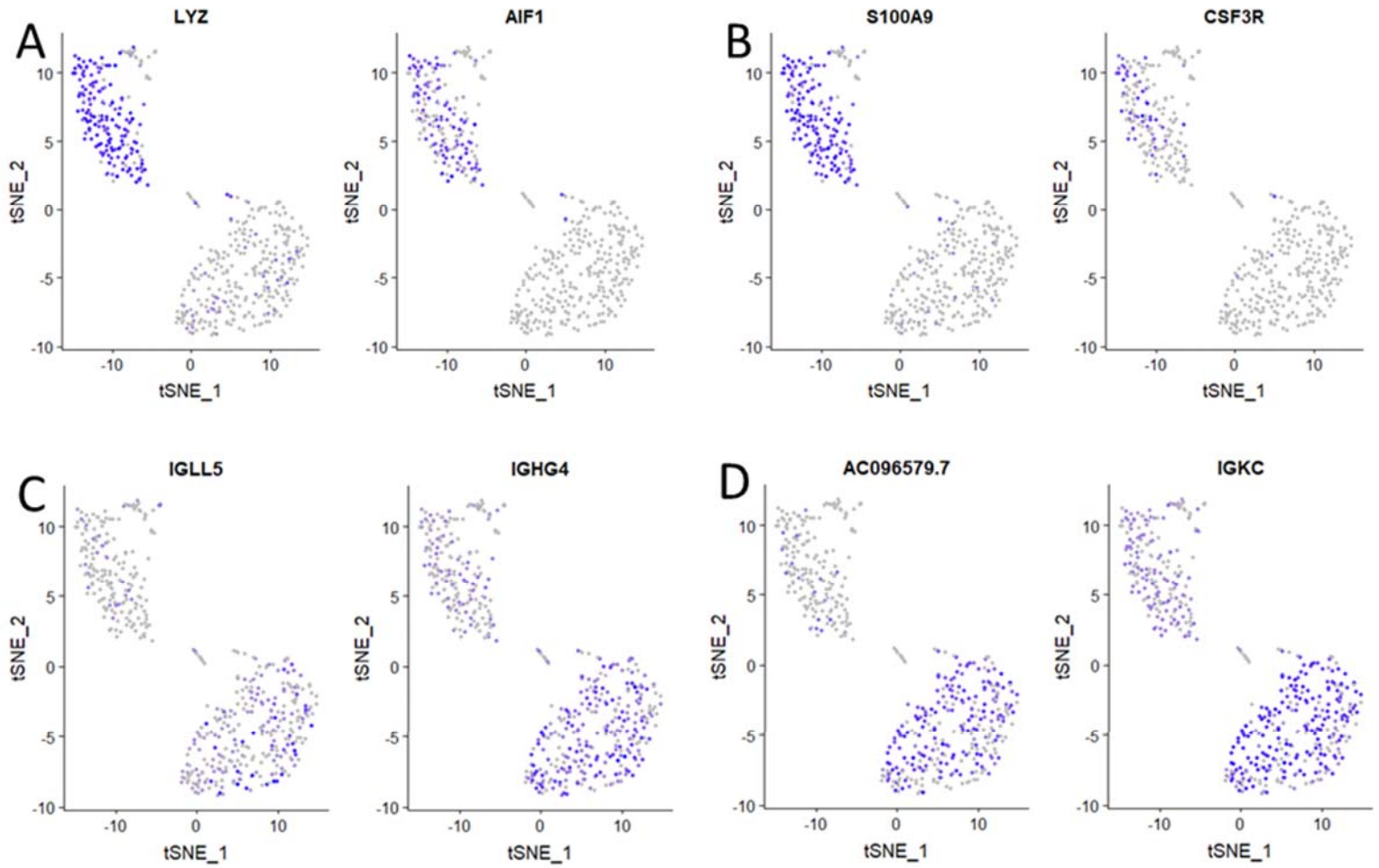
A
LYZ
AIF1
B
S100A9
CSF3R
C
IGLL5
IGHG4
D
AC096579.7
IGKC
tSNE_1
tSNE_2

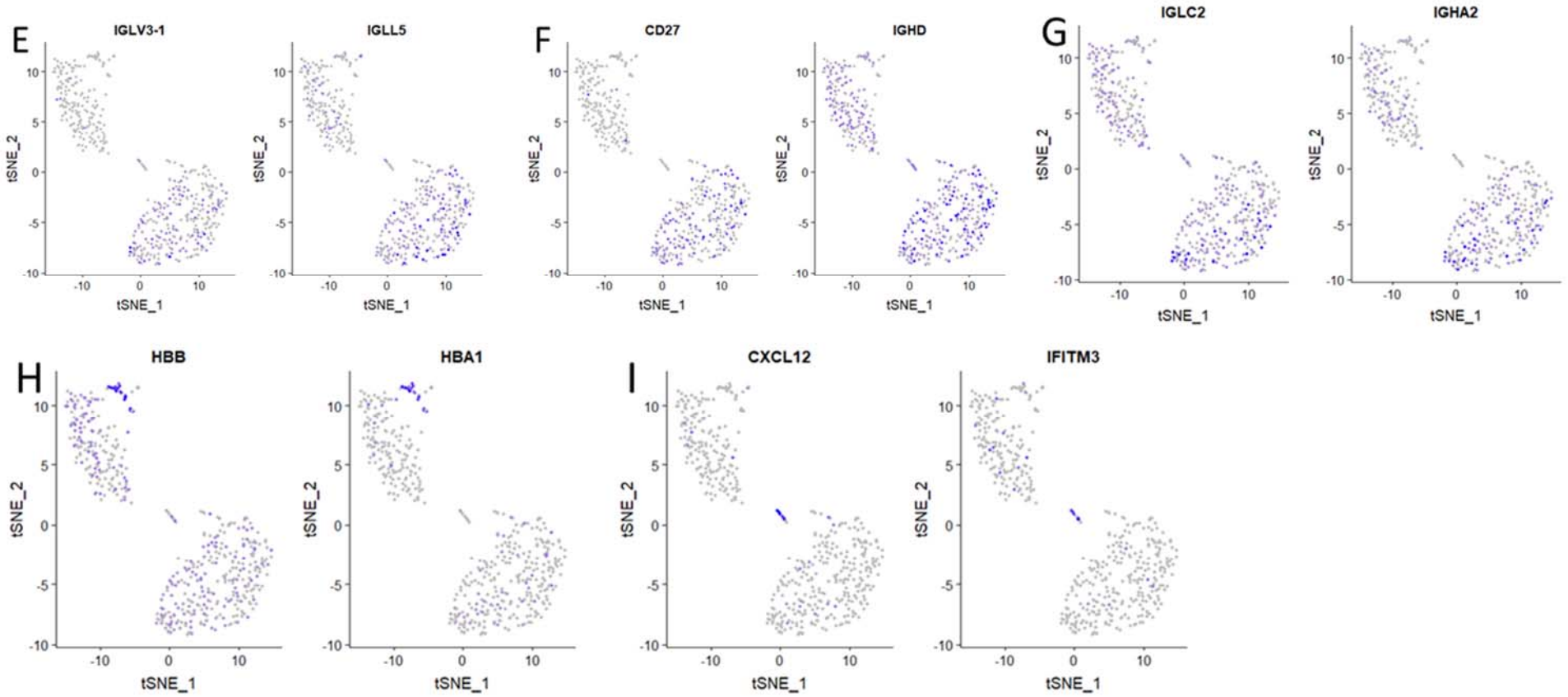

Figure 5-10 - Cells with positive gene expression overlaid onto the TSNE to highlight areas of abundant gene expression. The top two gene hits from each of the 9 identified clusters were overlaid on the cluster map. (A and B) Showed the top 2 genes from Cluster 0 and 1 overlaid with the TSNE plot. (C to G) Showed that the top 2 genes of the 5 Clusters (Clusters 2-6). (H) Showed the top 2 genes from Cluster 7. (I) showed genes from Cluster 8

.

The overlaying of the significant genes from each cluster on to the TSNE plot revealed that genes which were identified as significant within a specific cluster, were present within the larger group of clusters: for example, Figure 5-10 A and B show expression in the top left cluster grouping, where C and D show expression in the bottom right cluster grouping. Despite its grouping with Clusters 0 and 1, Cluster 7 did not share the gene expression profiles of Clusters 0 and 1. However, instead, Cluster 7 did display a unique set of genes (*HBB* and *HBA1*), present despite its proximity within the TSNE plot (Figure 5-10 H). The process of overlaying gene expressions onto the TSNE plot highlights the need for further investigation of the clusters and their localisation, rather than relying on TSNE plot cluster localisation, as Cluster 7 would have been grouped with Clusters 0 and 1 otherwise, despite a unique gene expression profile.

Cluster 8, as expected, did express its own set of genes which were not found within the other clusters (*CXCL12* and *IFITM3*) (Figure 5-10 I), showing that Cluster 8 was indeed a separate cell population from the upper and lower cluster groups, making this a unique and valuable population.

To further the analysis of the identified clusters, a heat map of gene expression was generated to verify expression of genes within clusters in an alternative way, while also incorporating more genes than were examined in Figure 5-10, as well as better represent the expression differences between the clusters and cluster groups (Figure 5-11).

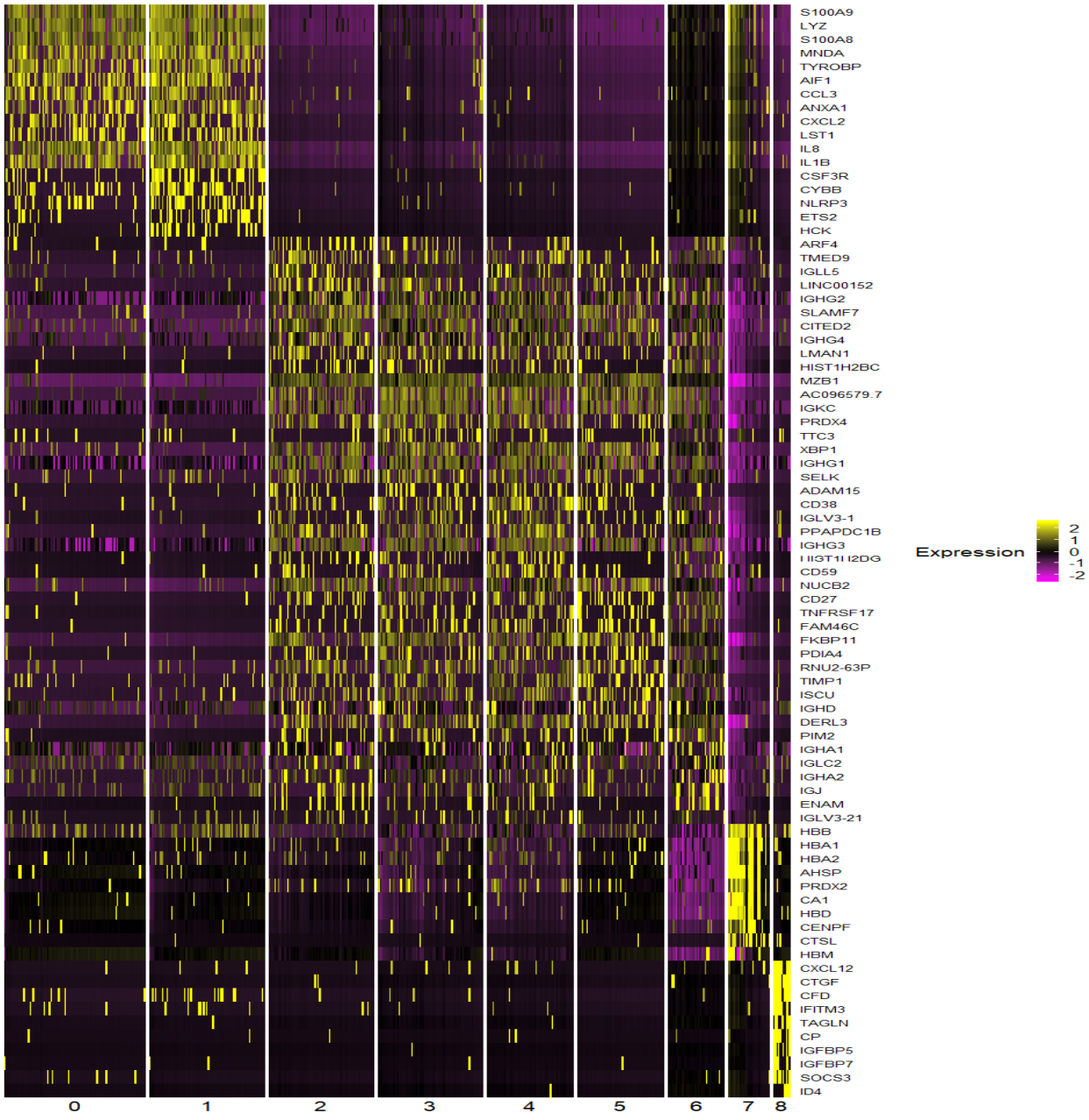

Figure 5-11 - A heat map of gene expression generated to assess gene expression differences between the cell clusters. The gene expression across the clusters highlighted several different cell populations with different gene expressions. Clusters 0 and 1 being one population, Clusters 2 to 6 being another, 7 another and 8 another. This data implies further that it was not just the top two genes expressed within the clusters which differentiate the clusters from one another. As shown in the key, yellow represents up-regulation, purple represents down-regulation, and black represents no expression.

From Figure 5-11 it was clear that there are 4 distinct cell populations with critical differing genes expression profiles. Clusters 0 and 1 shared almost all of the positive and negative expression, which suggested that these clusters are of one cell type from within the bone marrow. Further subtypes of cell populations may be present within the cluster groups; however: a more in-depth assessment, with more cells from that specific cluster grouping, would be required to identify the closely related subtypes. The same can be said of the group made up of Clusters 2 to 6, as they shared many of the same genes. Clusters 7 and 8 were two unique cell populations as their expression profiles were radically different from the other clusters and each other.

Comparing the gene expression of each of the clusters to literature describing known populations allowed for the identification of each of the clusters (Figure 5-12).

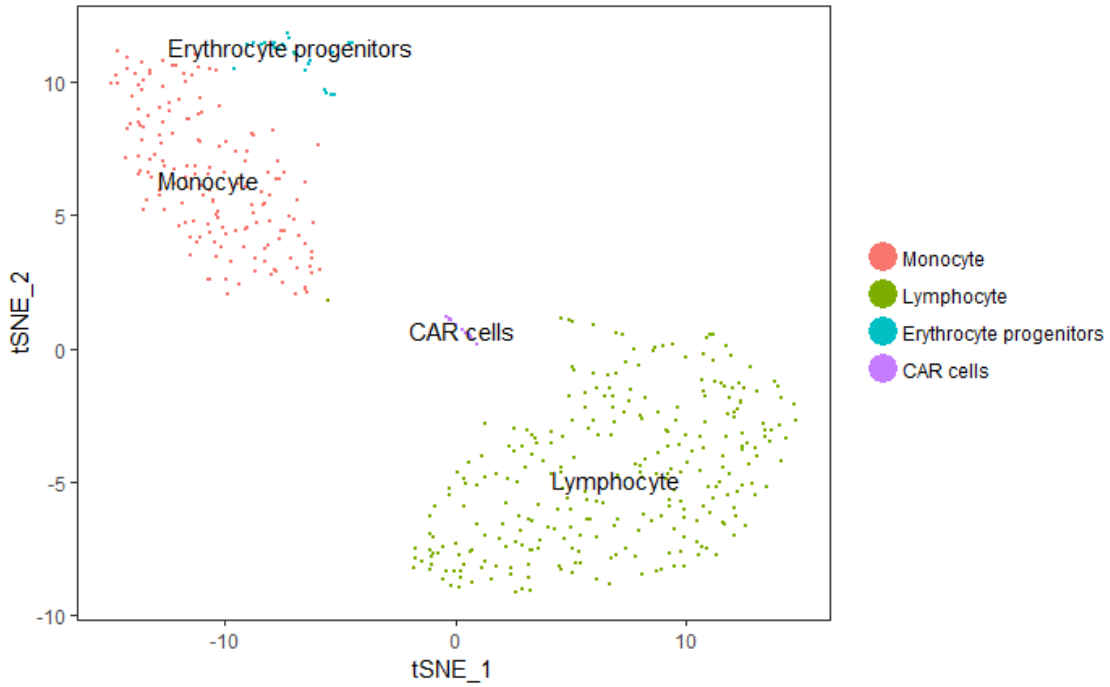

Figure 5-12 - Comparing the genes of significance to literature, each of the cluster groups allowed for the identification of the cell cluster groups. The gene expression profiles were used to identify the cell populations from which the cells were derived from within the bone marrow. This process used genes associated with specific populations to identify each of the cell populations; resulting in the identification of monocytes, lymphocytes, erythrocyte progenitors and CAR cells.

Genes such as *LYZ*, *MNDA*, and *CXCL2*, present in Clusters 0 and 1, were identified as the monocyte population. With Clusters 2 to 6 expressing many different immunoglobulins and *CD38*, this population was identified as lymphocytes. Cluster 7 featured expression of *HBB*, *HBA1*, and *HBA2* identifying these cells as erythroid progenitors. Finally, Cluster 8 with high expression of *CXCL12* helped identify this population as CXC chemokine ligand (CXCL) 12-abundant reticular (CAR) cells.

5.5 Discussion

This chapter aimed to utilise the existing antibody enrichment methods to sort for a specific cell population: the SSC. Using advanced sequencing techniques to interrogate cell populations allowed characterisation and further understanding of the heterogeneous bone marrow environment, and the SSC within it. Using the STRO-1 and CD146 epitopes for antibody binding allowed the isolation of a population, which was interrogated using Drop-Seq for gene expression profiling. Together, this revealed 4 different cell populations with unique expression; the monocytes, lymphocytes, erythrocyte progenitors, and CAR cells; the CAR cells being a highly intriguing population with direct association with the stem cell niche, regulating haematopoietic stem cells and also multipotent properties often attributed to the SSC population (Cordeiro Gomes et al., 2016, Bianco and Robey, 2015).

5.5.1 MACS and FACS sorting of primary cells

Cell sorting allows for assays of small cell populations, such as the CFU-F assays, but the process of cell sorting and the method affects the survival of the cells, and subsequently, any assays performed after sorting (Li et al., 2013). MACS provides a simple one-marker-based separation, but the survival of the cells is much higher than FACS. This trade-off may skew CFU-F assays with the higher purity: rarer cells sorted using FACS having a lower survival rate. A further issue with the sorting of rare populations is the lengthy sorting process. With cells being suspended in MACS buffer, this may limit cell survival, thus contributing to variability in the following CFU-F assays.

5.5.2 CFU-F assays of sorted cells

The differences between samples were not only found as noted previously in the population changes after MACS, but also within the colony forming unit assays using the same sorting conditions. The variation between samples prevents any statistically significant differences between the STRO-1^{BRIGHT}+ CD146+ and the

STRO-1+ alone being detected (Figure 5-5). Despite this, the STRO-1^{BRIGHT}+ CD146+ population demonstrated a higher colony forming unit capacity compared to the other makers alone, or when in combination. However, the combination of the STRO-1^{BRIGHT} and CD146 epitopes, and sorting based on antibody binding, led to a tiny population (48 cells out of 10,000). This population, regrettably, would not provide adequate cells for the Drop-Seq analysis, as over 20 million STRO-1 MACS enriched cells would need to be sorted to provide enough cells. The sorting time and sample size required for this would not be practical: therefore, a population utilising both markers (STRO-1 and CD146), but not utilising the ^{BRIGHT} fraction, was used instead to allow for cell population analysis, which allowed for cell sorting in a reasonable time, and an adequate number for both Drop-Seq and CFU-F analysis.

5.5.3 Drop-Seq of enriched SSC

The pipeline of the Drop-Seq is incredibly crucial for effective cluster identification, and subsequent gene expression identification within those clusters. Eliminating noise from the sequencing data allows for easier identification of clusters and, therefore, the genes associated with them. To this end, identifying how many PCs to use for cluster identification has the potential to eliminate some statistical noise. As the PCs identify important genes for population clustering, fewer, more varied PCs allow identification of fewer clusters with more certainty. Therefore, only the first 3 PCs were used within the analysis pipeline, as further PCs had little variation (Figure 5-8). Analysis of PCs allowed for the identification of 9 different Clusters (0-8) (Figure 5-9), at which point the analysis of which genes are important for each of the clusters could take place.

Statistical analysis of the identified clusters used the “Likelihood-ratio test for gene expression” statistical test (McDavid et al., 2013), due to it being explicitly designed for Drop-Seq data sets with large volumes of data, as well as being used within the original Drop-Seq paper (Macosko et al., 2015).

The genes identified as important for each of the clusters allowed for cell population identification, with Clusters 0 and 1 expressing *LYZ* and *S100A9* (Leculier et al., 1992, Keshav et al., 1991, Manitz et al., 2003, Zhao et al., 2012) (Figure 5-11 A and B), both of which are associated with the monocyte population, allowing for a more efficient identification of that population.

Lysozyme (*LYZ*) has long been associated from within the monocyte and macrophage populations (Keshav et al., 1991, Leculier et al., 1992), though seems to be elevated in rheumatoid arthritis (Torsteinsdóttir et al., 1999). However, detection of this gene gives a key indicator as to the type of cell population which was detected in Clusters 0 and 1.

S100A9 has been demonstrated to be a marker of Myeloid-derived suppressor cells (MDSC), which is a heterogeneous population of macrophages, granulocytes and other cells (Manitz et al., 2003, Zhao et al., 2012). The MDSC are responsible for suppressing immune responses but, in humans, do not have a defined set of markers. The fact that this marker shows up across the group of Clusters 0 and 1 suggests these cells are from myeloid origin as *S100A9* and *S100A8* are found in monocytes and early differentiation phases of macrophages (Foell et al., 2007).

Myeloid cell nuclear differentiation antigen (*MNDA*) codes for a protein expressed exclusively by monocytes, macrophages, granulocytes, their precursors (Briggs et al., 1992), and B lymphocytes (Briggs et al., 1994, Miranda et al., 1999). Building again on the evidence that the Clusters 0 and 1 are monocytes of some description, most likely with many subpopulations within them; however, more detailed population dissection would require more cells for more robust analysis.

Clusters 2-6 expressed many different immunoglobulins (Figure 5-10 C to G) (Alizadeh et al., 2000, Tallmadge et al., 2015) (Figure 5-11) which are associated with the lymphocyte population.

Cluster 7 was identified as erythrocyte progenitor cells, due to the exclusive expression of genes which encode for haemoglobin (*HBB*, *HBA1*, *HBA2*, and *HBD*), haemoglobin stabilisation (*AHSP*, *PRDX2*), or have high levels of expression on erythrocytes (*CA1*) (Bhattacharya et al., 2010). These cells were

removed during cell processing as governed by the red blood lysis protocol. These data suggest that the cells within Cluster 7 are an erythrocyte progenitor population responsible for generating erythrocytes.

Finally, Cluster 8 was found to have yet another unique expression profile, with high expression of *CXCL12* identifying the cell population as CAR cells. These CAR cells have been demonstrated to be a cell population found closely associated with and regulate the haematopoietic stem cells, as well as being multipotent, and regulators of lymphocyte development (Sugiyama et al., 2006, Cordeiro Gomes et al., 2016).

CXCL12 has been associated with a stem cell niche within the bone marrow, responsible for homing and maintenance of the haematopoietic stem cell pool through CXCL12 interacting with the CXCR4 receptor on the haematopoietic stem cells (Sugiyama et al., 2006). CXCL12 is found on the above-mentioned CAR cells (Ara et al., 2003, Tokoyoda et al., 2004), stromal cells (Nagasawa et al., 1996), osteoblasts (Dar et al., 2005), endothelial cells (Okada et al., 2002), and nestin-expressing cells (Mendez-Ferrer et al., 2010). CAR cells express high levels of the *CXCX12* compared to the other populations; express IL-7 (Cordeiro Gomes et al., 2016); and have adipo- and osteogenic genes (Sugiyama et al., 2006, Tzeng et al., 2011); have regulatory effects on haematopoietic stem cells; immune suppressing activity; and multipotent potential. These are all characteristics associated with the SSC population (Chamberlain et al., 2007, Bianco and Robey, 2015), suggesting the SSC population may be a subset of the CAR cells. Previous works have shown CAR cells isolated when enriching for SSCs within mouse bone marrow, and demonstrated a close relationship between the CAR cells and the stem cell niche (Zhou et al., 2014). In a recent paper, a group have used an alternative set of markers (PDPN+CD146−CD73+CD164+) to enrich for a cell population which is heterogeneous, displays differentiation to osteogenic and chondrogenic cell types, but not lipogenic, sharing the characteristics of the CAR cells identified within this chapter (Chan et al., 2018).

Interestingly pericytes were not identified as one of the clusters found within the STRO-1+ CD146+ population, despite their markers being identified as CD146+ NG2+ PDGFRb+ ALP+ CD34- CD45- vWF- CD144- (Crisan et al., 2008) as well as STRO-1(Simmons and Torok-Storb, 1991). Despite two of these markers being used to isolate the population which was then analysed by Drop-Seq, pericyte population was not highlighted as a main cluster. This was due to the markers identified as pericyte identifiers were not detected in the Drop-Seq analysis. As the Drop-Seq detects mRNA transcripts which are actively being transcribed, rather than protein markers which are already translated and on the surface of the cell, (like CD146 was not detected in Drop-Seq despite the cells being sorted for that marker). This may be due to a significant difference in the half-life between mRNA and protein (Vogel and Marcotte, 2012), which would explain the lack of gene expression of the CD146 and low levels of HSC70 detected in the cells isolated using these protein markers. Therefore the pericyte markers may be present at the protein level, but not at the RNA level which is what is analysed by Drop-Seq.

As literature points towards the pericytes encompassing the SSC population (Bianco and Robey, 2004, Bianco and Robey, 2015),(Alhadlaq and Mao, 2004, Avital et al., 2001, Caplan, 1991, Chan et al., 2018), with the use of two protein markers which are known markers of the pericytes, the cells which were analysed using Drop-Seq are likely to contain mainly pericytes, but identified other populations as the RNA expression profiles pointed more heavily to other populations. Therefore the SSC is likely within the pericyte population, closely associated with the HSC population, and the CAR cell population around the venous sinusoids.

Whether the SSC population is the CAR cell population (Zhou et al., 2014) or a closely related population is unclear at this point, and requires further protein expression analysis, and localisation studies. Studies on the CAR cells have shown a number of characteristics associated with the SSC population to be present, as well as speculated as possible osteogenic progenitors, one thing is clear, if these cells are not the same population, they are very closely related as shown in the schematic in Figure 5-13.

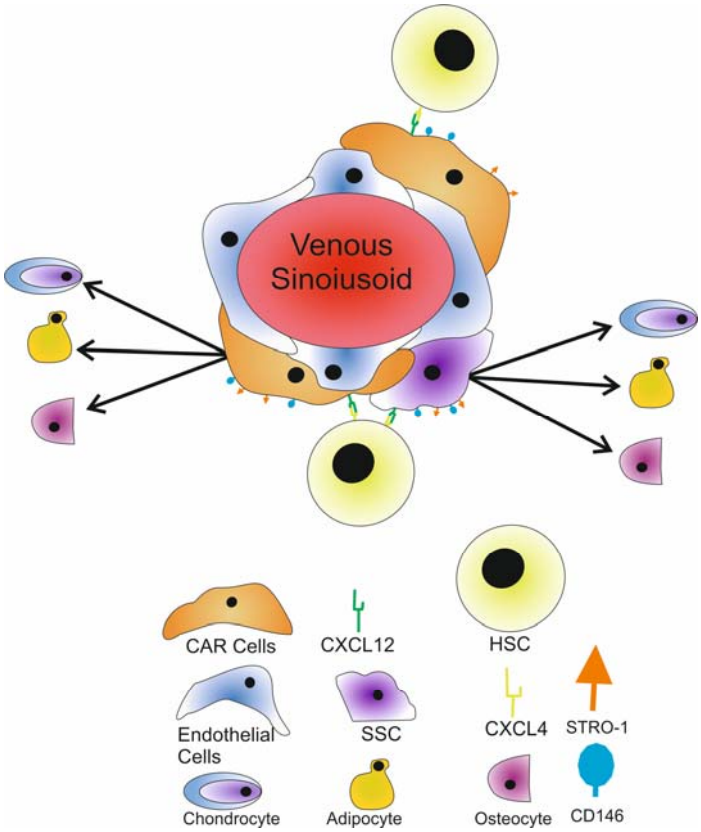

Figure 5-13 - A Schematic of where the potential SSC and CAR cells fit in the venous sinusoid. The enrichment for the SSC was performed with the STRO-1 and CD146 markers. The SSC while not identified after this work, has shown a close relationship with the CAR cells. A population which shares many characteristics associated with the SSC, and some papers even claiming the CXCL12/LEPR+ cells are the SSCs. One thing is clear, that further work is needed to narrow the search for these SSCs, but the inclusion of this Drop-Seq data does point towards a pericyte origin, with multi-lineage differentiation capability, and regulatory effects on the HSC. Despite the incomplete identification of the SSC, this diagram shows the venous sinusoid, and surrounding cells, including the CAR and SSC working together to regulate the HSC cells, with both the CAR cells and SSC cells are capable of differentiation (represented by the black arrows) into the chondrogenic, osteogenic, and adipogenic lineages. The CAR cells and the SSCs regulate the HSC through CXCL12 interaction with CXCL4.

Figure 5-13 represents the author's opinion on how the SSC system may be with the information from this thesis and literature surrounding the CAR cells taken into consideration. However, the author realises that this is with limited

information and with further works on the subject related to protein localisation of the CXCL12, as well as potential differentiation studies after isolating the CAR cells, or IL-7 expressing cells will further clarification.

In conclusion, the combination of the STRO-1^{BRIGHT} and CD146 markers identified a population of cells which had higher colony forming capacity than each other marker individually. Subsequent Drop-Seq analysis of the STRO-1+ CD146+ population, due to cell sorting limitations making STRO-1^{BRIGHT}+ CD146+ enrichment not possible, then identified the CAR cells. The CAR cells have been described within a stem cell niche in the bone marrow, and regulate haematopoietic stem cell proliferation, immune cell differentiation as well as being multipotent. These characteristics are attributed to both the CAR cell and SSC populations, and suggest that the SSC population may be a closely related to the CAR cells. Utilising the marker known to be found on the CAR cells, IL-7, it may be a possible to further the enrichment process, which may be used to select for the SSC population for further characterisation, CFU-F assessment, and ultimately clinical use, should more accurate markers not be identified following further investigation

Chapter 6 Final discussion

This thesis aimed to investigate the SSC population and improve our understanding of its characteristics. The SSCs are critical in bone regeneration and homeostasis: therefore, a better understanding of the SSCs may allow for their manipulation and potential in preventing the need for, or improving, the treatments for bone fractures and non-unions, and prevalent age-related diseases such as osteoarthritis and osteoporosis. To this end, the protein and gene expression profiles were investigated using the aptamer and Drop-Seq technologies respectively.

6.1 Overview of findings

6.1.1 Aptamer selection and methodology development against the skeletal cell line SAOS-2

Chapter 2 focused on developing methods to investigate protein expression within the SSC population, by performing and refining an aptamer selection against a human osteosarcoma cell line: the SAOS-2 cell line as a positive selection target, and the Raji cell line as a negative selection target to further refine the aptamer pool. This refinement of the aptamer pool allowed for the development of methodologies specific to adherent human bone-derived cells. Tracking of the aptamer pool recovery after each round using qPCR indicated an increase in aptamer materials bound to the SAOS-2 cells (2.2.10.2). After two rounds of selection with improved recovery, the stringency in which the selection took place was increased (Table 3-1). This increase further narrowed the aptamer pool, with the maintenance of the selection at these levels of stringency enabling the aptamer pool to be refined to a point where improved specificity of aptamer

selection was reached (Figure 3-12). After nine rounds of selection, the negative cell target of the Raji cell line was introduced to generate two aptamer pools with differing results in the materials recovered. Splitting both of the aptamer pools into two selection conditions resulted in four distinct results from each of the aptamer pools. The pool which had been exposed to the Raji cells performed better in both conditions, demonstrating the highest recovery against the SAOS-2 cells alone.

The aptamer materials which were recovered from the highest stringency selection in Round 13 (SAOS-2 cont.) were taken and clones generated from the materials. The cloning and subsequent colony picking allowed for the generation of single sequence aptamers.

Testing of these single aptamers revealed considerable variability within aptamer performance (Figure 3-15). A small number of the cloned-out aptamers showed favourable binding to the SAOS-2 cell line, demonstrating the efficacy of the aptamer approach.

6.1.2 Aptamer selection against skeletal stem cell populations

Following the establishment of the aptamer selection methodology in Chapter 3, aptamer selection was then performed on primary cells isolated from bone marrow. The aptamer selection performed against the BM-derived cells failed, as an aberrant products were generated after only two rounds of selection (Figure 4-4). Using new buffers, media, primers and naïve aptamer pool, a second selection was undertaken to incorporate FACS into the aptamer selection. The inclusion of FACS within the selection allowed for characterisation of the bone marrow cells during each round of selection, allowed for more details on the target cells to be gathered (Figure 4-5 and Figure 4-7). Despite the changing of the materials between the FACS selection and the previous selection against the BM cells, the same 120 - 140 bp aberrant products were produced, causing the

selection to fail again (Figure 4-9). Given time constraints and the ability for foetal cells to proliferate rapidly when cultured, an aptamer selection was performed using the foetal derived bone cells as the positive selection target. The main drawback of using the foetal cells resides in the fact that these cells are adherent, restricting aptamer selection through FACS of the foetal cells without disrupting the surface markers with trypsin. The foetal aptamer selection continued to Round 5 where again, despite using new materials for the foetal cell selection, the 120 - 140 bp aberrant products were generated which in the detailed analysis was found to originate from the target cells. Unfortunately, the aptamer selections against the BM and foetal cells failed due to sequences within the cells, which was readily amplifiable with the primers and aptamer library used in this work. However, with the verification of the methods of selection from Chapter 3, altering the primers and the aptamer library should allow for a more successful selection against the primary cells, and aid in identifying surface markers for SSC isolation.

6.1.3 Skeletal stem cell enrichment and characterisation utilising FACS and Drop-Seq

Isolation of several cell populations using the STRO-1+ and CD146+ markers enabled five different populations to be isolated; STRO-1+, CD146+, STRO-1^{BRIGHT}, STRO-1+ CD146+, and STRO-1^{BRIGHT}+ CD146+ populations. The STRO-1^{BRIGHT}+ CD146+ cells were not phenotypically distinct from the STRO-1+ isolated cells typically used within the Bone and Joint group (Figure 5-6) but displayed the highest number of CFU-F (Figure 5-5). However, the use of the STRO-1^{BRIGHT}+ CD146+ cells was not possible due to the cell numbers needed during the Drop-Seq protocol. Therefore, the STRO-1+ CD146+ cell population was used for Drop-Seq due to higher cell numbers isolated post FACS but which still incorporated both of the identified markers. Drop-Seq analysis revealed four distinct populations: monocytes, lymphocytes, erythrocyte progenitors, and CAR cells (Sugiyama et al., 2006, Zheng et al., 2007) (Figure 5-12). The monocytes

and lymphocytes are cells seen within the FACS analysis of the BM (Figure 5-3). The erythrocyte progenitors are known to be within the red bone marrow (Bianco et al., 1988, J B Vogler and Murphy, 1988), and the CXCL12 cells located around the venous sinusoids, closely related to the haematopoietic stem cell population (Sugiyama et al., 2006). The Drop-Seq analysis of the STRO-1+ CD146+ cells showed not only the cell populations expected and seen during the FACS but the erythrocyte progenitors and CAR cells. The CAR cells are of great interest due to their characteristics, close association with the haematopoietic stem cell population, and multipotent differentiation (Zhou et al., 2014, Zheng et al., 2007, Tzeng et al., 2011, Sugiyama et al., 2006, Nagasawa et al., 1996, Nagasawa, 2014).

6.2 Contribution to knowledge

6.2.1 Aptamer selection and methodology development against the skeletal cell line SAOS-2

Chapter 3 demonstrated successful aptamer selection against a bone-derived cell population (the SAOS-2 cell line). Cloning of the aptamers from this study provided several aptamers found to bind readily to the SAOS-2 population demonstrating successful aptamer selection, with robust methods which could then be applied to more precious primary cell samples.

6.2.2 Aptamer selection against skeletal stem cell populations

Primer design is critical for aptamer selection, and extensive testing should be performed on the primers alone before aptamer pools are generated. Chapter 4 shows that despite a number of QC steps, aberrant products were detected and, although removed, the ultimate failure of the selections was due to PCR products generated during PCR from the original cell material. To this end, aptamer

primers and subsequently aptamer libraries should be designed and tested to ensure that cell materials are not amplified in any of the amplification steps.

6.2.3 Skeletal stem cell enrichment and characterisation utilising FACS and Droplet Sequencing

The STRO-1^{BRIGHT}+ CD146+ cells isolated using MACS and FACS show a clear enrichment for the SSC population. However, the limited number of cells isolated prevented this population from being used for the Drop-Seq analysis. Therefore the STRO-1+ CD146+ cells were used instead to preserve the usage of both markers, but provide the cell numbers needed for Drop-Seq. The identification of the CXCL12 gene within the STRO-1+ CD146+ isolated cells links the CAR cells identified in mice as important in regulating the HSC population, (Zhou et al., 2014), and to hold multipotent potential (Cordeiro Gomes et al., 2016). This link of the CAR cells to the STRO-1+ CD146+ cells suggests that the rare SSC population is related to the rare CAR cell population, as characteristics attributed to each of these populations were found to overlap: specifically, the characteristics of the close association with the venous sinusoids, and the haematopoietic stem cells, multipotent differentiation, and regulatory effects on the haematopoietic stem cells (Bianco and Robey, 2004, Zhou et al., 2014, Sugiyama et al., 2006, Omatsu et al., 2010).

6.3 Limitations

6.3.1 Aptamer selection and methodology development against the skeletal cell line SAOS-2

The limitations in Chapter 3 which should be considered when interpreting the data are that the clones which demonstrated a higher affinity to the SAOS-2 cells compared to the Raji cell lines remain to be sequenced. This lack of sequencing is not uncommon within cell aptamer selection literature (Guo et al., 2008, Chang et al., 2013, Shangguan et al., 2015). However, in this case, although samples

were sent off for sequencing, the results proved inconclusive with aptamer sequences.

6.3.2 Aptamer selection against skeletal stem cell populations

Detection of aberrant products from the original cell material proved a significant issue. Furthermore, the slow growth of the BM cells limited the speed at which rounds of selection could be completed, and culturing of the BM cells for extended periods of time, to enable expansion, may have affected protein expression (Siissalo et al., 2007, Januszyk et al., 2015), which could have impacted on the effectiveness of the aptamer selection.

Altering the cell target to the foetal derived bone cells may have affected, ultimately, aptamer selection. While the adult and foetal BM cells are similar, there are reported differences in these two populations (Gotherstrom, 2016). Differences in cell protein expression would result in different epitopes targeted by the naive aptamer pool. However, given selection against either of these cell sources proved unsuccessful, comparison of the final aptamer pool was not possible.

6.3.3 Skeletal stem cell enrichment and characterisation utilising FACS and Droplet Sequencing

The main limitation faced in the characterisation of the SSC population is the absence of a specific unique marker or set of markers to isolate the population. Therefore the use of other markers can be exploited to enrich for the SSC population, but limitations reside therein. The reduction in cell purity post MACS or FACS, therefore, limits the accuracy of any characterisation following enrichment steps.

Following SSC enrichment, only one sample was isolated and taken to Drop-Seq. While there were many cells within this sample which contributed to the Principal Component analysis and subsequent clustering of the cells, these cells were from a single sample, and therefore any abnormalities from the sample will be incorporated into the analysis. Limitations in cell enrichment by MACS/FACS and processing may also have impacted on data generated.

6.4 Areas for further research

The outcomes of the work within this thesis provide new avenues to characterise further and develop strategies to aid the isolation of the SSC population.

- The establishing of robust aptamer selection methods.
- Identification of an enrichment methodology which provides a small population of cells with high CFU-F capacity.
- Characterisation of the STRO-1+ CD146+ cells providing four distinct populations, including one fraction displaying an association with HSC population.

These outcomes provide new avenues to be expanded upon in the future. These areas include the testing of the CAR cells to determine whether the SSC population is a subpopulation or encompass the CAR cell population.

Aptamer technology is a very viable approach to SSC marker discovery and exploitation, however as this study has shown primer design and subsequent aptamer libraries need to be designed with the cell nucleic materials in mind.

After isolation using either CAR cells based markers, the aptamers generated once a selection is completed, or the PDPN+ CD146- CD73+ CD164+ markers, the cell populations should be compared. Further to comparisons, pathways of stem cells may then be further studied to identify areas where the cells may be

manipulated to combat known disease states such as osteoarthritis and osteoporosis, or grown more readily to aid in the repair of broken bones and joints.

6.5 Conclusion

The SSC is an essential element within the skeletal system for repair and homeostasis. With little known about this rare cell population, further characterisation would expand not only the knowledge base within the skeletal system but offer potential treatments for musculoskeletal diseases.

A protein expression profile was undertaken using the aptamer technology to identify new markers for the SSC. Aptamer selection is a cyclical process of narrowing a diverse range of nucleic acid sequences to a refined pool of sequences, in this case, which would bind specifically to the SSC cell epitopes. A gene expression profile was approached using the Drop-Seq methodology, where tissues were isolated based on markers, and individual cells compartmentalised with functionalised beads. The cells were then lysed, with all the mRNA binding to the beads for subsequent reverse transcription, incorporating unique sequences from each individual bead with the number of mRNA molecules reverse transcribed to give a snapshot of expression within many cells, rather than an average expression of many cells. The expression of each cell was then analysed to rebuild the cell expressions, and group cells with similar expressions.

The aptamer selection approach was established and validated against the SAOS-2 cell line, but when applied to the primary cells from the bone marrow the process produces aberrant products, which impeded aptamer selection. The aberrant products appeared to be generated from the interaction between the primers and the cell's nucleic acids during PCR, resulting in many attempts being made using various newly generated materials and buffers to result in the same generation of 120 -140 bp nucleic acid strands.

The Drop-Seq methodology generated exciting data in which four unique clusters of cells were identified from the STRO-1+ CD146+ cell population, specifically: i) monocytes, ii) lymphocytes, iii) erythroid progenitors, and iv) CAR cells. The monocytes and lymphocytes were expected, as these were known to be present from the FACS analysis. The erythroid progenitors reside within the red bone marrow to produce red blood cells. Finally, the CAR cells are an intriguing cell population which is known to have proximity to, and proliferation regulatory effects on, the haematopoietic stem cells. As well as being multipotent, with the capacity to differentiate into osteo, chondro, and adipocytes, characteristics which are shared with the SSC population. The overlapping nature of these characteristics, and the finding of CAR cells within the same cell population fraction as SSC, suggests that the SSC population may be part of or a subset of the CAR cells. With further investigations, the differences between the CAR and SSC populations may be better identified to determine what relationship the two cell populations share. However, currently sharing so many characteristics determined from literature from the SSC and CAR cell populations suggests a relationship between both cell types.

References

A. DRABOVICH, M. BEREZOVSKI & KRYLOV, S. N. 2005. Selection of Smart Aptamers by Equilibrium Capillary Electrophoresis of Equilibrium Mixtures (ECEEM). *Journal of the american chemical society*.

ABAD, M., MOSTEIRO, L., PANTOJA, C., CANAMERO, M., RAYON, T., ORS, I., GRANA, O., MEGIAS, D., DOMINGUEZ, O., MARTINEZ, D., MANZANARES, M., ORTEGA, S. & SERRANO, M. 2013. Reprogramming in vivo produces teratomas and iPS cells with totipotency features. *Nature,* 502**,** 340-5.

ADAMIS, A. P., ALTAWEEL, M., BRESSLER, N. M., CUNNINGHAM, E. T., JR., DAVIS, M. D., GOLDBAUM, M., GONZALES, C., GUYER, D. R., BARRETT, K., PATEL, M. & MACUGEN DIABETIC RETINOPATHY STUDY, G. 2006. Changes in retinal neovascularization after pegaptanib (Macugen) therapy in diabetic individuals. *Ophthalmology,* 113**,** 23-8.

AGEUK 2016. Later Life in the United Kingdom. ageuk.org.uk: AgeUK.

ALEJANDRA LOPEZ-VERRILLI, M., CAVIEDES, A., CABRERA, A., SANDOVAL, S., WYNEKEN, U. & KHOURY, M. 2016. Mesenchymal stem cell derived exosomes from different sources selectively promote neuritic outgrowth. *Neuroscience*.

ALHADLAQ, A. & MAO, J. J. 2003. Tissue-engineered neogenesis of human-shaped mandibular condyle from rat mesenchymal stem cells. *J Dent Res,* 82**,** 951-6.

ALHADLAQ, A. & MAO, J. J. 2004. Mesenchymal stem cells: isolation and therapeutics. *Stem Cells Dev,* 13**,** 436-48.

ALIZADEH, A. A., EISEN, M. B., DAVIS, R. E., MA, C., LOSSOS, I. S., ROSENWALD, A., BOLDRICK, J. C., SABET, H., TRAN, T., YU, X., POWELL, J. I., YANG, L., MARTI, G. E., MOORE, T., HUDSON, J., JR., LU, L., LEWIS, D. B., TIBSHIRANI, R., SHERLOCK, G., CHAN, W. C., GREINER, T. C., WEISENBURGER, D. D., ARMITAGE, J. O., WARNKE, R., LEVY, R., WILSON, W., GREVER, M. R., BYRD, J. C., BOTSTEIN, D., BROWN, P. O. & STAUDT, L. M. 2000. Distinct types of diffuse large B-cell lymphoma identified by gene expression profiling. *Nature,* 403**,** 503-11.

ARA, T., TOKOYODA, K., SUGIYAMA, T., EGAWA, T., KAWABATA, K. & NAGASAWA, T. 2003. Long-Term Hematopoietic Stem Cells Require Stromal Cell-Derived Factor-1 for Colonizing Bone Marrow during Ontogeny. *Immunity,* 19**,** 257-267.

AUTEBERT, J., COUDERT, B., BIDARD, F. C., PIERGA, J. Y., DESCROIX, S., MALAQUIN, L. & VIOVY, J. L. 2012. Microfluidic: an innovative tool for efficient cell sorting. *Methods,* 57**,** 297-307.

AVITAL, I., INDERBITZIN, D., AOKI, T., TYAN, D. B., COHEN, A. H., FERRARESSO, C., ROZGA, J., ARNAOUT, W. S. & DEMETRIOU, A. A. 2001. Isolation, characterization, and

transplantation of bone marrow-derived hepatocyte stem cells. *Biochem Biophys Res Commun,* 288**,** 156-64.

BAKER, N., BOYETTE, L. B. & TUAN, R. S. 2015. Characterization of bone marrow-derived mesenchymal stem cells in aging. *Bone,* 70**,** 37-47.

BAKSH, D., DAVIES, J. E. & ZANDSTRA, P. W. 2003. Adult human bone marrow–derived mesenchymal progenitor cells are capable of adhesion-independent survival and expansion. *Experimental Hematology,* 31**,** 723-732.

BALDWIN, T. 2009. Morality and human embryo research. Introduction to the Talking Point on morality and human embryo research. *EMBO Rep,* 10**,** 299-300.

BARKER, N. 2014. Adult intestinal stem cells: critical drivers of epithelial homeostasis and regeneration. *Nat Rev Mol Cell Biol,* 15**,** 19-33.

BELTRAMI, A. P., BARLUCCHI, L., TORELLA, D., BAKER, M., LIMANA, F., CHIMENTI, S., KASAHARA, H., ROTA, M., MUSSO, E., URBANEK, K., LERI, A., KAJSTURA, J., NADAL-GINARD, B. & ANVERSA, P. 2003. Adult cardiac stem cells are multipotent and support myocardial regeneration. *Cell,* 114**,** 763-76.

BEREZOVSKI, M. V., LECHMANN, M., MUSHEEV, M. U., MAK, T. W. & KRYLOV, S. N. 2008. Aptamer-facilitated biomarker discovery (AptaBiD). *J Am Chem Soc,* 130**,** 9137-43.

BHATTACHARYA, D., SAHA, S., BASU, S., CHAKRAVARTY, S., CHAKRAVARTY, A., BANERJEE, D. & CHAKRABARTI, A. 2010. Differential regulation of redox proteins and chaperones in HbEbeta-thalassemia erythrocyte proteome. *Proteomics Clin Appl,* 4**,** 480-8.

BIANCO, P., CAO, X., FRENETTE, P. S., MAO, J. J., ROBEY, P. G., SIMMONS, P. J. & WANG, C. Y. 2013. The meaning, the sense and the significance: translating the science of mesenchymal stem cells into medicine. *Nat Med,* 19**,** 35-42.

BIANCO, P., COSTANTINI, M., DEARDEN, L. C. & BONUCCI, E. 1988. Alkaline phosphatase positive precursors of adipocytes in the human bone marrow. *Br J Haematol,* 68**,** 401-3.

BIANCO, P., RIMINUCCI, M., GRONTHOS, S. & ROBEY, P. G. 2001. Bone marrow stromal stem cells: nature, biology, and potential applications. *Stem Cells,* 19**,** 180-92.

BIANCO, P. & ROBEY, P. G. 2004. Skeletal Stem Cells. *In:* ATALA, A. & LANZA, R. P. (eds.) *Handbook of stem cells.* ACADEMIC PRESS.

BIANCO, P. & ROBEY, P. G. 2015. Skeletal stem cells. *Development,* 142**,** 1023-7.

BIANCO, P., ROBEY, P. G. & SIMMONS, P. J. 2008. Mesenchymal stem cells: revisiting history, concepts, and assays. *Cell Stem Cell,* 2**,** 313-9.

BIELBY, R., JONES, E. & MCGONAGLE, D. 2007. The role of mesenchymal stem cells in maintenance and repair of bone. *Injury,* 38 Suppl 1**,** S26-32.

BISWAS, A. & HUTCHINS, R. 2007. Embryonic stem cells. *Stem Cells Dev,* 16**,** 213-22.

BLACK, C. R., GORIAINOV, V., GIBBS, D., KANCZLER, J., TARE, R. S. & OREFFO, R. O. 2015. Bone Tissue Engineering. *Curr Mol Biol Rep,* 1**,** 132-140.

BLANK, M., WEINSCHENK, T., PRIEMER, M. & SCHLUESENER, H. 2001. Systematic evolution of a DNA aptamer binding to rat brain tumor microvessels. selective targeting of endothelial regulatory protein pigpen. *J Biol Chem,* 276**,** 16464-8.

BLIND, M. & BLANK, M. 2015. Aptamer Selection Technology and Recent Advances. *Molecular Therapy - Nucleic Acids,* 4**,** e223.

BONE, L. B. J., K D. 1986. Treatment of tibial fractures by reaming and intramedullary... : JBJS. *JBJS,* 68**,** 877-887.

BONNER, W. A. 1972. Fluorescence Activated Cell Sorting. *Review of Scientific Instruments,* 43**,** 404.

BOPPART, M. D., DE LISIO, M. & WITKOWSKI, S. 2015. Exercise and Stem Cells. *Prog Mol Biol Transl Sci,* 135**,** 423-56.

BOXALL, S. A. & JONES, E. 2012. Markers for characterization of bone marrow multipotential stromal cells. *Stem Cells Int,* 2012**,** 975871.

BRIGGS, J. A., BURRUS, G. R., STICKNEY, B. D. & BRIGGS, R. C. 1992. Cloning and expression of the human myeloid cell nuclear differentiation antigen: regulation by interferon alpha. *J Cell Biochem,* 49**,** 82-92.

BRIGGS, R. C., KAO, W. Y., DWORKIN, L. L., BRIGGS, J. A., DESSYPRIS, E. N. & CLARK, J. 1994. Regulation and specificity of MNDA expression in monocytes, macrophages, and leukemia/B lymphoma cell lines. *J Cell Biochem,* 56**,** 559-67.

BRUNO, J. G., CARRILLO, M. P. & PHILLIPS, T. 2008. In vitro antibacterial effects of antilipopolysaccharide DNA aptamer-C1qrs complexes. *Folia Microbiol (Praha),* 53**,** 295-302.

BRUNO, J. G. & KIEL, J. L. 1999. In vitro selection of DNA aptamers to anthrax spores with electrochemiluminescence detection. *Biosens Bioelectron,* 14**,** 457-64.

BRUNO, J. G., RICHARTE, A. M., CARRILLO, M. P. & EDGE, A. 2012. An aptamer beacon responsive to botulinum toxins. *Biosens Bioelectron,* 31**,** 240-3.

BUCHANAN, D. D., JAMESON, E. E., PERLETTE, J., MALIK, A. & KENNEDY, R. T. 2003. Effect of buffer, electric field, and separation time on detection of aptamer-ligand complexes for affinity probe capillary electrophoresis. *Electrophoresis,* 24**,** 1375-82.

BUDA, R., CASTAGNINI, F., CAVALLO, M., RAMPONI, L., VANNINI, F. & GIANNINI, S. 2015. "One-step" bone marrow-derived cells transplantation and joint debridement for osteochondral lesions of the talus in ankle osteoarthritis: clinical and radiological outcomes at 36 months. *Arch Orthop Trauma Surg*.

BURMEISTER, P. E., LEWIS, S. D., SILVA, R. F., PREISS, J. R., HORWITZ, L. R., PENDERGRAST, P. S., MCCAULEY, T. G., KURZ, J. C., EPSTEIN, D. M., WILSON, C. & KEEFE, A. D. 2005. Direct in vitro selection of a 2'-O-methyl aptamer to VEGF. *Chem Biol,* 12**,** 25-33.

CAMPAGNOLI, C., ROBERTS, I. A., KUMAR, S., BENNETT, P. R., BELLANTUONO, I. & FISK, N. M. 2001. Identification of mesenchymal stem/progenitor cells in human first-trimester fetal blood, liver, and bone marrow. *Blood,* 98**,** 2396-402.

CAMPBELL, M. A. & WENGEL, J. 2011. Locked vs. unlocked nucleic acids (LNA vs. UNA): contrasting structures work towards common therapeutic goals. *Chem Soc Rev,* 40**,** 5680-9.

CANI, P. D., AMAR, J., IGLESIAS, M. A., POGGI, M., KNAUF, C., BASTELICA, D., NEYRINCK, A. M., FAVA, F., TUOHY, K. M., CHABO, C., WAGET, A., DELMEE, E., COUSIN, B., SULPICE, T., CHAMONTIN, B., FERRIERES, J., TANTI, J. F., GIBSON, G. R., CASTEILLA, L., DELZENNE, N. M., ALESSI, M. C. & BURCELIN, R. 2007. Metabolic endotoxemia initiates obesity and insulin resistance. *Diabetes,* 56**,** 1761-72.

CAPLAN, A. I. 1991. Mesenchymal stem cells. *J Orthop Res,* 9**,** 641-50.

CAREY, J. J., LICATA, A. A. & DELANEY, M. F. 2006. Biochemical Markers of Bone Turnover. *Clinical Reviews in Bone and Mineral Metabolism,* 4**,** 197-212.

CARLSON, M. E. & CONBOY, I. M. 2007. Loss of stem cell regenerative capacity within aged niches. *Aging Cell,* 6**,** 371-382.

CATHERINE, A. T., SHISHIDO, S. N., ROBBINS-WELTY, G. A. & DIEGELMAN-PARENTE, A. 2014. Rational design of a structure-switching DNA aptamer for potassium ions. *FEBS Open Bio,* 4**,** 788-95.

CENTI, S., TOMBELLI, S., MINUNNI, M. & MASCINI, M. 2007. Aptamer-based detection of plasma proteins by an electrochemical assay coupled to magnetic beads. *Anal Chem,* 79**,** 1466-73.

CHAMBERLAIN, G., FOX, J., ASHTON, B. & MIDDLETON, J. 2007. Concise review: Mesenchymal stem cells: Their phenotype, differentiation capacity, immunological features, and potential for homing. *Stem Cells,* 25**,** 2739-2749.

CHAN, C. K. F., GULATI, G. S., SINHA, R., TOMPKINS, J. V., LOPEZ, M., CARTER, A. C., RANSOM, R. C., REINISCH, A., WEARDA, T., MURPHY, M., BREWER, R. E., KOEPKE, L. S., MARECIC, O., MANJUNATH, A., SEO, E. Y., LEAVITT, T., LU, W. J., NGUYEN, A., CONLEY, S. D., SALHOTRA, A., AMBROSI, T. H., BORRELLI, M. R., SIEBEL, T., CHAN, K., SCHALLMOSER, K., SEITA, J., SAHOO, D., GOODNOUGH, H., BISHOP, J., GARDNER, M., MAJETI, R., WAN, D. C., GOODMAN, S., WEISSMAN, I. L., CHANG, H. Y. & LONGAKER, M. T. 2018. Identification of the Human Skeletal Stem Cell. *Cell,* 175**,** 43-56 e21.

CHANG, Y. M., DONOVAN, M. J. & TAN, W. 2013. Using aptamers for cancer biomarker discovery. *J Nucleic Acids,* 2013**,** 817350.

CHE ABDULLAH, C. A., AZAD, C. L., OVALLE-ROBLES, R., FANG, S., LIMA, M. D., LEPRO, X., COLLINS, S., BAUGHMAN, R. H., DALTON, A. B., PLANT, N. J. & SEAR, R. P. 2014. Primary liver cells cultured on carbon nanotube substrates for liver tissue engineering and drug discovery applications. *ACS Appl Mater Interfaces,* 6**,** 10373-80.

CHENG, A. K., SEN, D. & YU, H. Z. 2009. Design and testing of aptamer-based electrochemical biosensors for proteins and small molecules. *Bioelectrochemistry,* 77**,** 1-12.

CHOI, S., SONG, S., CHOI, C. & PARK, J. K. 2007. Continuous blood cell separation by hydrophoretic filtration. *Lab Chip,* 7**,** 1532-8.

CHORY, J. & POLLARD, J. D., JR. 2001. Separation of small DNA fragments by conventional gel electrophoresis. *Curr Protoc Mol Biol,* Chapter 2**,** Unit2 7.

COLLINS, C. A., OLSEN, I., ZAMMIT, P. S., HESLOP, L., PETRIE, A., PARTRIDGE, T. A. & MORGAN, J. E. 2005. Stem cell function, self-renewal, and behavioral heterogeneity of cells from the adult muscle satellite cell niche. *Cell,* 122**,** 289-301.

COOPER, M. D. 2015. The early history of B cells. *Nat Rev Immunol,* 15**,** 191-7.

CORDEIRO GOMES, A., HARA, T., LIM, V. Y., HERNDLER-BRANDSTETTER, D., NEVIUS, E., SUGIYAMA, T., TANI-ICHI, S., SCHLENNER, S., RICHIE, E., RODEWALD, H. R., FLAVELL, R. A., NAGASAWA, T., IKUTA, K. & PEREIRA, J. P. 2016. Hematopoietic Stem Cell Niches Produce Lineage-Instructive Signals to Control Multipotent Progenitor Differentiation. *Immunity,* 45**,** 1219-1231.

CORREIA, S. I., PEREIRA, H., SILVA-CORREIA, J., VAN DIJK, C. N., ESPREGUEIRA-MENDES, J., OLIVEIRA, J. M. & REIS, R. L. 2014. Current concepts: tissue engineering and regenerative medicine applications in the ankle joint. *J R Soc Interface,* 11**,** 20130784.

COX, S. C., THORNBY, J. A., GIBBONS, G. J., WILLIAMS, M. A. & MALLICK, K. K. 2015. 3D printing of porous hydroxyapatite scaffolds intended for use in bone tissue engineering applications. *Mater Sci Eng C Mater Biol Appl,* 47**,** 237-47.

CRISAN, M., YAP, S., CASTEILLA, L., CHEN, C. W., CORSELLI, M., PARK, T. S., ANDRIOLO, G., SUN, B., ZHENG, B., ZHANG, L., NOROTTE, C., TENG, P. N., TRAAS, J., SCHUGAR, R., DEASY, B. M., BADYLAK, S., BUHRING, H. J., GIACOBINO, J. P., LAZZARI, L., HUARD, J. & PÉAULT, B. 2008. A perivascular origin for mesenchymal stem cells in multiple human organs. *Cell Stem Cell,* 3**,** 301-13.

D'ATRI, V., OLIVIERO, G., AMATO, J., BORBONE, N., D'ERRICO, S., MAYOL, L., PICCIALLI, V., HAIDER, S., HOORELBEKE, B., BALZARINI, J. & PICCIALLI, G. 2012. New anti-HIV aptamers based on tetra-end-linked DNA G-quadruplexes: effect of the base sequence on anti-HIV activity. *Chem Commun (Camb),* 48**,** 9516-8.

D'IPPOLITO, G., SCHILLER, P. C., RICORDI, C., ROOS, B. A. & HOWARD, G. A. 1999. Age-related osteogenic potential of mesenchymal stromal stem cells from human vertebral bone marrow. *J Bone Miner Res,* 14**,** 1115-22.

DAR, A., GOICHBERG, P., SHINDER, V., KALINKOVICH, A., KOLLET, O., NETZER, N., MARGALIT, R., ZSAK, M., NAGLER, A., HARDAN, I., RESNICK, I., ROT, A. & LAPIDOT, T. 2005. Chemokine receptor CXCR4-dependent internalization and resecretion of functional chemokine SDF-1 by bone marrow endothelial and stromal cells. *Nat Immunol,* 6**,** 1038-46.

DAVIS, K. 1998. Staining of cell surface human CD4 with 2'-F-pyrimidine-containing RNA aptamers for flow cytometry. *Nucleic Acids Research,* 26**,** 3915-3924.

References

DAWSON, J. I., KANCZLER, J., TARE, R., KASSEM, M. & OREFFO, R. O. 2014. Concise review: bridging the gap: bone regeneration using skeletal stem cell-based strategies - where are we now? *Stem Cells,* 32**,** 35-44.

DE LOS ANGELES, A., FERRARI, F., XI, R., FUJIWARA, Y., BENVENISTY, N., DENG, H., HOCHEDLINGER, K., JAENISCH, R., LEE, S., LEITCH, H. G., LENSCH, M. W., LUJAN, E., PEI, D., ROSSANT, J., WERNIG, M., PARK, P. J. & DALEY, G. Q. 2015. Hallmarks of pluripotency. *Nature,* 525**,** 469-78.

DE WERT, G. & MUMMERY, C. 2003. Human embryonic stem cells: research, ethics and policy. *Hum Reprod,* 18**,** 672-82.

DEY, A. K. 2005. Structural characterization of an anti-gp120 RNA aptamer that neutralizes R5 strains of HIV-1. *Rna,* 11**,** 873-884.

DI RUSSO, N. V., ESTRIN, D. A., MARTI, M. A. & ROITBERG, A. E. 2012. pH-Dependent conformational changes in proteins and their effect on experimental pK(a)s: the case of Nitrophorin 4. *PLoS Comput Biol,* 8**,** e1002761.

DIAMANDIS, E. P. 2004. Mass spectrometry as a diagnostic and a cancer biomarker discovery tool: opportunities and potential limitations. *Mol Cell Proteomics,* 3**,** 367-78.

DIMITRIOU, R., JONES, E., MCGONAGLE, D. & GIANNOUDIS, P. V. 2011. Bone regeneration: current concepts and future directions. *BMC Med,* 9**,** 66.

DOUGAN, H., LYSTER, D. M., VO, C. V., STAFFORD, A., WEITZ, J. I. & HOBBS, J. B. 2000. Extending the lifetime of anticoagulant oligodeoxynucleotide aptamers in blood. *Nucl Med Biol,* 27**,** 289-97.

DU, J., HONG, J., XU, C., CAI, Y., XIANG, B., ZHOU, C. & XU, X. 2015. Screening and Identification of ssDNA Aptamer for Human GP73. *Biomed Res Int,* 2015**,** 610281.

DUMETZ, A. C., CHOCKLA, A. M., KALER, E. W. & LENHOFF, A. M. 2008. Effects of pH on protein-protein interactions and implications for protein phase behavior. *Biochim Biophys Acta,* 1784**,** 600-10.

ELLINGTON, A. D. & SZOSTAK, J. W. 1990. In vitro selection of RNA molecules that bind specific ligands. *Nature,* 346**,** 818-22.

ELLINGTON, A. D. & SZOSTAK, J. W. 1992. Selection in vitro of single-stranded DNA molecules that fold into specific ligand-binding structures. *Nature,* 355**,** 850-2.

ELLIOTT, K. A. & JASPER, H. H. 1949. Physiological salt solutions for brain surgery; studies of local pH and pial vessel reactions to buffered and unbuffered isotonic solutions. *J Neurosurg,* 6**,** 140-52.

ERCIN, E., HURMEYDAN, O. M. & KARAHAN, M. 2017. Bone Anatomy and the Biologic Healing Process of a Fracture. *In:* GOBBI, A., ESPREGUEIRA-MENDES, J., LANE, J. G. & KARAHAN, M. (eds.) *Bio-orthopaedics: A New Approach.* Berlin, Heidelberg: Springer Berlin Heidelberg.

ESPELUND, M., STACY, R. A. & JAKOBSEN, K. S. 1990. A simple method for generating single-stranded DNA probes labeled to high activities. *Nucleic Acids Res,* 18**,** 6157-8.

ESPINOSA, E., MOLINS, E. & LECOMTE, C. 1998. Hydrogen bond strengths revealed by topological analyses of experimentally observed electron densities. *Chemical Physics Letters,* 285**,** 170-173.

ETZIONI, D. A., LIU, J. H., MAGGARD, M. A. & KO, C. Y. 2003. The aging population and its impact on the surgery workforce. *Ann Surg,* 238**,** 170-7.

EVANS, M. J. & KAUFMAN, M. H. 1981. Establishment in culture of pluripotential cells from mouse embryos. *Nature,* 292**,** 154-6.

FAMULOK, M. & SZOSTAK, J. W. 1992. Stereospecific recognition of tryptophan agarose by in vitro selected RNA. *Journal of the American Chemical Society,* 114**,** 3990-3991.

FANG, X. & TAN, W. 2010. Aptamers generated from cell-SELEX for molecular medicine: a chemical biology approach. *Acc Chem Res,* 43**,** 48-57.

FITTER, S., GRONTHOS, S., OOI, S. S. & ZANNETTINO, A. C. 2017. The Mesenchymal Precursor Cell Marker Antibody STRO-1 Binds to Cell Surface Heat Shock Cognate 70. *Stem Cells,* 35**,** 940-951.

FOELL, D., WITTKOWSKI, H., VOGL, T. & ROTH, J. 2007. S100 proteins expressed in phagocytes: a novel group of damage-associated molecular pattern molecules. *J Leukoc Biol,* 81**,** 28-37.

FORRISTAL, C. E., WRIGHT, K. L., HANLEY, N. A., OREFFO, R. O. & HOUGHTON, F. D. 2010. Hypoxia inducible factors regulate pluripotency and proliferation in human embryonic stem cells cultured at reduced oxygen tensions. *Reproduction,* 139**,** 85-97.

FRIEDENSTEIN, A. J., CHAILAKHJAN, R. K. & LALYKINA, K. S. 1970. The Development of Fibroblast Colonies in Monolayer Cultures of Guinea-Pig Bone Marrow and Spleen Cells. *Cell Proliferation,* 3**,** 393-403.

FRIEDENSTEIN, A. J., CHAILAKHYAN, R. K., LATSINIK, N. V., PANASYUK, A. F. & KEILISS-BOROK, I. V. 1974. Stromal cells responsible for transferring the microenvironment of the hemopoietic tissues. Cloning in vitro and retransplantation in vivo. *Transplantation,* 17**,** 331-40.

FRIEDENSTEIN, A. J., PIATETZKY, S., II & PETRAKOVA, K. V. 1966. Osteogenesis in transplants of bone marrow cells. *J Embryol Exp Morphol,* 16**,** 381-90.

FRIEDLAENDER, G. E., PERRY, C. R., DEAN COLE, J., COOK, S. D., CIERNY, G., MUSCHLER, G. F., ZYCH, G. A., CALHOUN, J. H., LAFORTE, A. J. & YIN, S. 2001. Osteogenic Protein-1 (Bone Morphogenetic Protein-7) in the Treatment of Tibial Nonunions: A Prospective, Randomized Clinical Trial Comparing rhOP-1 with Fresh Bone Autograft*. *J Bone Joint Surg Am,* 83-A Suppl 1**,** S151-8.

FU, X., CHEN, Y., XIE, F. N., DONG, P., LIU, W. B., CAO, Y., ZHANG, W. J. & XIAO, R. 2015. Comparison of immunological characteristics of mesenchymal stem cells derived from human embryonic stem cells and bone marrow. *Tissue Eng Part A,* 21**,** 616-26.

FUKUI, H. 2005. Relation of Endotoxin, Endotoxin Binding Proteins and Macrophages to Severe Alcoholic Liver Injury and Multiple Organ Failure. *Alcoholism: Clinical & Experimental Research,* 29**,** 172S-179S.

GANSON, N. J., POVSIC, T. J., SULLENGER, B. A., ALEXANDER, J. H., ZELENKOFSKE, S. L., SAILSTAD, J. M., RUSCONI, C. P. & HERSHFIELD, M. S. 2016. Pre-existing anti-polyethylene glycol antibody linked to first-exposure allergic reactions to pegnivacogin, a PEGylated RNA aptamer. *J Allergy Clin Immunol,* 137**,** 1610-1613 e7.

GE, Y. & FUCHS, E. 2018. Stretching the limits: from homeostasis to stem cell plasticity in wound healing and cancer. *Nat Rev Genet,* 19**,** 311-325.

GENTILE, P., CHIONO, V., CARMAGNOLA, I. & HATTON, P. V. 2014. An overview of poly(lactic-co-glycolic) acid (PLGA)-based biomaterials for bone tissue engineering. *Int J Mol Sci,* 15**,** 3640-59.

GERSTENFELD, L. C., CULLINANE, D. M., BARNES, G. L., GRAVES, D. T. & EINHORN, T. A. 2003. Fracture healing as a post-natal developmental process: molecular, spatial, and temporal aspects of its regulation. *J Cell Biochem,* 88**,** 873-84.

GIANNONI, P., MASTROGIACOMO, M., ALINI, M., PEARCE, S. G., CORSI, A., SANTOLINI, F., MURAGLIA, A., BIANCO, P. & CANCEDDA, R. 2008. Regeneration of large bone defects in sheep using bone marrow stromal cells. *J Tissue Eng Regen Med,* 2**,** 253-62.

GIMBLE, J. & GUILAK, F. 2003. Adipose-derived adult stem cells: isolation, characterization, and differentiation potential. *Cytotherapy,* 5**,** 362-9.

GOLDFARB, S. B., KASHLAN, O. B., WATKINS, J. N., SUAUD, L., YAN, W., KLEYMAN, T. R. & RUBENSTEIN, R. C. 2006. Differential effects of Hsc70 and Hsp70 on the intracellular trafficking and functional expression of epithelial sodium channels. *Proc Natl Acad Sci U S A,* 103**,** 5817-22.

GORDON, M. Y., LEWIS, J. L., SCOTT, M. A., ROBERTS, I. A. & GOLDMAN, J. M. 1995. Probability of progenitor renewal (PPR) and production of clonogenic progeny (CFU-GM) by primitive adherent progenitor cells in adult human bone marrow and umbilical cord blood. *Br J Haematol,* 90**,** 744-9.

GOTHARD, D., CHEUNG, K., KANCZLER, J. M., WILSON, D. I. & OREFFO, R. O. 2015a. Regionally-derived cell populations and skeletal stem cells from human foetal femora exhibit specific osteochondral and multi-lineage differentiation capacity in vitro and ex vivo. *Stem Cell Res Ther,* 6**,** 251.

GOTHARD, D., DAWSON, J. I. & OREFFO, R. O. 2013. Assessing the potential of colony morphology for dissecting the CFU-F population from human bone marrow stromal cells. *Cell Tissue Res,* 352**,** 237-47.

GOTHARD, D., GREENHOUGH, J., RALPH, E. & OREFFO, R. O. 2014. Prospective isolation of human bone marrow stromal cell subsets: A comparative study between Stro-1-, CD146- and CD105-enriched populations. *J Tissue Eng,* 5**,** 2041731414551763.

GOTHARD, D., SMITH, E. L., KANCZLER, J. M., BLACK, C. R., WELLS, J. A., ROBERTS, C. A., WHITE, L. J., QUTACHI, O., PETO, H., RASHIDI, H., ROJO, L., STEVENS, M. M., EL HAJ, A. J., ROSE, F. R., SHAKESHEFF, K. M. & OREFFO, R. O. 2015b. In Vivo Assessment of Bone Regeneration in Alginate/Bone ECM Hydrogels with Incorporated Skeletal Stem Cells and Single Growth Factors. *PLoS One,* 10**,** e0145080.

GOTHARD, D., TARE, R. S., MITCHELL, P. D., DAWSON, J. I. & OREFFO, R. O. 2011. In search of the skeletal stem cell: isolation and separation strategies at the macro/micro scale for skeletal regeneration. *Lab Chip,* 11**,** 1206-20.

GOTHERSTROM, C. 2016. Human Foetal Mesenchymal Stem Cells. *Best Pract Res Clin Obstet Gynaecol,* 31**,** 82-7.

GOTHERSTROM, C., RINGDEN, O., TAMMIK, C., ZETTERBERG, E., WESTGREN, M. & LE BLANC, K. 2004. Immunologic properties of human fetal mesenchymal stem cells. *Am J Obstet Gynecol,* 190**,** 239-45.

GOURRONC, F. A., ROCKEY, W. M., THIEL, W. H., GIANGRANDE, P. H. & KLINGELHUTZ, A. J. 2013. Identification of RNA aptamers that internalize into HPV-16 E6/E7 transformed tonsillar epithelial cells. *Virology,* 446**,** 325-33.

GOVENDER, S., CSIMMA, C., GENANT, H. K., VALENTIN-OPRAN, A., AMIT, Y., ARBEL, R., ARO, H., ATAR, D., BISHAY, M., BORNER, M. G., CHIRON, P., CHOONG, P., CINATS, J., COURTENAY, B., FEIBEL, R., GEULETTE, B., GOVENDER, S., GRAVEL, C., HAAS, N., RASCHKE, M., HAMMACHER, E., VAN DER VELDE, D., HARDY, P., HOLT, M., JOSTEN, C., KETTERL, R. L., LINDEQUE, B., LOB, G., MATHEVON, H., MCCOY, G., MARSH, D., MILLER, R., MUNTING, E., OEVRE, S., NORDSLETTEN, L., PATEL, A., POHL, A., RENNIE, W., REYNDERS, P., ROMMENS, P. M., RONDIA, J., ROSSOUW, W. C., DANEEL, P. J., RUFF, S., RUTER, A., SANTAVIRTAL, S., SCHIDHAUER, T. A., GEKLE, C., SCHNETTLER, R., SEGAL, D., SEILER, H., SNOWDOWNE, R. B., J., S., G., T., R., V. & VOGELS. L. <SPAN STYLE="COLOR: RGB(169 2002. RECOMBINANT HUMAN BONE MORPHOGENETIC PROTEIN-2 FOR TREATMENT OF OPEN TIBIAL FRACTURES A PROSPECTIVE, CONTROLLED, RANDOMIZED STUDY OF FOUR HUNDRED AND FIFTY PATIENTS. *JBJS,* 84**,** 2123-2134.

GOWRI, A. M., KAVITHA, G., RAJASUNDARI, M., FATHIMA, S. M., KUMAR, T. M. & RAJ, G. D. 2013. Foetal stem cell derivation & characterization for osteogenic lineage. *Indian J Med Res,* 137**,** 308-15.

GRANELI, C., THORFVE, A., RUETSCHI, U., BRISBY, H., THOMSEN, P., LINDAHL, A. & KARLSSON, C. 2014. Novel markers of osteogenic and adipogenic differentiation of human bone marrow stromal cells identified using a quantitative proteomics approach. *Stem Cell Res,* 12**,** 153-65.

GREEN, L. S., JELLINEK, D., BELL, C., BEEBE, L. A., FEISTNER, B. D., GILL, S. C., JUCKER, F. M. & JANJIC, N. 1995. Nuclease-resistant nucleic acid ligands to vascular permeability factor/vascular endothelial growth factor. *Chem Biol,* 2**,** 683-95.

GRONTHOS, S. 2003. Molecular and cellular characterisation of highly purified stromal stem cells derived from human bone marrow. *Journal of Cell Science,* 116**,** 1827-1835.

GRÜTTNER, C., RUDERSHAUSEN, S. & TELLER, J. 2001. Improved properties of magnetic particles by combination of different polymer materials as particle matrix. *Journal of Magnetism and Magnetic Materials,* 225**,** 1-7.

GUET, D., BURNS, L. T., MAJI, S., BOULANGER, J., HERSEN, P., WENTE, S. R., SALAMERO, J. & DARGEMONT, C. 2015. Combining Spinach-tagged RNA and gene localization to image gene expression in live yeast. *Nat Commun,* 6**,** 8882.

GUILLOT, P. V., GOTHERSTROM, C., CHAN, J., KURATA, H. & FISK, N. M. 2007. Human first-trimester fetal MSC express pluripotency markers and grow faster and have longer telomeres than adult MSC. *Stem Cells,* 25**,** 646-54.

GUO, K. T., SCHAFER, R., PAUL, A., GERBER, A., ZIEMER, G. & WENDEL, H. P. 2006. A new technique for the isolation and surface immobilization of mesenchymal stem cells from whole bone marrow using high-specific DNA aptamers. *Stem Cells,* 24**,** 2220-31.

GUO, K. T., ZIEMER, G., PAUL, A. & WENDEL, H. P. 2008. CELL-SELEX: Novel perspectives of aptamer-based therapeutics. *Int J Mol Sci,* 9**,** 668-78.

GURALNIK, J. M., FRIED, L. P. & SALIVE, M. E. 1996. Disability as a public health outcome in the aging population. *Annual Review of Public Health,* 17**,** 25-46.

GUTIERREZ-ARANDA, I., RAMOS-MEJIA, V., BUENO, C., MUNOZ-LOPEZ, M., REAL, P. J., MACIA, A., SANCHEZ, L., LIGERO, G., GARCIA-PAREZ, J. L. & MENENDEZ, P. 2010. Human induced pluripotent stem cells develop teratoma more efficiently and faster than human embryonic stem cells regardless the site of injection. *Stem Cells,* 28**,** 1568-70.

GÖTHERSTRÖM, C. 2011. Immunomodulation by mesenchymal stem cells and clinical experience. *Placenta,* 32**,** S327.

HADJIDAKIS, D. J. & ANDROULAKIS, II 2006. Bone remodeling. *Ann N Y Acad Sci,* 1092**,** 385-96.

HAWKINS, T. L., OCONNORMORIN, T., ROY, A. & SANTILLAN, C. 1994. DNA Purification and Isolation Using a Solid-Phase. *Nucleic Acids Research,* 22**,** 4543-4544.

HEIER, J. S., BROWN, D. M., CHONG, V., KOROBELNIK, J. F., KAISER, P. K., NGUYEN, Q. D., KIRCHHOF, B., HO, A., OGURA, Y., YANCOPOULOS, G. D., STAHL, N., VITTI, R., BERLINER, A. J., SOO, Y., ANDERESI, M., GROETZBACH, G., SOMMERAUER, B., SANDBRINK, R., SIMADER, C., SCHMIDT-ERFURTH, U., VIEW & GROUPS, V. S. 2012. Intravitreal aflibercept (VEGF trap-eye) in wet age-related macular degeneration. *Ophthalmology,* 119**,** 2537-48.

HEO, K., MIN, S. W., SUNG, H. J., KIM, H. G., KIM, H. J., KIM, Y. H., CHOI, B. K., HAN, S., CHUNG, S., LEE, E. S., CHUNG, J. & KIM, I. H. 2016. An aptamer-antibody complex (oligobody) as a novel delivery platform for targeted cancer therapies. *J Control Release,* 229**,** 1-9.

HERRERA, M. B., BRUNO, S., BUTTIGLIERI, S., TETTA, C., GATTI, S., DEREGIBUS, M. C., BUSSOLATI, B. & CAMUSSI, G. 2006. Isolation and characterization of a stem cell population from adult human liver. *Stem Cells,* 24**,** 2840-50.

HIANIK, T., OSTATNA, V., SONLAJTNEROVA, M. & GRMAN, I. 2007. Influence of ionic strength, pH and aptamer configuration for binding affinity to thrombin. *Bioelectrochemistry,* 70**,** 127-33.

HOGAN, B. L., BARKAUSKAS, C. E., CHAPMAN, H. A., EPSTEIN, J. A., JAIN, R., HSIA, C. C., NIKLASON, L., CALLE, E., LE, A., RANDELL, S. H., ROCK, J., SNITOW, M., KRUMMEL, M., STRIPP, B. R., VU, T., WHITE, E. S., WHITSETT, J. A. & MORRISEY, E. E. 2014. Repair and regeneration of the respiratory system: complexity, plasticity, and mechanisms of lung stem cell function. *Cell Stem Cell,* 15**,** 123-38.

HOU, Z., MEYER, S., PROPSON, N. E., NIE, J., JIANG, P., STEWART, R. & THOMSON, J. A. 2015. Characterization and target identification of a DNA aptamer that labels pluripotent stem cells. *Cell Res,* 25**,** 390-3.

HOWARD, D., BUTTERY, L. D., SHAKESHEFF, K. M. & ROBERTS, S. J. 2008. Tissue engineering: strategies, stem cells and scaffolds. *J Anat,* 213**,** 66-72.

HUANG, C. C., HUANG, Y. F., CAO, Z., TAN, W. & CHANG, H. T. 2005. Aptamer-modified gold nanoparticles for colorimetric determination of platelet-derived growth factors and their receptors. *Anal Chem,* 77**,** 5735-41.

HUANG, Z. 2003. Evolution of aptamers with a new specificity and new secondary structures from an ATP aptamer. *Rna,* 9**,** 1456-1463.

HUGHES, M. P. 2002. Strategies for dielectrophoretic separation in laboratory-on-a-chip systems. *Electrophoresis,* 23**,** 2569-2582.

HUIZENGA, D. E. & SZOSTAK, J. W. 1995. A DNA Aptamer That Binds Adenosine and Atp. *Biochemistry,* 34**,** 656-665.

HUNG, S. C., CHEN, N. J., HSIEH, S. L., LI, H., MA, H. L. & LO, W. H. 2002. Isolation and characterization of size-sieved stem cells from human bone marrow. *Stem Cells,* 20**,** 249-58.

HUNTER, C. A. & SANDERS, J. K. M. 1990. The nature of .pi.-.pi. interactions. *Journal of the American Chemical Society,* 112**,** 5525-5534.

IIDA, J., CLANCY, R., DORCHAK, J., SOMIARI, R. I., SOMIARI, S., CUTLER, M. L., MURAL, R. J. & SHRIVER, C. D. 2014. DNA aptamers against exon v10 of CD44 inhibit breast cancer cell migration. *PLoS One,* 9**,** e88712.

IN 'T ANKER, P. S., NOORT, W. A., SCHERJON, S. A., KLEIJBURG-VAN DER KEUR, C., KRUISSELBRINK, A. B., VAN BEZOOIJEN, R. L., BEEKHUIZEN, W., WILLEMZE, R., KANHAI, H. H. & FIBBE, W. E. 2003. Mesenchymal stem cells in human second-trimester bone marrow, liver, lung, and spleen exhibit a similar immunophenotype but a heterogeneous multilineage differentiation potential. *Haematologica,* 88**,** 845-52.

INGLIS, D. W., DAVIS, J. A., AUSTIN, R. H. & STURM, J. C. 2006. Critical particle size for fractionation by deterministic lateral displacement. *Lab Chip,* 6**,** 655-8.

ISMAIL, A., HUGHES, M. P., MULHALL, H. J., OREFFO, R. O. & LABEED, F. H. 2015. Characterization of human skeletal stem and bone cell populations using dielectrophoresis. *J Tissue Eng Regen Med,* 9**,** 162-8.

J B VOGLER, R. & MURPHY, W. A. 1988. Bone marrow imaging. *Radiology,* 168**,** 679-693.

JACKSON, E. L. & LU, H. 2013. Advances in microfluidic cell separation and manipulation. *Curr Opin Chem Eng,* 2**,** 398-404.

JAENISCH, R. & BIRD, A. 2003. Epigenetic regulation of gene expression: how the genome integrates intrinsic and environmental signals. *Nat Genet,* 33 Suppl**,** 245-54.

JAISWAL, N., HAYNESWORTH, S. E., CAPLAN, A. I. & BRUDER, S. P. 1997. Osteogenic differentiation of purified, culture-expanded human mesenchymal stem cells in vitro. *J Cell Biochem,* 64**,** 295-312.

JANUSZYK, M., RENNERT, R. C., SORKIN, M., MAAN, Z. N., WONG, L. K., WHITTAM, A. J., WHITMORE, A., DUSCHER, D. & GURTNER, G. C. 2015. Evaluating the Effect of Cell Culture on Gene Expression in Primary Tissue Samples Using Microfluidic-Based Single Cell Transcriptional Analysis. *Microarrays (Basel),* 4**,** 540-50.

JAROCHA, D., LUKASIEWICZ, E. & MAJKA, M. 2008. Adventage of mesenchymal stem cells (MSC) expansion directly from purified bone marrow CD105+ and CD271+ cells. *Folia Histochem Cytobiol,* 46**,** 307-14.

JENISON, R. D., JENNINGS, S. D., WALKER, D. W., BARGATZE, R. F. & PARMA, D. 1998. Oligonucleotide inhibitors of P-selectin-dependent neutrophil-platelet adhesion. *Antisense Nucleic Acid Drug Dev,* 8**,** 265-79.

JI, H. M., SAMPER, V., CHEN, Y., HENG, C. K., LIM, T. M. & YOBAS, L. 2008. Silicon-based microfilters for whole blood cell separation. *Biomed Microdevices,* 10**,** 251-7.

JIN, C., ZHENG, J., LI, C., QIU, L., ZHANG, X. & TAN, W. 2015. Aptamers Selected by Cell-SELEX for Molecular Imaging. *J Mol Evol*.

JOHANSSON, C. B., MOMMA, S., CLARKE, D. L., RISLING, M., LENDAHL, U. & FRISEN, J. 1999. Identification of a neural stem cell in the adult mammalian central nervous system. *Cell,* 96**,** 25-34.

JONES, D. L. & WAGERS, A. J. 2008. No place like home: anatomy and function of the stem cell niche. *Nat Rev Mol Cell Biol,* 9**,** 11-21.

KANCZLER, J. M. & OREFFO, R. O. C. 2008. Osteogenesis and angiogenesis: The potential for engineering bone. *European Cells and Materials,* 15**,** 100-114.

KARUSSIS, D., KARAGEORGIOU, C., VAKNIN-DEMBINSKY, A., GOWDA-KURKALLI, B., GOMORI, J. M., KASSIS, I., BULTE, J. W., PETROU, P., BEN-HUR, T., ABRAMSKY, O. & SLAVIN, S. 2010. Safety and immunological effects of mesenchymal stem cell transplantation in patients with multiple sclerosis and amyotrophic lateral sclerosis. *Arch Neurol,* 67**,** 1187-94.

KATILIUS, E., FLORES, C. & WOODBURY, N. W. 2007. Exploring the sequence space of a DNA aptamer using microarrays. *Nucleic Acids Res,* 35**,** 7626-35.

KEBRIAEI, P., ISOLA, L., BAHCECI, E., HOLLAND, K., ROWLEY, S., MCGUIRK, J., DEVETTEN, M., JANSEN, J., HERZIG, R., SCHUSTER, M., MONROY, R. & UBERTI, J. 2009. Adult human mesenchymal stem cells added to corticosteroid therapy for the treatment of acute graft-versus-host disease. *Biol Blood Marrow Transplant,* 15**,** 804-11.

KELLENBERGER, C. A. & HAMMOND, M. C. 2015. In vitro analysis of riboswitch-Spinach aptamer fusions as metabolite-sensing fluorescent biosensors. *Methods Enzymol,* 550**,** 147-72.

KELLER, G. 2005. Embryonic stem cell differentiation: emergence of a new era in biology and medicine. *Genes Dev,* 19**,** 1129-55.

KERAMARIS, N. C., CALORI, G. M., NIKOLAOU, V. S., SCHEMITSCH, E. H. & GIANNOUDIS, P. V. 2008. Fracture vascularity and bone healing: a systematic review of the role of VEGF. *Injury,* 39 Suppl 2**,** S45-57.

KERN, S., EICHLER, H., STOEVE, J., KLUTER, H. & BIEBACK, K. 2006. Comparative analysis of mesenchymal stem cells from bone marrow, umbilical cord blood, or adipose tissue. *Stem Cells,* 24**,** 1294-301.

KESHAV, S., CHUNG, P., MILON, G. & GORDON, S. 1991. Lysozyme Is an Inducible Marker of Macrophage Activation in Murine Tissues as Demonstrated by In Situ Hybridization. *The Journal of Experimental Medicine,* 174**,** 1049-1058.

KEYES, B. E. & FUCHS, E. 2018. Stem cells: Aging and transcriptional fingerprints. *J Cell Biol,* 217**,** 79-92.

KHARAZIHA, P., HELLSTROM, P. M., NOORINAYER, B., FARZANEH, F., AGHAJANI, K., JAFARI, F., TELKABADI, M., ATASHI, A., HONARDOOST, M., ZALI, M. R. & SOLEIMANI, M. 2009. Improvement of liver function in liver cirrhosis patients after autologous mesenchymal stem cell injection: a phase I-II clinical trial. *Eur J Gastroenterol Hepatol,* 21**,** 1199-205.

KIM, K., LEE, S., RYU, S. & HAN, D. 2014. Efficient isolation and elution of cellular proteins using aptamer-mediated protein precipitation assay. *Biochem Biophys Res Commun,* 448**,** 114-9.

KIM, S., KIM, S. S., LEE, S. H., EUN AHN, S., GWAK, S. J., SONG, J. H., KIM, B. S. & CHUNG, H. M. 2008. In vivo bone formation from human embryonic stem cell-derived osteogenic cells in poly(d,l-lactic-co-glycolic acid)/hydroxyapatite composite scaffolds. *Biomaterials,* 29**,** 1043-53.

KIM, Y., DENNIS, D. M., MOREY, T., YANG, L. & TAN, W. 2010. Engineering dendritic aptamer assemblies as superior inhibitors of protein function. *Chem Asian J,* 5**,** 56-9.

KINSELLA, K. & PHILLIPS, D. R. 2005. Global aging: The challenge of success. *Population Bulletin,* 60**,** 3-40.

KLIMES, J. & MICHAELIDES, A. 2012. Perspective: Advances and challenges in treating van der Waals dispersion forces in density functional theory. *J Chem Phys,* 137**,** 120901.

KOBORI, S., NOMURA, Y., MIU, A. & YOKOBAYASHI, Y. 2015. High-throughput assay and engineering of self-cleaving ribozymes by sequencing. *Nucleic Acids Res,* 43**,** e85.

KOLF, C. M., CHO, E. & TUAN, R. S. 2007. Mesenchymal stromal cells. Biology of adult mesenchymal stem cells: regulation of niche, self-renewal and differentiation. *Arthritis Res Ther,* 9**,** 204.

KOLLMER, M., BUHRMAN, J. S., ZHANG, Y. & GEMEINHART, R. A. 2013. Markers Are Shared Between Adipogenic and Osteogenic Differentiated Mesenchymal Stem Cells. *J Dev Biol Tissue Eng,* 5**,** 18-25.

KRAMPERA, M., PIZZOLO, G., APRILI, G. & FRANCHINI, M. 2006. Mesenchymal stem cells for bone, cartilage, tendon and skeletal muscle repair. *Bone,* 39.

KUZMINA, L. A., PETINATI, N. A., PAROVICHNIKOVA, E. N., LUBIMOVA, L. S., GRIBANOVA, E. O., GAPONOVA, T. V., SHIPOUNOVA, I. N., ZHIRONKINA, O. A., BIGILDEEV, A. E., SVINAREVA, D. A., DRIZE, N. J. & SAVCHENKO, V. G. 2012. Multipotent Mesenchymal Stromal Cells for the Prophylaxis of Acute Graft-versus-Host Disease-A Phase II Study. *Stem Cells Int,* 2012**,** 968213.

KUZNETSOV, S. A., MANKANI, M. H., GRONTHOS, S., SATOMURA, K., BIANCO, P. & ROBEY, P. G. 2001. Circulating Skeletal Stem Cells. *The Journal of Cell Biology,* 153**,** 1133-1140.

LAING, C. & SCHLICK, T. 2011. Computational approaches to RNA structure prediction, analysis, and design. *Curr Opin Struct Biol,* 21**,** 306-18.

LAINO, G., D'AQUINO, R., GRAZIANO, A., LANZA, V., CARINCI, F., NARO, F., PIROZZI, G. & PAPACCIO, G. 2005. A New Population of Human Adult Dental Pulp Stem Cells: A Useful Source of Living Autologous Fibrous Bone Tissue (LAB). *Journal of Bone and Mineral Research,* 20**,** 1394-1402.

LAINO, G., GRAZIANO, A., D'AQUINO, R., PIROZZI, G., LANZA, V., VALIANTE, S., DE ROSA, A., NARO, F., VIVARELLI, E. & PAPACCIO, G. 2006. An approachable human adult stem cell source for hard-tissue engineering. *J Cell Physiol,* 206**,** 693-701.

LANE, A. N., CHAIRES, J. B., GRAY, R. D. & TRENT, J. O. 2008. Stability and kinetics of G-quadruplex structures. *Nucleic Acids Res,* 36**,** 5482-515.

LANGER, R. & VACANTI, J. P. 1993. Tissue engineering. *Science,* 260**,** 920-6.

LE BLANC, K., FRASSONI, F., BALL, L., LOCATELLI, F., ROELOFS, H., LEWIS, I., LANINO, E., SUNDBERG, B., BERNARDO, M. E., REMBERGER, M., DINI, G., EGELER, R. M., BACIGALUPO, A., FIBBE, W. & RINGDÉN, O. 2008. Mesenchymal stem cells for treatment of steroid-resistant, severe, acute graft-versus-host disease: a phase II study. *The Lancet,* 371**,** 1579-1586.

LE BLANC, K., G??THERSTR??M, C., RINGD??N, O., HASSAN, M., MCMAHON, R., HORWITZ, E., ANNEREN, G. R., AXELSSON, O., NUNN, J., EWALD, U., NORD??N-LINDEBERG, S., JANSSON, M., DALTON, A., STR??M, E. & WESTGREN, M. 2005. Fetal Mesenchymal Stem-Cell Engraftment in Bone after In Utero Transplantation in a Patient with Severe Osteogenesis Imperfecta. *Transplantation,* 79**,** 1607-1614.

LECULIER, C., COUPRIE, N., FRANCINA, A., ARCHIMBAUD, E., ADELEINE, P., TREILLE, D., DENOYEL, G. & FIERE, D. 1992. Specific Detection of Monocytic Lysozyme within Normal and Leukemic-Cells. *Blood,* 79**,** 760-764.

LEE, C. H., LEE, S. H., KIM, J. H., NOH, Y. H., NOH, G. J. & LEE, S. W. 2015. Pharmacokinetics of a Cholesterol-conjugated Aptamer Against the Hepatitis C Virus (HCV) NS5B Protein. *Mol Ther Nucleic Acids,* 4**,** e254.

LEE, J. H., CANNY, M. D., DE ERKENEZ, A., KRILLEKE, D., NG, Y. S., SHIMA, D. T., PARDI, A. & JUCKER, F. 2005. A therapeutic aptamer inhibits angiogenesis by specifically targeting the heparin binding domain of VEGF165. *Proceedings of the National Academy of Sciences,* 102**,** 18902-18907.

LEVRERO-FLORENCIO, F., MARGETTS, L., SALES, E., XIA, S., MANDA, K. & PANKAJ, P. 2016. Evaluating the macroscopic yield behaviour of trabecular bone using a nonlinear homogenisation approach. *Journal of the mechaincal behavior of biomedical materials,* 61**,** 384-396.

LI, Q., ZHANG, X., PENG, Y., CHAI, H., XU, Y., WEI, J., REN, X., WANG, X., LIU, W., CHEN, M. & HUANG, D. 2013. Comparison of the sorting efficiency and influence on cell function between the sterile flow cytometry and immunomagnetic bead purification methods. *Prep Biochem Biotechnol,* 43**,** 197-206.

LI, S., SENGERS, B. G., OREFFO, R. O. & TARE, R. S. 2015. Chondrogenic potential of human articular chondrocytes and skeletal stem cells: a comparative study. *J Biomater Appl,* 29**,** 824-36.

LI, Y., QI, H., PENG, Y., YANG, J. & ZHANG, C. 2007. Electrogenerated chemiluminescence aptamer-based biosensor for the determination of cocaine. *Electrochemistry Communications,* 9**,** 2571-2575.

LIAO, I. C., MOUTOS, F. T., ESTES, B. T., ZHAO, X. & GUILAK, F. 2013. Composite three-dimensional woven scaffolds with interpenetrating network hydrogels to create functional synthetic articular cartilage. *Adv Funct Mater,* 23**,** 5833-5839.

LIN, C. S., XIN, Z. C., DAI, J. & LUE, T. F. 2013. Commonly used mesenchymal stem cell markers and tracking labels: Limitations and challenges. *Histol Histopathol,* 28**,** 7.

LINCOFF, A. M., MEHRAN, R., POVSIC, T. J., ZELENKOFSKE, S. L., HUANG, Z., ARMSTRONG, P. W., STEG, P. G., BODE, C., COHEN, M. G., BULLER, C., LAANMETS, P., VALGIMIGLI, M., MARANDI, T., FRIDRICH, V., CANTOR, W. J., MERKELY, B., LOPEZ-SENDON, J., CORNEL, J. H., KASPRZAK, J. D., ASCHERMANN, M., GUETTA, V., MORAIS, J., SINNAEVE, P. R., HUBER, K., STABLES, R., SELLERS, M. A., BORGMAN, M., GLENN, L., LEVINSON, A. I., LOPES, R. D., HASSELBLAD, V., BECKER, R. C. & ALEXANDER, J. H. 2016. Effect of the REG1 anticoagulation system versus bivalirudin on outcomes after percutaneous coronary intervention (REGULATE-PCI): a randomised clinical trial. *The Lancet,* 387**,** 349-356.

LITMAN, G. W., RAST, J. P., SHAMBLOTT, M. J., HAIRE, R. N., HULST, M., ROESS, W., LITMAN, R. T., HINDS-FREY, K. R., ZILCH, A. & AMEMIYA, C. T. 1993. Phylogenetic diversification of immunoglobulin genes and the antibody repertoire. *Mol Biol Evol,* 10**,** 60-72.

LIU, B., ZHANG, B., CHEN, G. & TANG, D. 2014. An omega-like DNA nanostructure utilized for small molecule introduction to stimulate formation of DNAzyme-aptamer conjugates. *Chem Commun (Camb),* 50**,** 1900-2.

LO SURDO, J. & BAUER, S. R. 2012. Quantitative approaches to detect donor and passage differences in adipogenic potential and clonogenicity in human bone marrow-derived mesenchymal stem cells. *Tissue Eng Part C Methods,* 18**,** 877-89.

LOU, X., QIAN, J., XIAO, Y., VIEL, L., GERDON, A. E., LAGALLY, E. T., ATZBERGER, P., TARASOW, T. M., HEEGER, A. J. & SOH, H. T. 2009. Micromagnetic selection of aptamers in microfluidic channels. *PNAS,* 106**,** 5.

LV, F. J., TUAN, R. S., CHEUNG, K. M. & LEUNG, V. Y. 2014. Concise review: the surface markers and identity of human mesenchymal stem cells. *Stem Cells,* 32**,** 1408-19.

LYSAGHT, M. J. & REYES, J. 2001. The growth of tissue engineering. *Tissue Eng,* 7**,** 485-93.

M. CHO, Y. XIAO, J. NIE, R. STEWART, A. T. CSORDAS, S. SOO OH, J. A. THOMSON & H. TOM SOH 2010. Quantitative selection of DNA aptamers through microfluidic selection and high-throughput sequencing. *PNAS,* 107**,** 5.

MA, X., KONG, L. & ZHU, S. 2017. Reprogramming cell fates by small molecules. *Protein Cell,* 8**,** 328-348.

MACOSKO, E. Z., BASU, A., SATIJA, R., NEMESH, J., SHEKHAR, K., GOLDMAN, M., TIROSH, I., BIALAS, A. R., KAMITAKI, N., MARTERSTECK, E. M., TROMBETTA, J. J., WEITZ, D. A., SANES, J. R., SHALEK, A. K., REGEV, A. & MCCARROLL, S. A. 2015. Highly Parallel Genome-wide Expression Profiling of Individual Cells Using Nanoliter Droplets. *Cell,* 161**,** 1202-14.

MAHERALI, N., SRIDHARAN, R., XIE, W., UTIKAL, J., EMINLI, S., ARNOLD, K., STADTFELD, M., YACHECHKO, R., TCHIEU, J., JAENISCH, R., PLATH, K. & HOCHEDLINGER, K. 2007. Directly reprogrammed fibroblasts show global epigenetic remodeling and widespread tissue contribution. *Cell Stem Cell,* 1**,** 55-70.

MAHLA, R. S. 2016. Stem Cells Applications in Regenerative Medicine and Disease Therapeutics. *Int J Cell Biol,* 2016**,** 6940283.

MANITZ, M. P., HORST, B., SEELIGER, S., STREY, A., SKRYABIN, B. V., GUNZER, M., FRINGS, W., SCHONLAU, F., ROTH, J., SORG, C. & NACKEN, W. 2003. Loss of S100A9 (MRP14) Results in Reduced Interleukin-8-Induced CD11b Surface Expression, a Polarized Microfilament System, and Diminished Responsiveness to Chemoattractants In Vitro. *Molecular and Cellular Biology,* 23**,** 1034-1043.

MANNIRONI, C., DI NARDO, A., FRUSCOLONI, P. & TOCCHINI-VALENTINI, G. P. 1997. In vitro selection of dopamine RNA ligands. *Biochemistry,* 36**,** 9726-34.

MARIMUTHU, C., TANG, T. H., TOMINAGA, J., TAN, S. C. & GOPINATH, S. C. 2012. Single-stranded DNA (ssDNA) production in DNA aptamer generation. *Analyst,* 137**,** 1307-15.

MARTIN, D. F., MAGUIRE, M. G., FINE, S. L., YING, G. S., JAFFE, G. J., GRUNWALD, J. E., TOTH, C., REDFORD, M. & FERRIS, F. L., 3RD 2012. Ranibizumab and bevacizumab for treatment of neovascular age-related macular degeneration: two-year results. *Ophthalmology,* 119**,** 1388-98.

MARTIN, G. R. 1981. Isolation of a pluripotent cell line from early mouse embryos cultured in medium conditioned by teratocarcinoma stem cells. *Proc Natl Acad Sci U S A,* 78**,** 7634-8.

MASHIMA, T., MATSUGAMI, A., NISHIKAWA, F., NISHIKAWA, S. & KATAHIRA, M. 2009. Unique quadruplex structure and interaction of an RNA aptamer against bovine prion protein. *Nucleic Acids Res,* 37**,** 6249-58.

MASON, C. & DUNNILL, P. 2008. A brief definition of regenerative medicine. *Regen Med,* 3**,** 1-5.

MASON, C. & MANZOTTI, E. 2010. Regenerative medicine cell therapies: numbers of units manufactured and patients treated between 1988 and 2010. *Regen Med,* 5**,** 307-13.

MCDAVID, A., FINAK, G., CHATTOPADYAY, P. K., DOMINGUEZ, M., LAMOREAUX, L., MA, S. S., ROEDERER, M. & GOTTARDO, R. 2013. Data exploration, quality control and testing in single-cell qPCR-based gene expression experiments. *Bioinformatics,* 29**,** 461-7.

MCFAUL, S. M., LIN, B. K. & MA, H. 2012. Cell separation based on size and deformability using microfluidic funnel ratchets. *Lab Chip,* 12**,** 2369-76.

MCNAMARA, J. O., 2ND, ANDRECHEK, E. R., WANG, Y., VILES, K. D., REMPEL, R. E., GILBOA, E., SULLENGER, B. A. & GIANGRANDE, P. H. 2006. Cell type-specific delivery of siRNAs with aptamer-siRNA chimeras. *Nat Biotechnol,* 24**,** 1005-15.

MEHRAN, R., ALEXANDER, J. & M., L. 2015. Effect of REG1 Anticoagulation System versus Bivalirudin on Cardiovascular Outcomes Following PCI:

The REGULATE-PCI Randomized Clinical Trial. Regulate-PCI.

MEIRELLES LDA, S. & NARDI, N. B. 2003. Murine marrow-derived mesenchymal stem cell: isolation, in vitro expansion, and characterization. *Br J Haematol,* 123**,** 702-11.

MENDEZ-FERRER, S., MICHURINA, T. V., FERRARO, F., MAZLOOM, A. R., MACARTHUR, B. D., LIRA, S. A., SCADDEN, D. T., MA'AYAN, A., ENIKOLOPOV, G. N. & FRENETTE, P. S. 2010. Mesenchymal and haematopoietic stem cells form a unique bone marrow niche. *Nature,* 466**,** 829-34.

MENSING, N., GASSE, H., HAMBRUCH, N., HAEGER, J.-D., PFARRER, C. & STASZYK, C. 2011. Isolation and characterization of multipotent mesenchymal stromal cells from the gingiva and the periodontal ligament of the horse. *BMC Veterinary Research,* 7**,** 42.

MERKLE, T., HOLDER, I. T. & HARTIG, J. S. 2016. The dual aptamer approach: rational design of a high-affinity FAD aptamer. *Org. Biomol. Chem.*

MILLS, L. A., AITKEN, S. A. & SIMPSON, A. 2017. The risk of non-union per fracture: current myths and revised figures from a population of over 4 million adults. *Acta Orthop,* 88**,** 434-439.

MILTENYI, S., MULLER, W., WEICHEL, W. & RADBRUCH, A. 1990. High gradient magnetic cell separation with MACS. *Cytometry,* 11**,** 231-8.

MIRANDA, R. N., BRIGGS, R. C., SHULTS, K., KINNEY, M. C., JENSEN, R. A. & COUSAR, J. B. 1999. Immunocytochemical analysis of MNDA in tissue sections and sorted normal bone marrow cells documents expression only in maturing normal and neoplastic myelomonocytic cells and a subset of normal and neoplastic B lymphocytes. *Hum Pathol,* 30**,** 1040-9.

MIRMALEK-SANI, S.-H., TARE, R. S., MORGAN, S. M., ROACH, H. I., WILSON, D. I., HANLEY, N. A. & OREFFO, R. O. C. 2006. Characterization and Multipotentiality of Human Fetal Femur-Derived Cells: Implications for Skeletal Tissue Regeneration. *Stem Cells,* 24**,** 1042-1053.

MOHAMED, H., TURNER, J. N. & CAGGANA, M. 2007. Biochip for separating fetal cells from maternal circulation. *J Chromatogr A,* 1162**,** 187-92.

MONTEIRO, I. P., SHUKLA, A., MARQUES, A. P., REIS, R. L. & HAMMOND, P. T. 2015. Spray-assisted layer-by-layer assembly on hyaluronic acid scaffolds for skin tissue engineering. *J Biomed Mater Res A,* 103**,** 330-40.

MORRIS, K. N., JENSEN, K. B., JULIN, C. M., WEIL, M. & GOLD, L. 1998. High affinity ligands from in vitro selection: complex targets. *Proc Natl Acad Sci U S A,* 95**,** 2902-7.

MOUSA, S. A. & MOUSA, S. S. 2010. Current status of vascular endothelial growth factor inhibition in age-related macular degeneration. *BioDrugs,* 24**,** 183-94.

MUIR, H. 1995. The chondrocyte, architect of cartilage. Biomechanics, structure, function and molecular biology of cartilage matrix macromolecules. *Bioessays,* 17**,** 1039-48.

MUSUMECI, D. & MONTESARCHIO, D. 2012. Polyvalent nucleic acid aptamers and modulation of their activity: a focus on the thrombin binding aptamer. *Pharmacol Ther,* 136**,** 202-15.

MUZYLAK, M., ARNETT, T. R., PRICE, J. S. & HORTON, M. A. 2007. The in vitro effect of pH on osteoclasts and bone resorption in the cat: implications for the pathogenesis of FORL. *J Cell Physiol,* 213**,** 144-50.

MÜLLER-SCHULTE, D., SCHMITZ-RODE, T. & BORM, P. 2005. Ultra-fast synthesis of magnetic and luminescent silica beads for versatile bioanalytical applications. *Journal of Magnetism and Magnetic Materials,* 293**,** 135-143.

NACHUM, R. & SHANBROM, E. 1981. Rapid detection of Gram-negative bacteriuria by Limulus amoebocyte lysate assay. *J Clin Microbiol,* 13**,** 158-62.

NAGASAWA, T. 2014. CXC chemokine ligand 12 (CXCL12) and its receptor CXCR4. *J Mol Med (Berl),* 92**,** 433-9.

NAGASAWA, T., HIROTA, S., TACHIBANA, K., TAKAKURA, N., NISHIKAWA, S., KITAMURA, Y., YOSHIDA, N., KIKUTANI, H. & KISHIMOTO, T. 1996. Defects of B-cell lymphopoiesis and

bone-marrow myelopoiesis in mice lacking the CXC chemokine PBSF/SDF-1. *Nature,* 382**,** 635-8.

NAVEIRAS, O., NARDI, V., WENZEL, P. L., HAUSCHKA, P. V., FAHEY, F. & DALEY, G. Q. 2009. Bone-marrow adipocytes as negative regulators of the haematopoietic microenvironment. *Nature,* 460**,** 259-63.

NEREM, R. M. & SAMBANIS, A. 1995. Tissue engineering: from biology to biological substitutes. *Tissue Eng,* 1**,** 3-13.

NESIC, D., WHITESIDE, R., BRITTBERG, M., WENDT, D., MARTIN, I. & MAINIL-VARLET, P. 2006. Cartilage tissue engineering for degenerative joint disease. *Adv Drug Deliv Rev,* 58**,** 300-22.

NEUMULLER, R. A. & KNOBLICH, J. A. 2009. Dividing cellular asymmetry: asymmetric cell division and its implications for stem cells and cancer. *Genes Dev,* 23**,** 2675-99.

NEVES, M. A. D., SLAVKOVIC, S., CHURCHER, Z. R. & JOHNSON, P. E. 2017. Salt-mediated two-site ligand binding by the cocaine-binding aptamer. *Nucleic Acids Res,* 45**,** 1041-1048.

NG, E. W., SHIMA, D. T., CALIAS, P., CUNNINGHAM, E. T., JR., GUYER, D. R. & ADAMIS, A. P. 2006. Pegaptanib, a targeted anti-VEGF aptamer for ocular vascular disease. *Nat Rev Drug Discov,* 5**,** 123-32.

NHS_ENGLAND 2015. NHS programme budgetting resource 2013 - 2014.

NI, S., YAO, H., WANG, L., LU, J., JIANG, F., LU, A. & ZHANG, G. 2017. Chemical Modifications of Nucleic Acid Aptamers for Therapeutic Purposes. *Int J Mol Sci,* 18.

NIMJEE, S. M., RUSCONI, C. P., HARRINGTON, R. A. & SULLENGER, B. A. 2005. The potential of aptamers as anticoagulants. *Trends Cardiovasc Med,* 15**,** 41-5.

NISHIDA, S., ENDO, N., YAMAGIWA, H., TANIZAWA, T. & TAKAHASHI, H. E. 1999. Number of osteoprogenitor cells in human bone marrow markedly decreases after skeletal maturation. *J Bone Miner Metab,* 17**,** 171-7.

NISSEN, P., HANSEN, J., BAN, N., MOORE, P. B. & STEITZ, T. A. 2000. The structural basis of ribosome activity in peptide bond synthesis. *Science,* 289**,** 920-30.

NOWAKOWSKI, J. & TINOCO, I. 1997. RNA structure and stability. *Seminars in Virology,* 8**,** 153-165.

O'BRIEN, E. P., BROOKS, B. R. & THIRUMALAI, D. 2012. Effects of pH on proteins: predictions for ensemble and single-molecule pulling experiments. *J Am Chem Soc,* 134**,** 979-87.

O'DONOGHUE, K. & FISK, N. M. 2004. Fetal stem cells. *Best Pract Res Clin Obstet Gynaecol,* 18**,** 853-75.

ODORICO, J. S., KAUFMAN, D. S. & THOMSON, J. A. 2001. Multilineage differentiation from human embryonic stem cell lines. *Stem Cells,* 19**,** 193-204.

OH, J., LEE, Y. D. & WAGERS, A. J. 2014. Stem cell aging: mechanisms, regulators and therapeutic opportunities. *Nat Med,* 20**,** 870-80.

OH, S. S., AHMAD, K. M., CHO, M., KIM, S., XIAO, Y. & SOH, H. T. 2011. Improving Aptamer Selection Efficiency through Volume Dilution, Magnetic Concentration, and Continuous Washing in Microfluidic Channels. *Anal. Chem.,* 83**,** 6.

OKA, M., USHIO, K., KUMAR, P., IKEUCHI, K., HYON, S. H., NAKAMURA, T. & FUJITA, H. 2000. Development of artificial articular cartilage. *Proc Inst Mech Eng H,* 214**,** 59-68.

OKADA, T., NGO, V. N., EKLAND, E. H., FÖRSTER, R., LIPP, M., LITTMAN, D. R. & CYSTER, J. G. 2002. Chemokine Requirements for B Cell Entry to Lymph Nodes and Peyer's Patches. *The Journal of Experimental Medicine,* 196**,** 65-75.

OKITA, K., ICHISAKA, T. & YAMANAKA, S. 2007. Generation of germline-competent induced pluripotent stem cells. *Nature,* 448**,** 313-7.

OKITA, K., MATSUMURA, Y., SATO, Y., OKADA, A., MORIZANE, A., OKAMOTO, S., HONG, H., NAKAGAWA, M., TANABE, K., TEZUKA, K., SHIBATA, T., KUNISADA, T., TAKAHASHI, M., TAKAHASHI, J., SAJI, H. & YAMANAKA, S. 2011. A more efficient method to generate integration-free human iPS cells. *Nat Methods,* 8**,** 409-12.

OMATSU, Y., SUGIYAMA, T., KOHARA, H., KONDOH, G., FUJII, N., KOHNO, K. & NAGASAWA, T. 2010. The essential functions of adipo-osteogenic progenitors as the hematopoietic stem and progenitor cell niche. *Immunity,* 33**,** 387-99.

OREFFO, R. O., COOPER, C., MASON, C. & CLEMENTS, M. 2005. Mesenchymal stem cells: lineage, plasticity, and skeletal therapeutic potential. *Stem Cell Rev,* 1**,** 169-78.

ORRISS, I. R., UTTING, J. C., BRANDAO-BURCH, A., COLSTON, K., GRUBB, B. R., BURNSTOCK, G. & ARNETT, T. R. 2007. Extracellular nucleotides block bone mineralization in vitro: evidence for dual inhibitory mechanisms involving both P2Y2 receptors and pyrophosphate. *Endocrinology,* 148**,** 4208-16.

OWEN, M. & FRIEDENSTEIN, A. J. 1988. Stromal stem cells: marrow-derived osteogenic precursors. *Ciba Found Symp,* 136**,** 42-60.

PAIGE, J. S., WU, K. Y. & JAFFREY, S. R. 2011. RNA mimics of green fluorescent protein. *Science,* 333**,** 642-6.

PERA, M. F., REUBINOFF, B. & TROUNSON, A. 2000. Human embryonic stem cells. *J Cell Sci,* 113 (Pt 1)**,** 5-10.

PETERSON, P. G. 1999. Gray dawn: The global aging crisis. *Foreign Affairs,* 78**,** 42-+.

PHILIPPOU, S., MASTROYIANNOPOULOS, N. P., MAKRIDES, N., LEDERER, C. W., KLEANTHOUS, M. & PHYLACTOU, L. A. 2018. Selection and Identification of Skeletal-Muscle-Targeted RNA Aptamers. *Mol Ther Nucleic Acids,* 10**,** 199-214.

PITTENGER, M. F. 1999. Multilineage Potential of Adult Human Mesenchymal Stem Cells. *Science,* 284**,** 143-147.

PITTENGER, M. F., MACKAY, A. M., BECK, S. C., JAISWAL, R. K., DOUGLAS, R., MOSCA, J. D., MOORMAN, M. A., SIMONETTI, D. W., CRAIG, S. & MARSHAK, D. R. 1999. Multilineage potential of adult human mesenchymal stem cells. *Science,* 284**,** 143-7.

POTHOULAKIS, G., CERONI, F., REEVE, B. & ELLIS, T. 2014. The spinach RNA aptamer as a characterization tool for synthetic biology. *ACS Synth Biol,* 3**,** 182-7.

POVSIC, T. J., COHEN, M. G., CHAN, M. Y., ZELENKOFSKE, S. L., WARGIN, W. A., HARRINGTON, R. A., ALEXANDER, J. H., RUSCONI, C. P. & BECKER, R. C. 2011. Dose selection for a direct and selective factor IXa inhibitor and its complementary reversal agent: translating pharmacokinetic and pharmacodynamic properties of the REG1 system to clinical trial design. *J Thromb Thrombolysis,* 32**,** 21-31.

POVSIC, T. J., VAVALLE, J. P., ABERLE, L. H., KASPRZAK, J. D., COHEN, M. G., MEHRAN, R., BODE, C., BULLER, C. E., MONTALESCOT, G., CORNEL, J. H., RYNKIEWICZ, A., RING, M. E., ZEYMER, U., NATARAJAN, M., DELARCHE, N., ZELENKOFSKE, S. L., BECKER, R. C., ALEXANDER, J. H. & INVESTIGATORS, R. 2013. A Phase 2, randomized, partially blinded, active-controlled study assessing the efficacy and safety of variable anticoagulation reversal using the REG1 system in patients with acute coronary syndromes: results of the RADAR trial. *Eur Heart J,* 34**,** 2481-9.

PRODĚLALOVÁ, J., RITTICH, B., ŠPANOVÁ, A., PETROVÁ, K. & BENEŠ, M. J. 2004. Isolation of genomic DNA using magnetic cobalt ferrite and silica particles. *Journal of Chromatography A,* 1056**,** 43-48.

PROKHOROVA, T. A., HARKNESS, L. M., FRANDSEN, U., DITZEL, N., SCHRODER, H. D., BURNS, J. S. & KASSEM, M. 2009. Teratoma formation by human embryonic stem cells is site dependent and enhanced by the presence of Matrigel. *Stem Cells Dev,* 18**,** 47-54.

PRZYBORSKI, S. A. 2005. Differentiation of human embryonic stem cells after transplantation in immune-deficient mice. *Stem Cells,* 23**,** 1242-50.

QUIRICI, N., SOLIGO, D., BOSSOLASCO, P., SERVIDA, F., LUMINI, C. & DELILIERS, G. L. 2002. Isolation of bone marrow mesenchymal stem cells by anti-nerve growth factor receptor antibodies. *Exp Hematol,* 30**,** 783-91.

R. K. MOSING, S. D. MENDONSA & BOWSER, M. T. 2005. Capillary Electrophoresis-SELEX Selection of Aptamers with Affinity for HIV-1 Reverse Transcriptase. *Anal. Chem.*

RAJESH, K., RANA, K. V. & SURI, C. R. 2013. Characterization of Hapten-Protein Conjugates: Antibody Generation and Immunoassay Development for Pesticides Monitoring. *Bionanoscience,* 3**,** 137-144.

RAMIREZ-ZACARIAS, J. L., CASTRO-MUNOZLEDO, F. & KURI-HARCUCH, W. 1992. Quantitation of adipose conversion and triglycerides by staining intracytoplasmic lipids with Oil red O. *Histochemistry,* 97**,** 493-7.

RAY, P., RIALON-GUEVARA, K. L., VERAS, E., SULLENGER, B. A. & WHITE, R. R. 2012. Comparing human pancreatic cell secretomes by in vitro aptamer selection identifies cyclophilin B as a candidate pancreatic cancer biomarker. *J Clin Invest,* 122**,** 1734-41.

REINEMANN, C., FREIIN VON FRITSCH, U., RUDOLPH, S. & STREHLITZ, B. 2016. Generation and characterization of quinolone-specific DNA aptamers suitable for water monitoring. *Biosens Bioelectron,* 77**,** 1039-47.

REZNIKOV, N., SHAHAR, R. & WEINER, S. 2014. Bone hierarchical structure in three dimensions. *Acta Biomater,* 10**,** 3815-26.

RHO, J.-Y. K.-S. Z., PETER. 1998. Mechanical properties and the hierarchical structure of bone. *Medical Engineering & Physics,* 20**,** 92-102.

RHO, J.-Y. T., TING Y. PHARR, GEORGE M. 1997. Elastic properties of human cortical and trabecular lamellar bone measured by nanoindentation. *Biomaterials,* 18**,** 1325-1330.

RICHARDSON, S. M., KALAMEGAM, G., PUSHPARAJ, P. N., MATTA, C., MEMIC, A., KHADEMHOSSEINI, A., MOBASHERI, R., POLETTI, F. L., HOYLAND, J. A. & MOBASHERI, A. 2016. Mesenchymal stem cells in regenerative medicine: Focus on articular cartilage and intervertebral disc regeneration. *Methods,* 99**,** 69-80.

RIFAI, N., GILLETTE, M. A. & CARR, S. A. 2006. Protein biomarker discovery and validation: the long and uncertain path to clinical utility. *Nat Biotechnol,* 24**,** 971-83.

RIFAS, L., FAUSTO, A., SCOTT, M. J., AVIOLI, L. V. & WELGUS, H. G. 1994. Expression of metalloproteinases and tissue inhibitors of metalloproteinases in human osteoblast-like cells: differentiation is associated with repression of metalloproteinase biosynthesis. *Endocrinology,* 134**,** 213-21.

ROBERTS, S. J., HOWARD, D., BUTTERY, L. D. & SHAKESHEFF, K. M. 2008. Clinical applications of musculoskeletal tissue engineering. *Br Med Bull,* 86**,** 7-22.

ROBERTSON, D. L. & JOYCE, G. F. 1990. Selection in vitro of an RNA enzyme that specifically cleaves single-stranded DNA. *Nature,* 344**,** 467-8.

ROBEY, P. G. 2011. Cell sources for bone regeneration: the good, the bad, and the ugly (but promising). *Tissue Eng Part B Rev,* 17**,** 423-30.

RODOLFA, K. T. & EGGAN, K. 2006. A transcriptional logic for nuclear reprogramming. *Cell,* 126**,** 652-5.

RODRIGUEZ, A. M., ELABD, C., AMRI, E. Z., AILHAUD, G. & DANI, C. 2005. The human adipose tissue is a source of multipotent stem cells. *Biochimie,* 87**,** 125-8.

RODRIGUEZ-ESTEBAN, G., GONZALEZ-SASTRE, A., ROJO-LAGUNA, J. I., SALO, E. & ABRIL, J. F. 2015. Digital gene expression approach over multiple RNA-Seq data sets to detect neoblast transcriptional changes in Schmidtea mediterranea. *BMC Genomics,* 16**,** 361.

RODRIGUEZ-MENOCAL, L., SHAREEF, S., SALGADO, M., SHABBIR, A. & VAN BADIAVAS, E. 2015. Role of whole bone marrow, whole bone marrow cultured cells, and mesenchymal stem cells in chronic wound healing. *Stem Cell Res Ther,* 6**,** 24.

ROSSI, J. J. 2007. Targeted cleavage: tuneable cis-cleaving ribozymes. *Proc Natl Acad Sci U S A,* 104**,** 14881-2.

ROUAH-MARTIN, E., MEHTA, J., VAN DORST, B., DE SAEGER, S., DUBRUEL, P., MAES, B. U., LEMIERE, F., GOORMAGHTIGH, E., DAEMS, D., HERREBOUT, W., VAN HOVE, F., BLUST, R. & ROBBENS, J. 2012. Aptamer-based molecular recognition of lysergamine, metergoline and small ergot alkaloids. *Int J Mol Sci,* 13**,** 17138-59.

RUCKMAN, J., GREEN, L. S., BEESON, J., WAUGH, S., GILLETTE, W. L., HENNINGER, D. D., CLAESSON-WELSH, L. & JANJIC, N. 1998. 2'-Fluoropyrimidine RNA-based aptamers to the 165-amino acid form of vascular endothelial growth factor (VEGF165). Inhibition of receptor binding and VEGF-induced vascular permeability through interactions requiring the exon 7-encoded domain. *J Biol Chem,* 273**,** 20556-67.

RUSCITO, A. & DEROSA, M. C. 2016. Small-Molecule Binding Aptamers: Selection Strategies, Characterization, and Applications. *Front Chem,* 4**,** 14.

RUSCONI, C. P., ROBERTS, J. D., PITOC, G. A., NIMJEE, S. M., WHITE, R. R., QUICK, G., JR., SCARDINO, E., FAY, W. P. & SULLENGER, B. A. 2004. Antidote-mediated control of an anticoagulant aptamer in vivo. *Nat Biotechnol,* 22**,** 1423-8.

SABETI, P. C., UNRAU, P. J. & BARTEL, D. P. 1997. Accessing rare activities from random RNA sequences: the importance of the length of molecules in the starting pool. *Chem Biol,* 4**,** 767-74.

SACCA, B., LACROIX, L. & MERGNY, J. L. 2005. The effect of chemical modifications on the thermal stability of different G-quadruplex-forming oligonucleotides. *Nucleic Acids Res,* 33**,** 1182-92.

SACCHETTI, B., FUNARI, A., MICHIENZI, S., DI CESARE, S., PIERSANTI, S., SAGGIO, I., TAGLIAFICO, E., FERRARI, S., ROBEY, P. G., RIMINUCCI, M. & BIANCO, P. 2007. Self-renewing osteoprogenitors in bone marrow sinusoids can organize a hematopoietic microenvironment. *Cell,* 131**,** 324-36.

SAKAGUCHI, Y., SEKIYA, I., YAGISHITA, K. & MUNETA, T. 2005. Comparison of human stem cells derived from various mesenchymal tissues: superiority of synovium as a cell source. *Arthritis Rheum,* 52**,** 2521-9.

SAMSONRAJ, R. M., RAI, B., SATHIYANATHAN, P., PUAN, K. J., ROTZSCHKE, O., HUI, J. H., RAGHUNATH, M., STANTON, L. W., NURCOMBE, V. & COOL, S. M. 2015. Establishing criteria for human mesenchymal stem cell potency. *Stem Cells,* 33**,** 1878-91.

SAZANI, P. L., LARRALDE, R. & SZOSTAK, J. W. 2004. A small aptamer with strong and specific recognition of the triphosphate of ATP. *J Am Chem Soc,* 126**,** 8370-1.

SCHAFER, R., WISKIRCHEN, J., GUO, K., NEUMANN, B., KEHLBACH, R., PINTASKE, J., VOTH, V., WALKER, T., SCHEULE, A. M., GREINER, T. O., HERMANUTZ-KLEIN, U., CLAUSSEN, C. D., NORTHOFF, H., ZIEMER, G. & WENDEL, H. P. 2007. Aptamer-based isolation and subsequent imaging of mesenchymal stem cells in ischemic myocard by magnetic resonance imaging. *Rofo,* 179**,** 1009-15.

SCHINDELER, A., MCDONALD, M. M., BOKKO, P. & LITTLE, D. G. 2008. Bone remodeling during fracture repair: The cellular picture. *Semin Cell Dev Biol,* 19**,** 459-66.

SCHOUSBOE, J. T., TAYLOR, B. C., FINK, H. A., KANE, R. L., CUMMINGS, S. R., ORWOLL, E. S., MELTON, L. J., 3RD, BAUER, D. C. & ENSRUD, K. E. 2007. Cost-effectiveness of bone densitometry followed by treatment of osteoporosis in older men. *JAMA,* 298**,** 629-37.

SEKIYA, S., NODA, K., NISHIKAWA, F., YOKOYAMA, T., KUMAR, P. K. & NISHIKAWA, S. 2006. Characterization and application of a novel RNA aptamer against the mouse prion protein. *J Biochem,* 139**,** 383-90.

SERAFINI, M., SACCHETTI, B., PIEVANI, A., REDAELLI, D., REMOLI, C., BIONDI, A., RIMINUCCI, M. & BIANCO, P. 2014. Establishment of bone marrow and hematopoietic niches in vivo by reversion of chondrocyte differentiation of human bone marrow stromal cells. *Stem Cell Res,* 12**,** 659-72.

SHANGGUAN, D., BING, T. & ZHANG, N. 2015. Cell-SELEX: Aptamer Selection Against Whole Cells. 13-33.

SHARMA, T. K., BRUNO, J. G. & DHIMAN, A. 2017. ABCs of DNA aptamer and related assay development. *Biotechnol Adv,* 35**,** 275-301.

SHENG, W., CHEN, T., KAMATH, R., XIONG, X., TAN, W. & FAN, Z. H. 2012. Aptamer-enabled efficient isolation of cancer cells from whole blood using a microfluidic device. *Anal Chem,* 84**,** 4199-206.

SHIELDS, C. W. T., REYES, C. D. & LOPEZ, G. P. 2015. Microfluidic cell sorting: a review of the advances in the separation of cells from debulking to rare cell isolation. *Lab Chip,* 15**,** 1230-49.

SHIH, I. M. 1999. The role of CD146 (Mel-CAM) in biology and pathology. *J Pathol,* 189**,** 4-11.

SHU, Y., CINIER, M., SHU, D. & GUO, P. 2011. Assembly of multifunctional phi29 pRNA nanoparticles for specific delivery of siRNA and other therapeutics to targeted cells. *Methods,* 54**,** 204-14.

SIISSALO, S., LAITINEN, L., KOLJONEN, M., VELLONEN, K. S., KORTEJARVI, H., URTTI, A., HIRVONEN, J. & KAUKONEN, A. M. 2007. Effect of cell differentiation and passage number on the expression of efflux proteins in wild type and vinblastine-induced Caco-2 cell lines. *Eur J Pharm Biopharm,* 67**,** 548-54.

SILVERMAN, S. K. 2009. Artificial Functional Nucleic Acids: Aptamers, Ribozymes, and Deoxyribozymes Identified by In Vitro Selection. *In:* YINGFU, L. & YI, L. (eds.) *Functional Nucleic Acids for Analytical Applications.* New York, NY: Springer New York.

SIMMONS, P. J. & TOROK-STORB, B. 1991. Identification of stromal cell precursors in human bone marrow by a novel monoclonal antibody, STRO-1. *Blood,* 78**,** 55-62.

SMESTAD, J. & MAHER, L. J., 3RD 2013. Ion-dependent conformational switching by a DNA aptamer that induces remyelination in a mouse model of multiple sclerosis. *Nucleic Acids Res,* 41**,** 1329-42.

SMITH, J. O., AARVOLD, A., TAYTON, E. R., DUNLOP, D. G. & OREFFO, R. O. 2011. Skeletal tissue regeneration: current approaches, challenges, and novel reconstructive strategies for an aging population. *Tissue Eng Part B Rev,* 17**,** 307-20.

SMITH, K. D., LIPCHOCK, S. V., AMES, T. D., WANG, J., BREAKER, R. R. & STROBEL, S. A. 2009. Structural basis of ligand binding by a c-di-GMP riboswitch. *Nat Struct Mol Biol,* 16**,** 1218-23.

SMUC, T., AHN, I. Y. & ULRICH, H. 2013. Nucleic acid aptamers as high affinity ligands in biotechnology and biosensorics. *J Pharm Biomed Anal,* 81-82**,** 210-7.

SONG, S., CHO, Y. S., LEE, S.-J. & HAH, S. S. 2014. Aptamer-Based Precipitation as an Alternative to the Conventional Immunoprecipitation for Purification of Target Proteins. *Bulletin of the Korean Chemical Society,* 35**,** 2665-2668.

SONG, S. P., WANG, L. H., LI, J., ZHAO, J. L. & FAN, C. H. 2008. Aptamer-based biosensors. *Trac-Trends in Analytical Chemistry,* 27**,** 108-117.

SORRENTINO, A., FERRACIN, M., CASTELLI, G., BIFFONI, M., TOMASELLI, G., BAIOCCHI, M., FATICA, A., NEGRINI, M., PESCHLE, C. & VALTIERI, M. 2008. Isolation and characterization of CD146+ multipotent mesenchymal stromal cells. *Exp Hematol,* 36**,** 1035-46.

SOSS, S. E., ROSE, K. L., HILL, S., JOUAN, S. & CHAZIN, W. J. 2015. Biochemical and Proteomic Analysis of Ubiquitination of Hsc70 and Hsp70 by the E3 Ligase CHIP. *PLoS One,* 10**,** e0128240.

SOULE, E. E., BOMPIANI, K. M., WOODRUFF, R. S. & SULLENGER, B. A. 2016. Targeting Two Coagulation Cascade Proteases with a Bivalent Aptamer Yields a Potent and Antidote-Controllable Anticoagulant. *Nucleic Acid Ther,* 26**,** 1-9.

STAHLBERG, J., JONSSON, B. & HORVATH, C. 1991. Theory for electrostatic interaction chromatography of proteins. *Anal Chem,* 63**,** 1867-74.

STEINER, T. & DESIRAJU, G. R. 1998. Distinction between the weak hydrogen bond and the van der Waals interaction. *Chemical Communications***,** 891-892.

STENDERUP, K., JUSTESEN, J., CLAUSEN, C. & KASSEM, M. 2003. Aging is associated with decreased maximal life span and accelerated senescence of bone marrow stromal cells. *Bone,* 33**,** 919-926.

STOLTENBURG, R., NIKOLAUS, N. & STREHLITZ, B. 2012. Capture-SELEX: Selection of DNA Aptamers for Aminoglycoside Antibiotics. *J Anal Methods Chem,* 2012**,** 415697.

STOLTENBURG, R., REINEMANN, C. & STREHLITZ, B. 2005. FluMag-SELEX as an advantageous method for DNA aptamer selection | SpringerLink. *Anal. Bioanal Chem,* 383**,** 8.

STOLZING, A., JONES, E., MCGONAGLE, D. & SCUTT, A. 2008. Age-related changes in human bone marrow-derived mesenchymal stem cells: consequences for cell therapies. *Mech Ageing Dev,* 129**,** 163-73.

STOVALL, G. 2004. Automated optimization of aptamer selection buffer conditions. *Journal of the Association for Laboratory Automation,* 9**,** 117-122.

SU, W., CHO, M., NAM, J.-D., CHOE, W.-S. & LEE, Y. 2013. Aptamer-Assisted Gold Nanoparticles/PEDOT Platform for Ultrasensitive Detection of LPS. *Electroanalysis,* 25**,** 380-386.

SU, W. & DING, X. 2015. Methods of Endotoxin Detection. *J Lab Autom,* 20**,** 354-64.

SU, W., LIN, M., LEE, H., CHO, M., CHOE, W. S. & LEE, Y. 2012. Determination of endotoxin through an aptamer-based impedance biosensor. *Biosens Bioelectron,* 32**,** 32-6.

SUBRAMANIAN, N., RAGHUNATHAN, V., KANWAR, J. R., KANWAR, R. K., ELCHURI, S. V., KHETAN, V. & KRISHNAKUMAR, S. 2012. Target-specific delivery of doxorubicin to retinoblastoma using epithelial cell adhesion molecule aptamer. *Molecular Vision,* 18**,** 2783-2795.

SUGIYAMA, T., KOHARA, H., NODA, M. & NAGASAWA, T. 2006. Maintenance of the hematopoietic stem cell pool by CXCL12-CXCR4 chemokine signaling in bone marrow stromal cell niches. *Immunity,* 25**,** 977-88.

SVOBODOVA, M., PINTO, A., NADAL, P. & CK, O. S. 2012. Comparison of different methods for generation of single-stranded DNA for SELEX processes. *Anal Bioanal Chem,* 404**,** 835-42.

TAICHMAN, R. S. & EMERSON, S. G. 1994. Human Osteoblasts Support Hematopoiesis through the Production of Granulocyte Colony-stimulating Factor. *J Exp Med,* 179**,** 1677-1682.

TAICHMAN, R. S., REILLY, M. J. & EMERSON, S. G. 1996. Human osteoblasts support human hematopoietic progenitor cells in vitro bone marrow cultures. *Blood,* 87**,** 518-24.

TAKAHASHI, M. 2018. Aptamers targeting cell surface proteins. *Biochimie,* 145**,** 63-72.

TALLMADGE, R. L., SHEN, L., TSENG, C. T., MILLER, S. C., BARRY, J. & FELIPPE, M. J. 2015. Bone marrow transcriptome and epigenome profiles of equine common variable immunodeficiency patients unveil block of B lymphocyte differentiation. *Clin Immunol,* 160**,** 261-76.

TANG, J., YU, T., GUO, L., XIE, J., SHAO, N. & HE, Z. 2007. In vitro selection of DNA aptamer against abrin toxin and aptamer-based abrin direct detection. *Biosens Bioelectron,* 22**,** 2456-63.

TARE, R. S., MITCHELL, P. D., KANCZLER, J. & OREFFO, R. O. 2012. Isolation, differentiation, and characterisation of skeletal stem cells from human bone marrow in vitro and in vivo. *Methods Mol Biol,* 816**,** 83-99.

TAVASSOLI, M. & CROSBY, W. H. 1968. Transplantation of marrow to extramedullary sites. *Science,* 161**,** 54-6.

TAYTON, E., PURCELL, M., SMITH, J. O., LANHAM, S., HOWDLE, S. M., SHAKESHEFF, K. M., GOODSHIP, A., BLUNN, G., FOWLER, D., DUNLOP, D. G. & OREFFO, R. O. 2015. The scale-up of a tissue engineered porous hydroxyapatite polymer composite scaffold for use in bone repair: an ovine femoral condyle defect study. *J Biomed Mater Res A,* 103**,** 1346-56.

THIEL, K. W., HERNANDEZ, L. I., DASSIE, J. P., THIEL, W. H., LIU, X., STOCKDALE, K. R., ROTHMAN, A. M., HERNANDEZ, F. J., MCNAMARA, J. O., 2ND & GIANGRANDE, P. H. 2012. Delivery of chemo-sensitizing siRNAs to HER2+-breast cancer cells using RNA aptamers. *Nucleic Acids Res,* 40**,** 6319-37.

THOMSON, J. A. 1998. Embryonic Stem Cell Lines Derived from Human Blastocysts. *Science,* 282**,** 1145-1147.

TOGARI, A., ARAI, M., MIZUTANI, S., MIZUTANI, S., KOSHIHARA, Y. & NAGATSU, T. 1997. Expression of mRNAs for neuropeptide receptors and β-adrenergic receptors in human osteoblasts and human osteogenic sarcoma cells. *Neuroscience Letters,* 233**,** 125-128.

TOH, S. Y., CITARTAN, M., GOPINATH, S. C. & TANG, T. H. 2015. Aptamers as a replacement for antibodies in enzyme-linked immunosorbent assay. *Biosens Bioelectron,* 64**,** 392-403.

TOKOYODA, K., EGAWA, T., SUGIYAMA, T., CHOI, B. I. & NAGASAWA, T. 2004. Cellular niches controlling B lymphocyte behavior within bone marrow during development. *Immunity,* 20**,** 707-18.

TOMA, J. G., AKHAVAN, M., FERNANDES, K. J., BARNABE-HEIDER, F., SADIKOT, A., KAPLAN, D. R. & MILLER, F. D. 2001. Isolation of multipotent adult stem cells from the dermis of mammalian skin. *Nat Cell Biol,* 3**,** 778-84.

TONDREAU, T., LAGNEAUX, L., DEJENEFFE, M., DELFORGE, A., MASSY, M., MORTIER, C. & BRON, D. 2004. Isolation of BM mesenchymal stem cells by plastic adhesion or negative selection: phenotype, proliferation kinetics and differentiation potential. *Cytotherapy,* 6**,** 372-9.

TORSTEINSDÓTTIR, I., HÅKANSSON, L., HÄLLGREN, R., GUDBJÖRNSSON, B., ARVIDSON, N. G. & VENGE, P. 1999. Serum lysozyme: a potential marker of monocyte/macrophage activity in rheumatoid arthritis. *Rheumatology,* 38**,** 1249-1254.

TOSTESON, A. N., MELTON, L. J., 3RD, DAWSON-HUGHES, B., BAIM, S., FAVUS, M. J., KHOSLA, S., LINDSAY, R. L. & NATIONAL OSTEOPOROSIS FOUNDATION GUIDE, C. 2008. Cost-effective osteoporosis treatment thresholds: the United States perspective. *Osteoporos Int,* 19**,** 437-47.

TRAVLOS, G. S. 2006. Normal structure, function, and histology of the bone marrow. *Toxicol Pathol,* 34**,** 548-65.

TSUMOTO, K., EJIMA, D., SENCZUK, A. M., KITA, Y. & ARAKAWA, T. 2007. Effects of salts on protein-surface interactions: applications for column chromatography. *J Pharm Sci,* 96**,** 1677-90.

TUERK, C. & GOLD, L. 1990. Systematic evolution of ligands by exponential enrichment: RNA ligands to bacteriophage T4 DNA polymerase. *Science,* 249**,** 505-10.

TZENG, Y. S., LI, H., KANG, Y. L., CHEN, W. C., CHENG, W. C. & LAI, D. M. 2011. Loss of Cxcl12/Sdf-1 in adult mice decreases the quiescent state of hematopoietic stem/progenitor cells and alters the pattern of hematopoietic regeneration after myelosuppression. *Blood,* 117**,** 429-39.

UHLMANN, E., PEYMAN, A., RYTE, A., SCHMIDT, A. & BUDDECKE, E. 2000. Use of minimally modified antisense oligonucleotides for specific inhibition of gene expression. *Antisense Technology, Pt A,* 313**,** 268-284.

ULRICH, H., MAGDESIAN, M. H., ALVES, M. J. & COLLI, W. 2002. In vitro selection of RNA aptamers that bind to cell adhesion receptors of Trypanosoma cruzi and inhibit cell invasion. *J Biol Chem,* 277**,** 20756-62.

UTERMOHLEN, O., BASCHUK, N., ABDULLAH, Z., ENGELMANN, A., SIEBOLTS, U., WICKENHAUSER, C., STOCKING, C. & KRONKE, M. 2009. Immunologic hurdles of therapeutic stem cell transplantation. *Biol Chem,* 390**,** 977-83.

UTTING, J. C., ROBINS, S. P., BRANDAO-BURCH, A., ORRISS, I. R., BEHAR, J. & ARNETT, T. R. 2006. Hypoxia inhibits the growth, differentiation and bone-forming capacity of rat osteoblasts. *Exp Cell Res,* 312**,** 1693-702.

VAVALLE, J. P. & COHEN, M. G. 2012. The REG1 anticoagulation system: a novel actively controlled factor IX inhibitor using RNA aptamer technology for treatment of acute coronary syndrome. *Future Cardiol,* 8**,** 371-82.

VEGA, A., MARTIN-FERRERO, M. A., DEL CANTO, F., ALBERCA, M., GARCIA, V., MUNAR, A., OROZCO, L., SOLER, R., FUERTES, J. J., HUGUET, M., SANCHEZ, A. & GARCIA-SANCHO, J. 2015. Treatment of Knee Osteoarthritis With Allogeneic Bone Marrow Mesenchymal Stem Cells: A Randomized Controlled Trial. *Transplantation,* 99**,** 1681-90.

VOGEL, C. & MARCOTTE, E. M. 2012. Insights into the regulation of protein abundance from proteomic and transcriptomic analyses. *Nat Rev Genet,* 13**,** 227-32.

VOGEL, W., GRUNEBACH, F., MESSAM, C. A., KANZ, L., BRUGGER, W. & BUHRING, H. J. 2003. Heterogeneity among human bone marrow-derived mesenchymal stem cells and neural progenitor cells. *Haematologica,* 88**,** 126-133.

WALTER, S., DOERING, A., LETIEMBRE, M., LIU, Y., HAO, W., DIEM, R., BERNREUTHER, C., GLATZEL, M., ENGELHARDT, B. & FASSBENDER, K. 2006. The LPS receptor, CD14, in experimental autoimmune encephalomyelitis and multiple sclerosis. *Cell Physiol Biochem,* 17**,** 167-72.

WAN, Y., LIU, Y., ALLEN, P. B., ASGHAR, W., MAHMOOD, M. A., TAN, J., DUHON, H., KIM, Y. T., ELLINGTON, A. D. & IQBAL, S. M. 2012. Capture, isolation and release of cancer cells with aptamer-functionalized glass bead array. *Lab Chip,* 12**,** 4693-701.

WANG, R. E., ZHANG, Y., CAI, J., CAI, W. & GAO, T. 2011. Aptamer-based fluorescent biosensors. *Curr Med Chem,* 18**,** 4175-84.

WANG, X., XU, S., ZHOU, S., XU, W., LEARY, M., CHOONG, P., QIAN, M., BRANDT, M. & XIE, Y. M. 2016. Topological design and additive manufacturing of porous metals for bone scaffolds and orthopaedic implants: A review. *Biomaterials,* 83**,** 127-41.

WANG, X.-B., YANG, J., HUANG, Y., VYKOUKAL, J., BECKER, F. F. & GASCOYNE, P. R. C. 2000. Cell Separation by Dielectrophoretic Field-flow-fractionation. *Analytical Chemistry,* 72**,** 832-839.

WANG, Y. S. & WHITE, T. D. 1999. The bacterial endotoxin lipopolysaccharide causes rapid inappropriate excitation in rat cortex. *J Neurochem,* 72**,** 652-60.

WARDLAW, D. C., STEVEN R.. VAN MEIRHAEGHE, JAN. BASTIAN, LEONARD. TILLMAN, JOHN B. RANSTAM, JONAS L U. EASTELL, RICHARD. SHABE, PETER. TALMADGE, KAREN. BOONEN, STEVEN. 2009. Efficacy and safety of balloon kyphoplasty compared with non-surgical care for vertebral compression fracture (FREE): a randomised controlled trial. *The Lancet,* 373**,** 1016-1024.

WEBER, P., OHLENDORF, D., WENDOLOSKI, J. & SALEMME, F. 1989. Structural origins of high-affinity biotin binding to streptavidin. *Science,* 243**,** 4.

WEN, A. Q., YANG, Q. W., LI, J. C., LV, F. L., ZHONG, Q. & CHEN, C. Y. 2009. A novel lipopolysaccharide-antagonizing aptamer protects mice against endotoxemia. *Biochem Biophys Res Commun,* 382**,** 140-4.

WERNIG, M., MEISSNER, A., FOREMAN, R., BRAMBRINK, T., KU, M., HOCHEDLINGER, K., BERNSTEIN, B. E. & JAENISCH, R. 2007. In vitro reprogramming of fibroblasts into a pluripotent ES-cell-like state. *Nature,* 448**,** 318-24.

WEXLER, S. A., DONALDSON, C., DENNING-KENDALL, P., RICE, C., BRADLEY, B. & HOWS, J. M. 2003. Adult bone marrow is a rich source of human mesenchymal 'stem' cells but umbilical cord and mobilized adult blood are not. *British Journal of Haematology,* 121**,** 368-374.

WHITE, R. R., SHAN, S., RUSCONI, C. P., SHETTY, G., DEWHIRST, M. W., KONTOS, C. D. & SULLENGER, B. A. 2003. Inhibition of rat corneal angiogenesis by a nuclease-resistant RNA aptamer specific for angiopoietin-2. *Proc Natl Acad Sci U S A,* 100**,** 5028-33.

WILLIAMS, E. L., WHITE, K. & OREFFO, R. O. 2013. Isolation and enrichment of Stro-1 immunoselected mesenchymal stem cells from adult human bone marrow. *Methods Mol Biol,* 1035**,** 67-73.

WILLIS, M. C., COLLINS, B. D., ZHANG, T., GREEN, L. S., SEBESTA, D. P., BELL, C., KELLOGG, E., GILL, S. C., MAGALLANEZ, A., KNAUER, S., BENDELE, R. A., GILL, P. S. & JANJIC, N. 1998. Liposome-anchored vascular endothelial growth factor aptamers. *Bioconjug Chem,* 9**,** 573-82.

WILSON, K. A., KELLIE, J. L. & WETMORE, S. D. 2014. DNA-protein pi-interactions in nature: abundance, structure, composition and strength of contacts between aromatic amino acids and DNA nucleobases or deoxyribose sugar. *Nucleic Acids Res,* 42**,** 6726-41.

WONG, W. L., SU, X., LI, X., CHEUNG, C. M. G., KLEIN, R., CHENG, C.-Y. & WONG, T. Y. 2014. Global prevalence of age-related macular degeneration and disease burden projection for 2020 and 2040: a systematic review and meta-analysis. *The Lancet Global Health,* 2**,** e106-e116.

WOOD, K. W., BUTTERMAN, G., MEHBOD, A., GARVEY, T., JHANJEE, R. & SECHRIEST, V. 2003. Operative Compared with Nonoperative Treatment of a Thoracolumbar Burst Fracture without Neurological Deficit. *JBJS,* 85**,** 773-781.

WORTHLEY, D. L., CHURCHILL, M., COMPTON, J. T., TAILOR, Y., RAO, M., SI, Y., LEVIN, D., SCHWARTZ, M. G., UYGUR, A., HAYAKAWA, Y., GROSS, S., RENZ, B. W., SETLIK, W., MARTINEZ, A. N., CHEN, X., NIZAMI, S., LEE, H. G., KANG, H. P., CALDWELL, J. M., ASFAHA, S., WESTPHALEN, C. B., GRAHAM, T., JIN, G., NAGAR, K., WANG, H., KHEIRBEK, M. A., KOLHE, A., CARPENTER, J., GLAIRE, M., NAIR, A., RENDERS, S., MANIERI, N., MUTHUPALANI, S., FOX, J. G., REICHERT, M., GIRAUD, A. S., SCHWABE, R. F., PRADERE, J. P., WALTON, K., PRAKASH, A., GUMUCIO, D., RUSTGI, A. K., STAPPENBECK, T. S., FRIEDMAN, R. A., GERSHON, M. D., SIMS, P., GRIKSCHEIT, T., LEE, F. Y., KARSENTY, G., MUKHERJEE, S. & WANG, T. C. 2015. Gremlin 1 identifies a skeletal stem cell with bone, cartilage, and reticular stromal potential. *Cell,* 160**,** 269-84.

WU, D. C., BOYD, A. S. & WOOD, K. J. 2008. Embryonic stem cells and their differentiated derivatives have a fragile immune privilege but still represent novel targets of immune attack. *Stem Cells,* 26**,** 1939-50.

WU, W., ZHANG, J., ZHENG, M., ZHONG, Y., YANG, J., ZHAO, Y., WU, W., YE, W., WEN, J., WANG, Q. & LU, J. 2012. An aptamer-based biosensor for colorimetric detection of Escherichia coli O157:H7. *PLoS One,* 7**,** e48999.

XAVIER, J. R., THAKUR, T., DESAI, P., JAISWAL, M. K., SEARS, N., COSGRIFF-HERNANDEZ, E., KAUNAS, R. & GAHARWAR, A. K. 2015. Bioactive nanoengineered hydrogels for bone tissue engineering: a growth-factor-free approach. *ACS Nano,* 9**,** 3109-18.

XAVIER, M., DE ANDRES, M. C., SPENCER, D., OREFFO, R. O. C. & MORGAN, H. 2017a. Size and dielectric properties of skeletal stem cells change critically after enrichment and expansion from human bone marrow: consequences for microfluidic cell sorting. *J R Soc Interface,* 14.

XAVIER, M., OREFFO, R. O. C. & MORGAN, H. 2017b. Skeletal stem cell isolation: A review on the state-of-the-art microfluidic label-free sorting techniques. *Biotechnology Advances,* 34**,** 15.

XU, J., WANG, W., LUDEMAN, M., CHENG, K., HAYAMI, T., LOTZ, J. C. & KAPILA, S. 2008. Chondrogenic differentiation of human mesenchymal stem cells in three-dimensional alginate gels. *Tissue Eng Part A,* 14**,** 667-80.

XU, Y., MIRMALEK-SANI, S. H., LIN, F., ZHANG, J. & OREFFO, R. O. 2007. Adipocyte differentiation induced using nonspecific siRNA controls in cultured human mesenchymal stem cells. *RNA,* 13**,** 1179-83.

YAMADA, M., KANO, K., TSUDA, Y., KOBAYASHI, J., YAMATO, M., SEKI, M. & OKANO, T. 2007. Microfluidic devices for size-dependent separation of liver cells. *Biomed Microdevices,* 9**,** 637-45.

YAMANAKA, S. 2007. Strategies and new developments in the generation of patient-specific pluripotent stem cells. *Cell Stem Cell,* 1**,** 39-49.

YAMANAKA, S. 2009. A fresh look at iPS cells. *Cell,* 137**,** 13-7.

YAN, W. & HUANG, L. 2009. The effects of salt on the physicochemical properties and immunogenicity of protein based vaccine formulated in cationic liposome. *Int J Pharm,* 368**,** 56-62.

YANG, J., HUANG, Y., WANG, X., WANG, X.-B., BECKER, F. F. & GASCOYNE, P. R. C. 1999a. Dielectric Properties of Human Leukocyte Subpopulations Determined by Electrorotation as a Cell Separation Criterion. *Biophysical Journal,* 76**,** 3307-3314.

YANG, J., HUANG, Y., WANG, X.-B., BECKER, F. F. & GASCOYNE, P. R. C. 1999b. Cell Separation on Microfabricated Electrodes Using Dielectrophoretic/Gravitational Field-Flow Fractionation. *Analytical Chemistry,* 71**,** 911-918.

YELURU, A., CUTHBERT, J. A., CASEY, L. & MITCHELL, M. C. 2016. Alcoholic Hepatitis: Risk Factors, Pathogenesis, and Approach to Treatment. *Alcohol Clin Exp Res,* 40**,** 246-55.

YU, X., CHEN, F., WANG, R. & LI, Y. 2018. Whole-bacterium SELEX of DNA aptamers for rapid detection of E.coli O157:H7 using a QCM sensor. *J Biotechnol,* 266**,** 39-49.

ZETHRAEUS, N., BORGSTROM, F., STROM, O., KANIS, J. A. & JONSSON, B. 2007. Cost-effectiveness of the treatment and prevention of osteoporosis--a review of the literature and a reference model. *Osteoporos Int,* 18**,** 9-23.

ZHANG, C., LV, X., HAN, X., MAN, Y., SAEED, Y., QING, H. & DENG, Y. 2015. Whole-cell based aptamer selection for selective capture of microorganisms using microfluidic devices. *Anal. Methods,* 7**,** 6339-6345.

ZHAO, F., HOECHST, B., DUFFY, A., GAMREKELASHVILI, J., FIORAVANTI, S., MANNS, M. P., GRETEN, T. F. & KORANGY, F. 2012. S100A9 a new marker for monocytic human myeloid-derived suppressor cells. *Immunology,* 136**,** 176-83.

ZHAO, Y., ZHAO, T., GUAN, J., ZHANG, X., FU, Y., YE, J., ZHU, J., MENG, G., GE, J., YANG, S., CHENG, L., DU, Y., ZHAO, C., WANG, T., SU, L., YANG, W. & DENG, H. 2015. A XEN-like State Bridges Somatic Cells to Pluripotency during Chemical Reprogramming. *Cell,* 163**,** 1678-91.

ZHENG, H., FU, G., DAI, T. & HUANG, H. 2007. Migration of endothelial progenitor cells mediated by stromal cell-derived factor-1alpha/CXCR4 via PI3K/Akt/eNOS signal transduction pathway. *J Cardiovasc Pharmacol,* 50**,** 274-80.

ZHOU, B. O., YUE, R., MURPHY, M. M., PEYER, J. G. & MORRISON, S. J. 2014. Leptin-receptor-expressing mesenchymal stromal cells represent the main source of bone formed by adult bone marrow. *Cell Stem Cell,* 15**,** 154-68.

ZHOU, J., LI, H., ZHANG, J., PIOTR, S. & ROSSI, J. 2011. Development of cell-type specific anti-HIV gp120 aptamers for siRNA delivery. *J Vis Exp*.

ZHU, J., HUANG, H., DONG, S., GE, L. & ZHANG, Y. 2014. Progress in aptamer-mediated drug delivery vehicles for cancer targeting and its implications in addressing chemotherapeutic challenges. *Theranostics,* 4**,** 931-44.

ZUK, P. A., ZHU, M., ASHJIAN, P., DE UGARTE, D. A., HUANG, J. I., MIZUNO, H., ALFONSO, Z. C., FRASER, J. K., BENHAIM, P. & HEDRICK, M. H. 2002. Human adipose tissue is a source of multipotent stem cells. *Mol Biol Cell,* 13**,** 4279-95.

ZULEWSKI, H., ABRAHAM, E. J., GERLACH, M. J., DANIEL, P. B., MORITZ, W., MULLER, B., VALLEJO, M., THOMAS, M. K. & HABENER, J. F. 2001. Multipotential nestin-positive stem cells isolated from adult pancreatic islets differentiate ex vivo into pancreatic endocrine, exocrine, and hepatic phenotypes. *Diabetes,* 50**,** 521-533.

ZURA, R., MEHTA, S., DELLA ROCCA, G. J. & STEEN, R. G. 2016. Biological Risk Factors for Nonunion of Bone Fracture. *JBJS Rev,* 4.

Appendix 1 Rstudio Code for analysis of Drop-Seq data

Open the analysis software

```
library (Seurat)

## Loading required package: ggplot2

## Loading required package: cowplot

##
## Attaching package: 'cowplot'

## The following object is masked from 'package:ggplot2':
##
##     ggsave

## Loading required package: Matrix

library(dplyr)

##
## Attaching package: 'dplyr'

## The following objects are masked from 'package:stats':
##
##     filter, lag

## The following objects are masked from 'package:base':
##
##     intersect, setdiff, setequal, union
```

Load the data from file location

```
bmmc.data <- read.table("~/F47 BMMC/F47_STRO1CD146.dge.txt.gz", sep='\t', hea
der=T, row.names=1)
```

Looks at data size and savings using sparse

```
dense.size <- object.size(x = as.matrix(x = bmmc.data))
dense.size

## 70130896 bytes

sparse.size <- object.size(x = bmmc.data)
sparse.size

## 70187008 bytes
```

```
dense.size/sparse.size

## 1 bytes
```

Creates a Seurat object for further analysis and manipulation

```
bmmc <- CreateSeuratObject(raw.data = bmmc.data, min.cells = 3, min.genes = 2
00, project = "MACSFACS")
```

Identifies the mitochondrial genes and shows the percentage of the data which is mitochondrial genes

```
mito.genes <- grep(pattern = "^MT-", x = rownames(x = bmmc@data), value = TRU
E)
percent.mito <- Matrix::colSums(bmmc@raw.data[mito.genes, ])/Matrix::colSums(
bmmc@raw.data)
```

Add meta data relating to the mitochondrial genes and plot the number of genes, number of unique molecule identifiers, and the percentage of mitochondrial genes within the data.

```
bmmc <- AddMetaData(object = bmmc, metadata = percent.mito, col.name = "perce
nt.mito")
VlnPlot(object = bmmc, features.plot = c("nGene", "nUMI", "percent.mito"), nC
ol = 3)
```

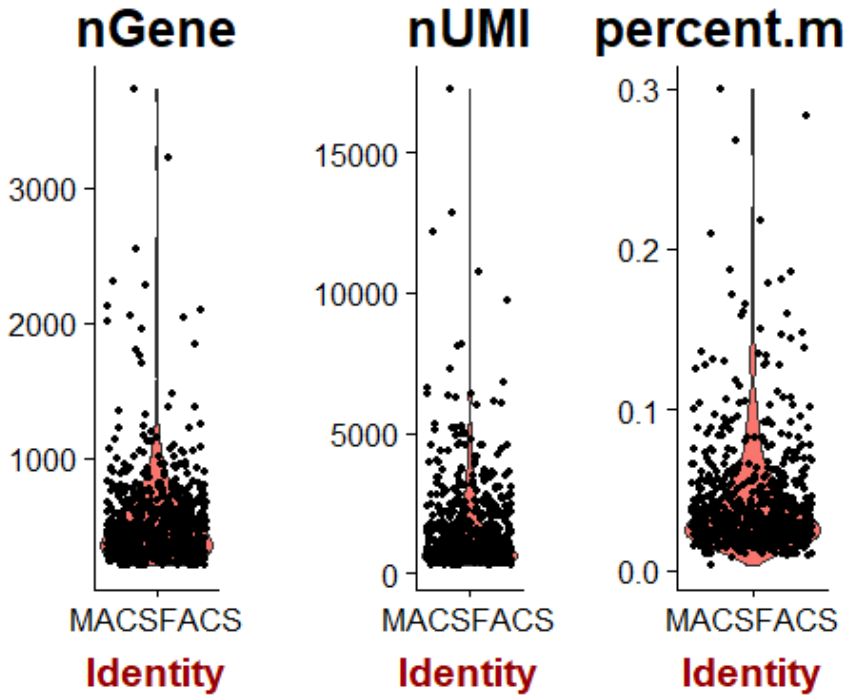

Gene plot to visualize gene-gene relations as well as to determine where threshold cutoffs should be made

```
par(mfrow = c(1, 2))
GenePlot(object = bmmc, gene1 = "nUMI", gene2 = "percent.mito")
GenePlot(object = bmmc, gene1 = "nUMI", gene2 = "nGene")
```

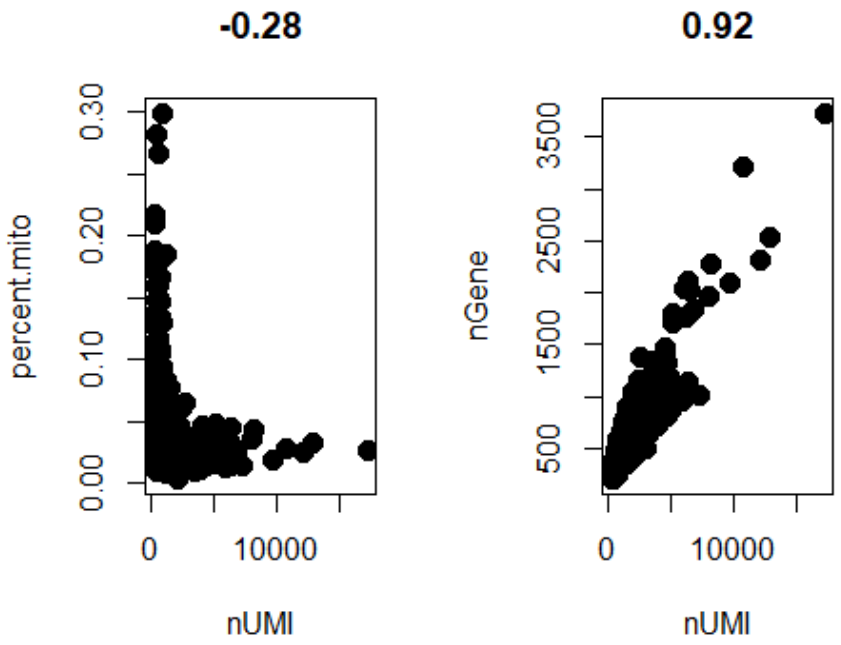

Filter of cells that have unique gene counts over 2500 or less than 200, and mitochondrial percentages above 0.05%

```
bmmc <- FilterCells(object = bmmc, subset.names = c("nGene", "percent.mito"),
 low.thresholds = c(200, -Inf), high.thresholds = c(2500, 0.05))
```

Normalise count data per cell and transform to log scale

```
bmmc <- NormalizeData(object = bmmc, normalization.method = "LogNormalize", s
cale.factor = 10000)
```

Detection of variable genes across single cells identifying those which may be important in PCA

```
bmmc <- FindVariableGenes(object = bmmc, mean.function = ExpMean, dispersion.
function = LogVMR, x.low.cutoff = 0.0125, x.high.cutoff = 3, y.cutoff = 0.5)
```

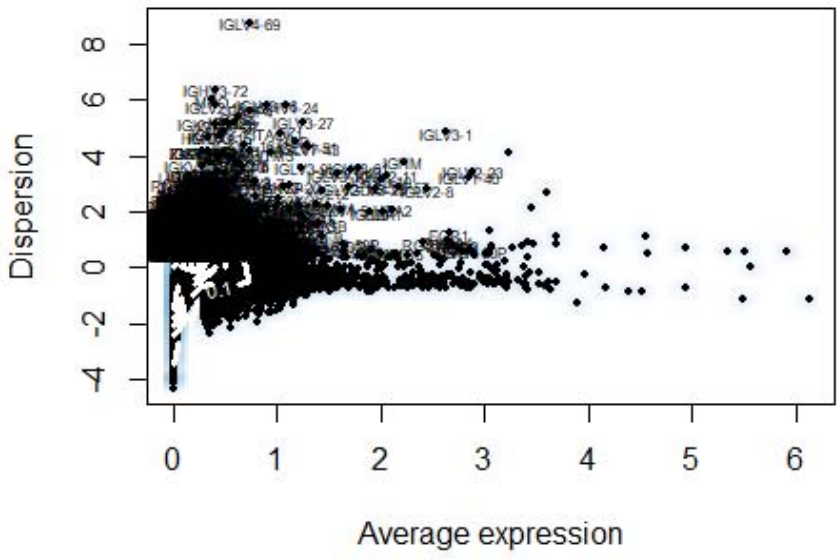


```
length(x = bmmc@var.genes)
```

```
## [1] 3364
```

Scaling the data and removing unwanted sources of variation

```
bmmc <- ScaleData(object = bmmc, vars.to.regress = c("nUMI"))
```

```
## Regressing out: nUMI

##
## Time Elapsed:  4.61014199256897 secs

## Scaling data matrix
```

Perform linear dimensional reduction, generating PCs which can then be assessed for use

```
bmmc <- RunPCA(object = bmmc, pc.genes = bmmc@var.genes, do.print = TRUE, pcs
.print = 1:11, genes.print = 5,pcs.compute = 40)
```

```
## [1] "PC1"
## [1] "CXCL12" "CP"     "CTGF"   "VCAM1"  "IGFBP5"
## [1] ""
## [1] "CITED2"  "RGS1"    "IGLL1"   "ENAM"    "SNORD13"
## [1] ""
## [1] ""
## [1] "PC2"
## [1] "CITED2"  "IGLV3-1" "RASD1"   "IGLL1"   "HSPA1B"
## [1] ""
```

```
## [1] "S100A4" "ACTB"   "SAT1"   "ANXA1"  "CTSS"
## [1] ""
## [1] ""
## [1] "PC3"
## [1] "CTSS"     "RNU1-60P" "CFD"      "CP"       "CD14"
## [1] ""
## [1] "CTSL"     "DNASE1L3" "HMBS"     "FABP4"    "ZMIZ2"
## [1] ""
## [1] ""
## [1] "PC4"
## [1] "VCAM1"   "C1QB"    "ITSN1"   "C1QA"    "SIGLEC1"
## [1] ""
## [1] "FABP4"    "DNASE1L3" "PEAK1"    "ZMIZ2"    "STK24"
## [1] ""
## [1] ""
## [1] "PC5"
## [1] "HBD"  "AHSP" "CA1"  "RHAG" "HBA1"
## [1] ""
## [1] "FABP4"    "DNASE1L3" "CLEC4G"   "IFT43"    "LRP5"
## [1] ""
## [1] ""
## [1] "PC6"
## [1] "LRCH1"    "VTRNA2-1" "OGFOD3"   "PARP11"   "VPS26B"
## [1] ""
## [1] "IFT43"   "SLC35B4" "SOCS3"   "CLEC4G"  "ROBO4"
## [1] ""
## [1] ""
## [1] "PC7"
## [1] "LGI4"          "LTBP2"         "ADAMTS1"       "KCNE4"
## [5] "RP11-109G23.3"
## [1] ""
## [1] "RALGAPA2" "NR2F2"    "FMO3"     "OLFML3"   "TNC"
## [1] ""
## [1] ""
## [1] "PC8"
## [1] "LHFP"    "MAF"     "SPARCL1" "APOE"    "ZNF608"
## [1] ""
## [1] "CTA-445C9.15" "DDR2"         "WBP5"         "NNMT"
## [5] "MAN1B1"
## [1] ""
## [1] ""
## [1] "PC9"
## [1] "MT-TN"   "MDN1"    "HYI-AS1" "SPTAN1"  "NR2C1"
## [1] ""
## [1] "FRMD4A" "ENG"    "LAMA4"  "LIMCH1" "SNHG17"
## [1] ""
## [1] ""
## [1] "PC10"
## [1] "PID1"     "RND3"     "VTRNA1-1" "INTS3"    "LCA5"
## [1] ""
## [1] "FMO2"   "DCN"    "PRSS23" "POGK"   "NNMT"
## [1] ""
## [1] ""
## [1] "PC11"
## [1] "LPL"     "COL16A1" "GSN"     "TCF7L1"  "PTPN13"
```

```
## [1] ""
## [1] "RARRES2" "KCNE4"   "FGF7"    "NOTCH3"  "LUM"
## [1] ""
## [1] ""
```

Visualisation of the PCA results in Gene vs significance (VizPCA), PCA plots which plot PCs against each other, in this case doesn't seem to show much other than the rarer gene expressions (PCAPlot), and heatmaps of each PCA showing genes and expression levels within the PCs (PCHeatmap)

```
PrintPCA(object = bmmc, pcs.print = 1:12, genes.print = 10, use.full = FALSE)
```

```
## [1] "PC1"
##  [1] "CXCL12"  "CP"      "CTGF"    "VCAM1"   "IGFBP5"  "ADAMTS1" "IGFBP7"
##  [8] "EBF3"    "LEPR"    "IGF2"
## [1] ""
##  [1] "CITED2"   "RGS1"     "IGLL1"    "ENAM"     "SNORD13"  "IGLJ3"
##  [7] "IGLV2-23" "IGHJ4"    "IGLV6-57" "CTSS"
## [1] ""
## [1] ""
## [1] "PC2"
##  [1] "CITED2"      "IGLV3-1"     "RASD1"       "IGLL1"       "HSPA1B"
##  [6] "RGS1"        "SNORD13"     "IGHJ4"       "KB-1980E6.3" "ENAM"
## [1] ""
##  [1] "S100A4" "ACTB"   "SAT1"   "ANXA1"  "CTSS"   "CXCL2"  "CD36"
##  [8] "CYBB"   "DEK"    "ZFAND5"
## [1] ""
## [1] ""
## [1] "PC3"
##  [1] "CTSS"     "RNU1-60P" "CFD"      "CP"       "CD14"     "IGFBP5"
##  [7] "EBF3"     "ACTB"     "MT1E"     "S100A12"
## [1] ""
##  [1] "CTSL"     "DNASE1L3" "HMBS"     "FABP4"    "ZMIZ2"    "LGMN"
##  [7] "STK24"    "HBA1"     "CCDC14"   "AHSP"
## [1] ""
## [1] ""
## [1] "PC4"
##  [1] "VCAM1"   "C1QB"    "ITSN1"   "C1QA"    "SIGLEC1" "SLC40A1" "IL1RAP"
##  [8] "LPCAT2"  "DIP2B"   "TWSG1"
## [1] ""
##  [1] "FABP4"    "DNASE1L3" "PEAK1"    "ZMIZ2"    "STK24"    "MGST2"
##  [7] "CLN5"     "PES1"     "PARP11"   "METTL13"
## [1] ""
## [1] ""
## [1] "PC5"
##  [1] "HBD"   "AHSP"  "CA1"   "RHAG"  "HBA1"  "PRDX2" "STMN1" "HBA2"
##  [9] "GYPB"  "PTTG1"
## [1] ""
##  [1] "FABP4"    "DNASE1L3" "CLEC4G"   "IFT43"    "LRP5"     "ROBO4"
##  [7] "CTSL"     "STK24"    "GNAQ"     "CYB5D1"
## [1] ""
## [1] ""
## [1] "PC6"
```

```
##  [1] "LRCH1"    "VTRNA2-1" "OGFOD3"   "PARP11"   "VPS26B"   "GTF2IRD2"
##  [7] "MAEA"     "CHMP1A"   "RC3H2"    "PSMB10"
## [1] ""
##  [1] "IFT43"    "SLC35B4"  "SOCS3"    "CLEC4G"   "ROBO4"    "LRP5"
##  [7] "RBM28"    "C10orf10" "MT-TN"    "GCFC2"
## [1] ""
## [1] ""
## [1] "PC7"
##  [1] "LGI4"          "LTBP2"         "ADAMTS1"       "KCNE4"
##  [5] "RP11-109G23.3" "FGF7"          "LPP"           "IRF9"
##  [9] "AC009506.1"    "YES1"
## [1] ""
##  [1] "RALGAPA2"   "NR2F2"      "FMO3"       "OLFML3"     "TNC"
##  [6] "CLDND2"     "CRH"        "AC025171.1" "SLC35B4"    "KIAA0930"
## [1] ""
## [1] ""
## [1] "PC8"
##  [1] "LHFP"    "MAF"     "SPARCL1" "APOE"    "ZNF608"  "ABCA6"   "UACA"
##  [8] "TF"      "ABCA8"   "CLDN23"
## [1] ""
##  [1] "CTA-445C9.15"  "DDR2"          "WBP5"          "NNMT"
##  [5] "MAN1B1"        "PLAC9"         "ID4"           "CH25H"
##  [9] "IGFBP5"        "RP11-109G23.3"
## [1] ""
## [1] ""
## [1] "PC9"
##  [1] "MT-TN"         "MDN1"          "HYI-AS1"       "SPTAN1"
##  [5] "NR2C1"         "CTD-2541M15.4" "SPATA6"        "GCFC2"
##  [9] "KDR"           "LPCAT1"
## [1] ""
##  [1] "FRMD4A" "ENG"    "LAMA4"  "LIMCH1" "SNHG17" "SUCLA2" "ATR"
##  [8] "ZNF143" "SLC9A8" "B3GNT5"
## [1] ""
## [1] ""
## [1] "PC10"
##  [1] "PID1"     "RND3"     "VTRNA1-1" "INTS3"    "LCA5"     "BOC"
##  [7] "PSEN1"    "SASH1"    "DALRD3"   "PDK4"
## [1] ""
##  [1] "FMO2"    "DCN"     "PRSS23"  "POGK"    "NNMT"    "DDR2"    "FAM127A"
##  [8] "ADAMTS1" "IGFBP7"  "FRMD4A"
## [1] ""
## [1] ""
## [1] "PC11"
##  [1] "LPL"      "COL16A1"  "GSN"      "TCF7L1"   "PTPN13"   "TNFRSF19"
##  [7] "MDFI"     "APP"      "MAP4K3"   "FAM134B"
## [1] ""
##  [1] "RARRES2"  "KCNE4"    "FGF7"     "NOTCH3"   "LUM"      "CYR61"
##  [7] "VTRNA2-1" "WDR86"    "LGI4"     "MT1M"
## [1] ""
## [1] ""
## [1] "PC12"
##  [1] "PLXND1"    "HPSE"      "RNF141"    "RHBDD2"    "LPAR2"
##  [6] "SLC16A7"   "C20orf194" "TPRA1"     "NMT2"      "IL18"
## [1] ""
##  [1] "CCL2"          "RP11-22P6.2"   "POLR2J3"       "RND3"
```

```
##  [5] "LCA5"          "ANO8"          "LTBP4"         "EXOC7"
##  [9] "OAF"           "RP11-206L10.2"
## [1] ""
## [1] ""
```

```
VizPCA(object = bmmc, pcs.use = 1:4)
```

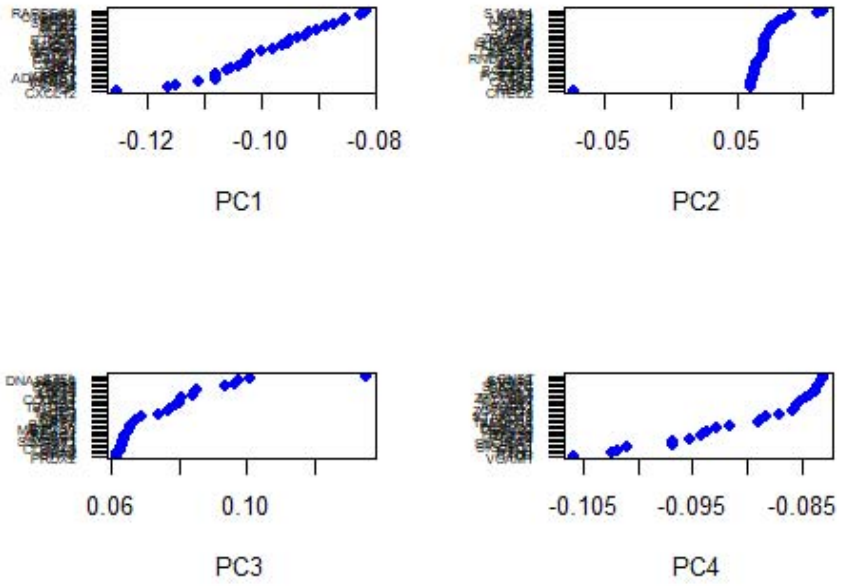


```
VizPCA(object = bmmc, pcs.use = 5:8)
```

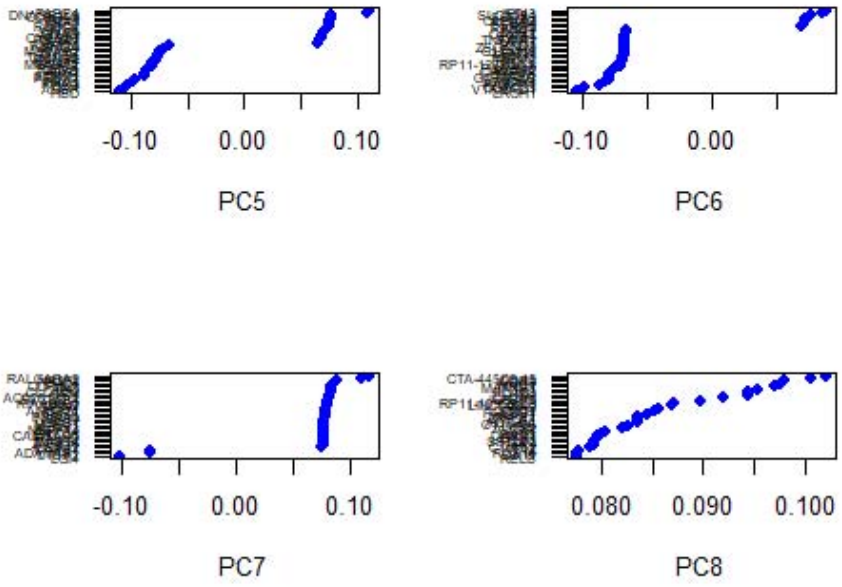


```
VizPCA(object = bmmc, pcs.use = 9:12)
```

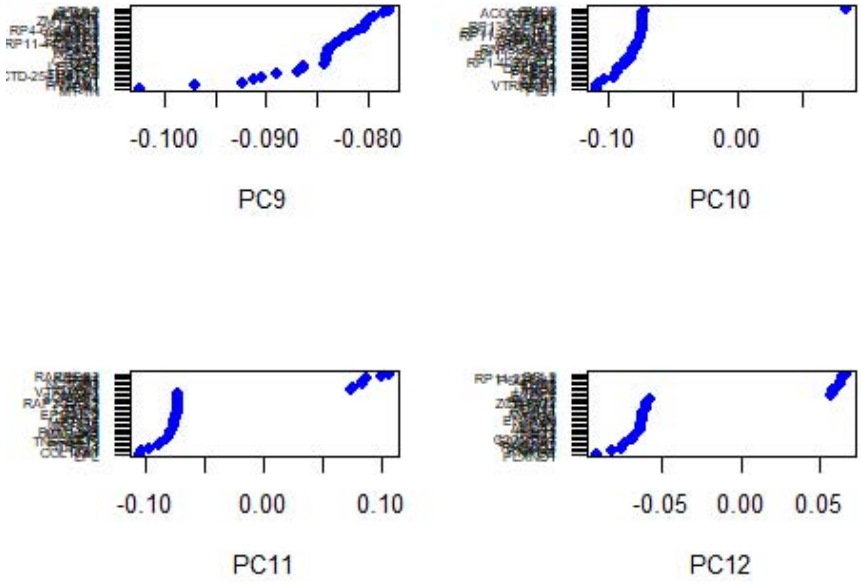


```
VizPCA(object = bmmc, pcs.use = 13:16)
```

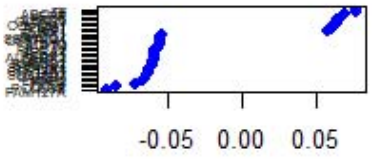

PC13

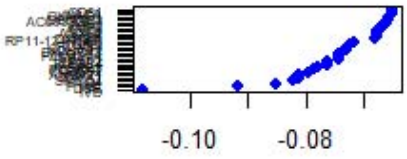

PC14

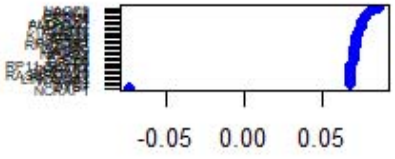

PC15

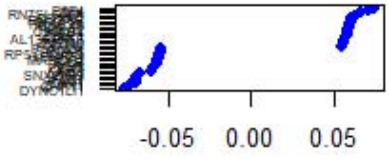

PC16

```
VizPCA(object = bmmc, pcs.use = 17:20)
```

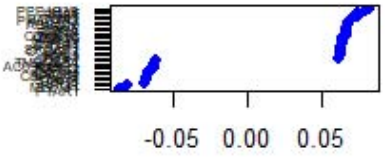

PC17

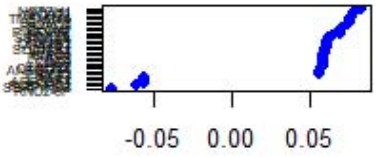

PC18

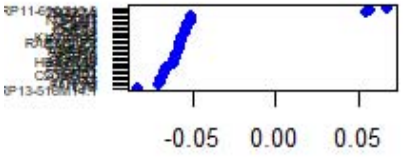

PC19

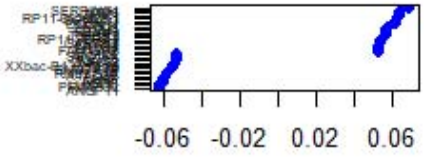

PC20

```
PCAPlot(object = bmmc, dim.1 = 1, dim.2 = 2)
```

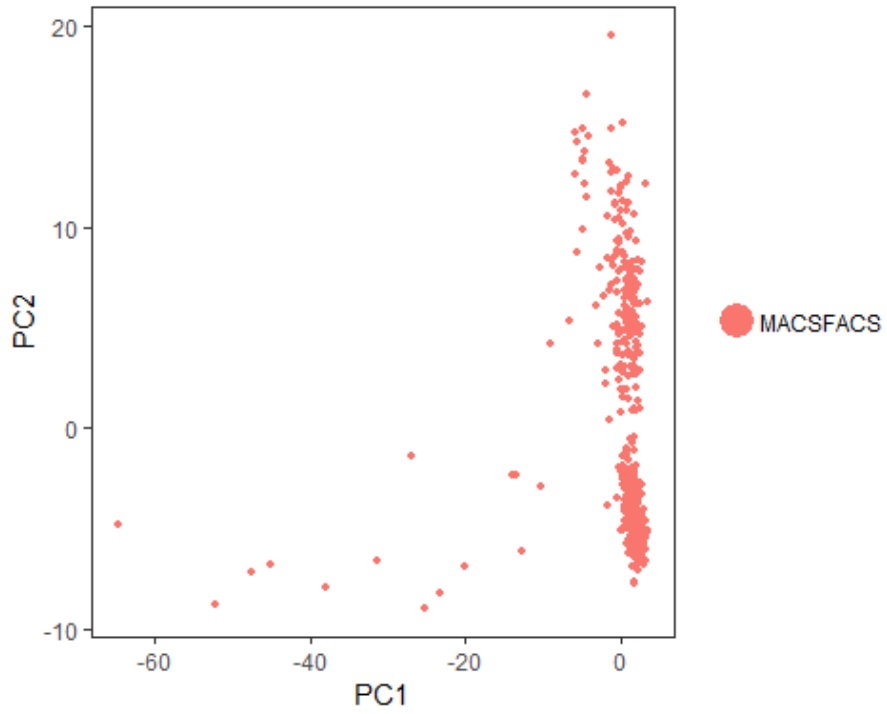


```
PCAPlot(object = bmmc, dim.1 = 1, dim.2 = 3)
```

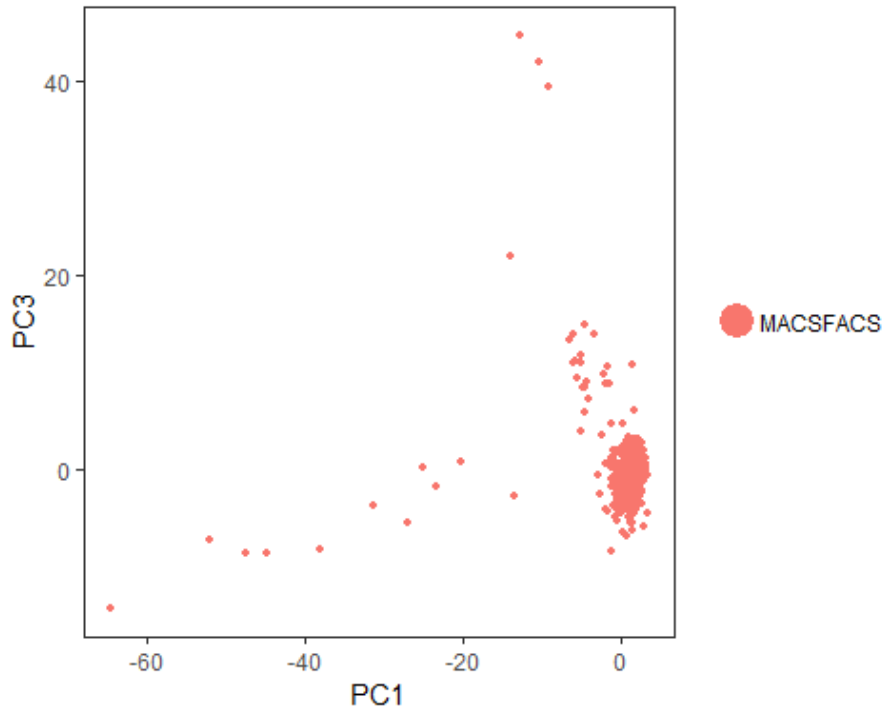


```
PCAPlot(object = bmmc, dim.1 = 1, dim.2 = 4)
```

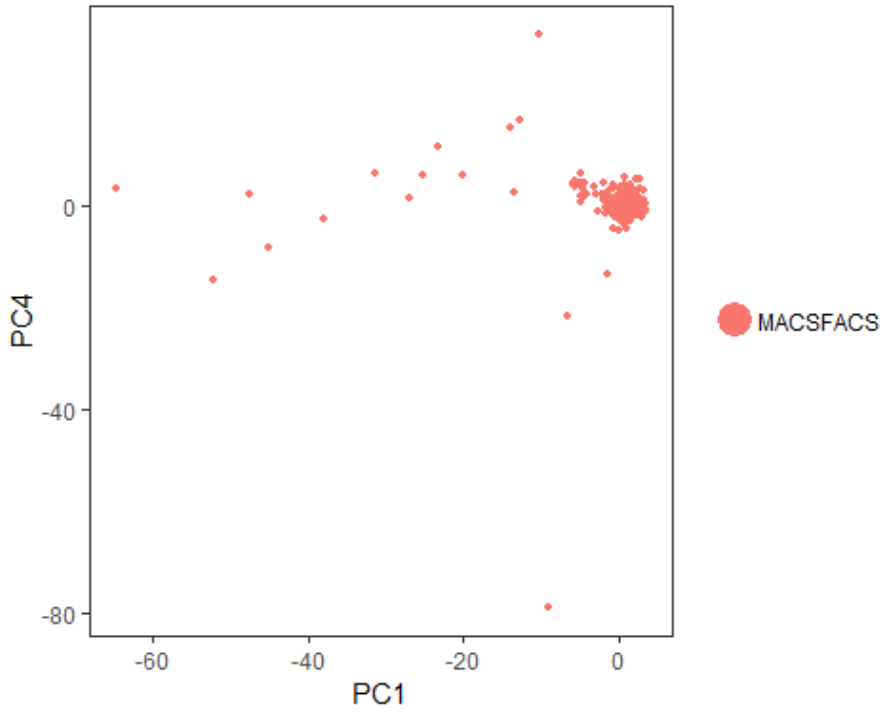


```
bmmc <- ProjectPCA(object = bmmc, do.print = FALSE)
PCHeatmap(object = bmmc, pc.use = 1:2, cells.use = 500, do.balanced = TRUE,
    label.columns = FALSE, use.full = T)
```

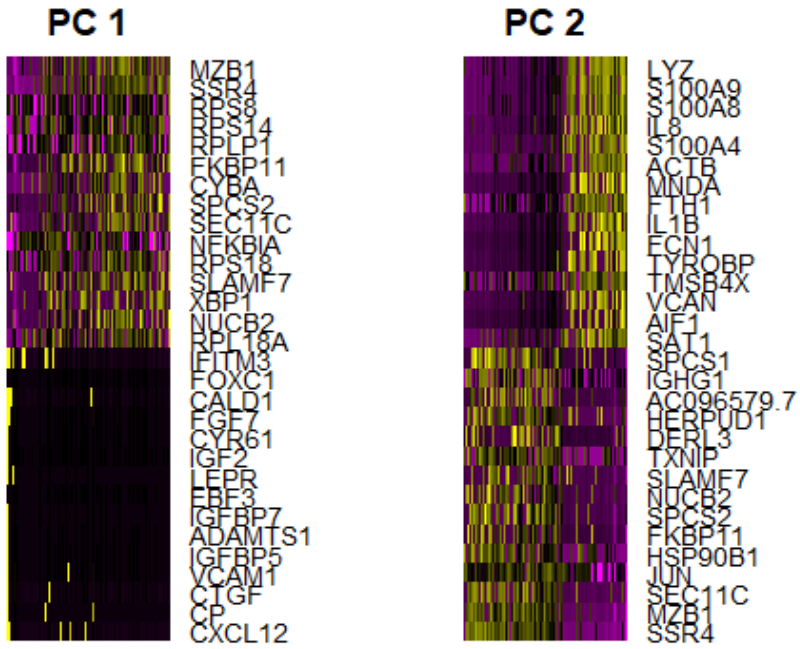


```
PCHeatmap(object = bmmc, pc.use = 3:4, cells.use = 500, do.balanced = TRUE,
    label.columns = FALSE, use.full = T)
```

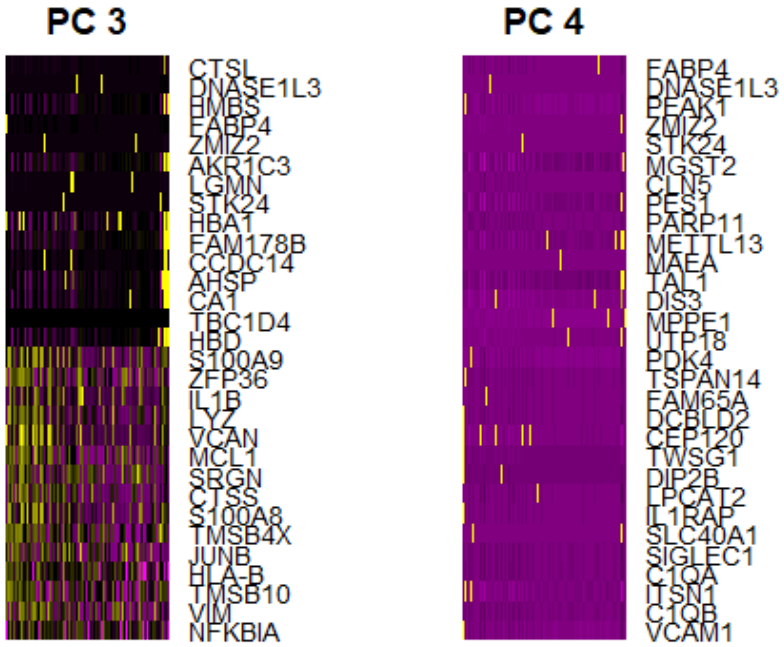


```
PCHeatmap(object = bmmc, pc.use = 5:6, cells.use = 500, do.balanced = TRUE,
    label.columns = FALSE, use.full = T)
```

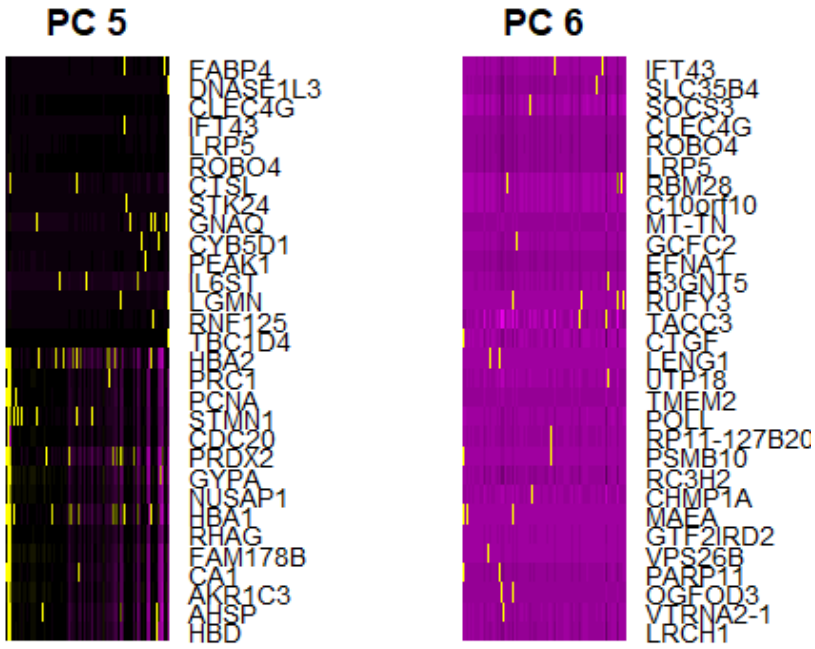

```
PCHeatmap(object = bmmc, pc.use = 7:8, cells.use = 500, do.balanced = TRUE,
    label.columns = FALSE, use.full = T)
```

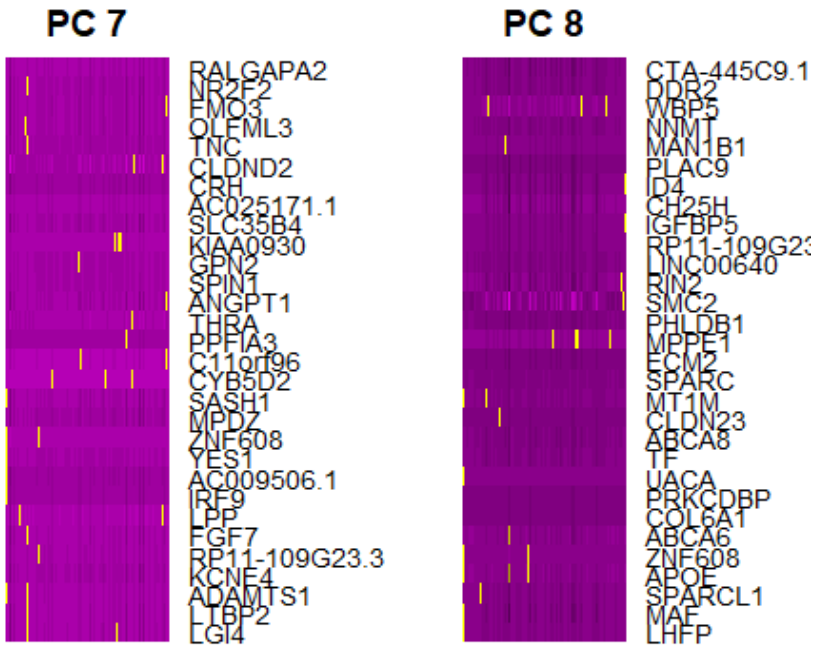


```
PCHeatmap(object = bmmc, pc.use = 9:10, cells.use = 500, do.balanced = TRUE,
    label.columns = FALSE, use.full = T)
```

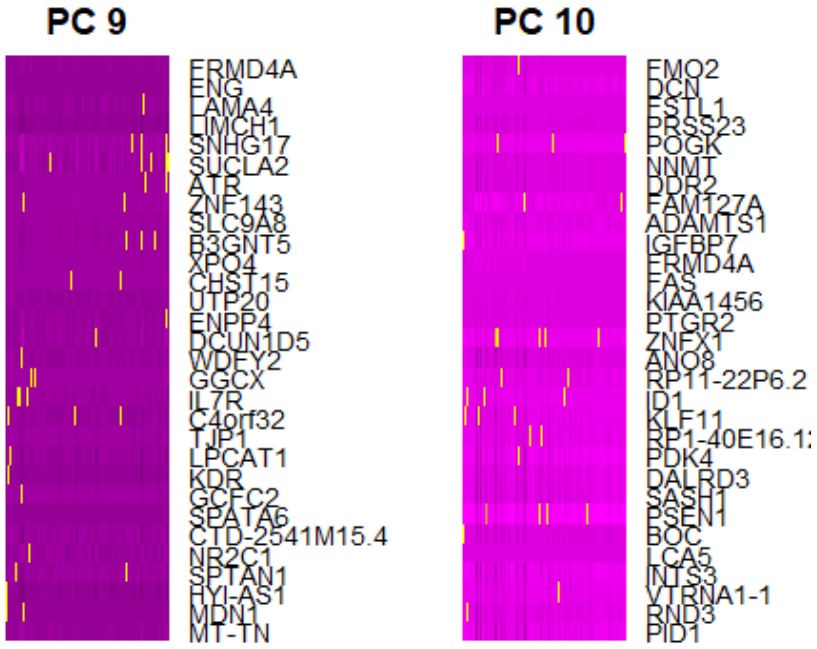

```
PCHeatmap(object = bmmc, pc.use = 11:12, cells.use = 500, do.balanced = TRUE,
    label.columns = FALSE, use.full = T)
```

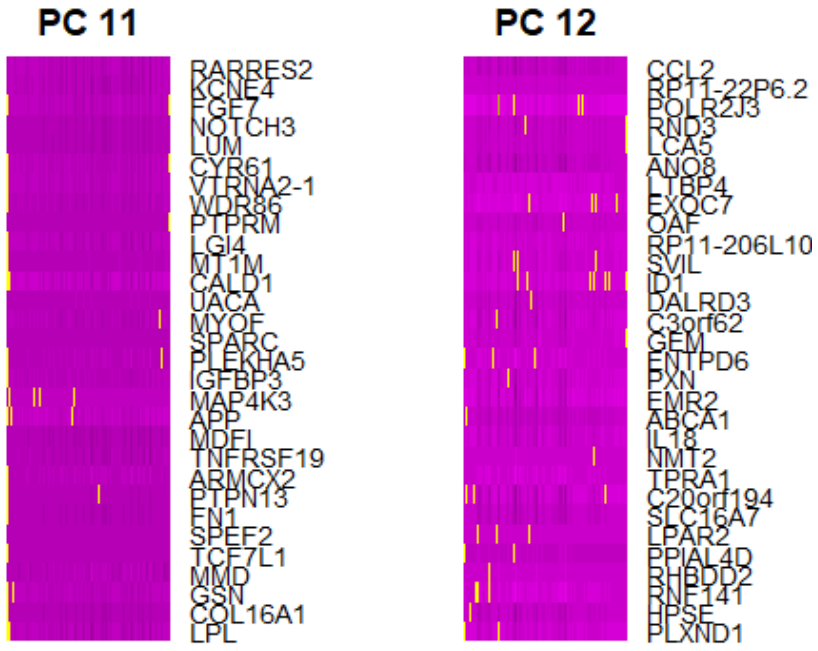


```
PCHeatmap(object = bmmc, pc.use = 13:14, cells.use = 500, do.balanced = TRUE,
    label.columns = FALSE, use.full = T)
```

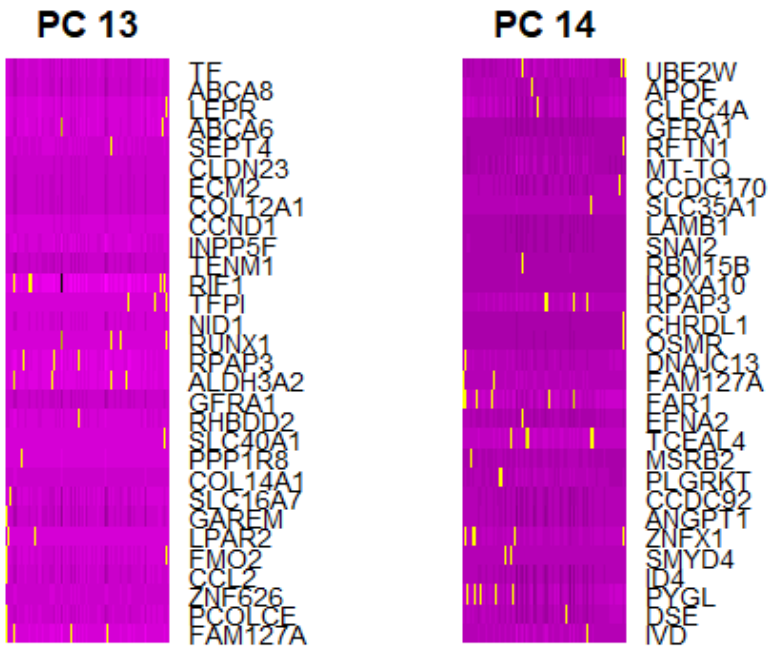


```
PCHeatmap(object = bmmc, pc.use = 15:16, cells.use = 500, do.balanced = TRUE,
    label.columns = FALSE, use.full = T)
```

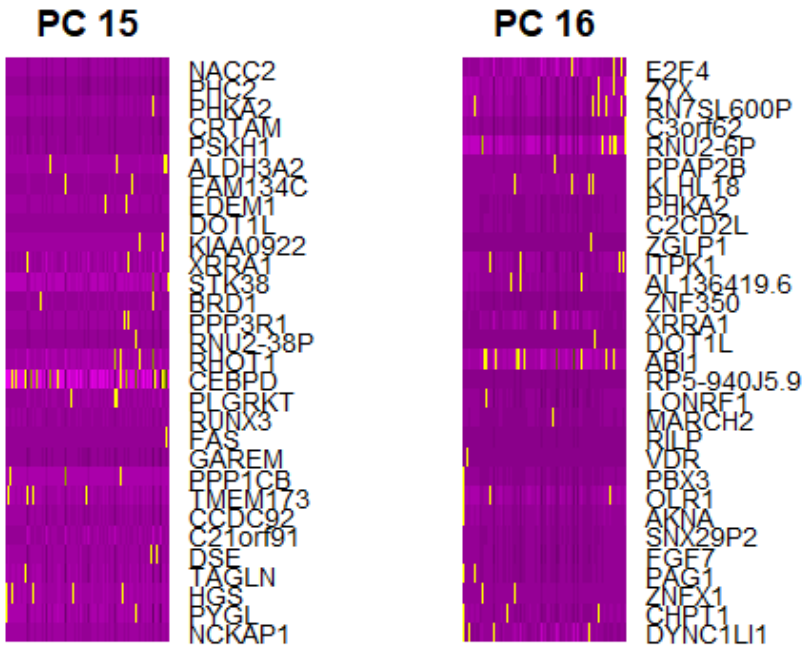

```
PCHeatmap(object = bmmc, pc.use = 17:18, cells.use = 500, do.balanced = TRUE,
    label.columns = FALSE, use.full = T)
```

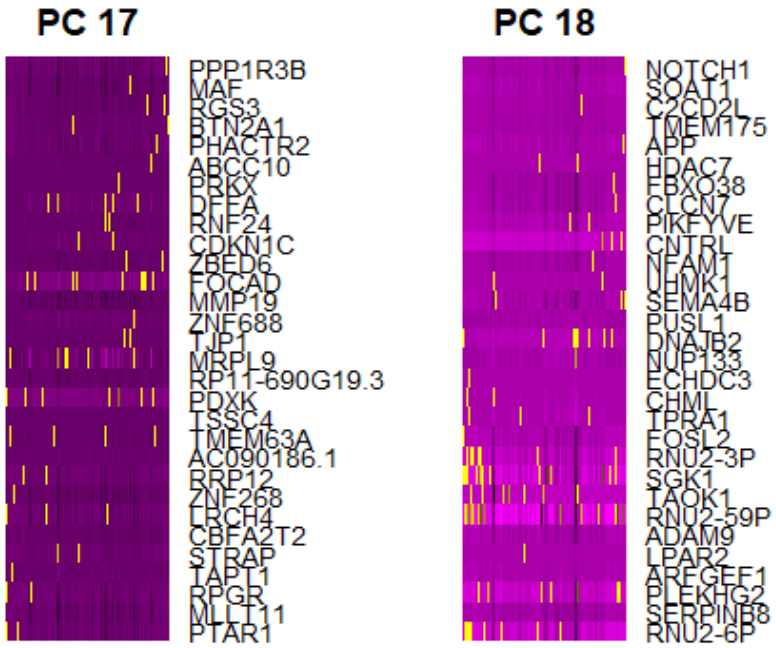


```
PCHeatmap(object = bmmc, pc.use = 19:20, cells.use = 500, do.balanced = TRUE,
    label.columns = FALSE, use.full = T)
```

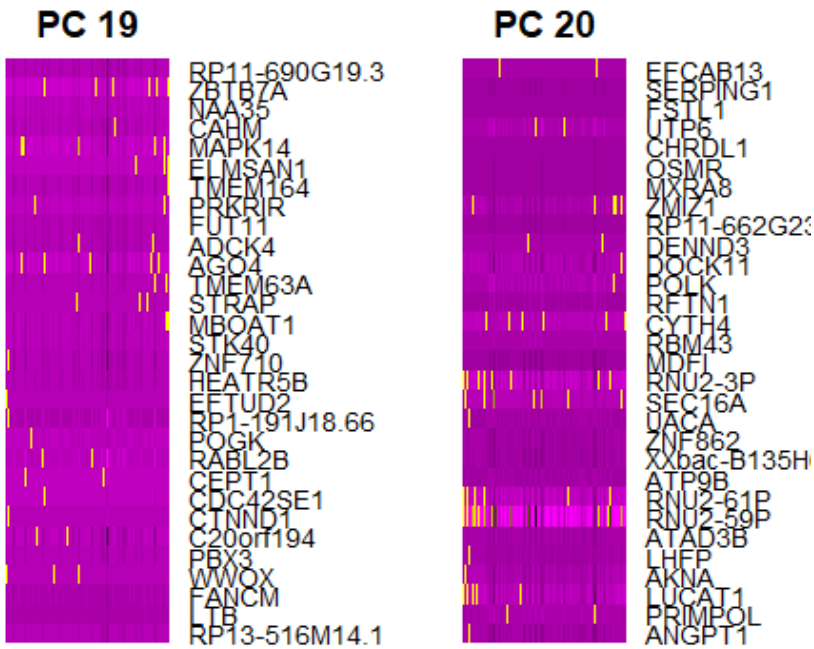

First 3

PCs which show variation

```
PCHeatmap(object = bmmc, pc.use = 1:3, cells.use = 500, do.balanced = TRUE,
    label.columns = FALSE, use.full = T)
```

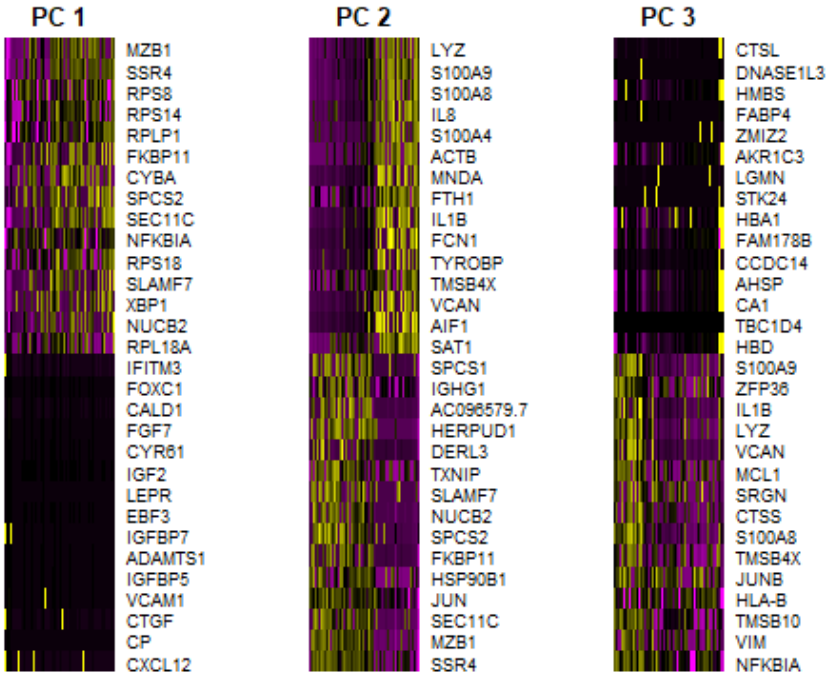

##

Jackstraw takes a long time to compute, shows the significance of each of the PCs,

though in this data is not as clear as the heatmaps #*{r} #bmmc <- JackStraw(object = bmmc, num.replicate = 100, display.progress = FALSE) #JackStrawPlot(object = bmmc, PCs = 1:20) #* ## Elbow plot of the PCs, the major bend in the data lines signifies where the PCs should stop being used.

```
PCElbowPlot(object = bmmc,num.pc = 40)
```

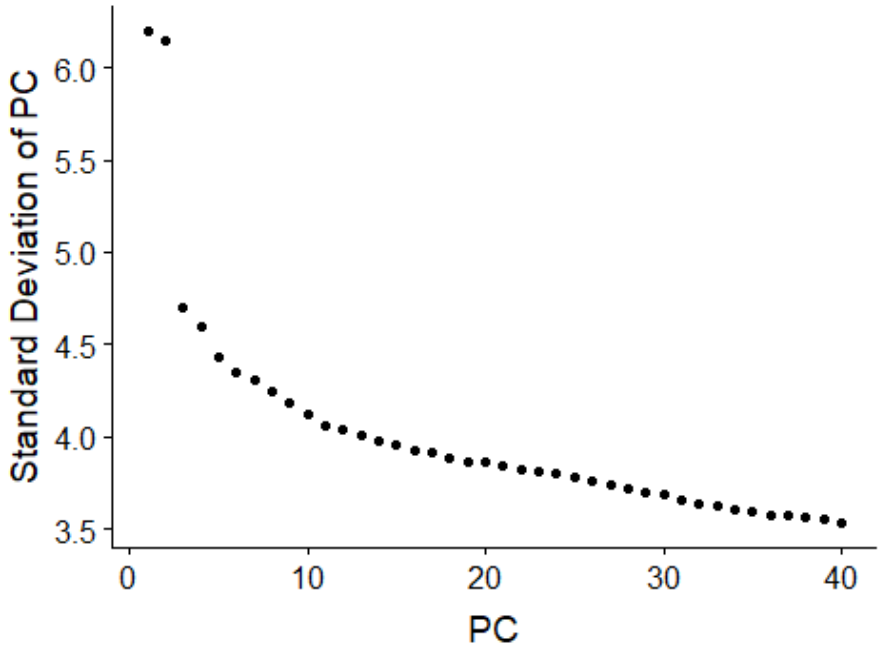

Two sets of data that look like either could be correct according to the PC data, from the elbow plot up to PC 11 could be used, though looking at the jackstraw only up to PC6 has standard deviation below 0.05, observing the heatmaps only the first 3 PCs have any clear expression differences using a resolution of 1.7 and only PCs 1 - 3

```
bmmc <- FindClusters(object = bmmc, reduction.type = "pca", dims.use = 1:3,
    resolution = 1.7, print.output = 0, save.SNN = TRUE)
PrintFindClustersParams(object = bmmc)

## Parameters used in latest FindClusters calculation run on: 2018-08-23 14:4
0:49
## ============================================================================
===
## Resolution: 1.7
## ----------------------------------------------------------------------------
---
## Modularity Function    Algorithm         n.start         n.iter
##      1                   1                 100             10
## ----------------------------------------------------------------------------
---
## Reduction used          k.param          prune.SNN
```

```
##      pca                   30                0.0667
## ----------------------------------------------------------------------
---
## Dims used in calculation
## ======================================================================
===
## 1 2 3

bmmc <- RunTSNE(object = bmmc, dims.use = 1:3, do.fast = TRUE, perplexity = 6
0)
TSNEPlot(object = bmmc, do.label = T, pt.size = 2, label.size = 4, plot.title
 = "1:3")
```

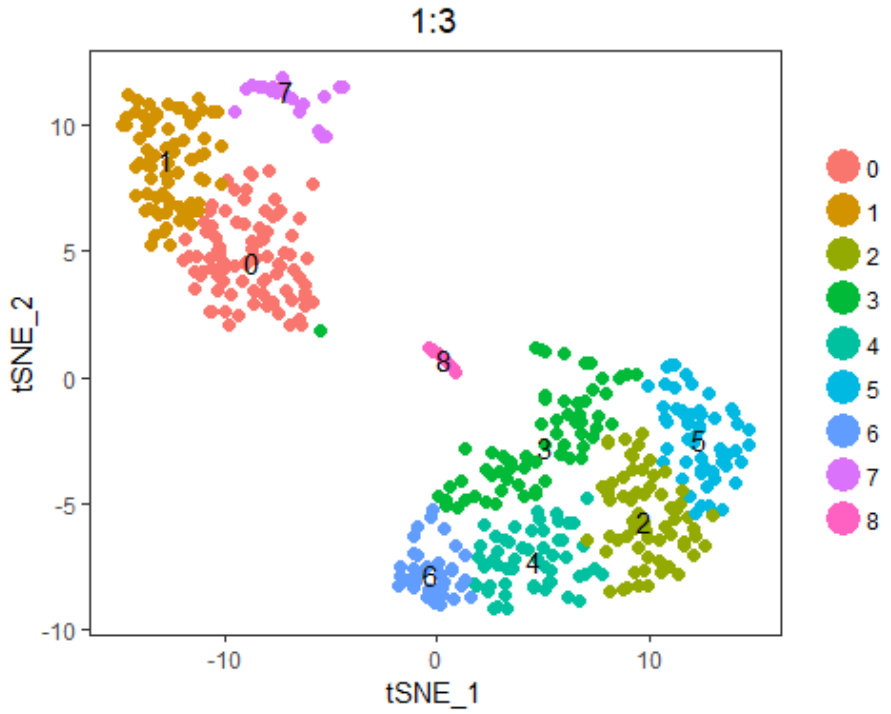

Find markers for every cluster compared to all other cells

```
bmmc.markers <- FindAllMarkers(object = bmmc, only.pos = TRUE, min.pct = 0.25
, return.thresh = 0.001, test.use = "bimod")
bmmc.markers %>% group_by(cluster) %>% top_n(2, avg_logFC)

## # A tibble: 18 x 7
## # Groups:   cluster [9]
##       p_val avg_logFC pct.1 pct.2 p_val_adj cluster gene
##       <dbl>     <dbl> <dbl> <dbl>     <dbl> <fct>   <chr>
##  1 3.46e-39     1.54  0.888 0.303  4.05e-35 0       LYZ
##  2 4.21e-17     1.54  0.573 0.123  4.92e-13 0       AIF1
##  3 2.61e-29     1.60  0.904 0.267  3.05e-25 1       S100A9
##  4 5.30e-16     1.68  0.438 0.049  6.19e-12 1       CSF3R
##  5 1.04e- 5     1.52  0.537 0.338  1.22e- 1 2       IGLL5
##  6 7.47e- 5     1.06  0.761 0.557  8.73e- 1 2       IGHG4
##  7 1.36e-10     0.784 0.742 0.345  1.58e- 6 3       AC096579.7
##  8 7.13e- 8     0.895 0.879 0.667  8.33e- 4 3       IGKC
##  9 6.48e- 7     1.79  0.545 0.194  7.57e- 3 4       IGLV3-1
```

```
## 10 1.10e- 5     1.52  0.6   0.336  1.29e- 1 4       IGLL5
## 11 3.56e- 8     0.903 0.291 0.208  4.16e- 4 5       CD27
## 12 7.04e- 5     1.05  0.6   0.622  8.23e- 1 5       IGHD
## 13 3.77e- 7     1.72  0.778 0.482  4.41e- 3 6       IGLC2
## 14 6.02e- 6     1.83  0.611 0.321  7.03e- 2 6       IGHA2
## 15 3.37e-66     4.72  0.769 0.42   3.94e-62 7       HBB
## 16 1.36e-32     4.16  0.769 0.1    1.59e-28 7       HBA1
## 17 4.97e-18     4.43  0.818 0.043  5.81e-14 8       CXCL12
## 18 3.88e-13     3.52  0.727 0.041  4.53e- 9 8       IFITM3
```

Visualisation of the top 2 genes from each cluster, overlaying the genes on the TSNE plot, and a violin plots

```
VlnPlot(object = bmmc, features.plot = c("LYZ", "AIF1"))
```

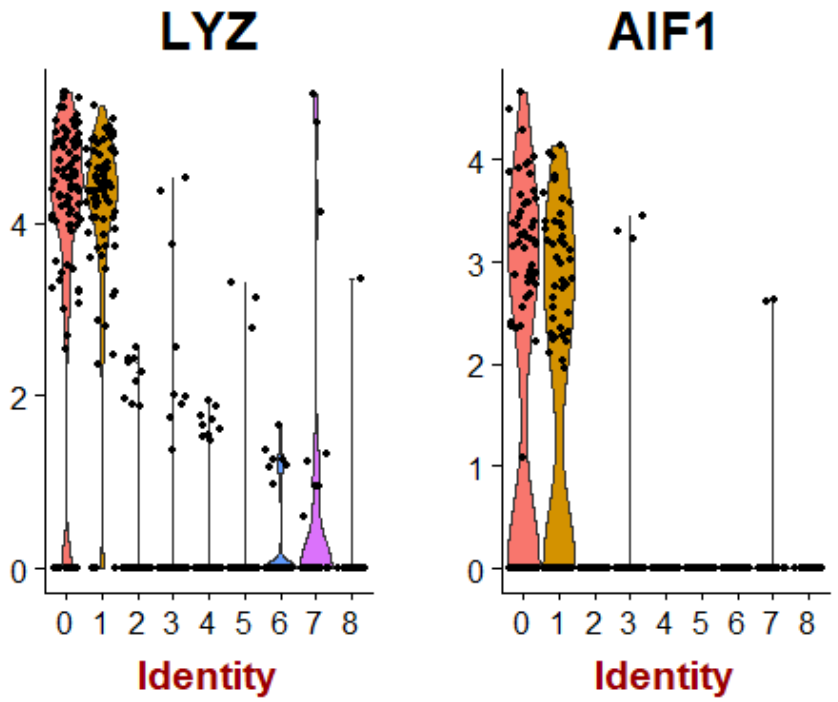


```
FeaturePlot(object = bmmc, features.plot = c("LYZ", "AIF1"), cols.use = c("gr
ey", "blue"),
    reduction.use = "tsne")
```

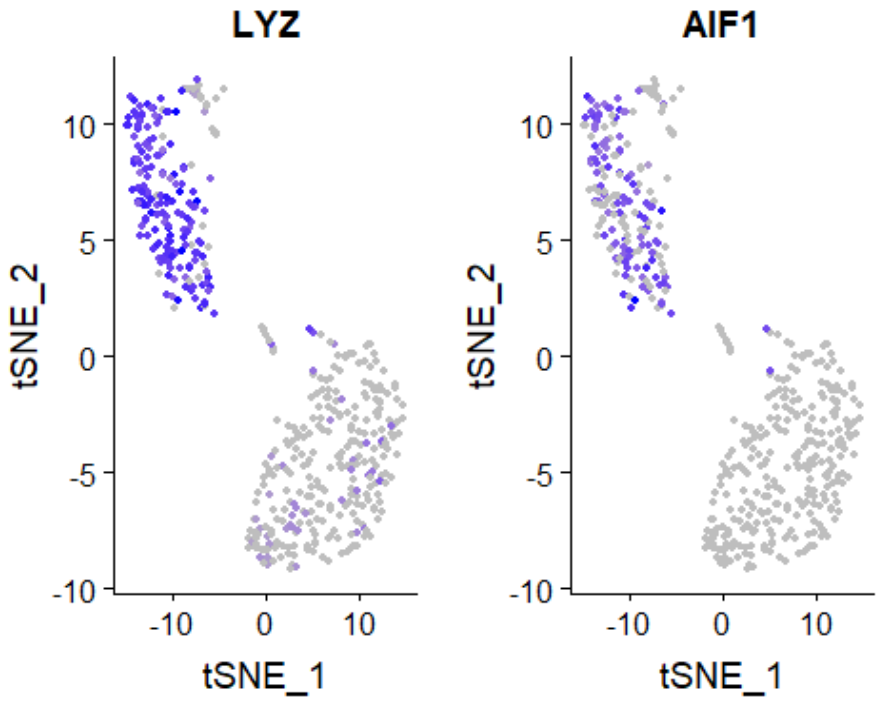


```
VlnPlot(object = bmmc, features.plot = c("S100A9", "CSF3R"))
```

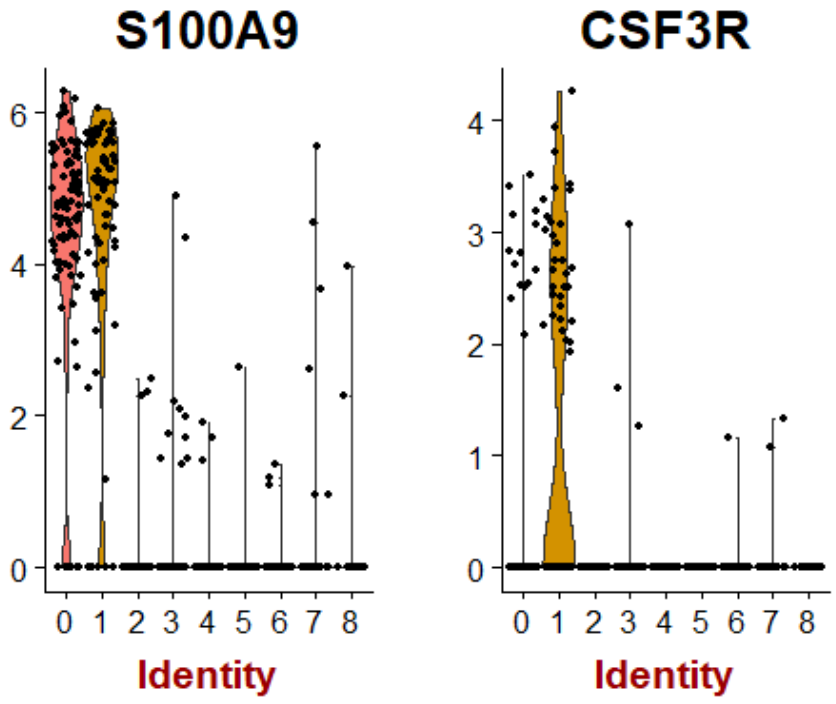


```
FeaturePlot(object = bmmc, features.plot = c("S100A9", "CSF3R"), cols.use = c
("grey", "blue"),
    reduction.use = "tsne")
```

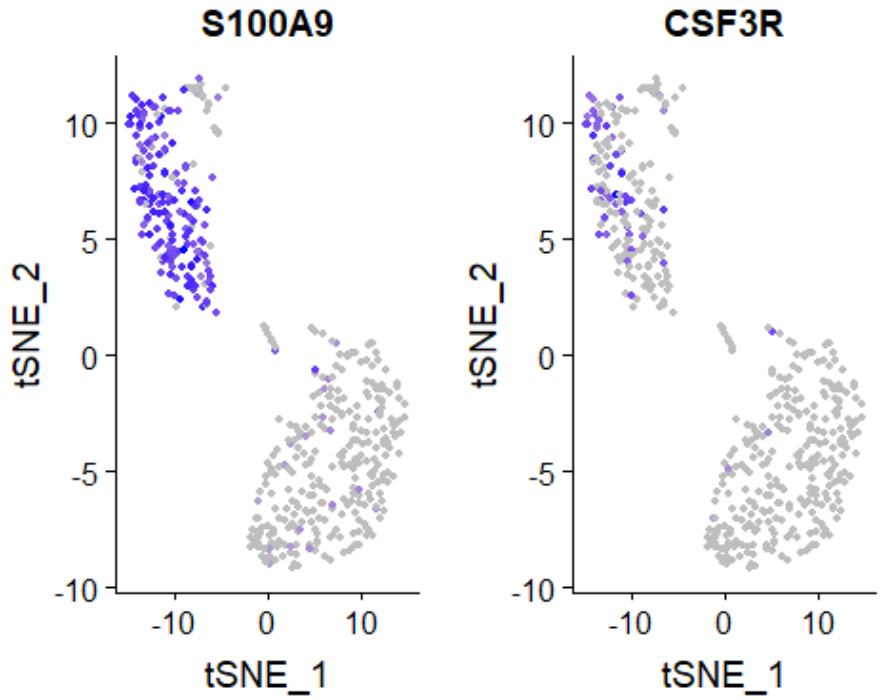


```
VlnPlot(object = bmmc, features.plot = c("IGLL5", "IGHG4"))
```

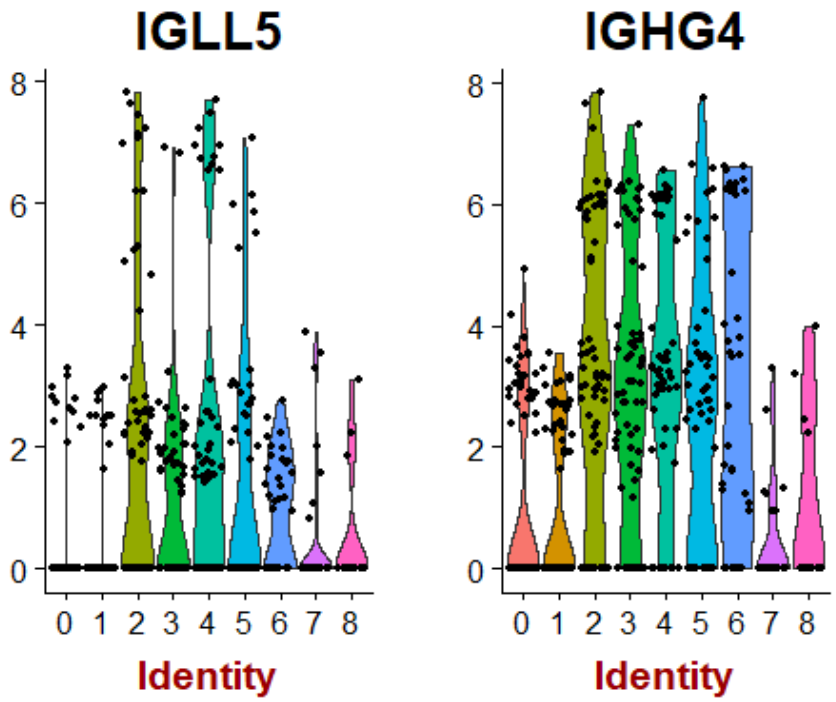

```
FeaturePlot(object = bmmc, features.plot = c("IGLL5", "IGHG4"), cols.use = c(
"grey", "blue"),
    reduction.use = "tsne")
```

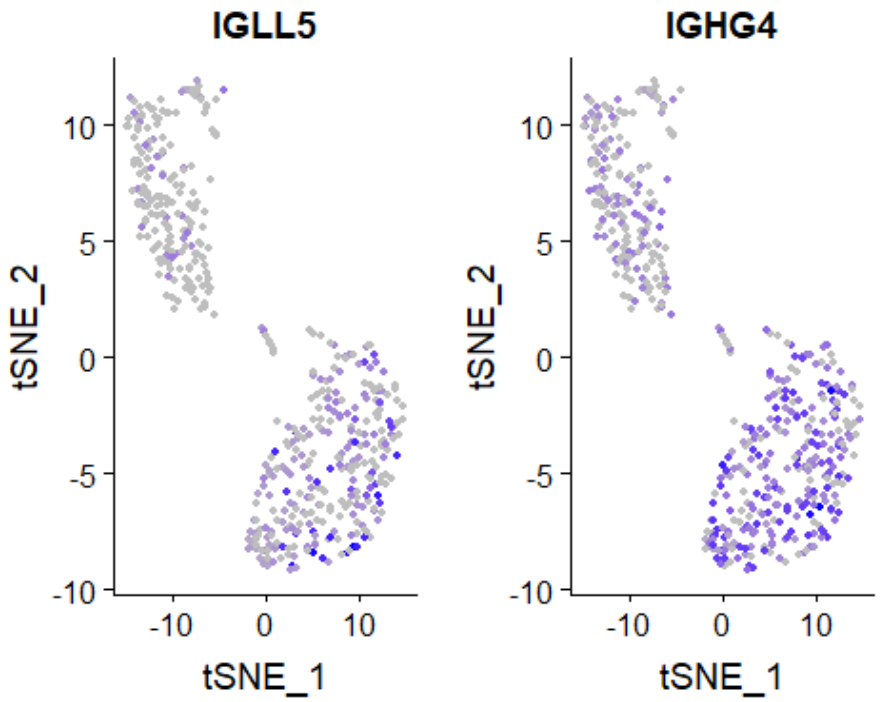


```
VlnPlot(object = bmmc, features.plot = c("AC096579.7", "IGKC"))
```

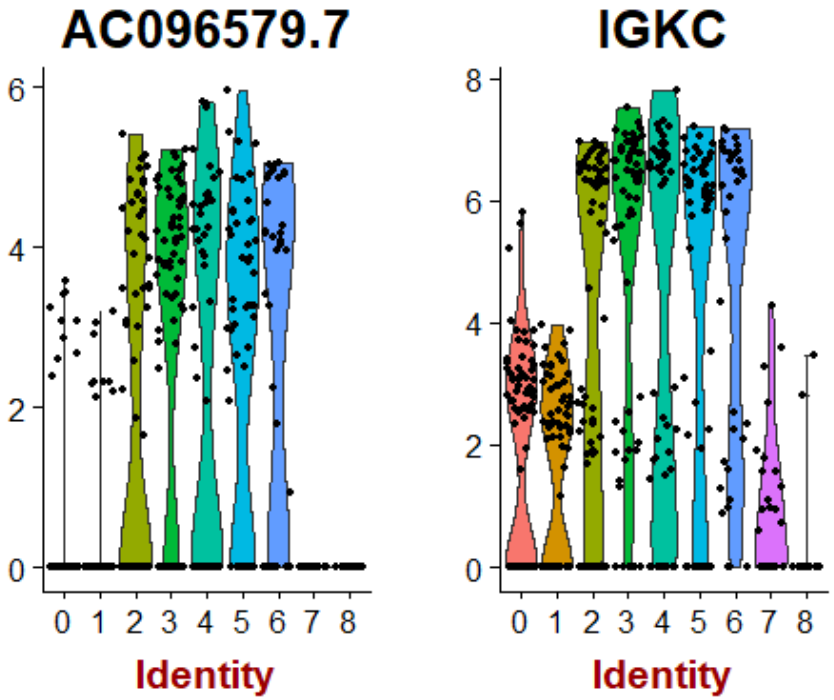

```
FeaturePlot(object = bmmc, features.plot = c("AC096579.7", "IGKC"), cols.use
= c("grey", "blue"),
    reduction.use = "tsne")
```

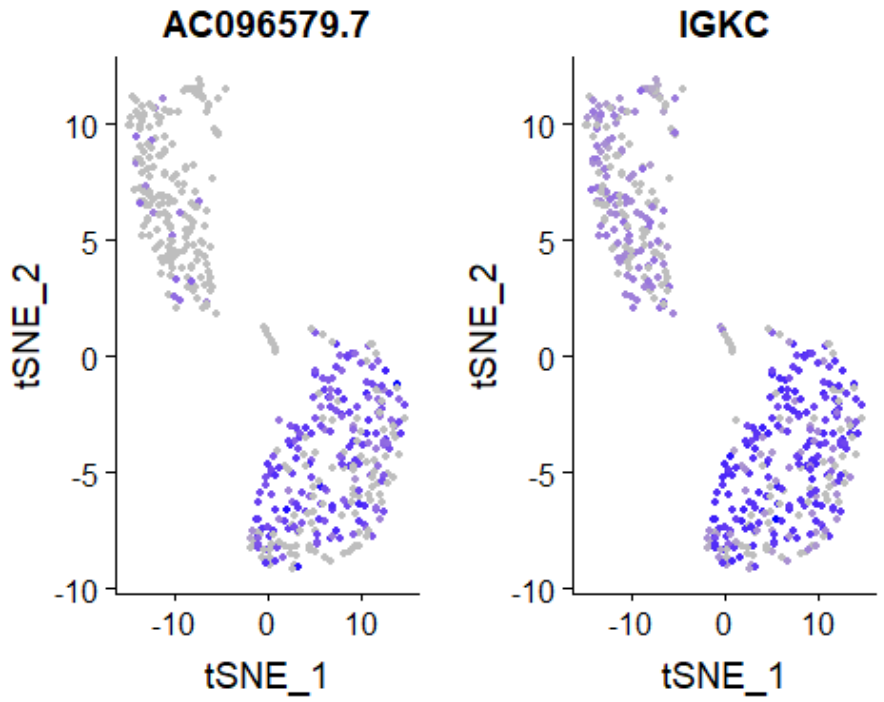


```
VlnPlot(object = bmmc, features.plot = c("IGLV3-1", "IGLL5"))
```

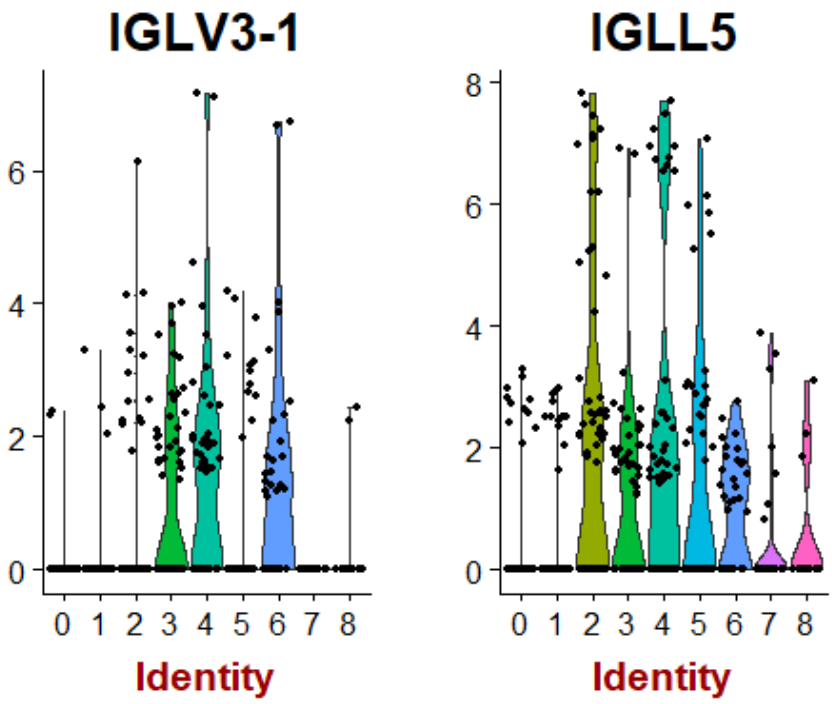


```
FeaturePlot(object = bmmc, features.plot = c("IGLV3-1", "IGLL5"), cols.use =
c("grey", "blue"),
    reduction.use = "tsne")
```

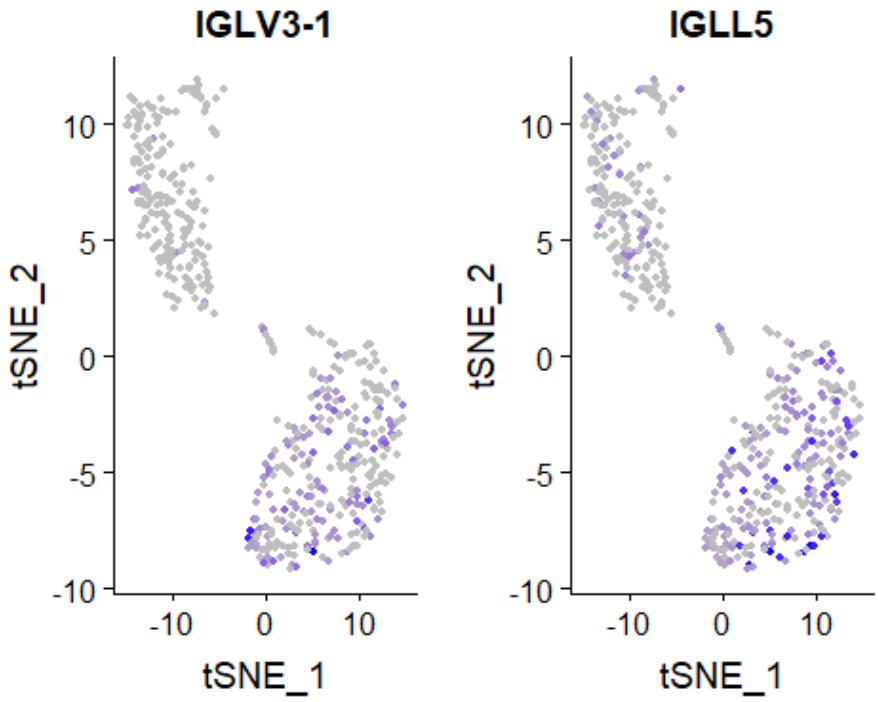


```
VlnPlot(object = bmmc, features.plot = c("CD27", "IGHD"))
```

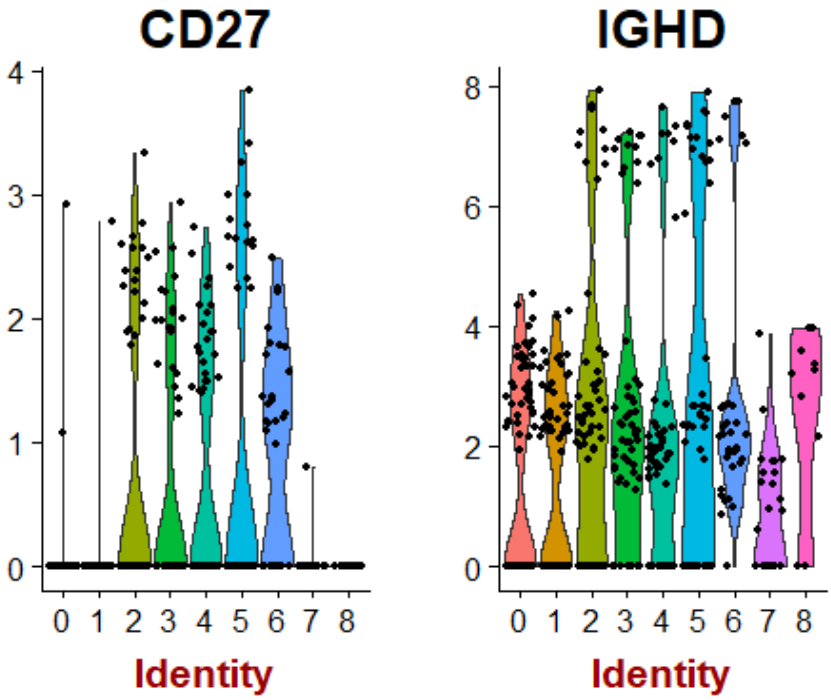


```
FeaturePlot(object = bmmc, features.plot = c("CD27", "IGHD"), cols.use = c("g
rey", "blue"),
    reduction.use = "tsne")
```

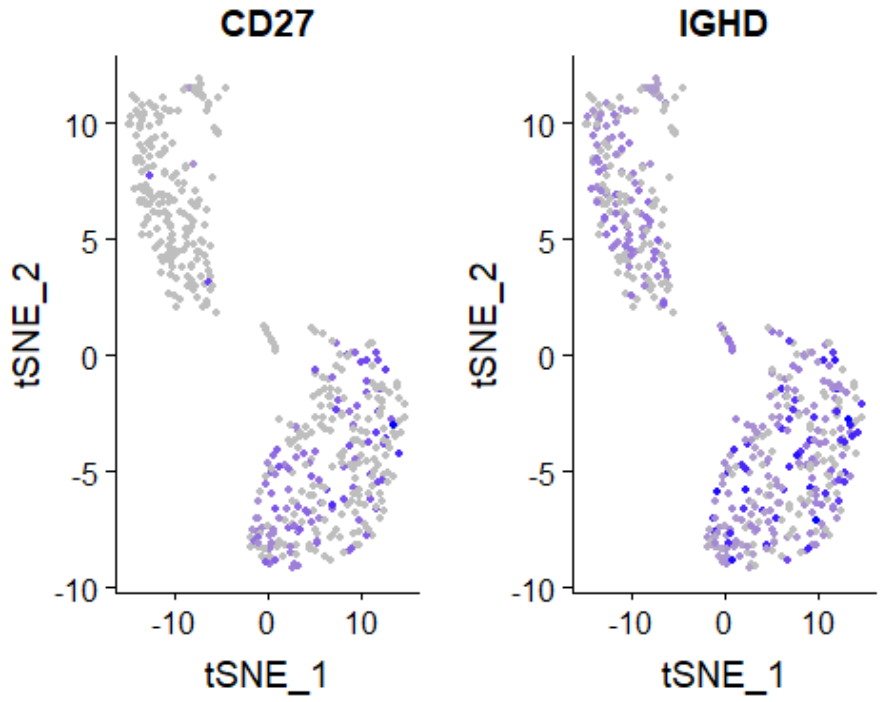

```
VlnPlot(object = bmmc, features.plot = c("IGLC2", "IGHA2"))
```

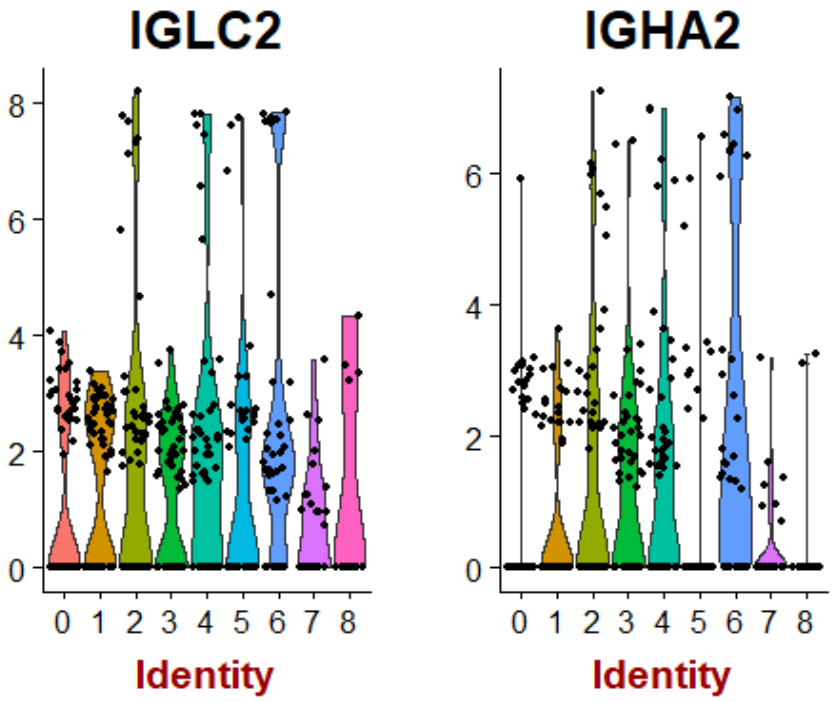


```
FeaturePlot(object = bmmc, features.plot = c("IGLC2", "IGHA2"), cols.use = c(
"grey", "blue"),
    reduction.use = "tsne")
```

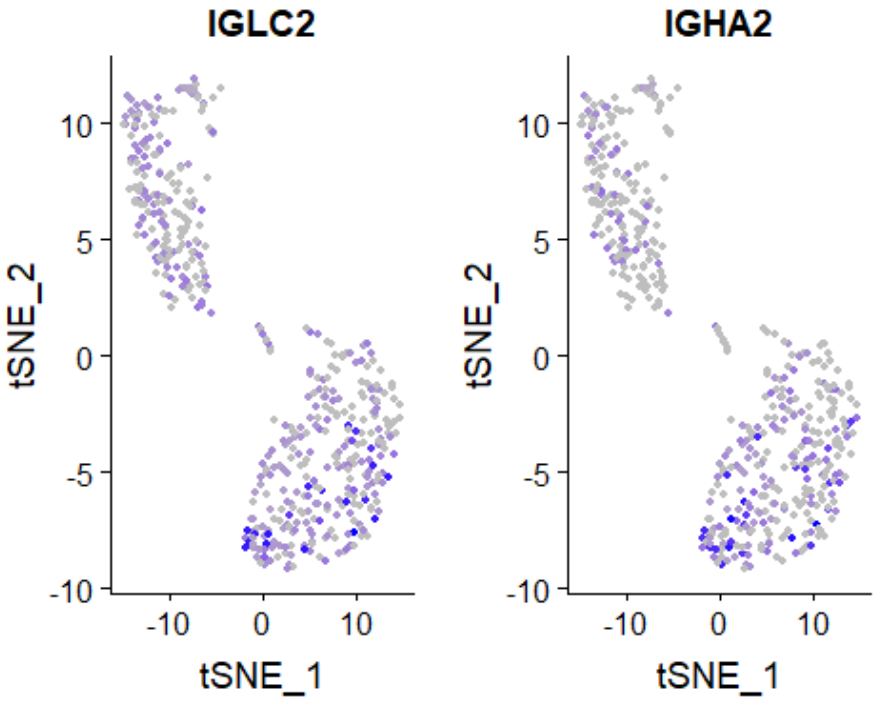

```
VlnPlot(object = bmmc, features.plot = c("HBB", "HBA1"))
```

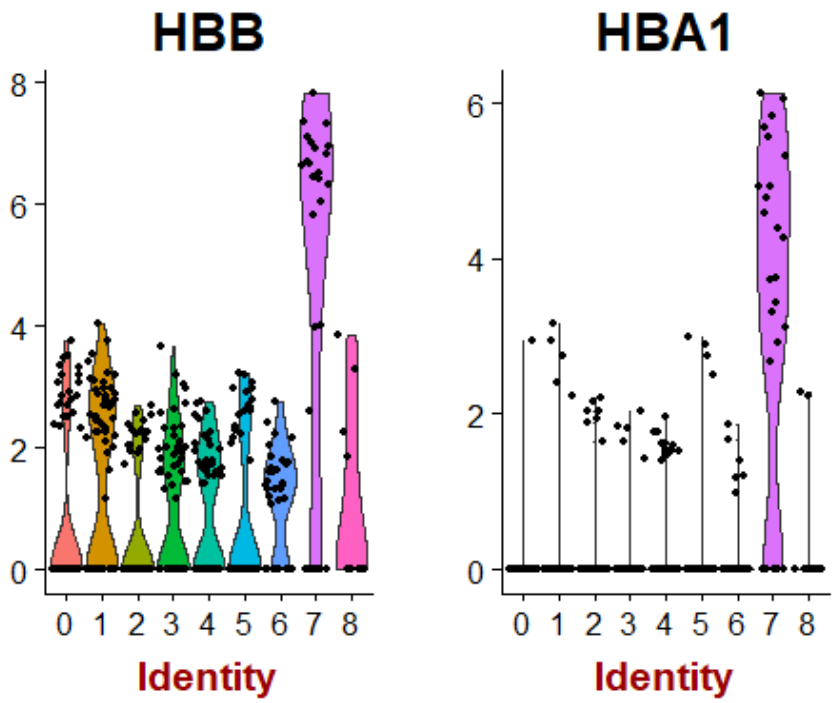


```
FeaturePlot(object = bmmc, features.plot = c("HBB", "HBA1"), cols.use = c("gr
ey", "blue"),
    reduction.use = "tsne")
```

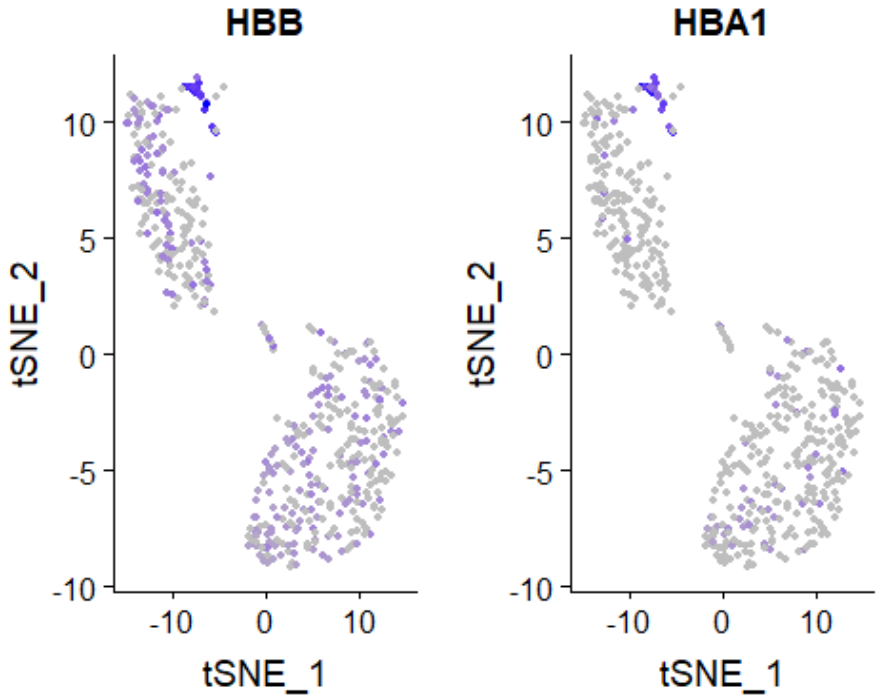


```
VlnPlot(object = bmmc, features.plot = c("CXCL12", "IFITM3"))
```

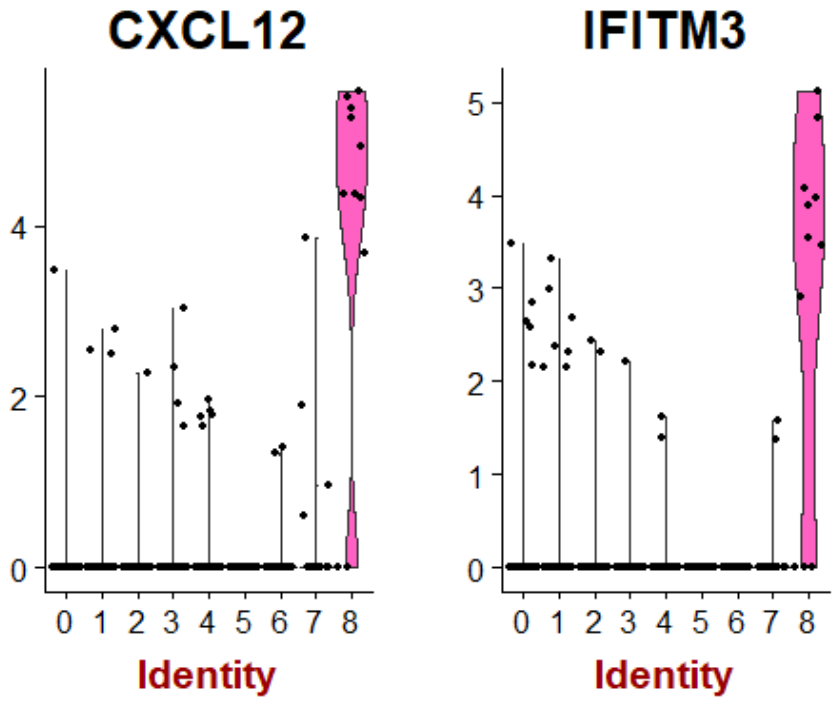


```
FeaturePlot(object = bmmc, features.plot = c("CXCL12", "IFITM3"), cols.use =
c("grey", "blue"),
    reduction.use = "tsne")
```

Appendix I

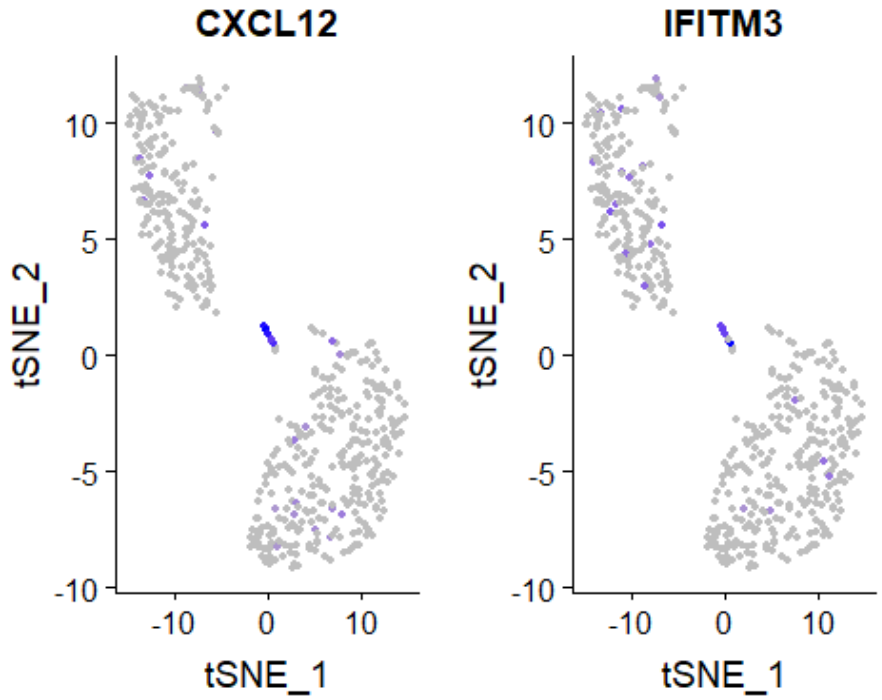

Checking of the expression on the markers used to isolate this population

```
VlnPlot(object = bmmc, features.plot = c("HSPA8", "MCAM"))
```

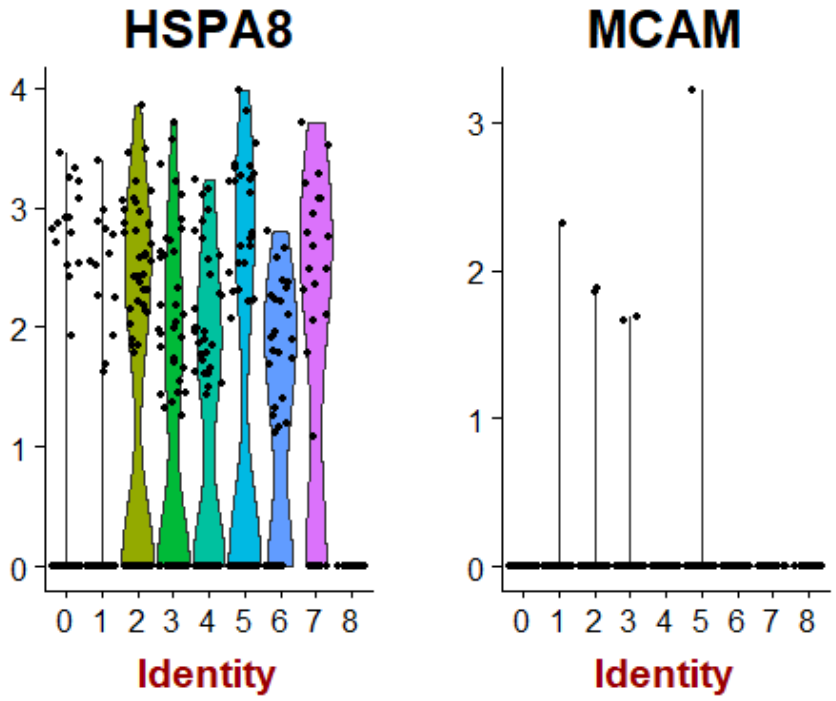

```
FeaturePlot(object = bmmc, features.plot = c("HSPA8", "MCAM"), cols.use = c("
grey", "blue"),
    reduction.use = "tsne")
```

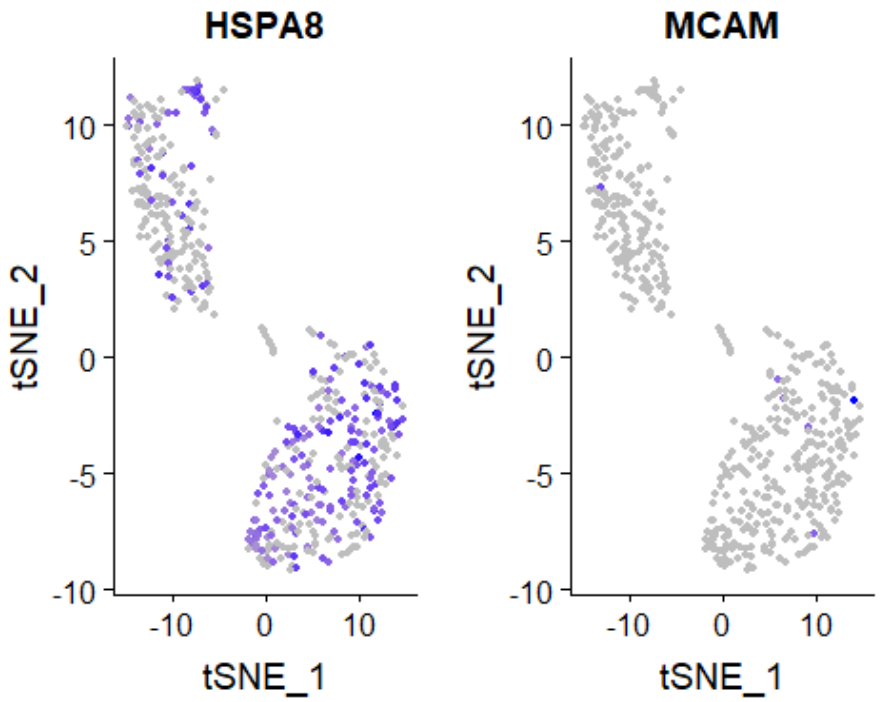

Finding genes and how they are varied between the clusters (top 10), and then producing a heat map across the clusters.

```
top10 <- bmmc.markers %>% group_by(cluster) %>% top_n(10, avg_logFC)
DoHeatmap(object = bmmc, genes.use = top10$gene, slim.col.label = TRUE, remov
e.key = FALSE, cex.row =10)
```

Appendix I

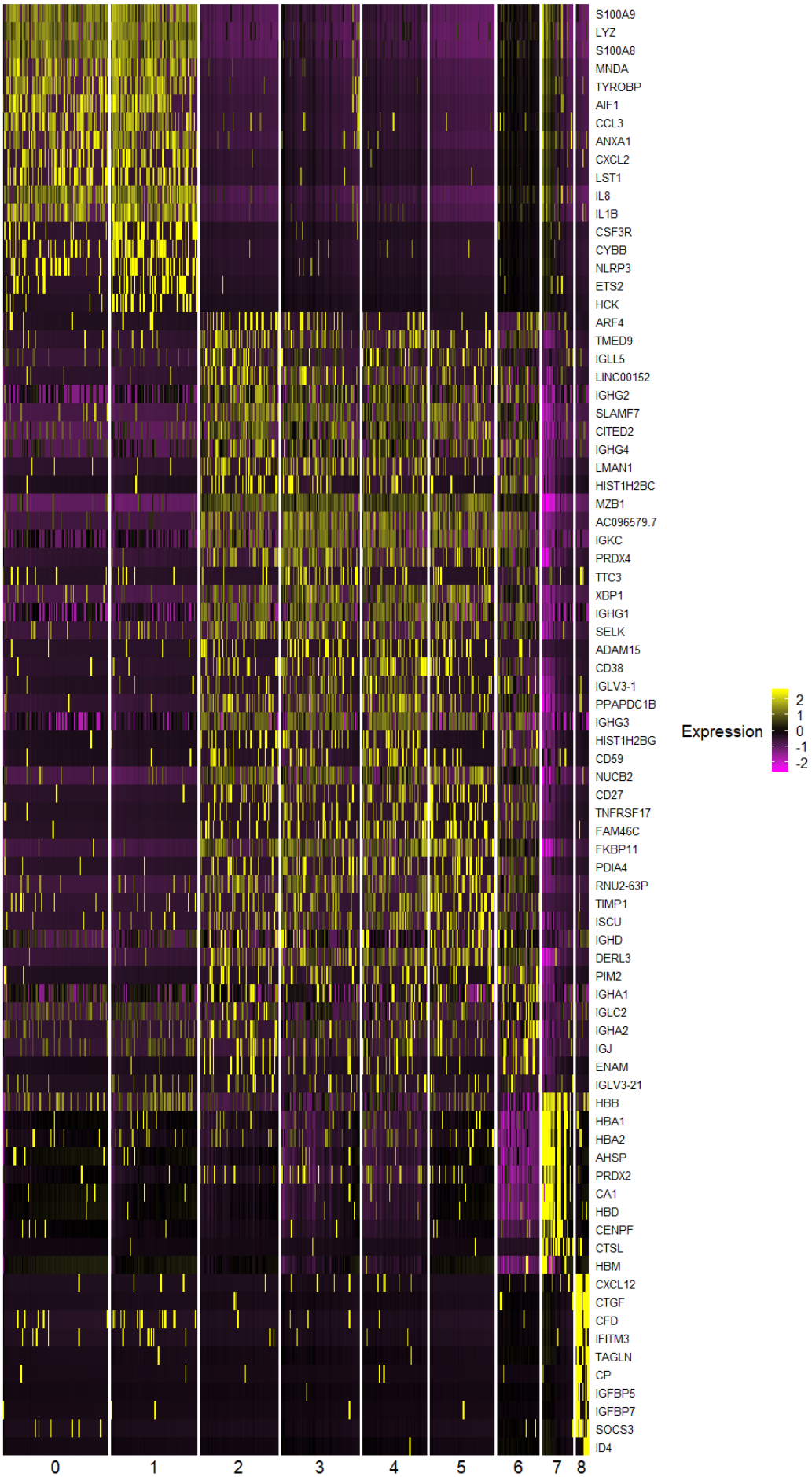
S100A9
LYZ
S100A8
MNDA
TYROBP
AIF1
CCL3
ANXA1
CXCL2
LST1
IL8
IL1B
CSF3R
CYBB
NLRP3
ETS2
HCK
ARF4
TMED9
IGLL5
LINC00152
IGHG2
SLAMF7
CITED2
IGHG4
LMAN1
HIST1H2BC
MZB1
AC096579.7
IGKC
PRDX4
TTC3
XBP1
IGHG1
SELK
ADAM15
CD38
IGLV3-1
PPAPDC1B
IGHG3
HIST1H2BG
CD59
NUCB2
CD27
TNFRSF17
FAM46C
FKBP11
PDIA4
RNU2-63P
TIMP1
ISCU
IGHD
DERL3
PIM2
IGHA1
IGLC2
IGHA2
IGJ
ENAM
IGLV3-21
HBB
HBA1
HBA2
AHSP
PRDX2
CA1
HBD
CENPF
CTSL
HBM
CXCL12
CTGF
CFD
IFITM3
TAGLN
CP
IGFBP5
IGFBP7
SOCS3
ID4
0
1
2
3
4
5
6
7
8
Expression
2
1
0
-1
-2

Naming of clusters based on markers found - not relevant for this population, need to look into markers - redo after cluster changes

```
current.cluster.ids <- c(0, 1, 2, 3, 4, 5, 6, 7, 8)
new.cluster.ids <- c("Monocyte", "Monocyte", "Lymphocyte", "Lymphocyte",
    "Lymphocyte", "Lymphocyte", "Lymphocyte", "Erythrocyte progenitors", "CAR
 cells")
bmmc@ident <- plyr::mapvalues(x = bmmc@ident, from = current.cluster.ids, to
= new.cluster.ids)
TSNEPlot(object = bmmc, do.label = TRUE, pt.size = 0.5)
```

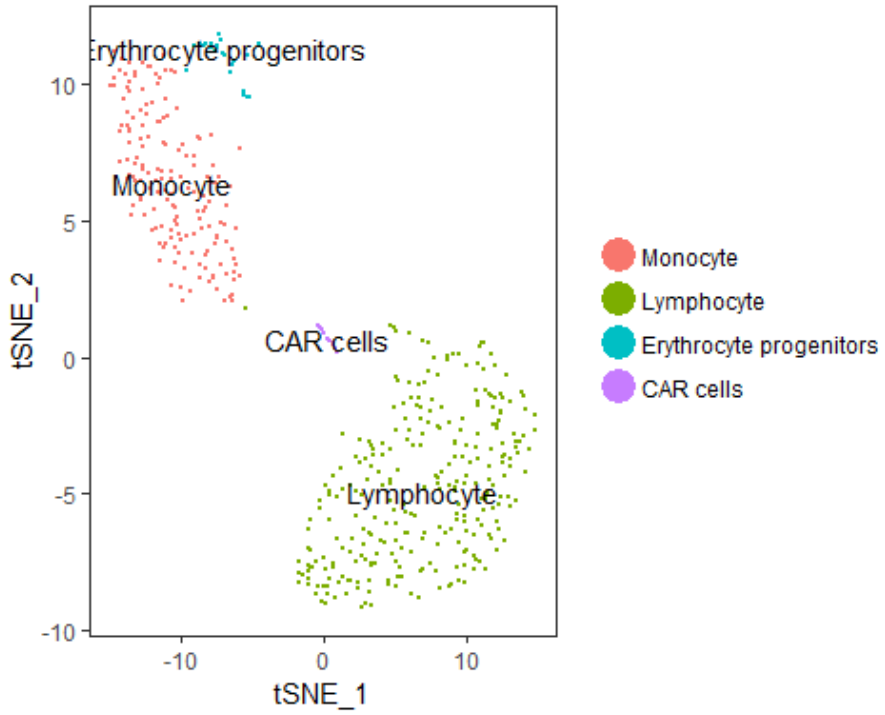

Saves files

```
bmmc <- SetAllIdent(object = bmmc, id = "ClusterNames_1.2")
saveRDS(bmmc, file = "~/F47 BMMC/F47_MACSFACS.rds")
```